SYNTHESIS OF PALM-BASED SELF-HEALING POLYURETHANE-LITHIUM PERCHLORATE

WONG CHEE SIEN

THESIS SUBMITTED IN FULFILMENT FOR THE DEGREE OF DOCTOR OF PHILOSOPHY

FACULTY OF SCIENCE AND TECHNOLOGY
UNIVERSITI KEBANGSAAN MALAYSIA
BANGI

2018

SINTESIS POLIURETANA-LITIUM PERKLORAT SWA-PULIH ASAS SAWIT

WONG CHEE SIEN

TESSIS YANG DIKEMUKAKAN UNTUK MEMPEROLEH IJAZAH
DOKTOR FALSAFAH

FAKULTI SAINS DAN TEKNOLOGI
UNIVERSITI KEBANGSAAN MALAYSIA
BANGI

2018

DECLARATION

I, hereby declare that this thesis is the result of my own investigation, except for quotations and summaries which have been appropriately acknowledged.

16 August 2018

WONG CHEE SIEN
P 67820

ACKNOWLEDGEMENTS

Thank God for giving me strength in completing my thesis.

I would like to extend my deepest gratitude towards my supervisors, Prof. Dr. Khairiah Haji Badri and Dr. Nurul Izzaty Hassan from School of Chemical Sciences and Food Technology (PPSKTM), Faculty of Science and Technology, Universiti Kebangsaan Malaysia (UKM) . Thank you so much for the guidance, supports, and encouragement during my research over the past years. I would like to also extend my personal appreciation to Dr Jose Alberto Mendez Gonzalez and Dr. Marie Angels Pelach Serra from School of Engineering, University of Girona, Spain for their guidance and supports during my attachment period. A special thanks to Erasmus Mundus Techno 2 mobility program by European Commission for giving me an opportunity for the research collaboration between UKM and University of Girona, Spain for the very warm welcome and excellent facilities provided.

I would also like to take this opportunity to thank the Ministry of Higher Education, Malaysia for MyPhD Scholarship under MyBrain15 scheme. This research work was supported by the Fundamental Research Grant Scheme, Ministry of Higher Education, Malaysia; FRGS/1/2011/TK/UKM/02/39, and Research University Grant provided by UKM, UKM-GUP-2011-228.

I would like to extend my appreciation towards all the lecturers, non-academic staffs and colleagues in PPSKTM, and Polymer Research Center (PORCE), Faculty of Science and Technology, UKM. Thank you for your valuable time, thoughts, ideas and useful arguments.

To my beloved family and friends, thank you so much for your moral supports, along my doctoral journey. Last but not least, I would like to acknowledge all of the supports that I was given throughout the process of this manuscript and all the people that I met along my journey of knowledge. Thanks for the inspiration.

SYNTHESIS OF PALM-BASED SELF-HEALING POLYURETHANE-LITHIUM PERCHLORATE

ABSTRACT

Palm-based self-healing polyurethane-$LiClO_4$ (PUC) was synthesized by pre-polymerization method. Self-healing agent namely 6,7-dihydroxycoumarin (DHC) was incorporated into palm-based polyurethane (PU). Blending mixture consisted of palm-based polyol (PKO-p), polyethylene glycol (PEG) and DHC were reacted with 4,4'-methylene diphenyl diisocyanate (MDI) in acetone under nitrogen gas environment at room temperature. Prior to that, lithium perchlorate ($LiClO_4$) salt at 5 %w/w in acetone was added into the blending mixture and the thin film was prepared via solution casting technique. PKO-p and PEG contributed the OH portion while MDI contributed the NCO portion. The studied variables were NCO/OH ratios (200/100, 150/100, 100/100 and 85/100), DHC content (24, 48, 72, 96 ratio to MDI), $LiClO_4$ loading percentage (0, 5, 10, 15, 20, 25 and 30 wt%). The formation of the urethane backbone (NHCO) in the main chain was indicated by the emergence of amine (secondary), carbonyl, carbamate, ether and ester groups in the FTIR spectra. The FTIR spectrum for the self-recovery polyurethane containing NCO/DHC ratio of 200/72 (PU200C72-5) showed increase in transmittance percentage at 830 cm^{-1} after exposure to ultraviolet (UV) radiation. This is due to the formation of cyclobutane bond in DHC along the polyurethane chain. PUC with inclusion of DHC at NCO/DHC ratios of 200/24 and 200/48 (PU200C24-5 and PU200C48-5 respectively) undergone degradation of the urethane bond indicated upon exposure to UV radiation. Sufficient DHC at NCO/DHC ratios of 200/72 and 200/96 could absorb more UV radiation and prevent degradation of urethane bonds. Glass transition temperature increased from 58 to 68 ℃ at higher DHC content (NCO/DHC ratios from 200/24 to 200/96 respectively). However, PU200C72-5 showed insignificant difference in the T_g (from 61.0 ℃ to 61.2℃). Micrographs obtained from optical and scanning electron microscopes (SEM) exhibited formation of new layer on top of the scratch wound in PU200C72-5. It is also able to retain its mechanical properties compared to other samples. The electrical conductivity of PU200C72-5 achieved 2.08×10^{-7} $S.cm^{-1}$. This study showed the potential of self-healing palm-based polyurethane in the production of conductive film for possible application in solar panel manufacturing.

ABSTRAK

Poliuretana-litium perklorat swa-pulih asas sawit (PUC) telah disintesiskan dengan kaedah prapempolimeran. Poliuretana (PU) sawit ini ditusukkan dengan 6,7-dihidroksikoumarin (DHC) bersaiz nano yang berfungsi sebagai agen swa-pulih. Campuran adunan PKO–p, polietilena glikol dan 6,7-dihidroksikoumarin dengan peratus berat yang berlainan (6, 8, 10 and 12 %w/w) ditindakbalaskan dengan 4,4'–difenil metilena diisosianat di dalam aseton dalam gas nitrogen pada suhu bilik. Garam litium perklorat ($LiClO_4$) pada peratus 5 % w/w dalam aseton ditambahkan ke dalam campuran dan filem nipis disediakan dengan menggunakan teknik penuangan larutan. Pembentukan tulang belakang uretana (NHCO) selepas tindak balas pempolimeran dan kemunculan puncak kumpulan amina (sekunder), karbonil, karbamat, eter dan ester dalam rantai PU diperhatikan dalam spektrum FTIR. Spektrum FTIR bagi poliuretana swa-pulih asas sawit dengan 10 %w/w DHC (PU200C72-5) menunjukkan penurunan intensity pada puncak di sekitar 830 cm^{-1} setelah pendedahan kepada sinaran ultraungu. Ini adalah kerana pembentukan ikatan siklobutana dalam DHC sepanjang rantaian poliuretana. Selain itu, poliuretana swa-pulih dengan 6 dan 8 %w/w DHC (PU200C24-5 and PU200C48-5) mengalami degradasi ikatan uretana dengan peningkatan peratus transmitans dari 65% ke 75% untuk puncak karbonil uretana selepas terdedah kepada sinaran ultraungu. DHC yang cukup boleh menyerap lebih banyak sinaran ultraungu dan mengelakkan degradasi ikatan uretana berlaku. Suhu peralihan kaca meningkat dari 58 ke 68 ℃ dengan kandungan DHC yang lebih tinggi dalam PUC. Tetapi setelah pendedahan kepada sinaran ultraungu, PU200C24-5 and PU200C48-5 mengalami penurunan suhu peralihan kaca. Tetapi, PU200C72-5 menunjukkan perbezaan ketara dalam T_g. Di samping itu, imej yang didapati daripada mikroskop optik dan mikrosop Imbasan Elektron (SEM) menunjukkan satu lapisan baru telah terbentuk pada permukaan calaran dalam PU200C72-5. Selain itu, PU200C72-5 ini dapat mengekalkan sifat mekanik berbanding dengan poliuretana yang lain. Di samping itu, sifat kekonduksian elektrik PU200C72-5 adalah paling cemerlang berbanding dengan poliuretana yang lain. Kajian ini menunjukkan potensi poliuretana swa-pulih asas sawit dalam pembuatan filem konduktif yang mungkin boleh digunakan dalam pembuatan panel solar.

TABLE OF CONTENT

LIST OF TABLES

LIST OF ILLUSTRATIONS

LIST OF SYMBOL

°	index (degree)
°C	temperature in Celcius
%	percentage
%T	percentage of transmission
λ	wavelength
π	pi
σ	conductivity
σ_o	pre-exponential factor
A	area
C	capacitance
cm	centimeter
cm^{-1}	wavenumber
g	gram
Hz	Hertz
I	current
K	temperature in Kelvin
l	thickness
MPa	megapascal
mm	millimeter
µm	micrometer
R	resistance
T_c	crystallization temperature
T_d	thermal degradation
T_g	glass transition temperature
T_m	melting temperature
T_{max}	maximum temperature
V	voltage
W_1	mass of sample before extraction
W_2	mass of sample after extraction
wt%	weight percentage
$S.cm^{-1}$	conductivity

LIST OF ABBREVIATIONS

AC	Alternating circuit
ASTM	American Society for Testing and Materials
ATR-FTIR	attenuated total reflectance-Fourier Transform Infrared spectroscopy
CPD	cyclopentadiene
DA	Diels-Alder
DAT	2,6-diaminotriaine
DCPD	dicyclopentadiene
DGEBA	diglycidyl ether bisphenol-A
DMF	dimethylformamide
DSC	differential scanning calorimetry
DTG	differential thermogravimetric
EIS	electrochemical impedance spectroscopy
EMI	electromagnetic interference
EV	electric vehicle
HFRA	high frequency resonance analyzer
HOMO	highest occupied molecular orbital
LUMO	lowest unoccupied molecular orbital
MDI	methylene diphenyl diisocyanate
MF	melamine-formaldehyde
MUF	melamine-urea formaldehyde
NCO/OH	nitrogen-carbon-oxygen/hydroxyl
PEG	polyethylene glycol
PEI	poly(ethyleneimine)
PEM	polyelectrolyte multilayer
PKO-p	palm kernel oil-based polyol
PMMA	poly(methylmethacrylate)
PSS	poly(styrene sulfonate)
PVdF	poly(vinylidene fluoride)

PU	polyurethane
PUC	self-healing polyurethane
ROMP	ring-opening metathesis polymerization
SEM-EDX	scanning electon microscope-energy dispersive X-ray spectroscopy
SHPU	self-healing conductive polyurethane
S_1	singlet
TGA	thermogravimetric analysis

LIST OF NOMENCLATURES

CO	carbon monoxide
CO_2	carbon dioxide
H_2O	water
Li^+	lithium ion
LiCl	lithium chloride
$LiClO_4$	lithium perchlorate
NaCl	Sodium chloride
$TiCl_4$	titanium tetrachloride
TiO_2	titanium dioxide

CHAPTER I

INTRODUCTION

1.1 RESEARCH BACKGROUND

Polyurethane (PU) is one of the most important polymers used in domestic goods and industries. It has great diversity of application types such as foams, fibers, coatings and adhesives due to excellent flexibility and durability of PU (Liu 2014; Simon 2015). The flexibility and durability of PU are attributed to the crosslinking in PU structural chain and interaction between urethane groups such as hydrogen bonds (Sami 2014; Lin 2012). Polyurethane is a synthetic polymer with urethane backbone (-NHCOO-). Polyurethanes with different types of molecular design could be manipulated for different applications. It is one of the most important polymers used in different fields such as foam, medical devices, adhesives, sealants, coatings and elastomers (Kim and Kim 2005; Kim et al. 2003). Natural polymers show the advantages of bio-degradability, bio-compatibility, non-toxic, high reactivity, low cost, and accessibility and therefore they have been counted as superb raw chemical substances for conserving petroleum resources and shielding the environment (Ermolovich 2005; Fomin & Guzeev 2001). Hence, palm kernel oil which is an abundant sustainable resource in Malaysia, is used to make polyurethane in this research (Badri 2011; Badri 2012; Wong et al. 2012; Zafar et al. 2012; Septevani 2015). The bio-based polyurethane film was prepared by solution casting technique (Wong et al. 2012). The chemical structure of the bio-based polyurethane is as shown in Figure 1.1:

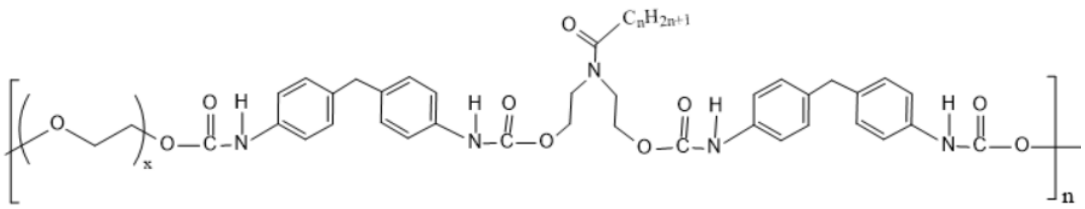

Figure 1.1 Predicted chemical structure of palm kernel oil-based polyurethane

PU is a good insulator and many efforts have been exerted to optimize the electrical conductivity of PU by incorporating conductive materials such as carbon nanotubes, metallic salts especially lithium salts and graphene into PU (Sun 2009; Segal 2001; Koerner 2005). The integration of lithium ions to the polymer matrix has attracted attention from academics and industries for several decades due to its wide applications in anti-static materials, electromagnetic interference (EMI) shielding, sensors and conductors and solar panels. However, PU is susceptible to UV degradation and it will shorten the lifespan of the electrical device such as solar panel. Hence, the device must be replaced regularly. Besides that, the damage inflicted to the polymer in the form of impact, fracture and puncture could lower the efficiency of the conductive polyurethane in the device. Hence, design of new materials with capabilities of "self-healing" is a new approach to solve the problem of emergence of damage, failure and degradation in the material. Self-healing materials exhibit the ability to repair or recover themselves using the resources inherently available to them. The repair can be autonomic or externally assisted (e.g. by heating or UV light). So, self-healing materials offer a new route toward safer, longer-lasting products and components (Blaiszik et al. 2010). For the past decade, different self-healing materials have been developed through the embedment of self-healing compounds into polymers through formation of covalent bonds (Xiangxu et al. 2002; Biswajit et al. 2009; Judit et al. 2011) and non covalent bonds (Rint et al. 1997; Philippe et al. 2008; Mark et al. 2011) activated by temperature, electromagnetic radiation, changes of chemical environments (pH, redox reactions, ionic strength). Light stimulated self-healing polymer is a promising approach as light is used to activate the self-healing ability in the polymer (Sheba et al. 2008; Zhang et al. 2012). Coumarin was used as a self-healing component in this research due to its ability to undergo [2+2] photocycloaddition reaction upon irradiation with UV light as shown below (Jun Ling 2012):

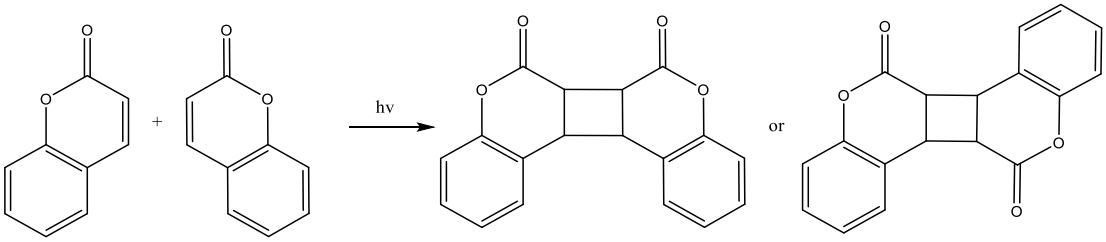

Figure 1.2 Photocycloaddition reaction

1.2 SCOPE

1.2.1 PROBLEM STATEMENT

One of the drawbacks in polyurethane-lithium salt is their limitation or drawback to repair the damaged sites due to photo-degradation in the polymer upon exposure to UV light. The damaged sites in the polymer could decrease thermal, mechanical and electrical conductivity of the polymer. One of the solutions to encounter this problem is by introducing 6,7-dihydroxycoumarin (DHC) into the polymer so it could heal the damaged site. The healing process can be triggered by UV irradiation. This process involves cycloaddition reaction of 6,7-dihydroxycoumarin in PU chain.

DHC was selected to give self-healing effect in the PU-$LiClO_4$ due to its ability to form urethane backbone by reacting its hydroxyl groups with isocyanate groups in MDI. Furthermore, the alkene group (C=C) in DHC is able to undergo photodimerization upon UV irradiation.

In this study, a bio-based polymer, PU was used as the host for the self-healing polymer-$LiClO_4$. PU provides desired flexibility and is easily molded compared to other petrochemical-based polymers such as polypropylene, polyvinyl chloride and polyethylene. This polyurethane is prepared at room temperature giving the advantage by the auto-catalyzed reaction as discovered by Wong and Badri (2012). Furthermore, the carbonyl group in urethane linkage might have interaction with cations.

In this research, the effect of DHC on the chemical, thermal and electrical conductivity of self-healing PU-$LiClO_4$ was investigated. PU-$LiClO_4$ with optimum NCO/OH ratio and $LiClO_4$ loading was selected to synthesize the self-healing PU-$LiClO_4$. This study is able to let us understand the effect of DHC onto the electrical conductivity and its relation to the chemical structure of PU-$LiClO_4$.

1.2.2 HYPOTHESIS

PU-$LiClO_4$ is susceptible to environmental stress such as energy from heat and light as well as moisture. It is common to have low resistivity towards UV irradiation resulting in photo-degradation. Hence discolouration, cracks, exfoliation as well as severe

damage are encountered. Thus, self-healing agents such as benzopyrone groups namely dihydroxycoumarin are required to treat the damaged sites. This is to ensure it remains resistant to UV degradation and able to recover the damage in the polymer by having the ability to undergo photo-cycloaddition reaction. The self-healing ability of the polymer can be assessible by FTIR spectroscopy, SEM-EDX and optical microscopies. In addition, DSC and TGA analyses, tensile strength determination, pendulum and pencil hardness tests were conducted to further confirm its potential.

1.2.3 RESEARCH OUTLINES

At the initial stage of the research, the polyurethane-$LiClO_4$ was prepared using optimum amount of $LiClO_4$ in polyurethane based on previous study conducted by the research team. The polyurethane-$LiClO_4$ was used as a control. Then, the self-healing PU-$LiClO_4$ was synthesized by embedding 6,7-dihydroxycoumarin into the polyurethane through prepolymerization method. Later, optimization of self-healing PU-$LiClO_4$ was carried out by varying the amount of 6,7-dihydroxycoumarin in the PU. Finally, the chemical, thermal, mechanical properties and morphology of self-healing PU-$LiClO_4$ were characterized. The chapters are divided into 5 parts which are the described as follow:

Chapter I is introducing the role of 6,7-dihydroxycoumarin as self-healing agent in the palm-based PU containing $LiClO_4$. In this chapter, the problem statement is highlighted which is stressed on the protocols of detecting the self-healing ability.

Chapter II is reporting on the recent research updates about polyurethane, self-healing agents especially coumarin, and also conductive polymers. Some of the ideas and findings are compared and interpreted in Chapter IV and V.

Chapter III is basically describing the methods and techniques used in preparing not only the palm-based PU, but also both the PU-$LiClO_4$ and self-healing PU-$LiClO_4$ containing DHC.

CHAPTER IV consists of ideas and results extracted from published paper and the research findings. It described the preparation and characterization of PU-$LiClO_4$ with different NCO/OH ratios and $LiClO_4$ loading percentage.

CHAPTER V consists of results and discussion for self-healing PU-$LiClO_4$. It also described and discussed the preparation and characterization of self-healing PU-$LiClO_4$ with different NCO/DHC ratios. In this chapter, the self-healing PU-$LiClO_4$ containing DHC was exposed to UV irradiation and compared to the pristine PU-$LiClO_4$

CHAPTER VI summarized the whole preparation and characterization of self-healing PU-$LiClO_4$ containing DHC. The possible future works were also stated to ensure continuity of this research.

1.3 OBJECTIVES

- To synthesize polyurethane-lithium perchlorate (PU-$LiClO_4$) with varying mass ratio of palm kernel oil-based polyol, diisocyanate and chain extender
- To prepare self-healing PU-$LiClO_4$ with the inclusion of DHC
- To investigate the effect of UV-light on the photodimerization reaction of self-healing PU-$LiClO_4$
- To determine the mechanical, thermal, ionic conductivity and chemical properties of the self-healing PU-$LiClO_4$

CHAPTER II

LITERATURE REVIEW

2.1 SELF-HEALING MATERIALS

Generally, self-healing materials can be categorized into 3 groups: capsule-based, vascular and intrinsic. Capsule-based self-healing entrapped the healing agent in discrete molecules as shown in Figure. 2.1 (a). The self-healing mechanism is stimulated through the release when the capsules are ruptured, resulted from damages. Self-healing via vascular system is an entrapment of the healing agent in a network in which it will be interconnected until damage triggers the self-healing. The first delivery of healing agent occurs after the vascular network is damaged. At this point, the network can be refilled by an exterior source or from an intact but connected part of the vascular network. This refilling action permits several healing events in the same area of damage. Intrinsic self-healing materials as shown in Figure 2.1(c) do not have an isolated healing agent. Damages or external stimulus, e.g. pH change, light, temperature and pressure are often described as underlying triggering factors to intrinsic self-healing mechanisms. In order to initiate the self-healing mechanism, these materials should rely on several factors such as chain mobility, cycloaddition chain entanglement, reversible polymerization, hydrogen bonding, thermoplastic melting phases or ionic interactions (Blaiszik et al. 2010).

Different recovery systems offer healing for different damage volume regimes as shown in Figure 2.2. Intrinsic self-healing materials are used for small damage and capable to heal the cracked faces at the molecular scale. Most intrinsic materials require small damage volume for efficient healing because intrinsic rebonding requires close proximity of the damaged surfaces.

Large damage volume could be recovered if vascular self-healing materials are used. The healing of vascular network only could be trigerred if the damage size is large enough. Capsule-based self-healing materials could heal the moderate damage volume which could not be filled by intrinsic and vascular approaches as shown in Figure 2.2 (Blaiszik et al. 2010).

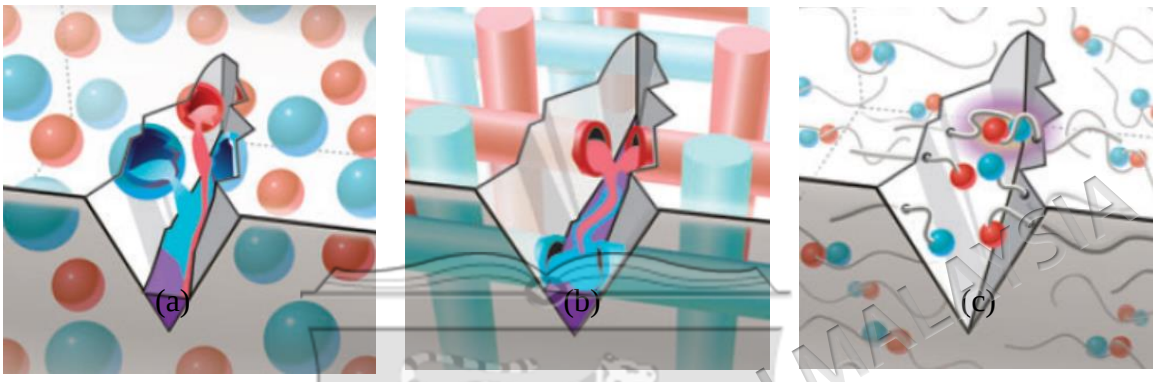

Figure 2.1 (a) Capsule-based self-healing materials, (b) Vascular self-healing materials and (c) Intrinsic self-healing materials

Source: Blaiszik et al. (2010)

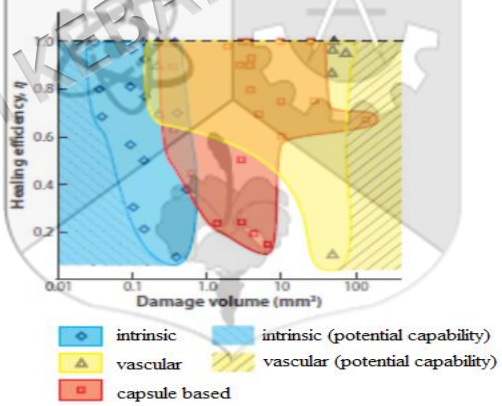

Figure 2.2 Healing for different damage volumes by different self-healing materials

Source: Blaiszik et al. (2010)

2.1.1 Capsule-based self-healing materials

In situ, interfacial and meltable dispersion are the most common encapsulation techniques. Encapsulated self-healing materials via in-situ and interfacial were made by urea-formaldehyde (UF) (Blaiszik et al. 2009; Keller et al. 2007; Brown et al. 2003), melamine-formaldehyde (MF) (Yuan et al. 2008), melamine-urea formaldehyde (MUF)

(Liu et al. 2009), PU (Cho et al. 2006), or acrylates (Xiao et al. 2009) followed by the formation of a polymer shell wall at the interface of droplets in an oil-in-water (o/w) emulsion. Meltable dispersion encapsulated self-healing material is prepared by dispersion of self-healing capsule in the melted polymer. Subsequently, it was emulsified to form droplets followed by forming a protective sphere around the self-healing capsule via heating or solvent removal process (Rule et al. 2005). The capsules could be prepared by inverse emulsion (Yeom et al. 2000), *Pickering* stabilization (Mookhoek et al. 2008), inverse *Pickering* stabilization and multiple emulsions (Abate et al. 2009).

2.1.2 Vascular Self-Healing Materials

The preparation of vascular self-healing materials is carried out by the incorporation of the healing agent into the hollow glass fibers (HGFs) with microsized diameter. Bleay and his friends (2001) embedded HGFs with the diameter of 15 μm into one-way plies for composite laminates. Under applied vacuum, the specimens of fibers within cured laminates were filled with various fluids and the fluids were released into damage zones. For a more effective fluid filling, Pang (2005) fabricated a 60-μm-diameter HGFs and incorporated both HGF and solid glass fiber layers into a hybrid laminate. A 2D networks self-healing fibers were constructed within composite panels by Williams and friends (2008). The network was assembled in a hierarchical pattern and contained two-part of epoxy system. Polyvinyl chloride tubes act as major vessels in the panel midplane and small size channels drilled vessels to extend through the foam core. Toohey and co-workers (2007) imitated the structure and functionality of epidermal tissue by producing a 3D vascular self-healing epoxy. They incorporated a brittle epoxy coating with Grubb's catalyst and later deposited on a flexible epoxy substrate. The epoxy substrate contained a 3D grid network of 200 μm microchannels filled with healing agent. The healing agent from the vascular substrate was released and subsequently polymerization occurred as the healing agent reacted with the catalyst in the coating. A complex and isolated interpenetrating network was made using direct-ink writing methods by Hansen and his friends (2009). This method can improve the mixing of two-part epoxy healing system as well as to optimize stoichiometry.

2.1.3 Intrinsic Self-Healing materials

Generally, there are 3 main schemes to demonstrate intrinsic self-healing materials. Covalent bonding as shown in Fig. 2.4 (a) makes use of the cycloaddition or Diels-Alder (DA) reactions and they are adapted to self-healing applications. These materials normally contain in the polymers that enable the cycloaddition reaction to take place. Xiang Chen et al. (2002) produced synthesized thermally activated self-healing furan-maleimide polymers which allowed DA reaction at 75ºC. Plaisted and Nemat-Nasser (2007) also made self-healing furan-maleimide polymer via DA reaction. Park (2008) synthesized cyclopentadiene containing polymer and the cyclopentadiene in polymer is able to undergo cycloaddition to have self-healing ability as shown in Figure 2.3 and it was applied in the composite (Park et al. 2009). Murphy et al. (2008) produced and characterized another type of cyclopentadiene containing polymer. The polymer is comprised of a dicyclopentadiene core which acts as both diene and dienophile in the DA reaction. Polymer specimens have been prepared from two monomeric units, monomers 400 and 401, and the thermal and mechanical properties of these materials have been studied via differential scanning calorimetry, dynamic mechanical analysis, and three-point bending, compression, and fracture tests. After fracture, these hard, colourless, transparent materials are capable of thermal mending at 120 °C, effectively healing cracks formed in the specimen.

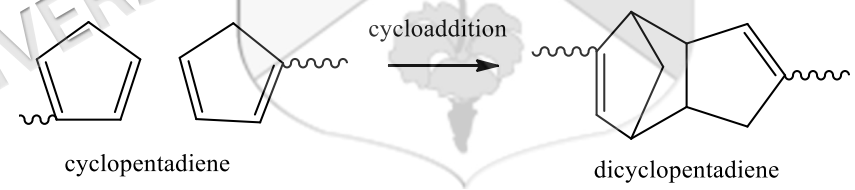

Figure 2.3 Cycloaddition reaction of cyclopentadiene

Source: Park (2008)

In the chain entanglement/diffusion approach (Figure 2.4 (b)), the molecular diffusion at crack faces could take place when the healing molecules such as epoxy containing phase-separated poly(carpolactone) span the crack surfaces and get entangled. Rahmathullah and Palmese (2008) prepared self-healing epoxy matrix with surplus amine functionality where molecular diffusion took place through thermal treatment. In addition, molecular diffusion is capable to heal the damage and also inhibit

corrosion. Aramaki (2008) prepared a solution of $CeCl_3$ and a sodium silicate containing 1,2-bis(triethoxysilyl)ethane polymer for cathode coating system. The silicate ion could move and cover the scratches. Andreeva and her friends (2008) prepared alternating layers of poly(ethyleneimine) (PEI) and poly(styrene sulfonate) (PSS) for polyelectrolyte multilayer (PEM) coatings. These copolymers could diffuse into cracked site via swelling method in water.

Figure 2.4 (c) shows a non-covalent bonding self-healing materials which exhibited self-healing properties via formation of ionic or hydrogen bonds. Copolymers namely poly(ethylene-*co* methacrylic acid) (EMAA) was prepared by Kalista and co-workers (2007). Further studies of this self-healing ionic polymer were carried out by Varley and van der Zwaag (2008). The self-healing phenomenon exhibited by the ionomer known as Surlyn 8940 (DuPont), a partially neutralized poly(ethylene-comethacrylic acid) random co-polymer has been investigated according to three separate strategies. Actual ballistic penetration studies confirmed that both elastomeric and viscous behaviour was evident throughout the impact regions. The outer impact regions exhibited ductile/elastic behaviour, while closer to the impact cavity elastomeric and viscous behaviour could be observed. It was also shown, however, that different weights and velocities of bullets could alter this balance and affect final healing. The elastic response (gelastic), critical to hole closure post-impact, was shown to be dependent upon the presence of ionic clusters when compared with related non-ionic polymers. Dynamic mechanical analysis also illustrated how the ionic clusters create a range of properties from elastic, elastomeric and then molten behaviour at different temperatures and play a critical role during high-energy impact. Repeatability of the self-healing process was demonstrated, confirming that healing is inherent to the chemical structure and morphology of the ionomer. The viscous healing response (gviscous) showed that, given sufficient molecular mobility and time, polymer chains will diffuse across discontinuous boundaries and heal. The balance between solid-like and liquid-like behaviour exhibited by Surlyn 8940 compared to non-ionic LLDPE, was shown to be critical to achieving appropriate healing. Cordier (2008) and Montarnal (2009) prepared a self-healing of a rubbery material through supramolecular assembly. The materials could be healed via hydrogen bonds as these supramolecular self-healing materials are destructed. Fatty diacid and triacid were condensed first with diethylene

triamine and then reacted with urea such as di(amidoethyl) urea and diamido tetraethyl triurea giving a mixture of oligomers. When the oligomers were broken or cut, they could be simply repaired by bringing together fractured surfaces to self-heal via hydrogen bonding at room temperature. Repaired samples recuperate their enormous extensibility. The process of breaking and healing can be repeated many times.

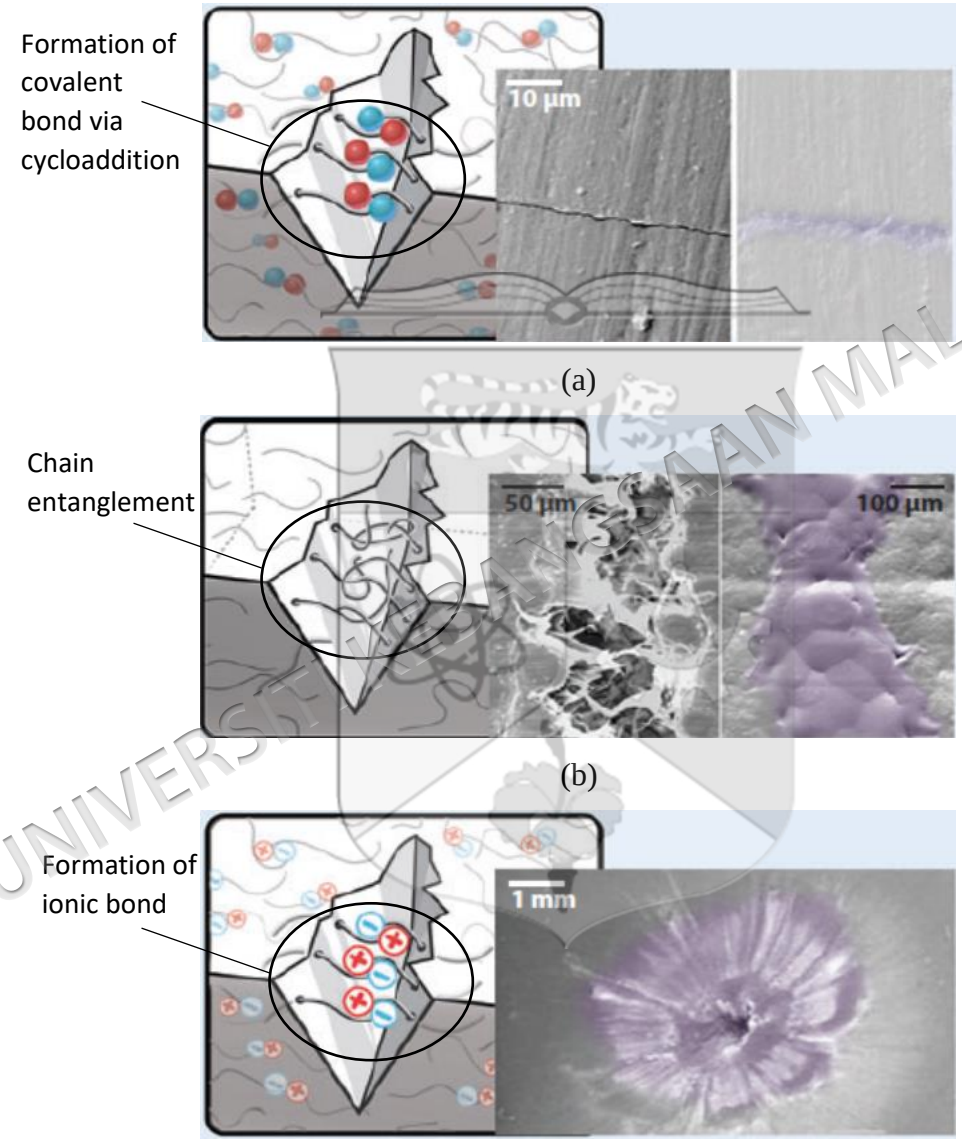

Figure 2.4 (a) Bonding, (b) chain entanglement and (c) Noncovalent bonding

Source: Blaiszik et al. (2010)

2.2 HEALING MECHANISM

2.2.1 Encapsulated healing

Incorporation of microcapsules and catalyst into the polymer matrix is a way to produce self-healing polymers. The catalyst could be solid particle or separately encapsulated liquid. Figure 2.5 shows the cracks created through the polymer matrix and rupturing several microcapsules. Subsequently, the liquid monomer moves from the broken capsules and onto the crack surface, while the healing agent polymerizes once in contact with the catalyst, thus adhering the two cracks faces together (White et al. 2008).

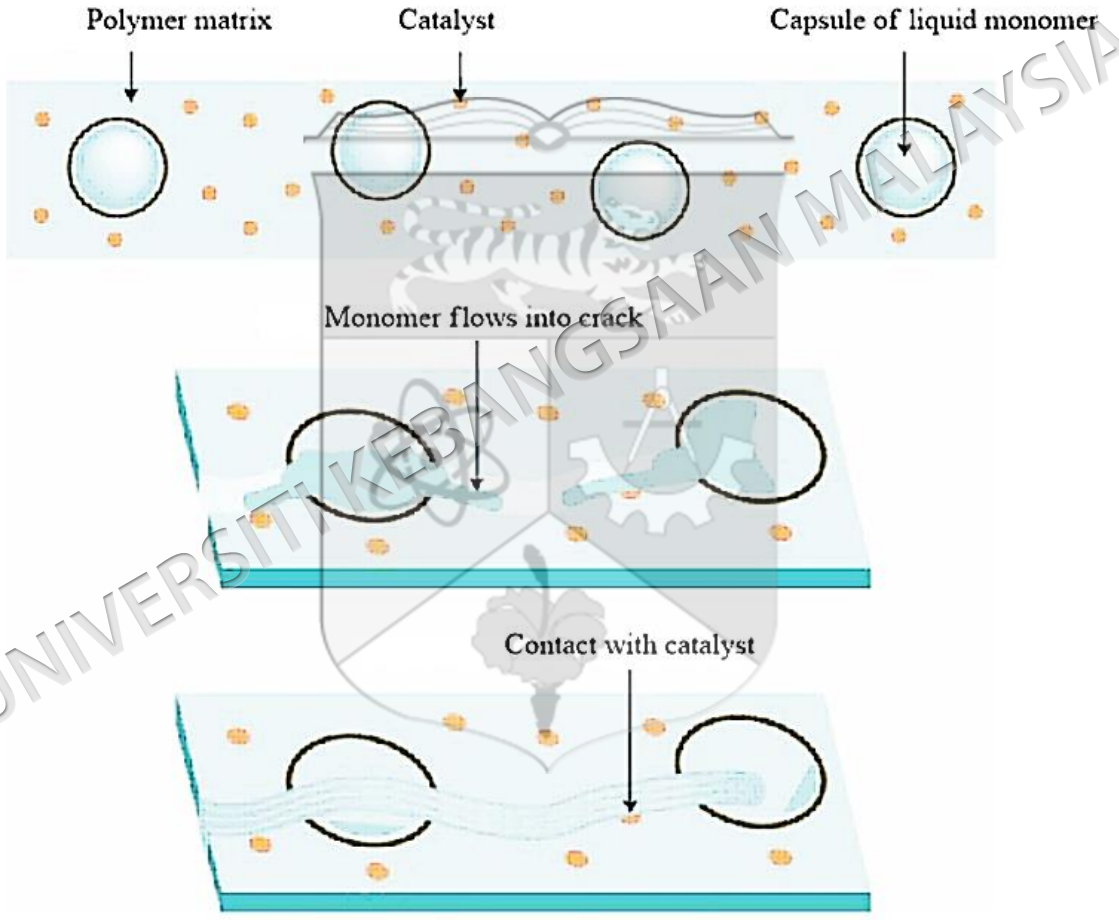

Figure 2.5 Microcapsule-based self-healing technique with a liquid, encapsulated monomer and a solid catalyst.

Source: White et al. (2008)

Healing agent and catalyst determine successful microcapsule-based self-healing effect. This can be achieved by having a long lifespan and stable healing agent and catalyst without leaking out of the microcapsule shell. Besides that, the healing

agent must completely fill the crack volume within a short time interval. In addition, the healing agent must have a rapid polymerization reaction with the catalyst and produced new polymer with a good mechanical strength. Microcapsules embedded styrene/polystyrene blends (Jung et al. 1997) and phenolic-based resins (Stephenson 2008) gave different results, but the healing mechanism is the ring-opening metathesis polymerization (ROMP) (Bielawski & Grubbs 2007; Nguyen et al. 1992; Kessler & White 2002) of dicyclopentadiene (DCPD) with ruthenium-based olefin metathesis catalyst Bis(tricyclohexylphosphine) benzylidene ruthenium dichloride or known as Grubbs‘ catalyst (Nguyen & Grubbs 1993; Dias et al. 1997; Trnka & Grubbs 2001; Sanford et al. 2001; Grubbs 2006). Firstly, the DCPD is co-ordinated to the ruthenium catalyst and forms a metallocyclobutane intermediate by a cycloaddition with the ruthenium catalyst. Finally, a cycloreversion took place in order to open

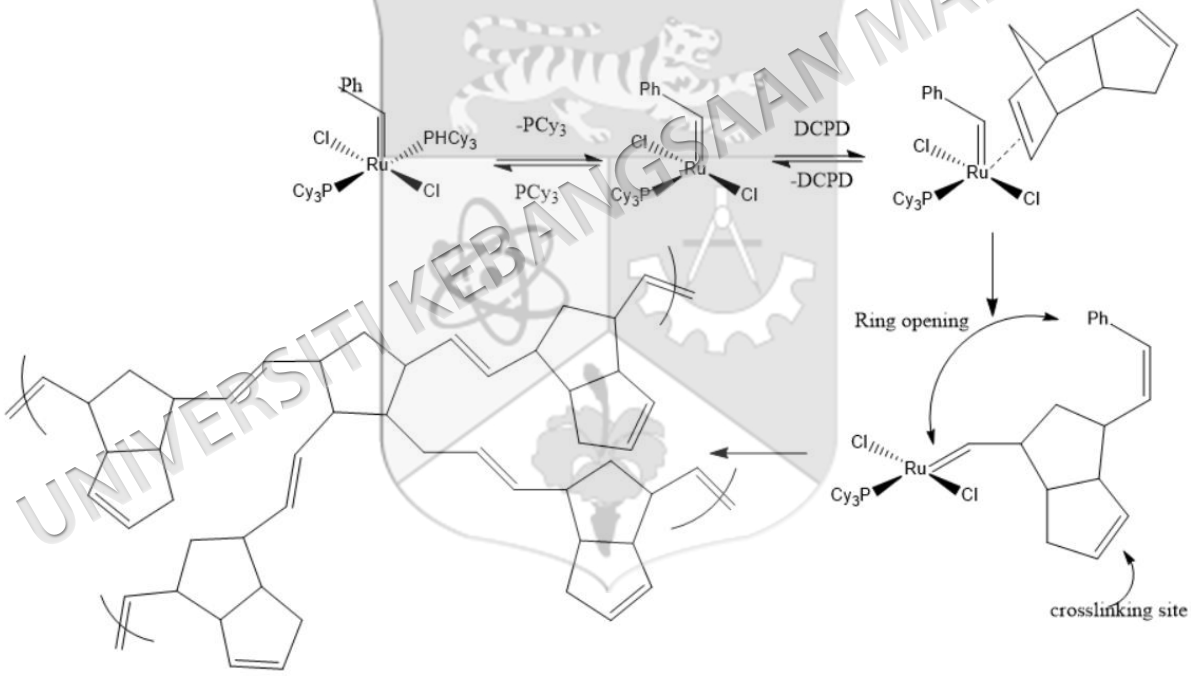

Figure 2.6 Polymerization mechanism of DCPD with Grubbs’ catalyst

Source: Grubbs et al. (2006)

A research by White et al. (2001) has reported the application of DCPD/Grubbs‘ catalyst in a self-healing material. The process involved the addition of encapsulated DCPD into a poly(urea-formaldehyde) and catalyst was embedded into an epoxy. The result shows that 90% toughness recovery could be achieved for the self-

healing polymer (Brown et al. 2002). Besides the healing large cracks, these polymers also showed increment to over 30 times longer lifespan compared to a polymer without self-healing properties (Brown et al. 2005; Brown et al. 2005; Jones et al. 2007). Polymers like PMMA bone cement (Lewis et al. 2009; Biggs et al. 2009), epoxy vinyl esters (Wilson et al. 2008), and poly(styrene-*b*-butadiene-*b*-styrene) (Chipara et al. 2009) used the DCPD/Grubbs‘ catalyst-based as a healing agent system. Another types of polymer matrices/healing agents based on epoxies and poly(dimethylsiloxane) (PDMS) polymers were developed. Rong et al. (2007), made a self-healing material by encapsulating diglycidyl ether bisphenol-A (DGEBA)-based epoxy resin in a urea-formaldehylde microcapsule and also with a capsulated imidazole hardener, embedded in an epoxy matrix made from the same DGEBA epoxy resin as in the microcapsules. Further improvements by Yi et al. (2007) were achieved where the capsulated imidazole was replaced with an epoxy-soluble imidazole that dissolved into the epoxy matrix during fabrication. One disadvantage of all imidazole hardener embedded epoxy-based self-healing polymers was that it required an external heat to polymerize the healing agent. Due to the growing interest for the development of a more autonomic epoxy-based self-healing system (i.e. without the need for external heat), more aggressive hardeners should come to play. Therefore, Keller et al. (2007) came with an idea of preparing PDMS elastomer with a healing agent that, when polymerized, is identical to the polymer matrix (Keller et al. 2007; Keller et al. 2008). A two-capsule healing agent was used in this polymer, where the first capsule comprised of a vinyl-functionalized PDMS resin and a platinum catalyst, and the second capsule was a liquid initiator containing a hydrosiloxane copolymer dissolved in 20% solvent to reduce its viscosity. These two components were then encapsulated in urea-formaldehyde shells. When the microcapsules were ruptured, the agents in the capsules would flow into the damage area, the platinum catalysed the reaction between hydrosiloxane copolymer and PDMS resin to cure and heal damage. Other PDMS self-healing polymers have been developed, as well. For instance, a tin-catalyzed condensation polymerization of polysiloxane-based healing agents was studied to heal damage area and able to withstand high pressure up to 101.3 kPa (Beiermann et al. 2009).

One of the crucial components for capsule healing is the microcapsules. Despite of the liquid healing agent should be stable in the microcapsules and should not leak out

of the capsules, nor should any other components permeate into the microcapsule, the encapsulation method should be simple and user-friendly. These capsules should be strong enough to tolerate the fabrication process of the self-healing polymer, but easy to shatter and are able to release the healing agent when the self-healing polymer is damaged. And most importantly, they must be compatible with the surrounding polymer. The encapsulation of DCPD in a poly(urea-formaldehyde) shell was among the first reports in the development of microcapsules (Figure 2.7) (Brown et al. 2003). One significant improvement of these capsules was the development of micro-sized microcapsules as shown below.

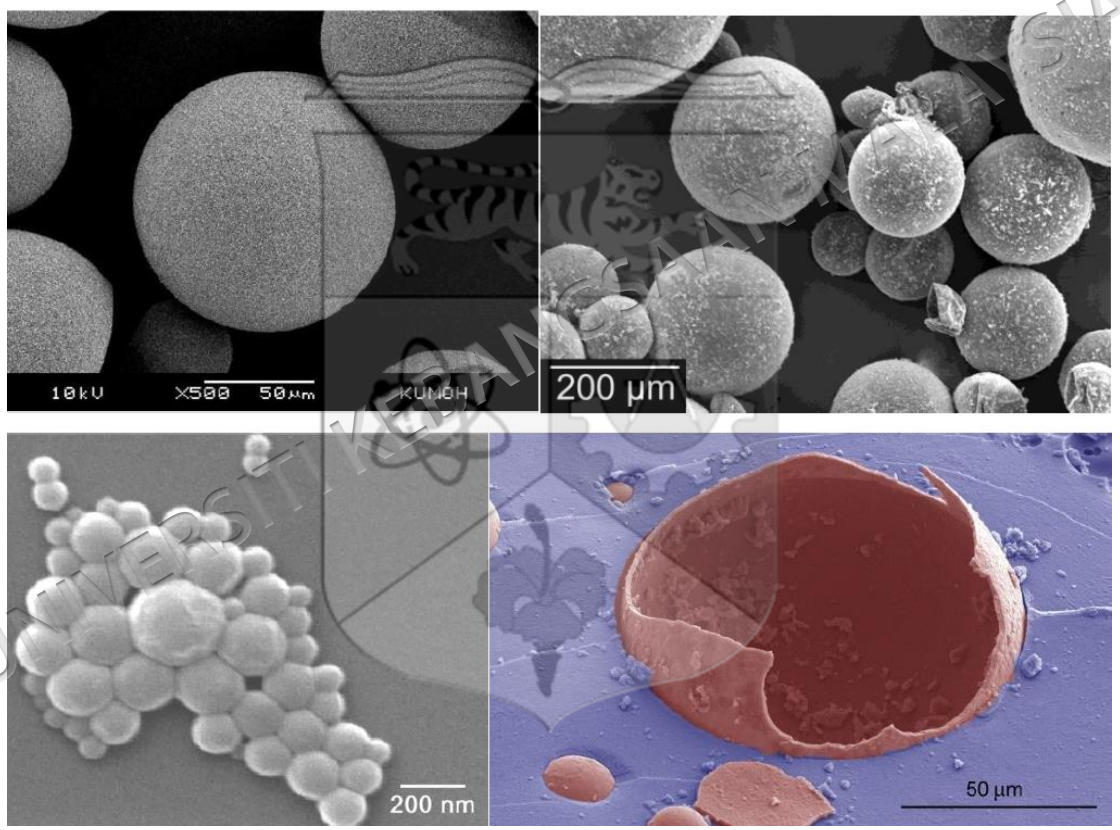

Figure 2.7 Micro-sized microcapsules

Source: Brown et al. (2003)

The optimization of the self-healing microcapsules can be conducted via numerous healing agent delivery methods such as the addition of epoxy and hardener into nano-porous silica, later embedded in a matrix (Kirk et al. 2009).

2.2.2 Vascular self-healing

Vascular self-healing polymer could repair the crack with large volume of healing agent as the vessel/channel able to store and release the healing agent when the vessel is broken or cut. But bigger size of vessel or channel might affect the mechanical properties of polymer host. Hence, the healing agent which could strengthen the structure of polymer while able to fill the damage site quickly is important. The hollow fibers with open ends or with pored are filled with healing agents as shown in Figure 2.8. Bleay et al. (2001) used a small diameter and strong fibers filled with healing agent, but the healing agent only could be activated by heat. A number of healing agents have been previously studied to treat the damage when incorporated into hollow fibers. Liu et al. (2008) introduced a coating with an improved ability to act as a water permeation barrier. In this study, water degradable poly(lactic acid) (PLA) fibers were filled with $TiCl_4$, and subsequently assembled into multilayer films. The moisture degraded the PLA fibers once damage reached the PLA layers and subsequently $TiCl_4$ was released into the damaged region. Then, the healing agent oxidized TiO_2 film to solidify.

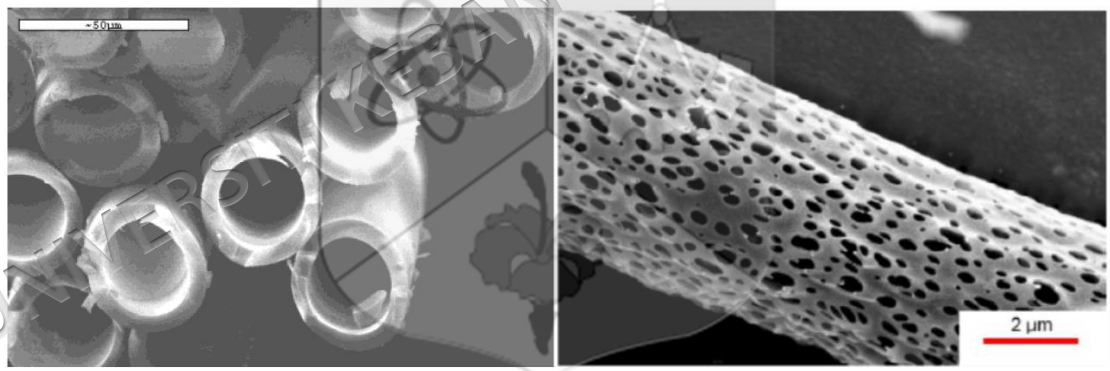

Figure 2.8 Hollow fibers with open ends (left) and with pores (right)

Source: Liu et al. (2008)

2.2.3 Thermal activated self-healing

Diels-Alder (DA) reaction between a diene and a dienophile, for several reasons, is ideal for self-healing mechanism. First, as diene and dienophile are chosen (i.e. furan and maleimide derivatives), DA reaction occurs at room temperature as soon as the self-healing mechanism is triggered in the polymer. In addition, the thermal degradation is avoidable since the controlled retro Diels-Alder (rDA) reaction of furan/maleimide-derived polymers is favored within the temperature range of 90-120 °C. Therefore, the

damage could be fixed at the molecular level. In 2002, thermoset polymers based on the Diels-Alder reaction between the multi-furan and multi-maleimide monomers were introduced (Chen et al. 2002). The reports demonstrated that this polymer could be heated higher than 120 °C and recovered about 57% from its original fracture load. Besides that, polymers with similar multi-furan and multimaleimide monomers have also been made and could get similar results (Liu & Hsieh 2006; Gotsmann et al. 2006; Adzima et al. 2008). Murphy et al. used cyclopentadiene (CPD) as both the diene and dieneophile for DA reaction in the self-healing polymer (Murphy et al. 2008). The heating temperature could be adjusted to control the healing of polymer as shown in Figure 2.9. Healing capability varied with the different mendomers shown in Figure 2.10.

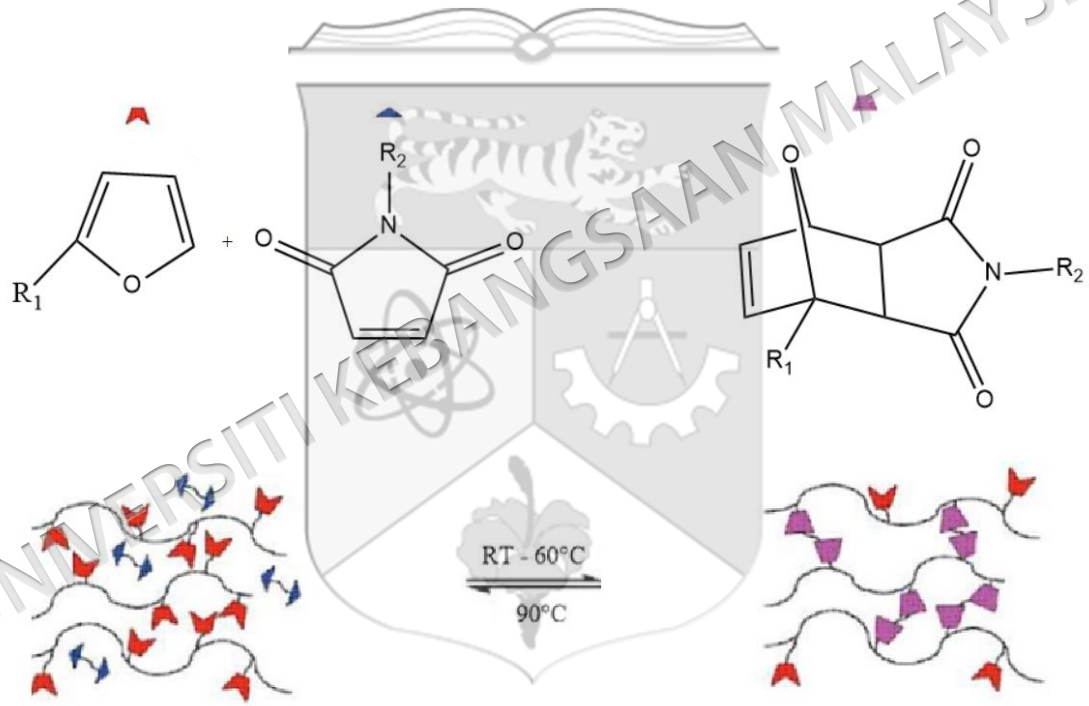

Figure 2.9 Self-healing with thermal activated furan-maleimide healing.

Source: Palmese et al. (2009)

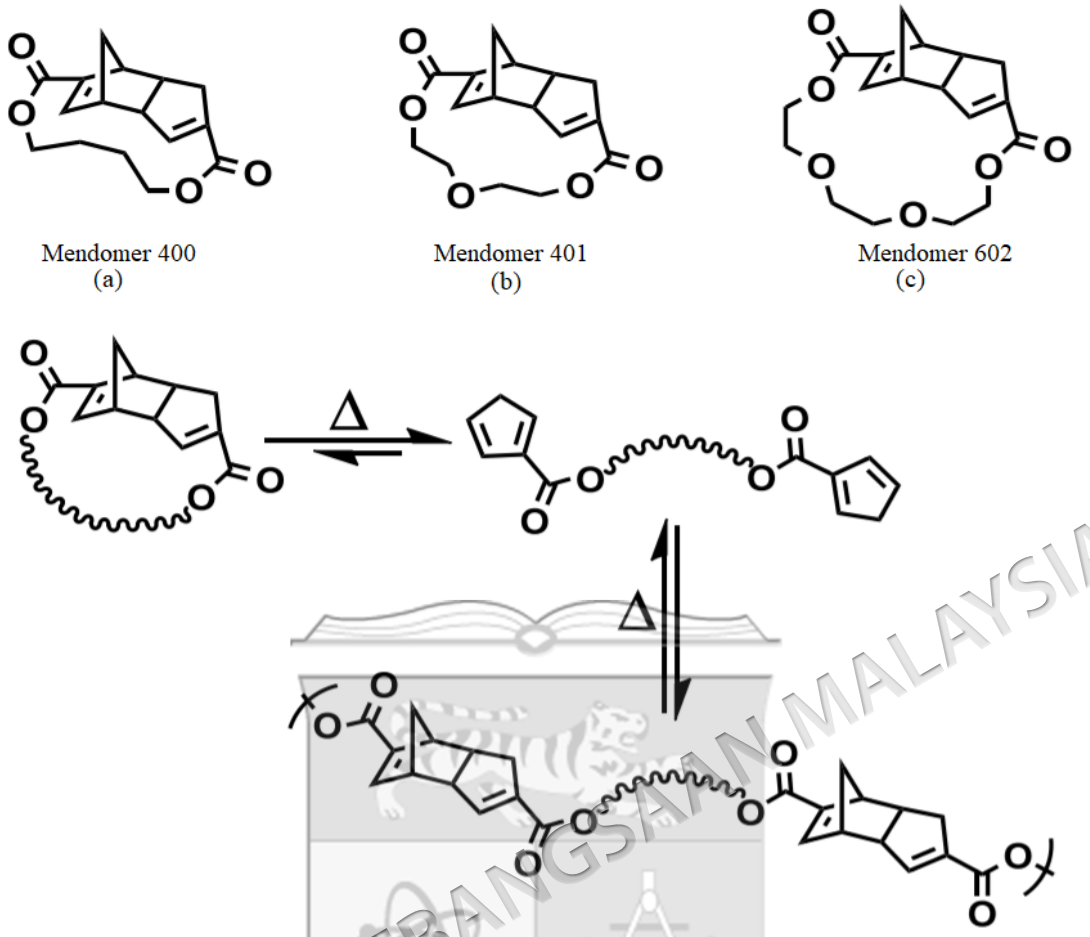

Figure 2.10 Three mendomers (a),(b) and (c) that could trigger self-healing after a heating

Source: Park et al. (2008)

Epoxy resins also could be incorporated with thermal activated furan/maleimide compounds (Figure 2.9). Tian et al. crosslinked synthesized furan-containing diepoxide resin with a commercially-available bismaleimide (Tian et al. 2009). When the polymer was ruptured, the crack size was reduced by heating.

2.2.4 UV activated self-healing

Besides that, UV light is able to activate healing in the polymer. It was found that cinnamoyl and conjugated C=C in coumarin groups could undergo [2+2] cycloaddition. Hence, tricinnamates and coumarin were incorporated into polymer to have self-healing functionality. Then, the polymer was UV irradiated to form cyclobutene in the polymer films (Cho et al. 2008; Chung et al. 2004)). Eriko Sato and co-workers (2013) produced film by reacting 7-methacryloyloxy-4-methylcoumarin (MMC) and 2,2'-

Azobis(isobutyronitrile) (AIBN) in dimethylformamide (DMF) which acted as solvent and studied the thickness control of the film through photodimerization process. Aguirresarobe and co-workers (2014) synthesized and studied the waterborne coumarin based PU. The dimerization of coumarin took place between the polymer chains as the conjugation disappeared when the cyclobutane is formed. Seoane et al. (2016) incorporated coumarin-containing polycaprolactone diol into PU by reacting with hexamethylenediisocyanate in dichloroethane. Non irradiated PU was found to have low mechanical strength and soft. However, crosslinking in UV irradiated PU produced tough elastomeric PU with the detection of increase in tensile strength from 1.9 MPa (non UV irradiated PU) to 6.7MPa (UV irradiated PU). Chan et al. (2014) embedded alkoxyamine into PU. The healing of cracked PU was carried out by treating the polymer at 80°C under atmosphere for 2.5 hours. Ling and co-workers (2012) successfully synthesized self-healing PUs by using 5,7-bis(2-hydroxyethoxy)-4-methylcoumarin (DHEOMC) as a crosslinker in order to give self-healing properties. The synthesized DHEOMC was incorporated into the PUs by reacting it with isophorone diisocyanate (IPDI) and different polyethylene glycols (PEG-400 (M_w=400) and PEG-800 (M_w=800)) to form a self-healing PU as shown in Figure 2.11. They found that the chain mobility plays an important role in crack healing because low chain mobility leads to detrimental to the contacts at the fractured surfaces. The soft segment with longer chain gives greater mobility of the PU chain. Performance of the self-healing PU can be improved by changing the ratio of hard segment and soft segment as well as the content of dihydroxyl coumarin derivatives.

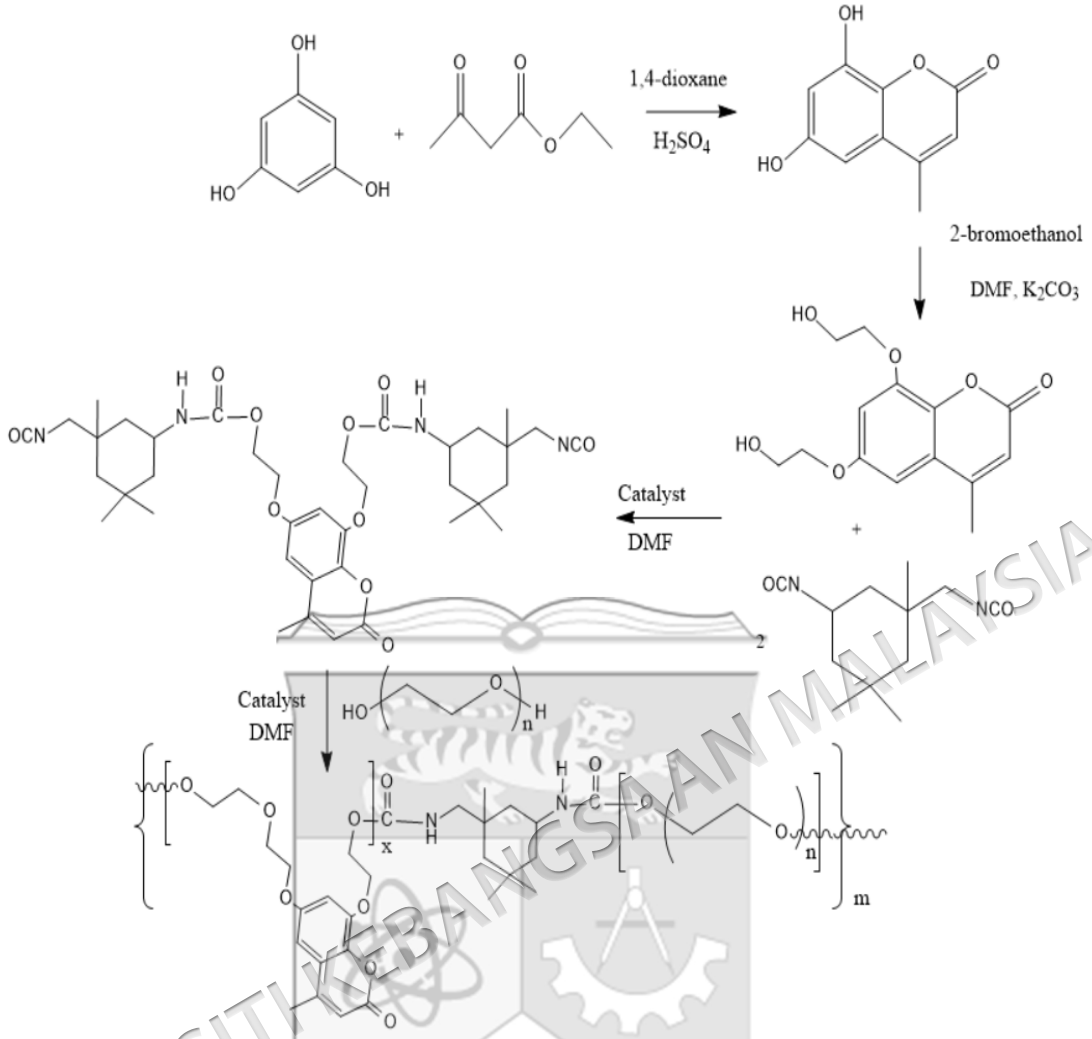

Figure 2.11 Synthesis of self-healing PU

Source: Ling et al. (2012)

2.2.5 Chain entanglement/Diffusion healing

Another healing is the chain entanglement or diffusion of polymer branches or dangling chains. These dangling chains can heal a polymer either by chemical interactions or mechanical interlocking after diffusion as shown in Figure 2.12. Caruso et al. (2007) showed epoxy/amine polymers with residual reactive groups that could have healing functionalities (Cruso et al. 2007). Solvents were found entrapped in urea formaldehyde microcapsules, which later embedded in the polymer matrix. As soon as the polymer matrix was ruptured, the microcapsules would then release the solvent to the damage site. As a result, the molecular mobility at the damage site increases while the diffusion rate of residual reactive groups is facilitated. Through the solvent facilitated diffusion

mechanism, the healing process of the residual epoxy/amine groups at room temperature is now possible. According to a research work, a complete recovery of the polymer mechanical strength can be achieved with the addition of epoxy resin solutes in the microcapsules (Cruso et al. 2008).

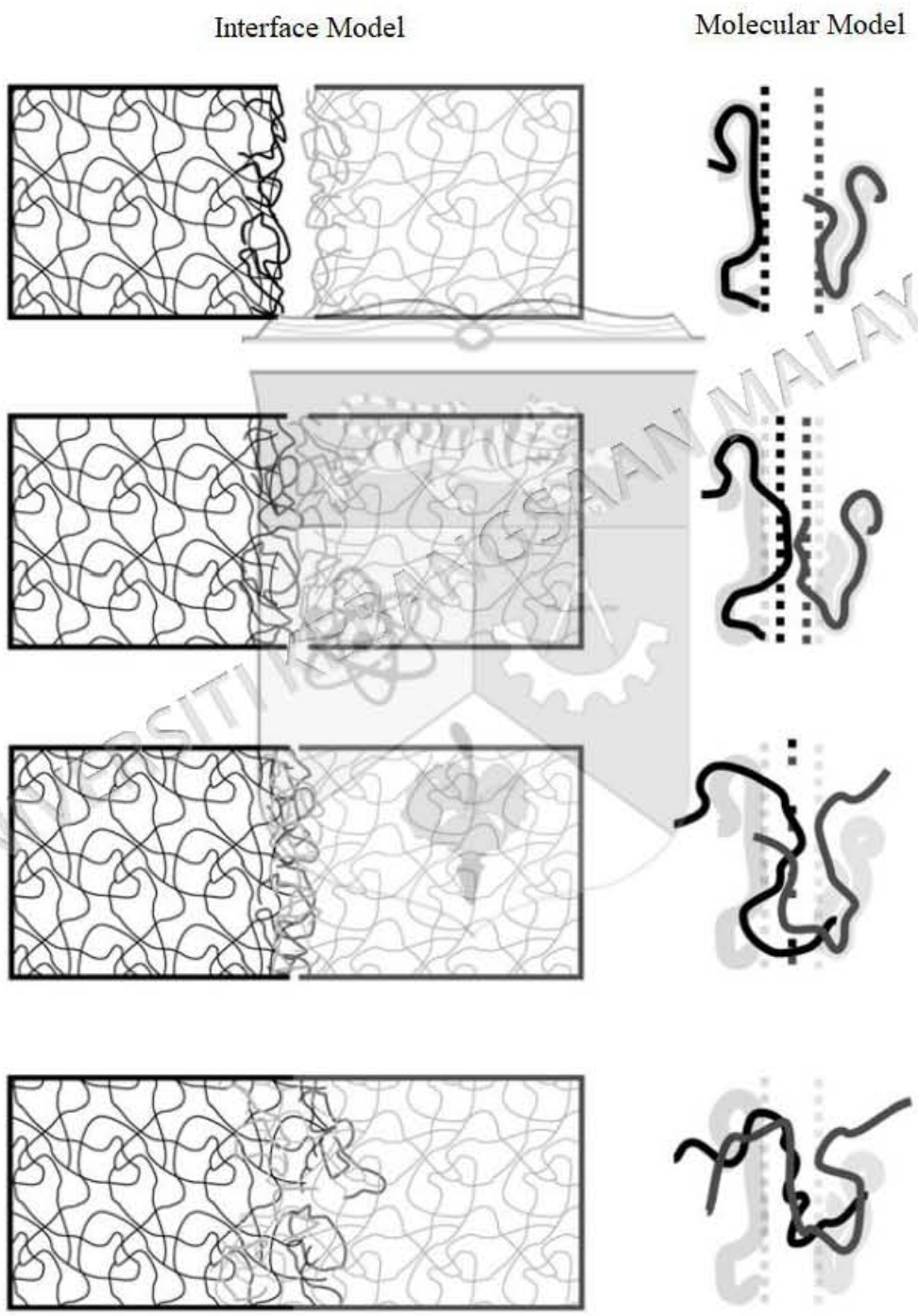

Figure 2.12 Healing through chain entanglement/diffusion process

Source: Blaiszik et al. (2010)

2.2.6 Non covalent bond healing

Hydrogen bond also could be used to give self-healing functionality in the polymer. However, hydrogen bond strength, polymer chain length and mobility determine the efficiency of self-healing via hydrogen bond formation. Another important factor is the presence of moisture will affect the hydrogen bond formation. Hence, the self-healing via hydrogen bond formation is harder to be triggered (Liu et al. 2007). The capability of forming multi-hydrogen bonds, such as triple hydrogen bonds between thymine (Thy) and 2,6-diaminotriaine (DAT) as shown in Figure 2.13 (a) (Moynot et al. 2008), quadruple hydrogen bonds of ureidopyrimidinone (Upy) as shown in Figure 2.13 (b) (Shchukin et al. 2008), could enhance the interaction between polymeric chains greatly.

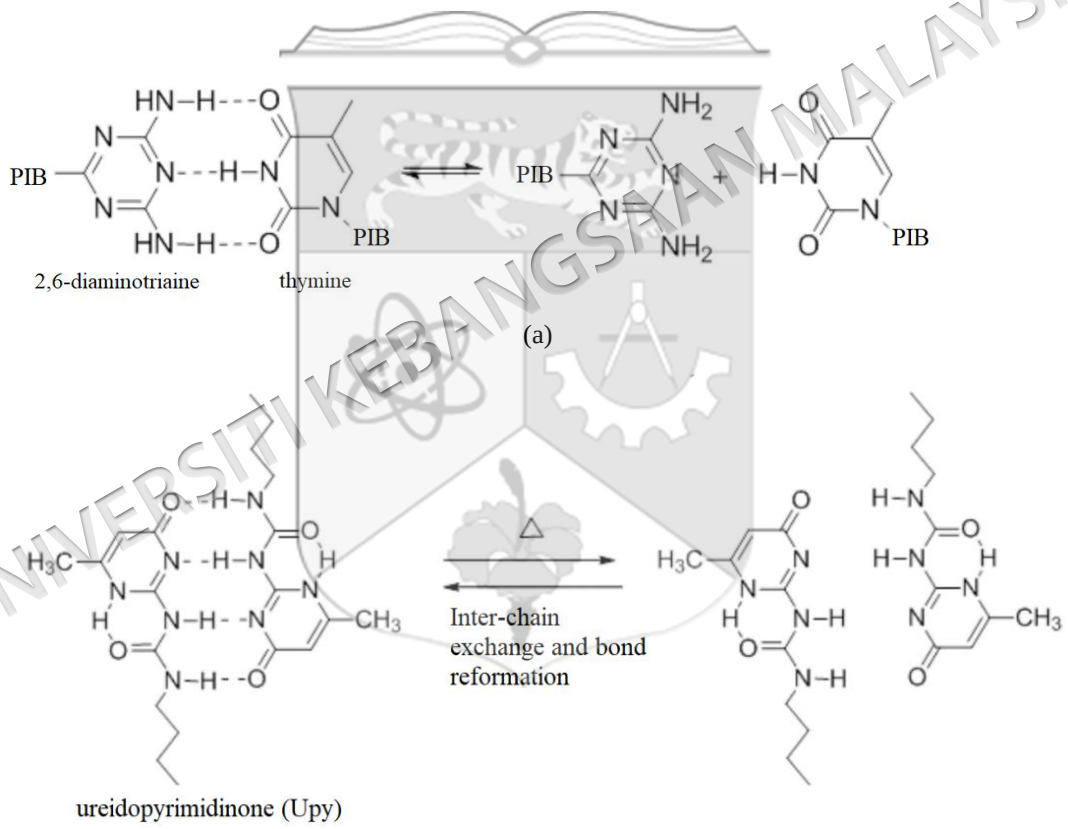

Figure 2.13 (a) Triple bond formation between thymine and 2,6-diaminotriaine (b) Quadruple hydrogen bond formation between ureidopyrimidinone (Upy)

Source: Moynot et al. (2008) and Shchukin et al. (2008)

Polyisobutylenes (PIBs) interacted with Thy and DAT end groups and formed strong materials by formation of triple hydrogen bonds (Brown 2003; Nelson & Kuo 1975). Besides that, Upy was able to be incorporated into flexible poly(ethylene-co-butylene) and PDMS, facilitates formation of multiple Upy-dimers through hydrogen bond formation (Larin et al. 2006; Lee et al. 2007). However, Upy is hard to be incorporated into polymer due to its low solubility in organic solvent.

Ionic interactions in ionomers could be utilized to demonstrated self-healing properties (Mookhoek 2009). For example, NaCl containing poly(acrylic acid) (PAA)/poly(allylamine hydrochloride) (PAH) copolymers shown in Figure 2.14 exhibited self-healing properties (Cosco et al. 2007). The self-healing ability became stronger with increasing concentration of NaCl salt, due to the greater ionic bond formation between ionomers as shown in Figure 2.15. Despite the higher ionic content increases healing capability, it will lower the mobility of polymer chains. Besides that, too high concentration of salt ions is hard to heal at low temperatur due to the high rigidity.

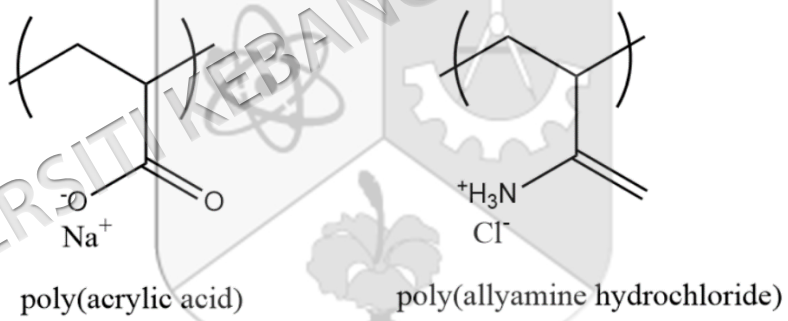

Figure 2.14 NaCl containing poly(acrylic acid) (PAA)/poly(allylamine hydrochloride) (PAH) copolymers

Source: Cosco et al. (2007)

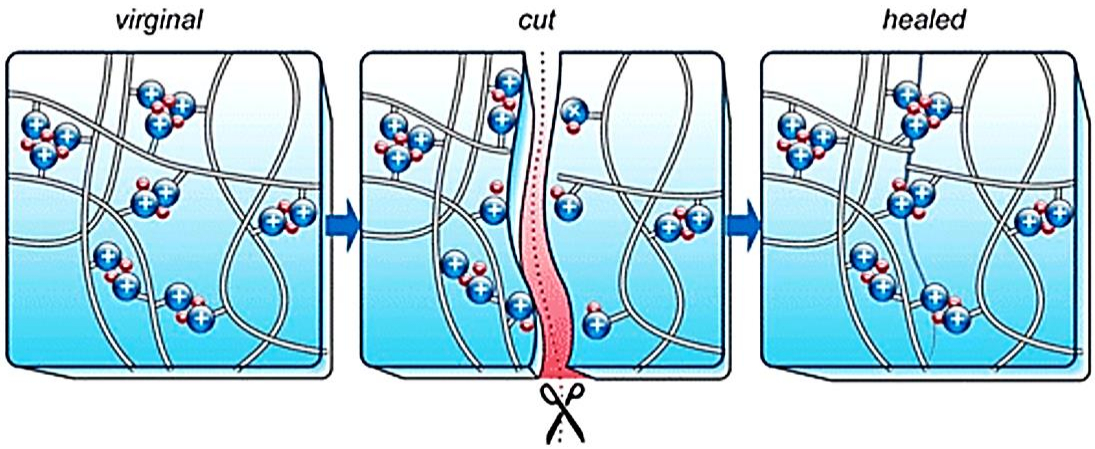

Figure 2.15 Healing via ionic bond formation between ionomers after cut is applied

Source: Cosco et al. (2007)

2.3 COUMARIN

2.3.1 Applications of Coumarin

Coumarin is widely used in material science applications. It is interesting that coumarin could be incorporated into polymer due to its ability to undergo dimerization. Poly(vinyl acetate) acted as a host to stabilize coumarin in thin films (Chen et al. 1995). Photon induced crosslinking (Chen et al. 1994; Ngai & Wu 2003; Chujo et al. 1990) of coumarin could be used to control the refractive index of the polymers (Trager et al. 2006; Trager et al. 2008). In the area of biochemistry, polymers with coumarin dimers in the main chain were used as a probe in detecting the effect of lipase (Chen et al. 1997). Besides that, the unique photochemical properties of coumarin was utilized by numerous research groups in silica based nanoparticles. A brief explanation of functionalization of silica nanoparticles with coumarin has been provided by Graf and co-workers (2000). Another research work by Mal et al. (2003) has successfully incorporated the photochemical properties of coumarin with silicon based nanotechnology by the modification of the mesoporous silica cavity where coumarin molecule served as a gate to either release or trap organic molecules. According to Fujiwara et al. (2003), synthesis of organic-inorganic hybrid polymers is possible through photo-cycloaddition reaction. Apart from that, photo-deformable spherical hybrid nanoparticles comprising coumarin dimers were successfully synthesized (Zhao

et al. 2006). Besides that, a research group utilized the fluorescence coumarin derivatives to synthesize biocompatible fluorescent silica nanoparticles, which could be used in vivo imaging (Ha et al. 2009). The effect of prolonged sunlight exposure onto the coumarin dimer, 7,7-[3-(tert-butyldimethylsilyloxy)propoxy]-dicoumarin (TBS-p-C dimer) has been studied by Kim and co-workers (2008). The synthetic route to the formation of TBS-p-C dimer is as illustrated in Figure 2.16.

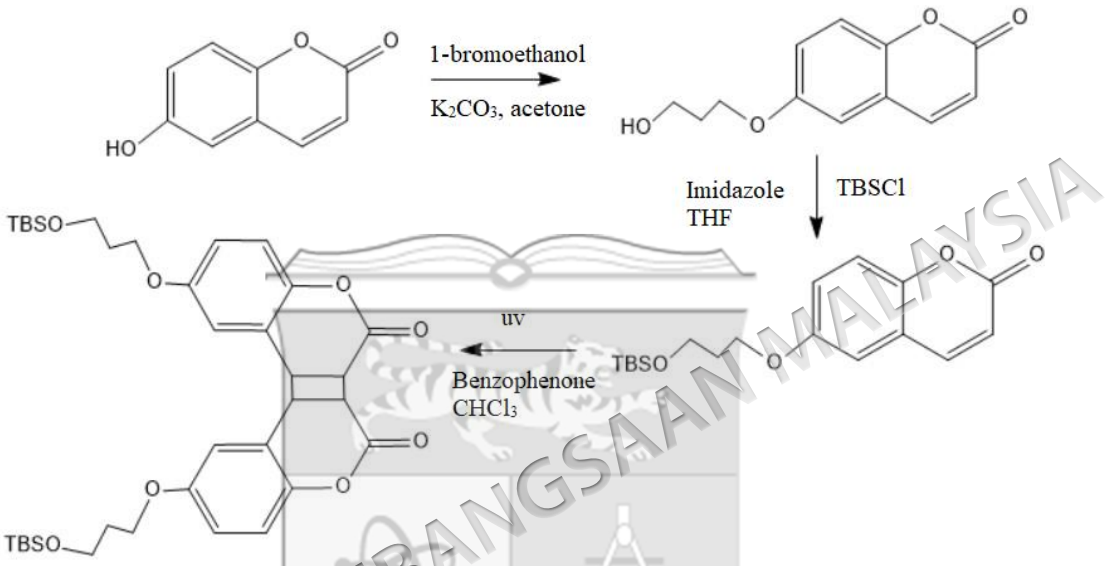

Figure 2.16 Formation of TBS-p-C dimer

Source: Kim et al. (2008)

2.3.2 Dimerization of coumarin

Coumarin is able to undergo photocycloaddition reaction since it could excite to singlet state by UV irradiation and subsequently undergoes intersystem crossing to triplet state. Single state is a molecular electronic state where the spin of 2 electrons is paired in an opposite direction. In a triplet state, the spin of electrons is parallel to each other. The mechanism of dimerization of coumarin is [2+2] photocycloaddition as shown below (Loutfy et al. 1972):

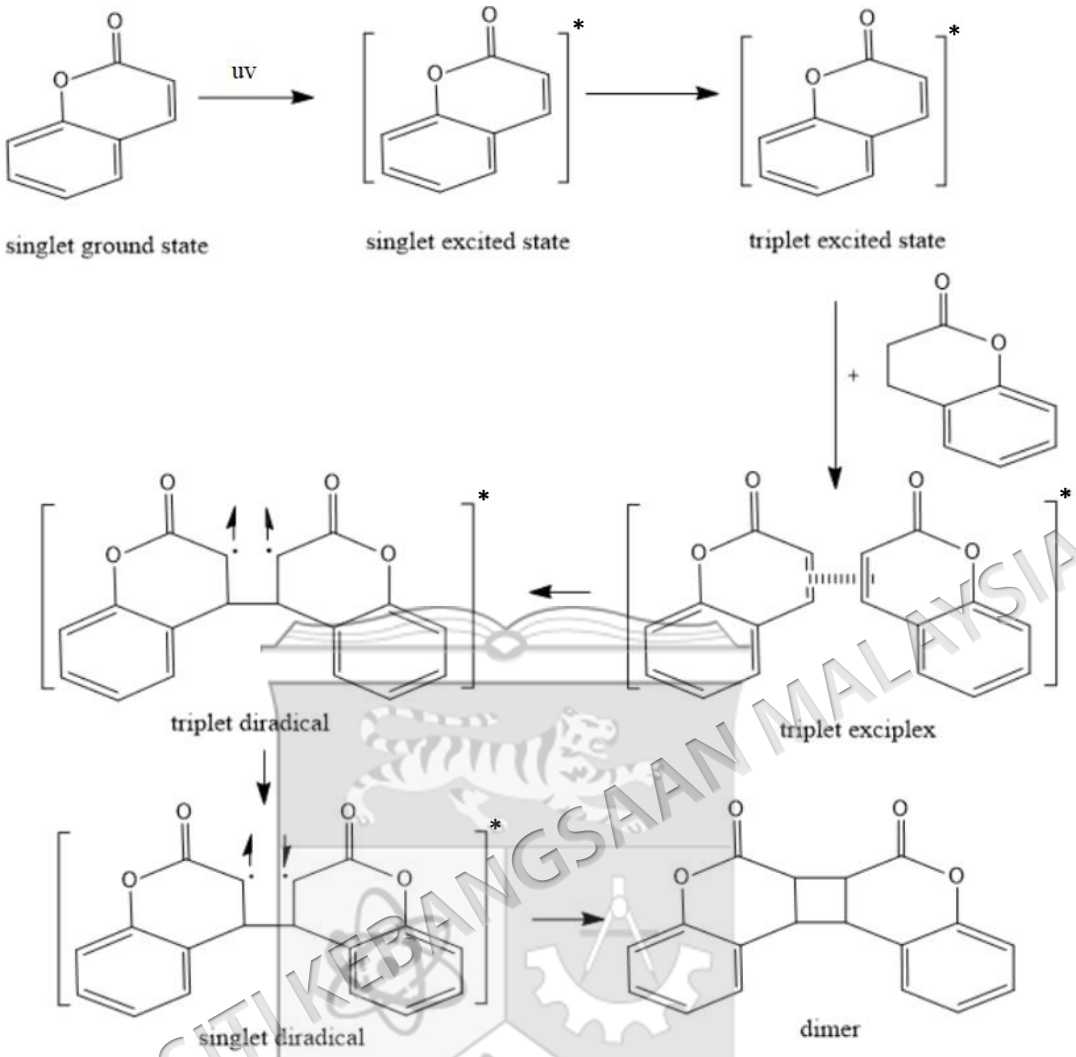

Figure 2.17 The photodimerization mechanism of coumarin

Source: Loutfy et al. (1972)

The conjugated π -system of coumarin molecules comprised of the phenyl ring connected through an additional double bond to the carbonyl functional group, leading to the excitation of two characteristic electronic transitions when irradiated with UV-light, a π-π* transition is observed between 310 nm and 340 nm, which is associated to the C=C in the cyclic structure (Ghouili et al. 2013). Another transition of π-π* can be observed at much higher energies between 250 nm and 300 nm, which is attributed to the conjugated π-system.

Photodimerization of coumarin is a regioselective reaction which leads to the formation of four possible types of dimers; syn head-to-head dimer, anti-head-to-head dimer, syn head-to-tail dimer and anti-head-to-tail dimer, as illustrated in Figure 2.18.

Direct irradiation of coumarin in polar solvent such as ethanol gives the syn head-to-head dimer, through single-excited state formation. Direct irradiation of coumarin cannot be carried out in benzene solution as it induces the self-quenching of S_1 state. The anti head-to-head dimer can be formed when benzophenone sensitized-irradiation of coumarin takes place in both polar and non polar solvent (Maurizio 2004). In this research, anti head-to-head dimer is at preference especially when acetone is used as solvent.

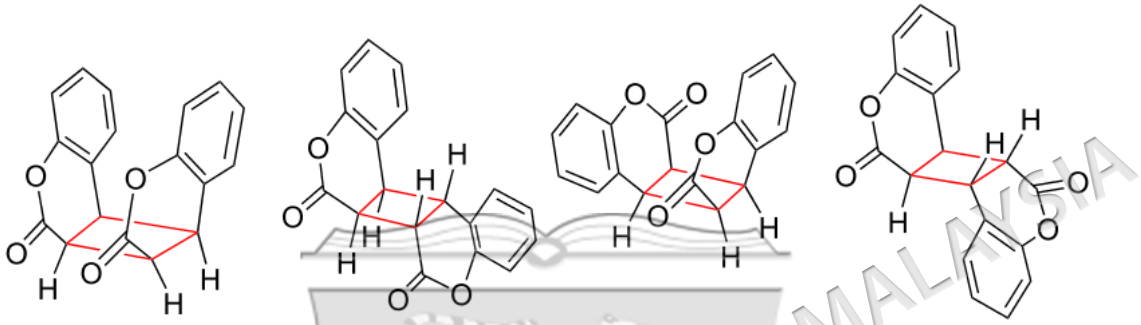

(a) (b) (c) (d)

Figure 2.18 (a) syn head-to-head dimer, (b) anti head-to-head dimer, (c) syn head-to-tail dimer and (d) anti head-to-tail dimer

Source: Maurizio (2004)

The calculated enthalpy change for the first excited singlet state formation was 83 kcal.mol^{-1}, consistent with the experimental results (82 kcal.mol^{-1}). In the sensitised reaction, the reaction has to take place through the first excited triplet state formation. The triplet state, however gave a much lower energy of 60 kcal.mol^{-1}. The sensitised photodimerization reaction involves the formation of biradical intermediates which is able to determine the stereochemistry of the product. Table 2.1 below shows the enthalpy of all the possible biradical intermediates formation.

Table 2.1 Energy change in the formation of biradical intermediates

Possible biradical intermediates formed in the sensitised photo-dimerisation of coumarin	
Biradical intermediates	Total enthalpy change (kcal.mol^{-1})
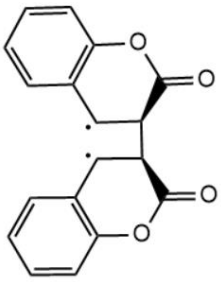 syn head-to-head biradical intermediate	-80489.974
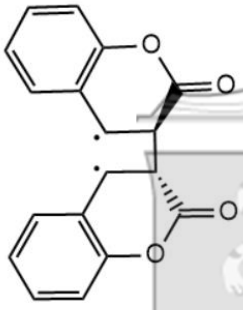 anti head-to-head biradical intermediate	-80491.167
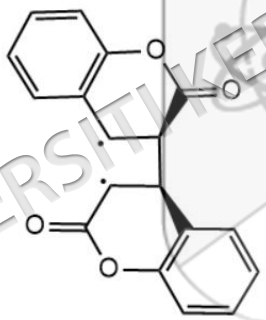 syn head-to-tail biradical intermediate	-80481.353
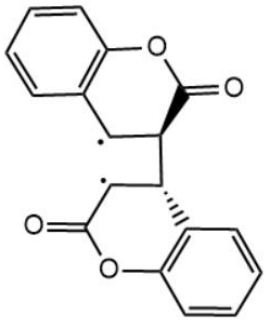 anti head-to-tail biradical intermediate	-80481.452

The formation of head-to-head trans biradical intermediate is favoured since the energy of formation of this intermediate is the most exothermic. Besides, the enthalpy change of formation of syn head-to-head dimer is more exothermic than anti head-to-head dimer, promoting the direct irradiation of coumarin without sensitizer.

A new coumarin chalcone 3-((2E)-3-(2-hydroxyphenyl) prop-2-enoyl)-4-hydroxy-2(H)-chromen-2-one was synthesized by Ghouili and co-workers (2013) through Claisen Schmidt reaction by condensation of 3-acetyl-4-hydroxycoumarin and 2-hydroxybenzaldehyde using a mild organic base. Intermolecular hydrogen bonding exists between coumarin molecules while π-π stacking interactions happen between the benzene rings of coumarin molecules.

Furthermore, photodimerization of coumarin could take place in solid state. Koichi et al. (2012) found that the hydrogen bond formed between C=O of coumarin and OH of diacetylenediol enabled the formation of coumarin dimer. The electron withdrawing group attached to benzene ring in diacetylenediol allowed the formation of anti-head-head dimer while the electron donating group attached to benzene ring in diacetylenediol allowed the formation of anti-head-tail dimer. Therefore, the absence of either electron donating or withdrawing group on the benzene ring of diacetylenediol inhibits the formation of dimer.

2.4 POLYURETHANE

PU has received broad attention nowadays due to its wide application in composites (Badri et al. 2005; Husić et al. 2005), medical engineering (Mondal and Martin 2012), coating and adhesives (Badri et al. 2004; Wong & Badri 2012) and electrochemical devices (da Conceição et al. 2003; Ren et al. 2005; Wang & Min 2011; Xiaobin et al. 2005). PU is a block copolymer synthesized by addition polymerization reaction between polyester or polyether polyols and diisocyanate (Badri 2012). It is formed through combination of both soft and hard segments of the polymeric chain, contributed by the polyols and isocyanates segments respectively. The physical stability and rigidity of PU are contributed by the hard segment. The hard segment could be selected from

various isocyanate compounds with two or more NCO groups. Aliphatic isocyanate is less reactive than the aromatic isocyanate. However, PU is susceptible to UV irradiation as studied by Boubakri et al. (2010). It was found that the colour change from colourless to yellow or brown was due to the formation of oxidized structure of PU after exposure to UV irradiation. Besides that, the glass transition temperature of PU decreased after exposure to UV irradiation. This is due to the increase of molecular mobility, resulted from the chain scission (oxidation reaction). Both stress and strain of PU were reduced because of the degradation of polymer.

Previous studies on PU pre-polymerization were conducted in aprotic solvents to induce the self-association of the alcohols, catalysts and reaction products through intermolecular hydrogen bonding. Consequently, the number of the available reacting hydroxyl groups is reduced (Respoet et al. 1998). However, the usage of toxic and carcinogenic volatile organic compound (VOC) such as tetrahydrofuran (THF) and dimethylformamide (DMF) in conventional PU pre-polymerization is crucial due to its high boiling point and is not easily removed from the film. Meanwhile, PU synthesized using acetone can quickly evaporate and may minimize the trapped residual that forms bubbles, which in turn reduce the mechanical properties of the film (Xu et al. 2008).

Conventional polyester polyols are based on virgin raw materials and manufactured by direct polyesterification of high-purity diacids and glycols. They are of course, distinguishable depending on the choice of monomers, molecular weight, and degree of branching. Polyether polyols are commonly derived from propylene by the petroleum cracking process, which later converted to polyols by oxidation and alkoxylation with an amine or hydroxyl containing initiator (Colvin 1995). However, the cost of petroleum-based materials is increasing while the production is limited since they require high processing technology. The renewable resources can replace petrochemicals as raw materials in producing polymer. Meanwhile, bio-based polyester polyols derived from vegetable oils provide better elastomeric properties, flexible and easy to be molded. It offers physical properties that could not be obtained by petrochemical-based polyether polyols such as PEG, including superior solvent, abrasion, low resistance and exhibited high thermal stability (Petrović 2008). Glycerol

is a by-product of bio-diesel process from transesterification of vegetable oils with methanol or ethanol (Ionescu & Petrović 2010).

PU based on bio-based polyester polyols derived from vegetable oils have been known to be more biodegradable and has better tuneable functionality than those derived from petrochemical-based polyether-based (Petrović 2008; Badri 2012; Radojčić et al. 2013). Biodegradability of PUs can be achieved by incorporating labile and hydrolyzable moieties into the polymer backbone such as utilizing polyols with hydrolyzable bonds as starting materials for the preparation of PUs (Yeganeh & Hojati-Talemi 2007). Various types of vegetable oils based polyester polyols are being used for PU polymerization such as palm oil, castor oil, soybean oil, sunflower seed oil, corn oil, and grape seed oil (Ooi et al. 2006; Yeganeh & Hojati-Talemi 2007; Petrović 2008; Pfister et al. 2011; Badri 2012; Pan & Webster 2012; Radojčić et al. 2013; Alam & Alandis 2014; Fridrihsone-Girone & Stirna 2014; Garrison et al. 2014).

The main composition of vegetable oils is triglycerides of fatty acids. Almost all of the most common vegetable oils contain these fatty acids; palmitic, stearic, oleic, linoleic, and linolenic acids (Pfister et al. 2011). Unsaturated vegetable oils with hydrolyzable bonds could be used to form polyols as a reagent for PU fabrication. Epoxidation and ring opening reaction with haloacids or alcohols, transesterfication, ozonolysis and hydration are among the techniques used (Pfister et al. 2011). Palm oil derived from mesocarp (reddish pulp) of the fruit of oil palm species, *Elaeis guineensis* and palm kernel oil (PKO) obtained from the kernel part of the palm oil fruit are among 17 major commodity oils and fats that are produced abundantly and traded widely in the world. The production of palm oil and palm kernel oil in 2016 occupied 38.7 % of global oils and fats with consumption of 6.6 % of global land use for cultivation area worldwide (European Palm Oil Alliance 2016). Research on palm oil based PU has been extensively studied (Chian & Gan 1998; Ooi et al. 2006; Chuayjuljit et al. 2007; Tanaka et al. 2008; Velayutham et al. 2009; Salleh et al. 2010; Ang et al. 2014; Clark & Hoong 2014; Khoon Poh et al. 2014; Lumcharoen & Saravari 2014; Salih et al. 2014). However, PKO obtained from the kernel part of the palm oil fruit differs greatly in its characteristics as compared to palm oil. Although it lies within the palm nut, PKO has a high content of saturated fats, which is more saturated than palm oil and comparable

to coconut oil (Badri et al. 2004; Ng et al. 2003; Nik Norulaini et al. 2004; Tan et al. 1997). It has a cloudy point at 23 °C and semi-solid appearence at room temperature. Research on bio-based PU from PKO has extensively been studied by Badri and co-workers (Badri et al. 2000; 2001; 2004; 2005; Badri 2011; 2012; Wong & Badri 2010; 2012) for various applications including composites, adhesives and coatings. Works by Wong and Badri (2010) revealed that the glass transition temperature (T_g) of PU derived from PKO polyol is lower than PU derived from soybean polyols. Lower T_g values implies an increase in segmental motion and free volume of the polymeric chain, thus leading to a significant increase in ionic conductivity (Gray 1991; Bruce 1995; Lu et al. 2003a; Tian et al. 2003; Noor et al. 2010). This has motivated our research group to explore the potential of bio-based PU from PKO polyols as polymeric host for conductive polymer application in electrochemical devices (Daud et al. 2013, 2014; Su'ait et al. 2014).

The study on PKO based polyester polyols has been pioneered by Badri and co-workers (2000, 2001, 2011, 2012). According to patent innovation by Badri (2004), polyester polyols of PKO based monoester-OH (PKO-p) was synthesized by polyesterification and polycondensation reaction between crude PKO and mixture of polyhydroxyl compound. Crude PKO is made to react with the polyhydroxyl compound under basic medium to ensure that complete reaction occurs. The selection of polyhydroxyl compound is the crucial part where it should offer high hydroxyl value, low moisture content, no toxic vapour and high functionality polyol possible to fully convert the crude PKO into polyol at the highest yield by involving polycondensation and esterification reaction (Badri 2012). Septevani and co-workers (2015) conducted a study about substituting polyether polyol with palm kernel oil based polyester polyol in rigid PU foam. In order to obtain a homogeneous mixture, polyol was blended with catalyst, surfactant and blowing agent. The mixture was mixed with polymeric methylene diphenyl diisocyanate (pMDI) to form rigid PU foam and their thermal stability was studied. The onset decomposition of urethane bonds started around 170 °C. The lower thermal stability of the increasing palm based polyol content corresponds to more unstable urethane groups, due to poor crosslink density.

2.5 CONDUCTIVE POLYMER

A conductive polymer can be described as a solvent–free system whereby through dissolution process of metals salts of low lattice energy in a polar polymer matrix of high molecular weight with aprotic solvent, an ionically conducting pathway is generated. Fundamentally, an ionic conduction in the conductive polymer is best described as carbon double bond between the polymer backbones in the presence ion hopping ionizing groups. Initially, the electron donating group in the polymer solvates the cation component in the dopant salt and assists the ion separation process prior to ionic hopping mechanism. Thus, ionic conductivity is generated. If these ions are however, immobile or unable to migrate, the well separated ions are then referred to as poor conductors. The host polymer must be adequately flexible in order to have enough space for facilitating the migration of these two ions (Gray 1997). In addition, Gray (1991) stated that the local relaxation processes in the polymer chains can be one of the factors that govern the ionic transportation within the conductive polymers, which may give identical properties as liquid electrolytes. In the ion transport mechanism, interaction occurs between the solvating group or donor atom of polymer and the cations in the salt. The coordination takes place when negative charge on the solvating group in contact with the positive charge on the cation through electrostatic interactions. The dissociation of the ion from the coordination initiates the ionic conduction in the polymer electrolytes. The solid conductive polymer can be classified into three major types; dry polymer electrolyte (or solid conductive polymer), gel conductive polymer and composite conductive polymer. Solid conductive polymers serve three primary roles in a lithium rechargeable battery. Firstly, it acts as an electrode separator that insulates the anode from the cathode in the battery so that the requirement of inclusion of inert porous spacer between the electrolytes and electrodes interface can be eliminated. To generate ionic conductivity, the conductive polymer should act as a channel through which ions are transported between the anode and cathode during charging and discharging processes. This would enhance the energy density in the batteries together with the formation of thin film. In addition, this type of polymers could as binders to ensure a superior electrical contact with electrodes. Eventually, the high temperature process of conventional liquid electrolytes can be eliminated (Gray 1991; Kang 2004).

Growing concern over the usage of harmful conventional liquid electrolytes has urged the interest for development of conductive polymers. The access to this type of polymers is intrinsic to eliminate the use of corrosive solvent leakage and harmful gas during operation, easy processability due to removal of liquid component, suppression of lithium dendrite growth, conformed in any shape due to high flexibility of polymer matrix, high automation potential for electrode application and no recent technology requirement as well as light in weight (Xu & Ye 2005; Gray 1991). Conductive polymers portrayed high elastic relaxation properties under stress and are easy to handle and process (Ibrahim et al. 2012). Fabrication of all solid–state electrochemical cells arises from the superior mechanical integrity of conductive polymers and the high flexibility of polymer matrix (Gray 1997). Electrochemical cells based on conductive polymers have been studied to have an excellent electrode–electrolyte interfacial contact as compared to crystalline or glassy electrolytes–based cells. The contact can be maintained under stresses at all the times of charging and discharging processes (Gray 1991; Gray 1997). According to Liew et al. (2013), conductive polymers may not cause the explosion during charge and discharge processes in the electrochemical cell since they do not build up any form of internal pressure. Other advantages of conductive polymers are no vapor pressure, wide operating temperature range, high energy density, ease of handling and manufacturing, low volatility, and relatively high ionic conductivity at room temperature (Baskaran et al. 2007; Rajendran et al. 2004). Unlike conventional liquid electrolytes, the electrochemical, structural, thermal, photochemical and chemical stabilities of conductive polymers can be improvised (Adebahr et al. 2003; Nicotera et al. 2006).

Conductive polymers cover a wide range of applications in the technology field, extending from small scale production of commercial secondary lithium ion batteries (or rechargeable batteries) to advanced high energy electrochemical devices, such as supercapacitors, chemical sensors, analog memory devices, fuel cells, thermoelectric generators and solar cells (Gray 1991; Rajendran et al. 2004). In the case of devices relative to lithium rechargeable batteries, there are wide applications ranging from portable electronic and personal communication devices such as laptop, mobile phone,

MP3 player, and hybrid electrical vehicle (EV) and act as a power source to generate electricity (Gray 1997; Ahmad et al. 2005).

In 1975, Wright and his group invented the first generation of conductive polymer from crystalline poly(ethylene oxide) (PEO)–based polymer electrolytes (Fenton et al. 1973; Quartarone et al. 1998). The effect of alkali metal salts such as sodium and potassium salts when incorporated in PEO has been reported, as well (Fenton et al. 1973; Wright 1975). Numerous ways have been implemented to inhibit the recrystallization of polymer complexes and/or reduce the degree of crystallinity in the polymer electrolytes, including polymer modifications, polymer blending, addition of semi–crystalline or amorphous polymer like poly(methyl methacrylate) (PMMA) and utilization of additives like plasticizers and inorganic fillers. There are several structural modifications onto the short chains of ethylene oxide in PEO polymer backbone have been proposed by Quartarone et al. (1998) to minimize recrystallization. These include cationic polymerization, epoxides copolymerization, radical polymerization cross–linking, random, block or comb polymerization. The use of lithium salt in the conductive polymer has gained so much attention among many researchers, for the past few decades. The first trial in crosslinking PEO with poly(dimethylsiloxane) (PDMS) was done by Bouridah and the co-workers in 1985. One year later, a research group carried out another reaction involving crosslinking of poly(propylene oxide) (PPO) with triol type of PEO (Watanabe *et al*. 1986). The ionic conductivity was found to be 5 times higher for $LiClO_4$-doped polymer networked compared to the PEO polymer electrolytes without cross–linked with PPO. Yuan et al. (2005) synthesized polyacrylonitrile–polyethylene oxide (PAN–PEO) copolymer. The effects of acrylonitrile (AN) wt% content and Mn(PEO) on ionic conductivity are investigated by alternating current (ac) impedance spectroscopy. By controlling and adjusting the AN wt% content and doping PEO with high molecular weight (M_n=3,000,000), the ionic conductivity of SPEs is optimized. The ionic conductivity of PAN–PEO solid polymer electrolytes is found to be high 6.79×10^{-4} S cm^{-1} at 25 °C with an [EO]/[Li] ratio of about 10, and are electrochemically stable up to about 4.8 V versus Li/Li^+. The conductivity and interfacial resistance remain almost constant even at 80 °C. Libin Liu and co-workers (2014) studied the PU based polymer-$LiClO_4$ with different alkyl chain length. Sukor and co-workers (2011) studied incorporated $LiClO_4$

into 49% poly(methyl methacrylate) grafted natural rubber (MG 49) and poly(methyl methacrylate) (PMMA) based solid polymer electrolytes. In addition, the result showed that the ionic conductivity of the polymer blend in the absence of salt is 1.1×10^{-12} Scm^{-1} and the value increased to 1.5×10^{-8} $S.cm^{-1}$ when 25 wt% of $LiClO_4$ was used. Baskaran and co-workers (2006) studied the effect of $LiClO_4$ concentration and PMMA on the ionic conductivities, and chemical structure of poly(vinyl acetate) (PVAc) and poly(methylmethacrylate) (PMMA) blend polymer electrolyte films. The conductivity of PVAc-PMMA-$LiClO_4$ was found to be higher than PVAc-$LiClO_4$. This may be attributed by the amorphous nature of the blended polymer matrix and the decrease in glass transition temperature. Rajendran and co-workers (2002) investigated the effect of different mole ratios of poly(methyl methacrylate) (PMMA) and poly(vinylidene fluoride) (PVdF) on the ionic conductivity, and chemical structures of the PMMA-PVdF polymer blend electrolyte with $LiClO_4$ as dopant. It is found that the ionic conductivity increases from 0.041×10^{-5} $S.cm^{-1}$ to 2.517×10^{-5} $S.cm^{-1}$ as the PVdF concentration increases. Higher content of PVdF in the electrolytes leads to higher viscosity which in turn lowers the mobility of the charge carriers and hence lowers the conductivity. Besides that, the conductivity increases when temperature increases. It is affected by the solubility of the salt in the amorphous phase and the mobility of the ion in the amorphous phase. Moreover, increase in free volume also leads to the increase in ion mobility and segmental mobility that assists ion transport.

Several factors could affect the conductivity of conducting polymers containing lithium salt. These conducting polymers (CP) comprised of both crystalline and amorphous regions. It has been reported that the ion transport occurs mainly in the amorphous region rather than the crystalline region, but the polymers host materials that are used in CP are often semi-crystalline (Aziz et al.2011). Thus, to overcome the disadvantages and improve conductivity, plasticizer is commonly added to improve conductivity. As a result, the amorphous region and ion aggregates in CP can be both increased and dissociated causing the conductivity of CP to be improved (Pradhan et al. 2009). The conductivity in plasticized CP increases with a decrease in mechanical strength and vice versa (Deka et al. 2011). In addition to high conductivity, CP must exhibit good thermal and mechanical properties. The concept of dissolving inorganic salts in functional (polar)polymer, thus creating an ion conducting solid electrolyte is

one of the methods to form conductive polymers (Edman et al. 2000). The interactions of metal ions with polar groups of polymers are mainly resulting from electrostatic forces and accordingly the formation of coordinating bonds. There are some important factors that may have effect on the polymer-metal ion interactions, such as nature of the functional groups attached to the polymer backbone, compositions and distance between functional groups, molecular weight, degree of branching, nature and charge of metal cation, and anions (Rivas et al. 2003). The cations can transfer from one coordinated site to another when subjected to an electric field.

CHAPTER III

MATERIALS AND METHOD

3. 1 MATERIALS

3.1.1 Polyurethane-$LiClO_4$

The palm kernel oil-based polyol (PKO-p) was obtained from the UKM Technology Sdn Bhd through its pilot plant at Bangi Lama, Selangor, Malaysia. 4,4'-methylene diphenyl diisocyanate (MDI) was purchased from Cosmopolyurethane (M) Sdn. Bhd, Kuala Lumpur, Malaysia. Acetone, polyethylene glycol (PEG, M_w=400), lithium perchlorate ($LiClO_4$) and 6,7-dihydroxycoumarin were purchased from Sigma Aldrich (M) Sdn. Bhd, Petaling Jaya, Malaysia

3.1.2 Self-healing Polyurethane-$LiClO_4$

Self-healing polyurethane-$LiClO_4$ was synthesized via the incorporation of 6,7-dihydroxycoumarin into polyurethane-$LiClO_4$.

3.2 METHOD

3.2.1 The effect of different NCO/OH ratios and $LiClO_4$ contents on the polyurethane-$LiClO_4$

PKO-p was mixed with MDI in acetone in a round-bottom flask under nitrogen gas atmosphere to form urethane prepolymer. Then 20 wt% of PEG was added into the mixture for the chain extension reaction. Then, 5, 10, 15, 20, 25 and 30 wt% of $LiClO_4$

were added respectively into the mixture and agitated at 200 rpm for an hour at 25 ºC. The mixture was then casted onto a Teflon plate. The film was cured at 55°C for 24 hours. Table 3.1 summarized the formulation used to develop PU-$LiClO_4$ by varying NCO/OH mass ratios and lithium salt loading percentage. The mixing ratio of PKO-p to PEG was fixed at 1:1.

Table 3.1 Polyurethane-$LiClO_4$ with different NCO/OH ratios and $LiClO_4$ contents

Sample	NCO/OH (g/g)	$LiClO_4$ (wt %)
PU200-0	200/100	0
PU200-5	200/100	5
PU150-5	150/100	5
PU100-5	100/100	5
PU85-5	85/100	5
PU200-10	200/100	10
PU200-15	200/100	15
PU200-20	200/100	20
PU200-25	200/100	25
PU200-30	200/100	30

The mechanism of formation of polyurethane is shown in Figure 3.1

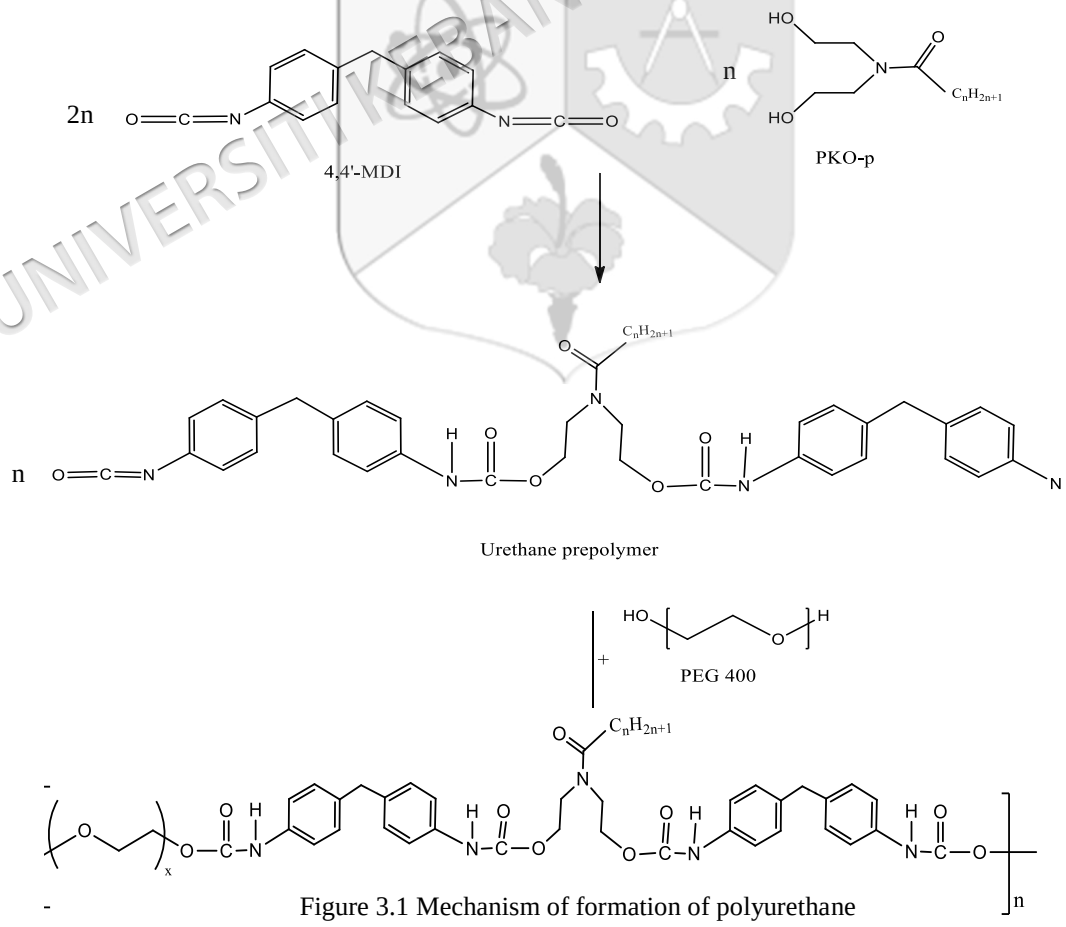

Figure 3.1 Mechanism of formation of polyurethane

3.2.2 Preparation of self-healing polyurethane-$LiClO_4$

Self-healing polyurethane-$LiClO_4$ was prepared by mixing PKO-p and MDI in acetone in a round-bottom flask under nitrogen gas atmosphere to form urethane prepolymer. Then PEG and 6,7-dihydroxycoumarin were added into the mixture for the further reaction. After that, 5 wt% of $LiClO_4$ which was the optimum $LiClO_4$ loading (as shown in Chap IV) was added into the solution and agitated at 200 rpm for an hour at 25 °C. The mixture was casted onto a Teflon plate. Then, the film was cured at 55 °C for 24 hours. The mechanism of formation of self-healing polyurethane-$LiClO_4$ is as shown below:

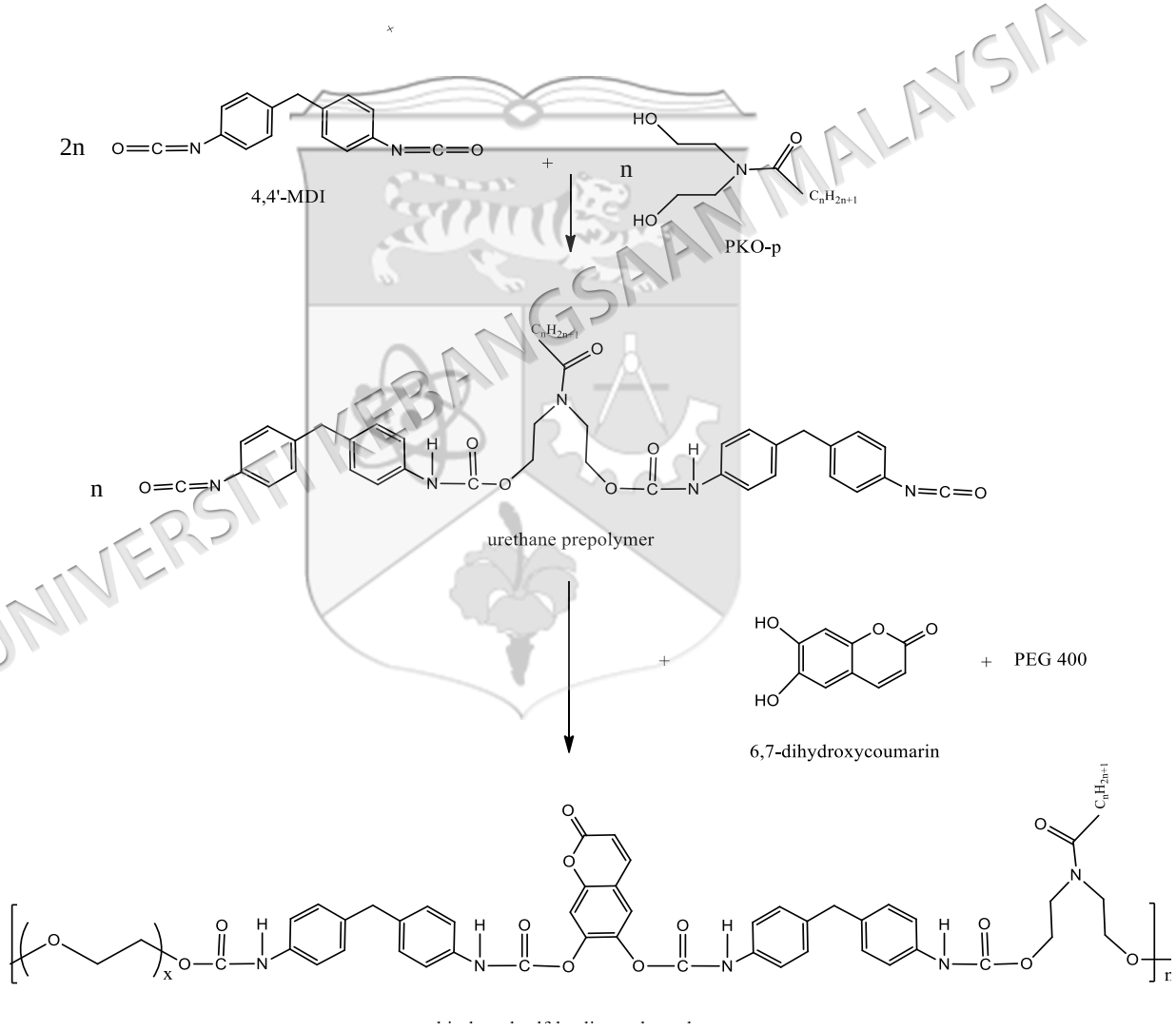

Figure 3.2 Mechanism of formation of self-healing PKO-based polyurethane

Self-healing polyurethanes with different MDI to 6,7-dihydroxycoumarin ratio (NCO/DHC) were synthesized as shown in the table below:

Table 3.2 Self-healing polyurethanes with different amount of 6,7-dihydroxycoumarin

Sample	NCO/DHC (g/g)	$LiClO_4$ (wt %)
PU200C24-5	200/24	5
PU200C48-5	200/48	5
PU200C72-5	200/72	5
PU200C96-5	200/96	5

All UV irradiated self-healing polyurethane samples were prepared by exposing the samples to 16 UV lamps (128 Watts) in the UV reactor for 100 hours as the energy needed is 4.608×10^7 J for the dimerization of 6,7-dihydroxycoumarin according to the equation shown below. This duration was obtained after finalized by observing the SEM micrographs on the healed cut wound. The UV irradiated self-healing polyurethanes were labelled as HPU200C24-5, HPU200C48-5, HPU200C72-5 and HPU200C96-5.

$$\text{Energy (J)} = \text{Power (Watt or J.}s^{-1}) \times \text{time (second)}$$

3.3 CHARACTERIZATION

3.3.1 Attenuated total reflectance Fourier transform infrared (ATR-FTIR) analysis

The main functional groups in pristine PU, PU-$LiClO_4$ and self-healing PU-$LiClO_4$ (HPU) were identified by ATR-FTIR analysis using spectrometer model Perkin-Elmer spotlight 400 imaging system with the scan resolution of 2 cm^{-1}. The peaks were detected at scan range from 4000 to 700 cm^{-1} to identify the presence of N-H, C=O, C-O-C and C-N of urethane group.

3.3.2 Cross-linking analysis

The percentage of gel content of PU-$LiClO_4$ films was determined by carrying out soxhlet method. The solvent (250 ml of toluene) was added to a round bottom flask, which was attached to a Soxhlet extractor and condenser (Figure 3.3) on a heating mantle. The samples loaded into the cellulose bag, which was placed inside the Soxhlet

extractor. The solvent was heated using the heating mantle and was let to evaporate and moving through the apparatus to the condenser. The condensate then dripped into the reservoir containing the cellulose bag. Once the level of solvent reached the siphon it poured back into the flask and the cycle began again. The process ran for a total of 24 hours (Coll et al. 2008). Then, the samples were extracted at 116 °C to obtain dry samples. The percentage of the solid content of the dry sample was calculated by using the equation below:

$$\text{gel content (\%)} = \frac{\text{mass of dried sample}}{\text{mass of sample}} \text{ x } 100\%$$

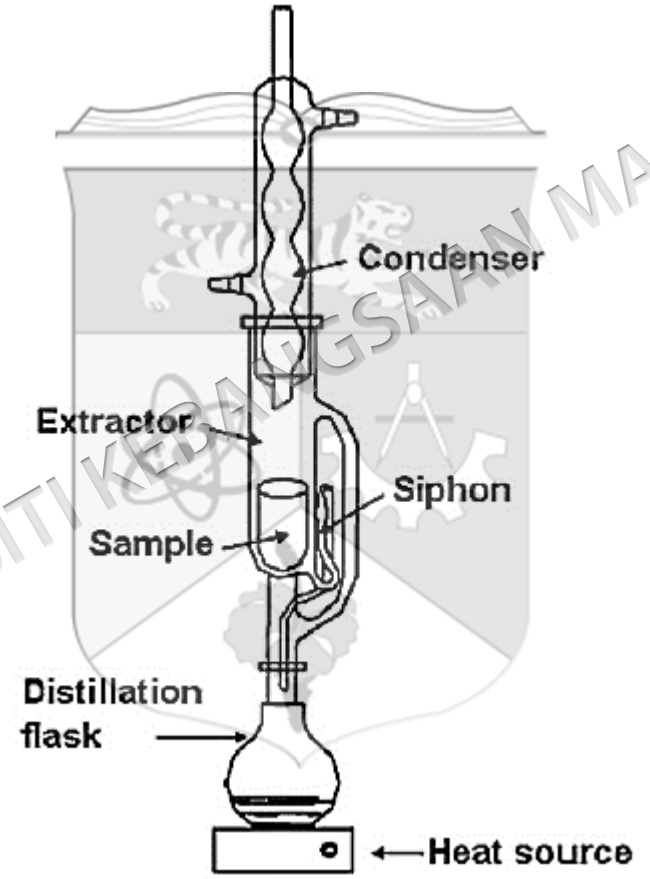

Figure 3.3 Soxhlet extractor equipment

3.3.3 Thermal analysis

The glass transition temperature (T_g) of samples was analysed by using a DSC analyser model Mettler Toledo 822*e* in nitrogen gas atmosphere. The thermal behavior of PU-$LiClO_4$ was observed by heating the samples with at temperature ranging from 30 °C

to 250 °C under nitrogen gas atmosphere at heating rate of 10 °C/min. 4 mg of sample was used in each measurement.

Thermal stability of samples was determined by thermogravimetric analysis. The analysis was carried out using a Mettler–Toledo TGA/SDTA 851 analyzer under nitrogen gas atmosphere from 30 °C to 600 °C at a heating rate of 10 °C/min. A sample size of ~10 mg was used to determine the weight loss of the samples.

3.3.4 Morphological analysis

The morphology of the PU-$LiClO_4$ was observed and recorded using Scanning Electron Microscope (SEM) model ZEISS, SUPRA 55VP at a depth of 10000× magnification at 10 kV electron beam. The average atomic percentage of carbon, nitrogen, oxygen and chlorine atoms in the PU-$LiClO_4$ was determined using SEM-EDX.

Qualitative evaluation of the healing efficiency was conducted by visual inspection. The film was cut using a razor blade. The film was then exposed to UV irradiation for 100 hours to determine its healing efficiency. The cut wounds of self-healing PUs before and after UV irradiation were observed and recorded using Leica DMRXA optical microscope at 40× magnification. The change in the cut wounds was confirmed from observations using SEM model ZEISS, SUPRA 55VP at 300× magnification using 10 kV electron beam.

3.3.5 X-ray Diffraction Analysis (XRD)

The crystallinity of samples was determined by X–ray diffractometer (XRD) model D–5000 Siemen with Cu radiation (Cu–Kα; α = 1.5418 Å). The data was collected in the range of diffraction angle, 2θ from 5 ° to 60 ° at a scanning rate 0.04 °.s^{-1}.

3.3.6 Electrochemical Impedance Spectroscopy (EIS)

The electrical conductivity of samples was measured by alternating current (ac) electrochemical impedance spectroscopy (EIS) using a high frequency resonance analyzer (HFRA) model 1255 with applied frequency from 1 Hz to 10 MHz at 100 mV amplitude at room conditions (25 °C, 1 atm). The 16 mm in diameter disc-shaped sample was sandwiched between two stainless steel blocking electrodes. The electrical

conductivity (σ) was calculated from the bulk resistance (Rb), determined from the equivalent circuit analysis by using the Zview analyzer software and the film thickness (l) and contact area of the thin film (A = 2.01 cm^2), in accordance with the equation shown below (Ahmad et al. 2012).

$$\sigma = \frac{l}{A.Rb}$$

3.3.7 Mechanical analysis

The hardness of samples was determined by pencil test according to ASTM D 3363-00 (Standard Test Method for Film Hardness by Pencil Test). A coated panel is placed on a firm horizontal surface. The pencil was held firmly against the film at a 45° angle (point away from the operator) and pushed away from the operator in a 6.5 mm (1⁄4-in.) stroke. The test began in descending order of the scale of hardness to the end point: the pencil that will not scratch the film (scratch hardness). H indicates hardness of pencils and B indicates blackness or softness of pencils. A set of calibrated drawing leads (preferred) or equivalent calibrated wood pencils meeting the following scale of hardness:

The hardness of samples was also determined by using Konig Pendulum hardness tester Cat. No. 5854 according to ASTM D-4366 (Standard Test Method for Hardness of Organic Coatings by Pendulum Damping Test). The assembly swings supported on 2 ball bearings of 5 mm diameter which rest on the surface of the sample. Then, the number of oscillations made by the pendulum with the amplitude of 6° on the sample was recorded. Thus, the hardness of the sample was calculated as shown below:

$$\frac{\text{number of oscillations (with sample)}}{\text{number of oscillations (without sample)}} \times 100\% = \text{hardness of sample (\%)}$$

Tensile test was carried out according to ASTM D638-14 (Standard Test Method for Tensile Properties of Plastics) by using the specimen with dumb-bell shape

(14 mm gauge length and 2 mm width using cutter ISO-37 type 4). Then the specimens were tested using INSTRON 5848 machine with 50 N load cell at a cross-head speed of 10 mm/min. in order to measure their tensile stress, strain and modulus.

3.3.8 Synthesis of chain extended dihydroxycoumarin

Several attempts had been carried out to synthesize the chain extended dihydroxycoumarin by referring to the following process flow.

The 6,7-dihydroxycoumarin was dissolved in DMF under continuous stirring. K_2CO_3 was added into the mixture. After that, 2-bromoethanol diluted in DMF was added into the mixture. The reaction proceeded at 85°C for 18 hours under nitrogen gas atmosphere and then cooled down to room temperature. DMF was removed by using vacuum pump at 55°C. Then the product was filtered and the solvent was evaporated by using rotary evaporator. The crude compound was isolated by conducting column chromatography and further verified by thin layer chromatography as shown in Figure 3.5. The solvents then were removed by rotary evaporator to give white solid which was the chain extended dihydroxycoumarin. Figure 3.4 below shows the mechanism of formation of chain extended dihydroxycoumarin.

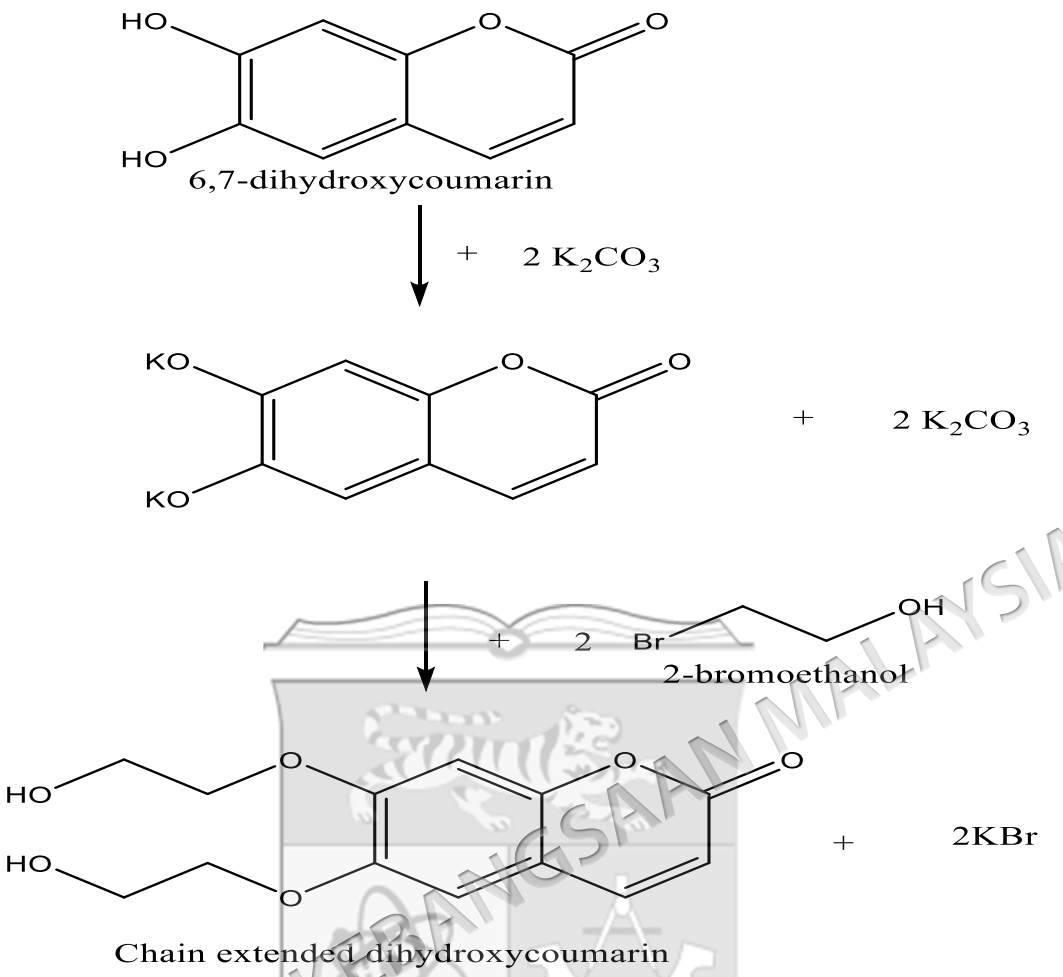

Figure 3.4 Mechanism of formation of chain extended dihydroxycoumarin via Williamson ether reaction

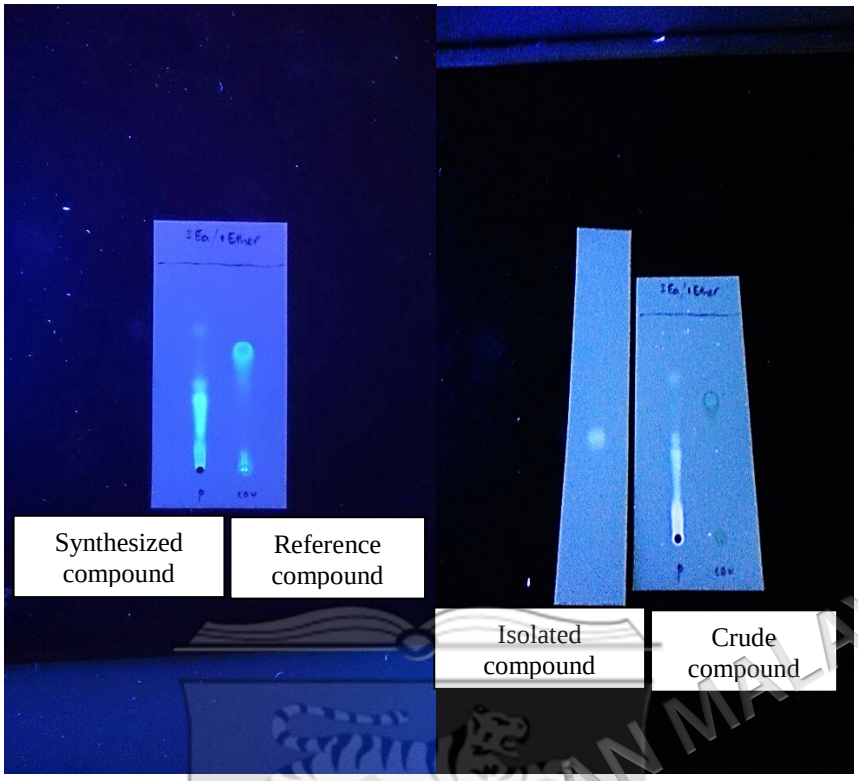

Figure 3.5 Thin layer chromatography of reference compound, crude compound and Isolated compound

Several attempts with various independent variables were conducted to synthesize chain extended dihydroxycoumarin as shown in Table 3.3 and the structure of product was determined by ^{1}H NMR. However, chain extended dihydroxycoumarin could not be obtained as the splitting patterns, chemical shifts and integration in ^{1}H NMR spectra of extracted products as shown in and Appendix A1-A8 do not match the ^{1}H NMR spectrum of desired chain extended dihydroxycoumarin as shown in Figure 3.6. This is because 2-bromoethanol is a very unstable compound with low boiling point (56 ℃). Hence, it might react with itself via nucleophilic substitution or evaporate during the synthesis of chain extended 6,7-dihydroxycoumarin.

For chain extended dihydrxycoumarin, 1H NMR (450 MHz, DMSO-d6, δ): 7.94 (1H, doublet), 6.98 (2H, singlet), 6.22 (1H, doublet), 4.9 (2H, singlet), 4.33 (4H, triplet), 3.69 (4H, triplet)

For experiment 1, 1H NMR (450 MHz, DMSO-d6, δ): 7.93 (1H, singlet), 6.93 (1H, quartet), 6.29 (1H, triplet), 5.03 (1H, singlet), 4.27 (4H, triplet)

For experiment 2, 1H NMR (450 MHz, DMSO-d6, δ): 7.88 (1H, doublet), 6.99 (2H, singlet), 6.24 (1H, singlet), 4.93 (1H, doublet), 4.22 (3H, doublet)

For experiment 3, 1H NMR (450 MHz, DMSO-d6, δ): 7.90 (3H, doublet), 7.00 (5H, singlet), 6.23 (3H, doublet), 5.00 (1H, doublet), 4.23 (2H, doublet)

For experiment 4, 1H NMR (450 MHz, DMSO-d6, δ): 7.90 (3H, doublet), 7.00 (4H, singlet), 6.40 (4H, singlet), 45.31 (1H, triplet), 4.23 (2H, triplet)

For experiment 5, 1H NMR (450 MHz, DMSO-d6, δ): 8.00 (7H, singlet), 7.09 (1H, doublet), 6.43 (1H, singlet), 4.41 (1H, doublet)

For experiment 6, 1H NMR (450 MHz, DMSO-d6, δ): 7.95 (1H, singlet), 7.00 (5H, singlet), 6.32 (2H, doublet), 4.10 (3H, singlet), 3.72 (3H, singlet)

For experiment 7, 1H NMR (450 MHz, DMSO-d6, δ): 7.90 (1H, doublet), 7.00 (3H, singlet), 6.33 (1H, singlet), 4.11 (2H, singlet), 3.83 (2H, singlet)

Table 3.3 Synthesis of chain extended dihydroxycoumarin with various ratios of 2-bromoethanol and K_2CO_3 (catalyst) and tetrabutylammonium iodide (Ling et al. 2012)

Experiment	6,7-dihydroxycoumarin (mol)	2-bromoethanol (mol)	DMF (mL)	K_2CO_3 (mol)	Tetrabutylammonium Iodide (wt %)
1	1	3.0	15	10	-
2	1	2.5	15	10	-
3	1	2.0	15	10	-
4	1	3.0	15	5	-
5	1	3.0	15	1	-
6	1	3.0	15	10	5
7	1	3.0	15	10	10

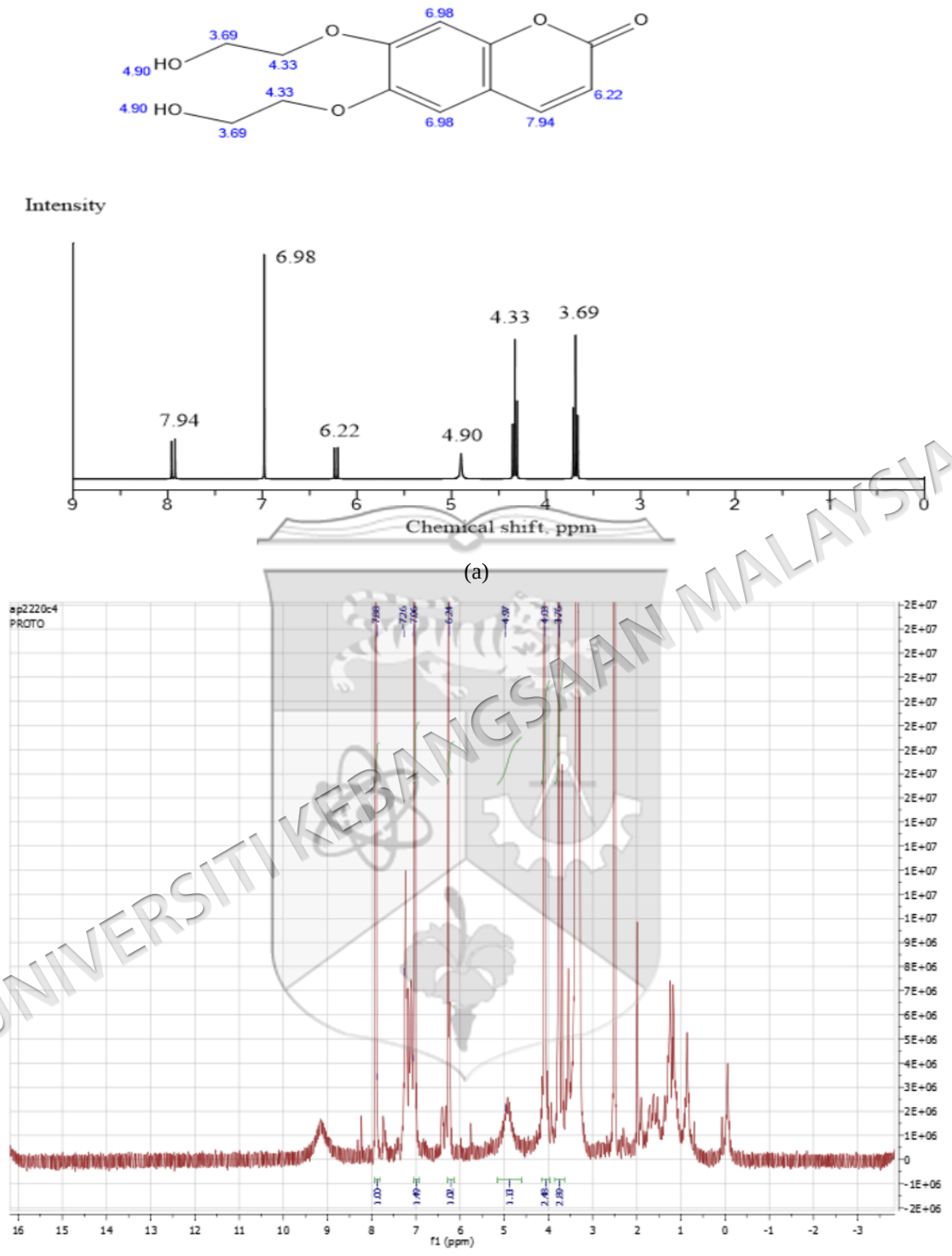

Figure 3.6 (a) Calculated ^{1}H NMR spectrum of chain extended 6,7-dihydroxycoumarin and (b) Selected ^{1}H NMR spectrum of the synthesized chain extended 6,7-dihydroxycoumarin from experiment 1

Hence, the attempt of synthesizing chain extended dihydroxycoumarin has been unsuccessful. The following discussion of this research will then focus only on the commercial 6,7-dihydroxycoumarin that will be discussed in Chapter V.

CHAPTER IV

SYNTHESIS OF PALM-BASED POLYURETHANE-LITHIUM PERCHLORATE

4.1 OVERVIEW

The work presented in this chapter was extracted from: Wong, C.S., Badri, K.H. and Hassan, N.I. 2015. Palm-Based Polyurethane as a potential precursor for bio-based polyurethane-$LiClO_4$. *International Journal of Chemical, Molecular, Nuclear, Materials and Metallurgical Engineering 8: 1168-1175.*

From this section onwards, PU-$LiClO_4$ with different NCO/OH ratios of 200/100 (PU200-5), 150/100 (PU150-5), 100/100 (PU100-5), 85/100 (PU85-5) and different $LiClO_4$ content with addition of 0 wt% (PU200-0), 5 wt% (PU200-5), 10 wt% (PU200-10), 15 wt% (PU200-15), 20 wt% (PU200-20), 25 wt% (PU200-25) and 30 wt% (PU200-30) were characterized and discussed. In this work, the effect of NCO/OH ratios and different $LiClO_4$ loadings on the morphology, chemical, mechanical and thermal properties as well as ionic conductivity of this novel bio-based PU-$LiClO_4$ were investigated to understand the ionic conductivity and ion binding mechanisms in this PU-$LiClO_4$. The PU-$LiClO_4$ films were prepared by curing the blends consist of $LiClO_4$, PKO-p, MDI and PEG in acetone via casting method at room temperature. The structures of PU-$LiClO_4$ were confirmed by FTIR spectroscopy. FTIR spectroscopy proved the coordination of lithium ion with the urethane group forming complex with the emergence of ordered C=O peak at 1649 cm^{-1} as shown in section 4.3.1. Inhibition of polymerization took place with more than 5 wt% of $LiClO_4$ content in PU-$LiClO_4$ in section 4.3.2. Besides that, DSC analysis exhibited higher glass transition temperature (49.09°C) at NCO/OH ratio of 200/100

and salt loading of 5 wt%. However, TGA analysis showed decrease in degradation temperature (from 239 °C to 191 °C) with the increase in $LiCLO_4$ content from 0 wt% to 5 wt% due to the lower molecular weight of polyurethane chain formed. Moreover, SEM micrographs revealed the cracks in PU-$LiClO_4$ with more than 5 wt% of $LiClO_4$ salt due to high crystallinity of $LiClO_4$ as shown in XRD analysis with emergence of sharp peaks at 13.5°, 21.1°, 22.1° 23.3°, 30.9°, 31.7°, 33.1°, and 46.2°.

4.2 Physical Observation

PU-$LiClO_4$ with different NCO/OH ratios were prepared as shown in Figures 4.1 (a) and (b). All the films prepared were flexible, void-free, free standing and with homogeneous surface. Besides that, PU-$LiClO_4$ with different $LiClO_4$ loading were prepared as shown in Figure 4.1 (c). PU200-0 and PU200-5 (refers to 0 and 5 wt% of $LiClO_4$ respectively) were flexible, void-free and with homogeneous surface. However, more voids were detected in PU200-10 to PU200-30 and they were not free-standing due to the incomplete polymerization in PU200-10 to PU200-30 as shown in section 4.3.2 that will be discussed later. The presence of lithium salt disturbed the polymerization process, thus resulted in incomplete polymerization. It becomes significant especially at higher loading percentage of lithium salt (15, 20, 25 and 30 wt%). In addition, the lithium salt was dissolved in acetone and it is possible to affect the polymerization kinetics.

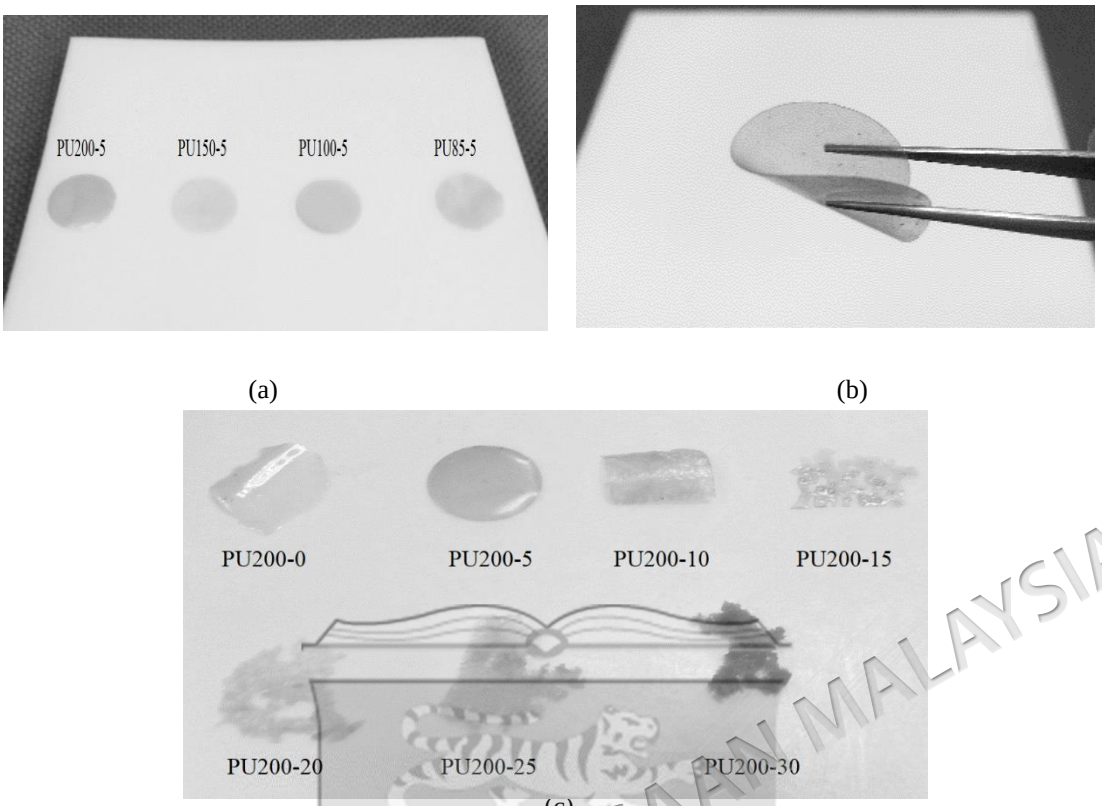

Figure 4.1 (a) PU-LiClO4 with different NCO/OH ratios of 200/100 (PU200-5), 150/100 (PU150-5), 100/100 (PU100-5) and 85/100 (PU85-5) (b) Flexible, free-standing and transparent PU-$LiClO_4$ (c) PU-$LiClO_4$ by varying $LiClO_4$ content with addition of 0 wt% (PU200-0), 5 wt% (PU200-5), 10 wt% (PU200-10), 15 wt% (PU200-15), 20 wt% (PU200-20), 25 wt% (PU200-25) and 30 wt% (PU200-30) of $LiClO_4$

4.3 FTIR spectroscopy analysis

4.3.1 Effect of NCO/OH ratio on properties of palm based PU-$LiClO_4$

The presence of N-H, C=O, C=C, and C-O-C of urethane group in the PU-$LiClO_4$ films with various NCO/OH ratios was detected as shown in Figure 4.4. and summarized in Appendix D1. The hydrogen bonded amine (N-H) stretching band was found at the range of 3296-3352 cm^{-1} which is similar to earlier works (Haddad et al. 2011; Mutsuhisa et al. 2007). The carbamate peaks were detected too at the range of 1597-1599 cm^{-1}. Besides that, the absence of NCO peak at the range of 2250-2270 cm^{-1} proved the complete polymerization of the NCO group in MDI and hydroxyl group in polyol and PEG as detected by Mishra et al. (2012) and as shown in Figure 4.6 (b). Besides, the free and hydrogen bonded C=O stretching bands of urethane group in PU200-0 were shown at 1725 cm^{-1} and 1711 cm^{-1} as in Appendix D2 and Figure 4.2(b). The hydrogen bonded C=O peak was found only in PU-$LiClO_4$ (PU200-5, PU150-5,

PU100-5 and PU85-5). Moreover, the hydrogen bonded C=O peak of these four PU-$LiClO_4$ shifted to 1708 cm^{-1} compared to 1711 cm^{-1} of PU200-0 as shown in Figure 4.2(b). This confirms coordination between Li^+ ions and carbonyl groups PU-$LiClO_4$ disrupted the C=O in the urethane bond as shown in Figure. 4.5. An ordered complexed C=O band in the PU chain was also detected at 1649 cm^{-1} for PU200-5 in Figure 4.2(c). It is attributed to the coordination between Li^+ ion and PU200-5 which has the greatest hard segment content contributed by the highest NCO/OH ratio. The interaction between Li^+ ion with oxygen atom of carbonyl group weakens the C=O bond by sharing the electron density of oxygen atom in the carbonyl group (Liu et al. 2014). Besides, the C-N and C-O-C peaks of the PU-$LiClO_4$ remained unchange at 1598 cm^{-1} and 1067 cm^{-1}. Hence, it implies the coordination of Li^+ ion is preferable with C=O and not with C-N and C-O-C due to higher electron density of oxygen of C=O compared to the oxygen atom of C-O-C and nitrogen atom of C-N (Michael 1996). The C=C peaks detected in FTIR spectra of all polyurethane-$LiClO_4$ samples are referred to the benzene ring of MDI used in synthesis of polyurethane-$LiClO_4$ (Xiong et al. 2012).

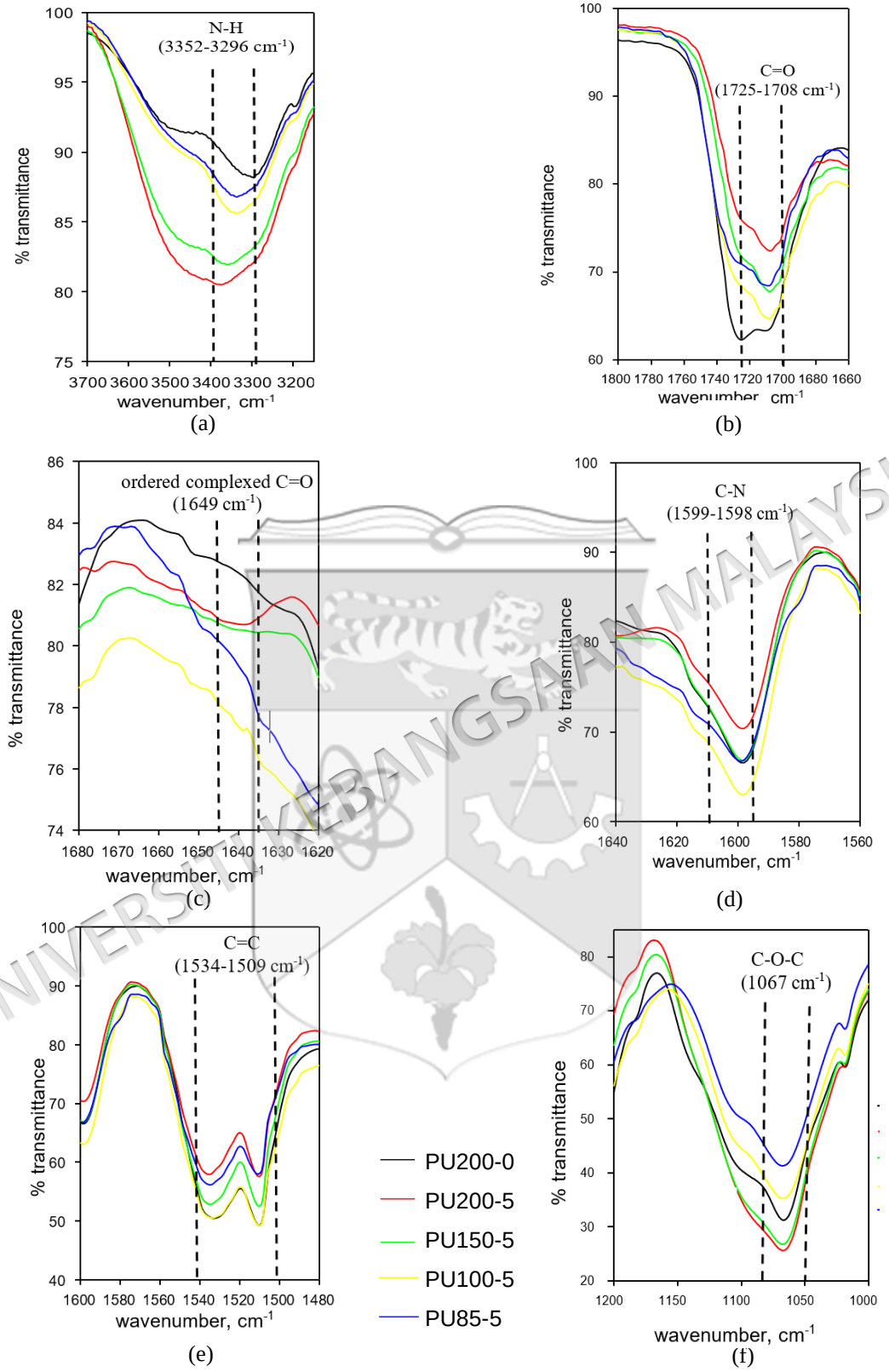

Figure 4.2 The vibration regions of (a) N-H, (b) C=O, (c) ordered complexed C=O, (d) C-N, (e) C=C and (f) C-O-C of urethane group in PU-$LiClO_4$ and pristine polyurethane

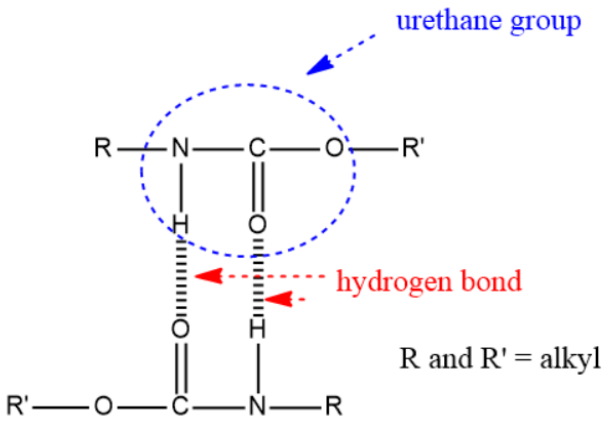

Figure 4.3 Suggested formation of hydrogen bond in the PU-$LiClO_4$

4.3.2 Effect of $LiClO_4$ loading

Figure 4.4 reveals the FTIR spectrum of PU200-0 (control), PU200-5, PU200-10, PU200-15, PU200-20, PU200-25 and PU200-30 (refers as 0, 5, 10, 15, 20, 25 and 30 wt% of $LiClO_4$ respectively) with various $LiClO_4$ content in the PU-$LiClO_4$. The important bands of the urethane bond located at 3393-3296 cm^{-1} (N-H stretching vibration), 1708-1707 cm^{-1} (non-hydrogen bonded and hydrogen bonded C=O stretching vibrations), 1070-1067 cm^{-1} (C-O-C stretching vibration) and 1598-1597 cm^{-1} (C-N stretching vibration) were observed in all the PU-$LiCLO_4$ as shown in Table 4.2. However, incomplete polymerization was seen in PU200-10, PU200-15, PU200-20, PU200-25 and PU200-30 with the emergence of N=C=O asymmetric stretching band (Sebenik et al. 2007) at 2282-2275 cm^{-1} which is associated with the free isocyanate groups in the urethane prepolymer as shown in Figure 4.6(b). It indicates the inhibition of the formation of polyurethane by $LiClO_4$ where Li^+ ion is a metal ion that could bind with nucleophiles strongly such as carbonyl and hydroxyl groups (Fukushima et al. 2001) as the formation of polyurethane is nucleophilic substitution (Wong et al. 2012). The C=C peak was also detected in all polyurethanes which was derived from the benzene ring of MDI.

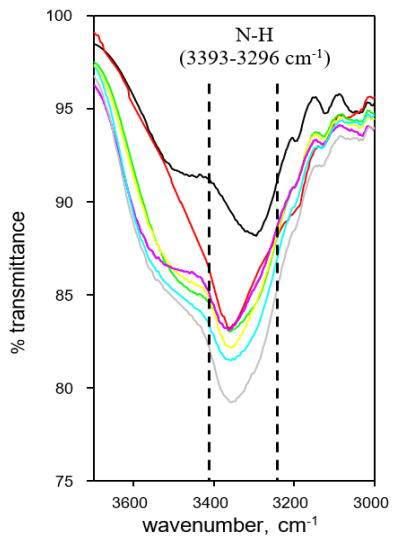

(a)

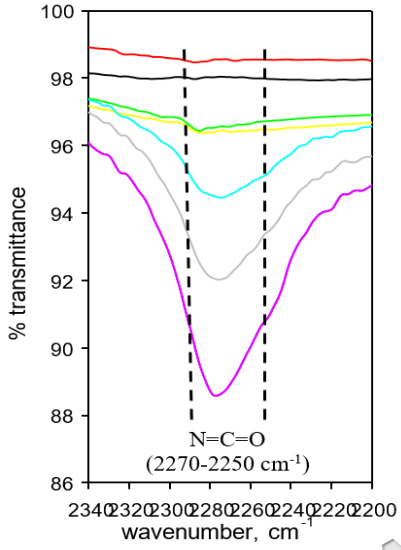

(b)

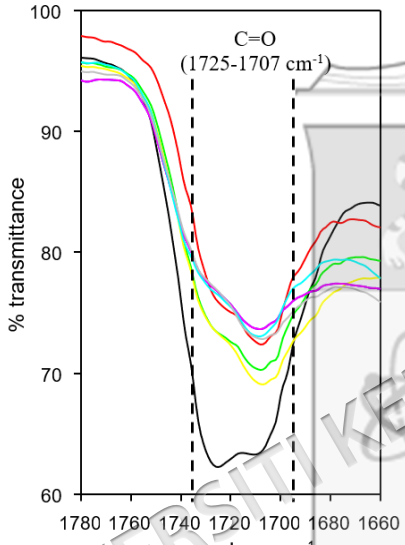

(c)

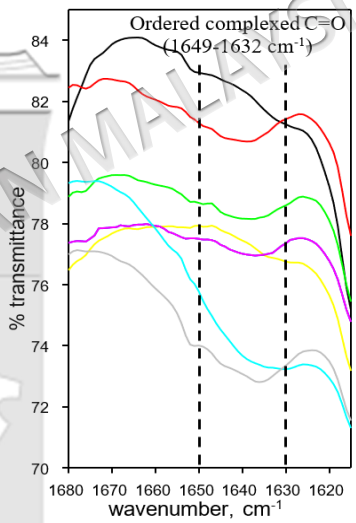

(d)

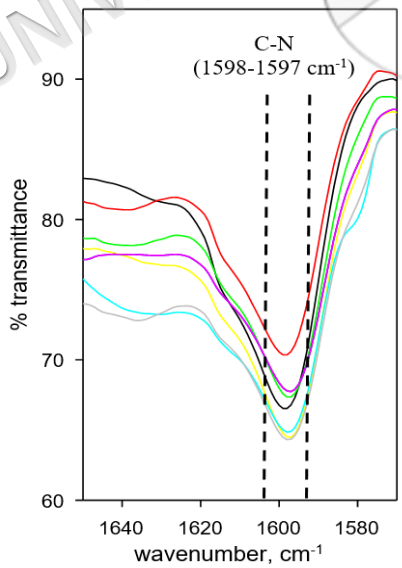

(e)

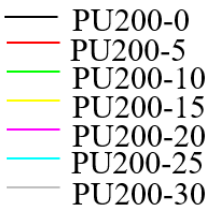

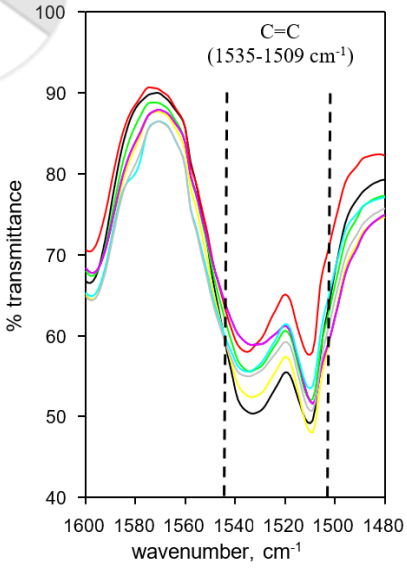

(f)

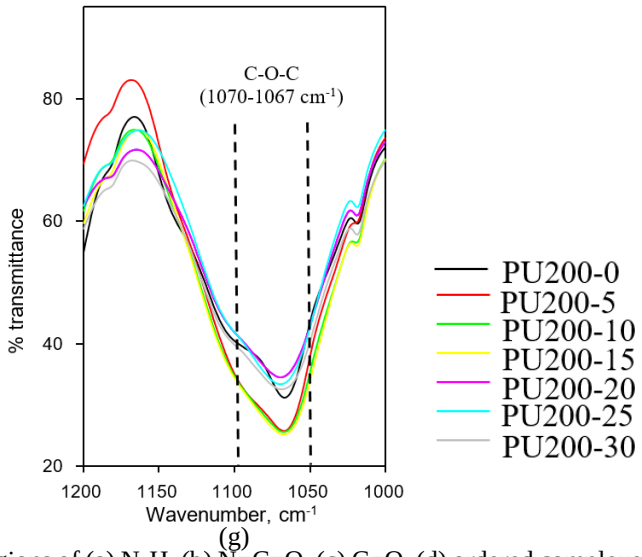

Figure 4.4 The vibration regions of (a) N-H, (b) N=C=O, (c) C=O, (d) ordered complexed C=O, (e) C-N, (f) C=C and (g) C-O-C of urethane group in PU-$LiClO_4$ with various $LiClO_4$ content and pristine polyurethane

4.4 Cross-linking analysis

4.4.1 Effect of NCO/OH ratios

Soxhlet analysis was used to determine the amount of hard segment in the PUs. The urethane group (hard segment) in PU is polar (Cuve et al. 1991). Hence, the hard segment of PU is hardly dissolved in toluene. The soxhlet test result as shown in Table 4.1 proves that PU200-5 has the greatest amount of hard segment (urethane group) followed by PU150-5, PU100-5 and PU85-5. Hard segment is formed by the reaction between isocyanate and the hydroxyl groups. PU200-5 with the greatest NCO/OH ratio gave the highest gel content. The obtained result is consistent with TGA analysis. PU200-0, the control sample shows the highest gel content (72.9%) indicating higher cross-linking compared to those samples at lower NCO contents.

4.4.2 Effect of $LiClO_4$ loading

As shown in Table 4.1, higher salt loading generally results in lower solid content of the PU-$LiClO_4$. This indicates the inhibition of the formation of hard segment in PU which leads to shorter polymer chain and lower solid content. Hence, the soxhlet analysis results confirmed the FTIR analysis data. Besides, the decrease in gel content

may be attributed to the high heating temperature (116 °C) facilitates the dissociation of lithium salt.

Table 4.1 Percentage of gel content of the pristine polyurethane and PU-$LiClO_4$ at various NCO/OH ratio and $LiClO_4$ content

Samples	Gel content (%)
PU200-0	72.90
PU200-5	69.18
PU150-5	59.50
PU100-5	39.80
PU85-5	31.80
PU200-10	64.29
PU200-15	60.18
PU200-20	56.23
PU200-25	54.12
PU200-30	50.36

4.5 DSC analysis

4.5.1 Effect of NCO/OH ratios

The glass transition of PU-$LiClO_4$ was obtained as summarized in Table 4.2 and shown in Appendix E1. The glass transition temperatures of PU200-5, PU150-5, PU100-5 and PU85-5 are above room temperature indicating the glassy state of polyurethane-$LiClO_4$. The glass transition temperatures of PU-$LiClO_4$ decreased by lowering NCO/OH ratio. Hence, the decrease of NCO/OH ratio gives flexible polyurethanes. The presence of MDI contributes to the formation of hard segment in PU. Upon polymerization, this hard segment might restrict the polymer chain mobility (Ren et al. 2013) due to the steric hindrance of benzene ring in the hard segment. The endothermic peak of acetone at 56℃ could not be detected in DSC analysis implying the acetone was removed from the PU-$LiClO_4$ during the curing process.

4.5.2 Effect of $LiClO_4$ loading

Glass transition temperatures (T_g) of hard segment of PU1-0, PU1-5, PU1-10, PU1-15, PU1-20, PU1-25 and PU1-30 were determined in the range of 30-60 °C as shown in Appendix E2 and Table 4.2 (Wang et al. 2000). An increase in the lithium salt loading in the PU-$LiClO_4$ led to the decrease of the glass transition temperature as shown in Table 4.6 and Appendix E2. This might be due to interaction between lithium ions with

the hard segments as proven by FTIR analysis. This effect decreases the extend of the hydrogen bond between the hard segments and soft segments (Liu et al. 2014). Besides that, addition of Li^+ ion reduces the crystalline region in PU-$LiClO_4$ as proven by XRD analysis. Hence, glass transition is lower (Gurusiddappa et al. 2016). Hence, lower temperature is needed to change the glassy state of polyurethane to rubbery state.

Table 4.2 Glass transition temperatures of PU-$LiClO_4$ with different NCO/OH ratios and $LiClO_4$ loading

Sample	Glass transition temperature, °C
PU200-5	49.1
PU150-5	35.0
PU100-5	29.3
PU85-5	24.5
PU200-0	58.2
PU200-10	37.0
PU200-15	34.9
PU200-20	34.6
PU200-25	33.1
PU200-30	31.7

4.6 Thermogravimetric analysis

4.6.1 Effect of NCO/OH ratios

Appendix F1 shows TGA thermograms and differential thermogravimetric (DTG) curves for PU-$LiClO_4$ films with different NCO/OH ratios. The percentage of weight loss (%) is listed in Table 4.3. In general, a slight weight loss was observed in Figure 4.4 at the region of 40-100 °C. This is attributed to the vaporization of moisture and solvent residue. The first thermal degradation (T_{d1}) stage of the PU-$LiClO_4$ films was observed at the region of 150-230 °C as shown in Appendix D5. PU200-5 had the highest maximum degradation temperature (T_{max}) and the greatest percentage of weight loss (wt.%) in the first thermal degradation stage (T_{d1}) followed by PU150-5, PU100-5 and PU85-5. T_{d1} corresponds to the degradation of hard segment for urethane linkages forming alcohol or degraded short chain polyol and free isocyanates (Berta et al. 2006), primary and secondary amines and carbon dioxide (Chattopadhyay & Webster 2009; Chuayjuljit et al. 2007; Corcuera et al. 2011; Lu et al. 2002; Pan and Webster 2012; Rueda-Larraz et al. 2009). PU200-5 contained higher amount of isocyanate which led to higher yield of urethane bonds. The second thermal degradation stage (T_{d2}) for

PU200-5 experienced 49.07% weight loss and decreased to 45.52% for PU85-5 which contained the lowest NCO/OH ratio. T_{d2} is referred to the dimerization of free isocyanates to form carbodiimides and releases CO_2. The carbodiimide formed reacts with alcohol to form urea (Berta et al. 2006). The third thermal degradation stage (T_{d3}) is related to the degradation of urea (Berta et al. 2006) and soft segments of PU. The weight loss in T_{d3} increased from 17.34% (PU1-5) to 29.42% (PU85-5). It is associated to the lowest NCO/OH ratio in PU4-5 which gives the highest soft segment content in PU85-5.

Table 4.3 The percentage of weight loss (wt%) of PU-$LiClO_4$ at varying NCO/OH contents

	% weight loss (wt%)					
Sample	T_{max}, ° C	T_{d1}, 150-230°C	T_{d2}, 230-430°C	T_{d3}, 430-520°C	Total weight loss (%)	Residue after 520°C (%)
PU200-5	219.69	4.95	49.07	17.34	71.36	28.64
PU150-5	202.35	4.82	47.88	20.48	73.19	26.81
PU100-5	197.10	4.15	46.64	26.27	77.06	22.94
PU85-5	196.89	3.74	45.52	29.42	78.68	21.32

4.6.2 Effect of $LiClO_4$ loading

Appendix F2 reveal the TGA thermograms, DTG curves and the percentage of weight loss for PU-$LiClO_4$ films with different $LiClO_4$ loading (5, 10, 15, 20, 25 and 30 wt%). The percentage of weight loss (%) is listed in Table 4.4. The thermal decomposition stage (T_d) of PU200-0, PU200-5, PU200-10, PU200-15, PU200-20, PU200-25 and PU200-30 (refers as 0, 5, 10, 15, 20, 25 and 30 wt% of $LiClO_4$ respectively) at the temperature regions of 150-230 °C, 230-430 °C, 430-520 °C was observed. $LiClO_4$ is a hygroscopic material, so the evaporation of some moisture was observed at the temperature region of 40-100°C. Among all the PU-$LiClO_4$ films, PU1-5 had the highest T_{max} and greatest wt% at T_{d1}. T_{max} and T_{d1} decreased with the increase in $LiClO_4$ loading percentage from PU200-10 to PU200-30. The greater the amount of $LiClO_4$ in the PU-$LiClO_4$ would disrupt the PU chains due to the coordination between oxygen atom and Li^+ ion bond as confirmed by FTIR analysis. During T_{d1}, the disruption of urethane bonds took place resulted in the decomposition of hard segment forming alcohols and free isocyanates, primary or secondary amine and CO_2 (Chattopadhyay & Webster 2009; Chuayjuljit et al. 2007; Corcuera et al. 2011; Lu et al. 2002; Pan & Webster 2012; Rueda-Larraz et al. 2009). T_{d2} is attributed to the dimerization of free isocyanates to form carbodiimides that involves the release of CO_2 followed by formation of urea

between the reaction of carbodiimides and the alcohols produced. Furthermore, T_{d3} was contributed by the rupture of ester linkages (Cangemi et al. 2006). At higher loading of $LiClO_4$ salts, DTG peak of T_{d2} region shifted to the right due to interaction between $LiClO_4$ salts and urethane groups as observed in the FTIR spectrum. This proved the formation of PU-salt complexes. Besides, the residue percentage increased from PU1-5 to PU1-30 as shown in Table 4.7 also proves the salt complex formation that induces higher degradation temperature. The degradation of $LiClO_4$ involves 3 main steps as shown below (Jian-He et al. 2010):

At temperature 235-260°C, $LiClO_4$(solid) → $LiClO_4$(liquid)

At temperature 260-580°C, $LiClO_4$(liquid) → LiCl(solid)+$2O_2$(gas)

At temperature 580-610°C, LiCl(solid) →LiCl(liquid)

Table 4.4 The percentage of weight loss (wt.%) of pristine PU and PU-$LiClO_4$ films at varying $LiClO_4$ content with 200/100 of NCO/OH ratio

		% weight loss (wt. %)			Total weight loss (%)	Residue after 520°C (%)
Sample	T_{max}, °C	T_{d1}, 150-230°C	T_{d2}, 230-430°C	T_{d3}, 430-520°C		
PU200-0	239.08	6.95	62.51	15.52	84.98	15.02
PU200-5	219.69	4.95	49.07	17.34	71.36	28.64
PU200-10	217.72	3.67	53.59	13.38	70.67	29.34
PU200-15	216.90	3.13	48.38	18.19	69.70	30.30
PU200-20	210.74	2.75	45.76	11.01	59.52	40.48
PU200-25	192.95	2.27	44.52	11.41	58.20	41.80
PU200-30	190.76	2.25	42.88	14.41	59.54	40.46

4.7 SEM-EDX Morphology analysis

4.7.1 Effect of NCO/OH ratios

The SEM micrographs in Figure 4.5 and 4.6 reveal the formation of homogeneous polymer via step-wise polymerization and the polymer films with 5 wt% of lithium salt were free of void. Prepolymerization method could prevent adverse reactions in the polymerization of PU-$LiClO_4$. Furthermore, no trace of phase separation in PUs was detected in the SEM micrographs indicating a good interaction between the 5 wt% of $LiClO_4$ and polyurethane (Su'ait et al. 2014). This is further justified by the FTIR spectrum. In EDX-SEM analysis, light elements such as lithium and hydrogen could not be detected (Kaur et al. 2012). Hence, the detection of Cl elements in different spots of PU-$LiClO_4$ is attributed to the lithium salts and it indicated the dispersion of lithium

salt in the PU-$LiClO_4$. Moreover, the agglomeration of lithium salts could not be detected in PU200-5, PU100-5 and PU85-5 as summarized in Appendix G1 indicating the homogeneity between 5 wt% lithium salt and PU matrix. However, there was an insignificant increase in Cl (6 wt%) based on the elemental composition analysis through EDX (Appendix G1) detected in PU150-5.

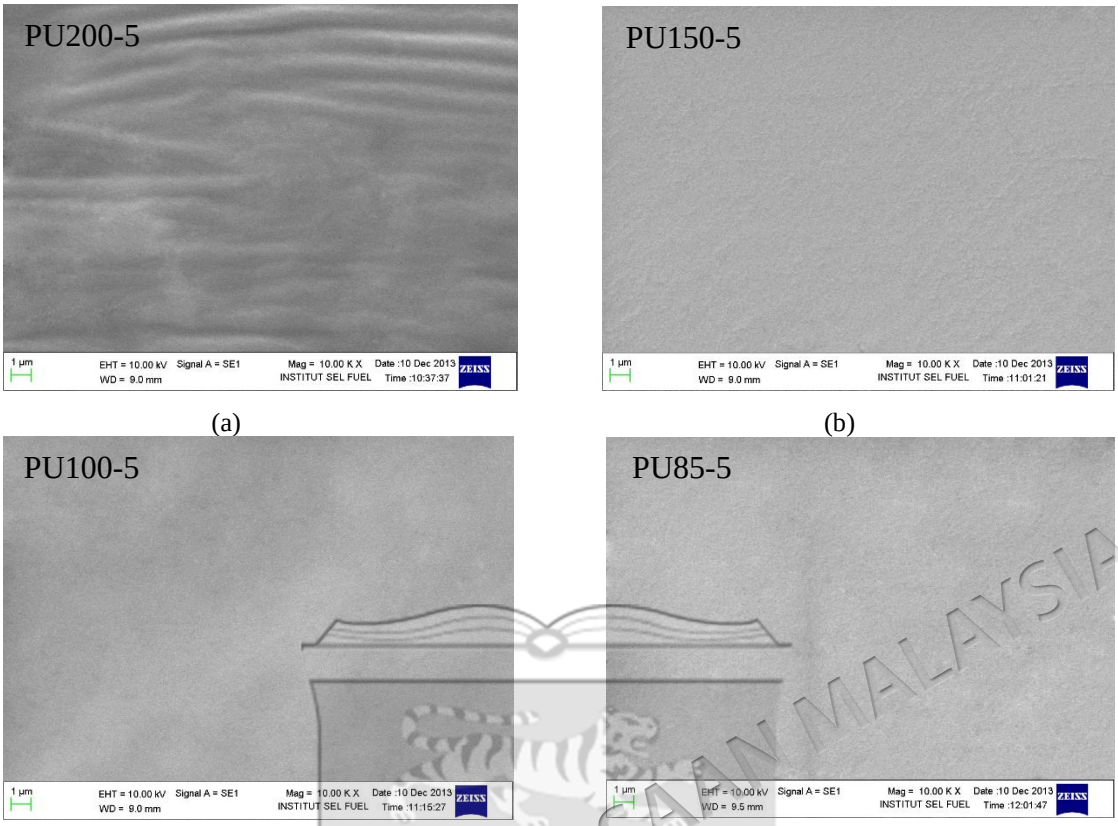

(a) (b)

(c) (d)

Figure 4.5 SEM analysis on the surfaces of (a) PU200-5,(b) PU150-5,(c) PU100-5 and (d) PU85-5

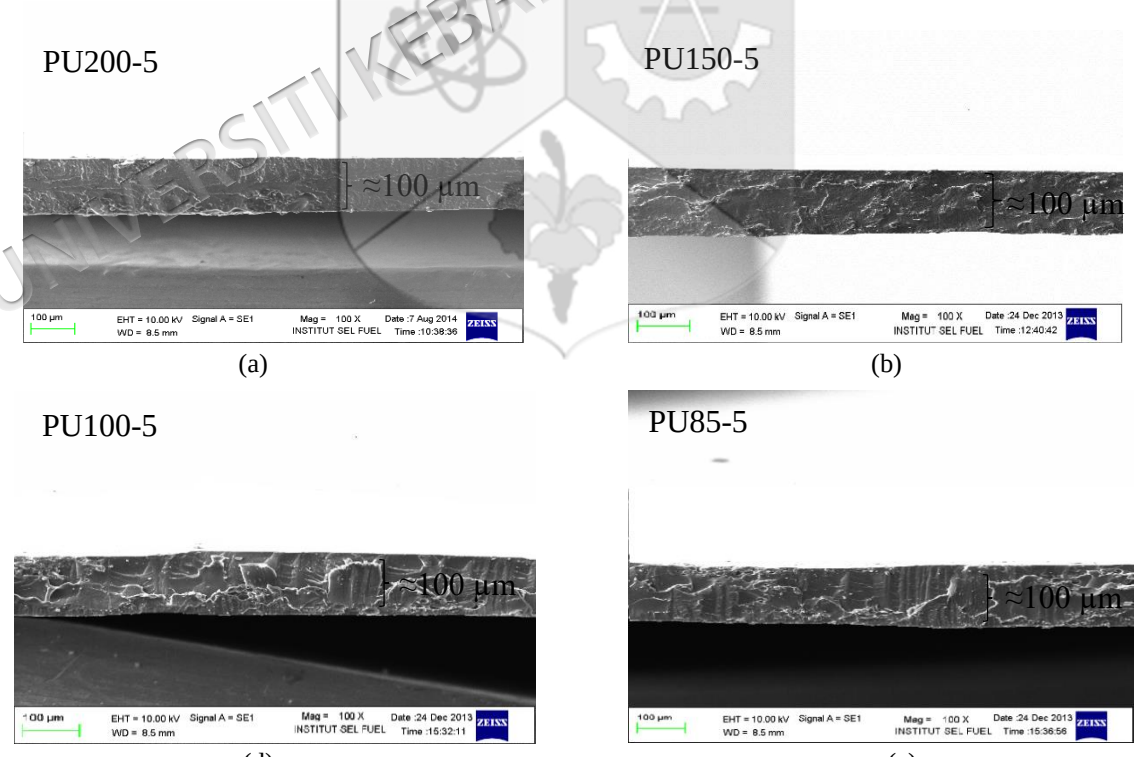

(a) (b)

(d) (e)

Figure 4.6 SEM analysis on the cross sections of (a) PU200-5, (b) PU150-5, (c) PU100-5 and (d) PU85-5

4.7.2 Effect of $LiClO_4$ loading

In Figure 4.8 (a), (b) and (c), no cracks or defects detected on the surface of the PU-$LiClO_4$ indicating good interfacial interaction between $LiClO_4$ and polyurethane. In reference to the work conducted by Sukor et al. (2011), the maximum and effective interactions between oxygen atoms and Li+ ion ([O/Li^+] ratio) is [6/1]. However, cracks were detected in the PU-$LiClO_4$ with more than 5 wt% of $LiClO_4$. This is associated to incomplete polymerization in the PU-$LiClO_4$ and high crystallinity of $LiClO_4$ which increased the rigidity of the PU-$LiClO_4$ films resulting in weak as supported by the XRD analysis. The micrographs shown in Figure 4.9 (a) and (b) reveal the cross sections of PU-$LiClO_4$ with 0 wt% and 5 wt% of $LiClO_4$ which are bubbleless. However, the increase in $LiClO_4$ content of polyurethane from 10 wt% to 30 wt% as shown in Figure 4.9 (c), (d), (e) and (f) led to greater formation of bubbles. This is attributed to the hygroscopic properties of $LiClO_4$ and free isocyanate groups in PU200-10, PU200-15, PU200-20, PU200-25 and PU200-30 as proven by the FTIR spectra shown in Figure 4.4 (b). The reaction between H_2O absorbed by $LiClO_4$ which has hygroscopic properties and the free isocyanate groups induced the formation of urea and CO_2 in the PU films (Clemitson 2008) as shown below:

Figure 4.7 Formation of urea and CO_2 by the reaction between isocyanate groups of urethane prepolymer and water

Moreover, the vigorous formation of CO_2 resulted in the formation of uneven surface in PU200-15, PU200-20, PU200-25 and PU200-30. Therefore, ionic conductivity analysis could not be performed on PU200-15, PU200-20 and PU200-25 and PU200-30 because even surface films are needed. EDX-SEM analysis shown in Appendix G2 shows higher percentage of Cl in the polyurethane matrix at higher $LiClO_4$ content, retrieved from the elemental analysis of SEM-EDX.

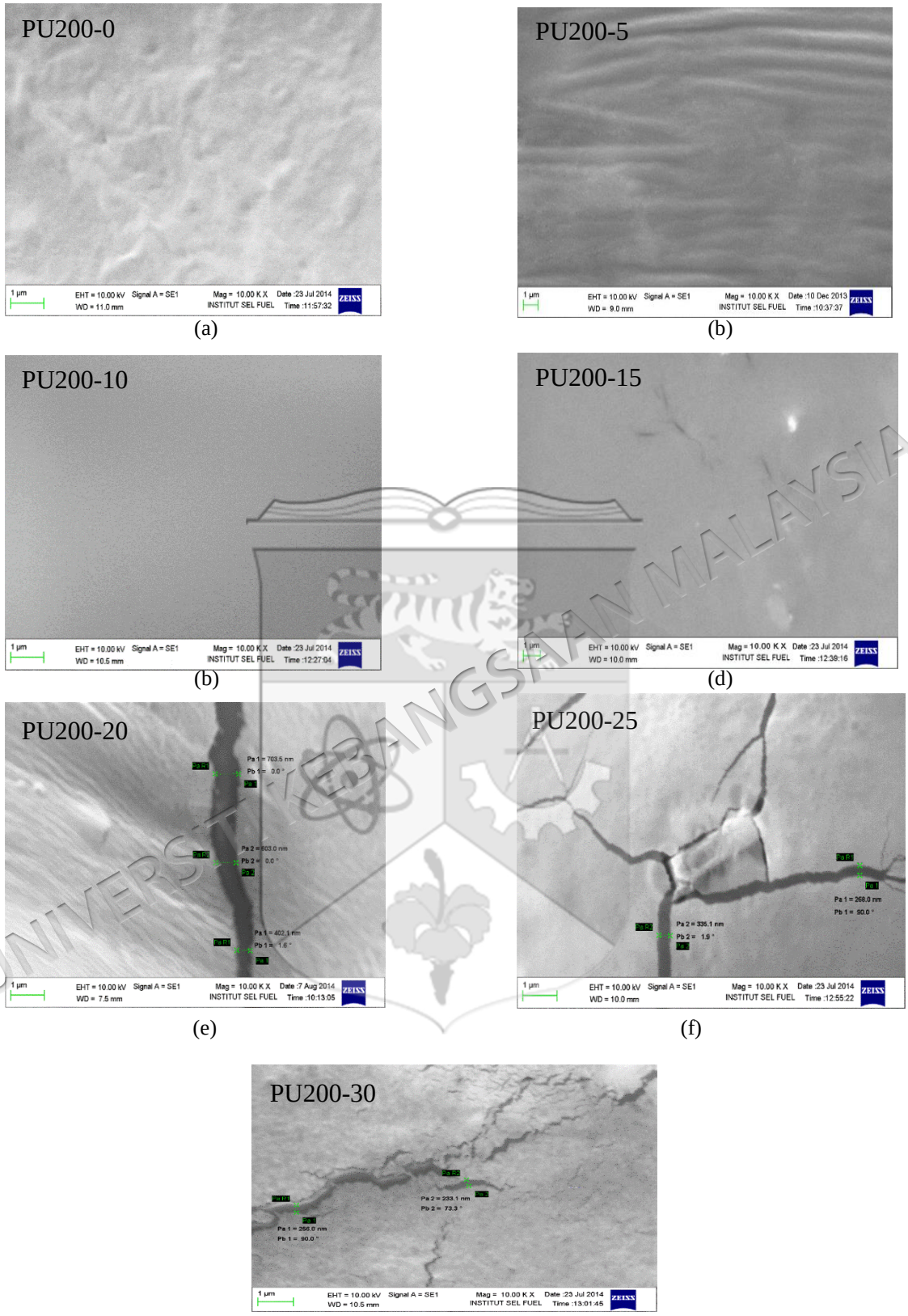

Figure 4.8 SEM analysis on the surfaces of (a) PU200-0, (b) PU200-5, (c) PU200-10, (d) PU200-15, (e) PU200-20, (f) PU200-25, (g) PU200-30

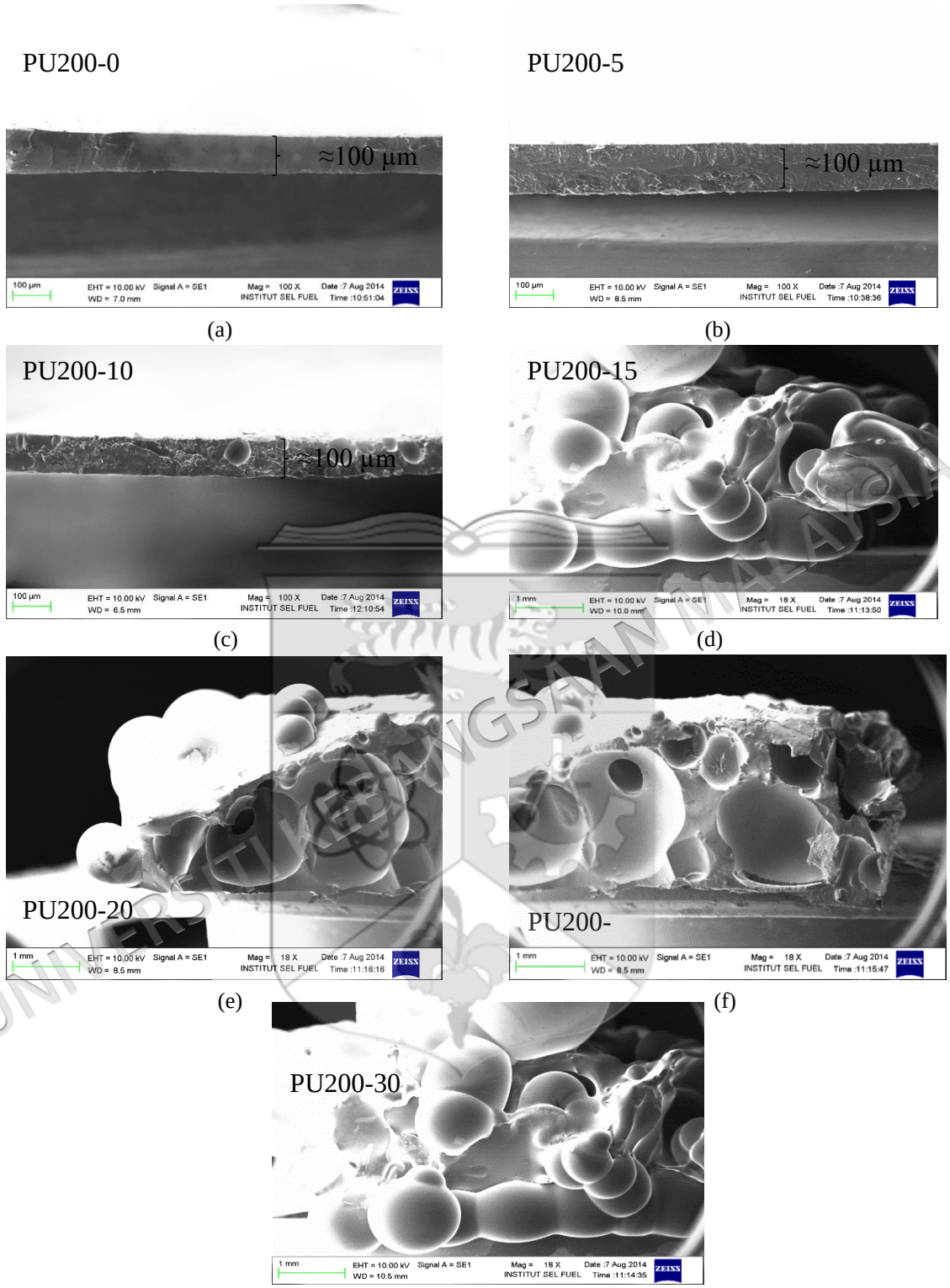

Figure 4.9 SEM analysis on the cross sections of (a) PU200-0, (b) PU200-5, (c) PU200-10, (d) PU200-15, (e) PU200-20, (f) PU200-25 and (g) PU200-30

4.8 X-ray Diffraction analysis

4.8.1 Effect of NCO/OH ratio

The XRD analysis was conducted to determine the phase and crystallizing of the PU-$LiClO_4$ complexes. The presence of the crystalline or the amorphous region in the PU-$LiCLO_4$ was determined. Figure 4.10 shows the XRD patterns of the PU-$LiClO_4$ indicating an increase in crystallinity. The crystalline region was detected in PU200-5, PU150-5, PU100-5 and PU85-5 with the emergence of broad peak at 20.0°. This region is associated to the segregation of the hard and soft segments in the polyurethane blocks (Ajit et al. 2010). The intensity of hump at the range of 15-27° remained unchange due to the same weight percentage of $LiClO_4$ for all samples resulted in same degree of crystallinity.

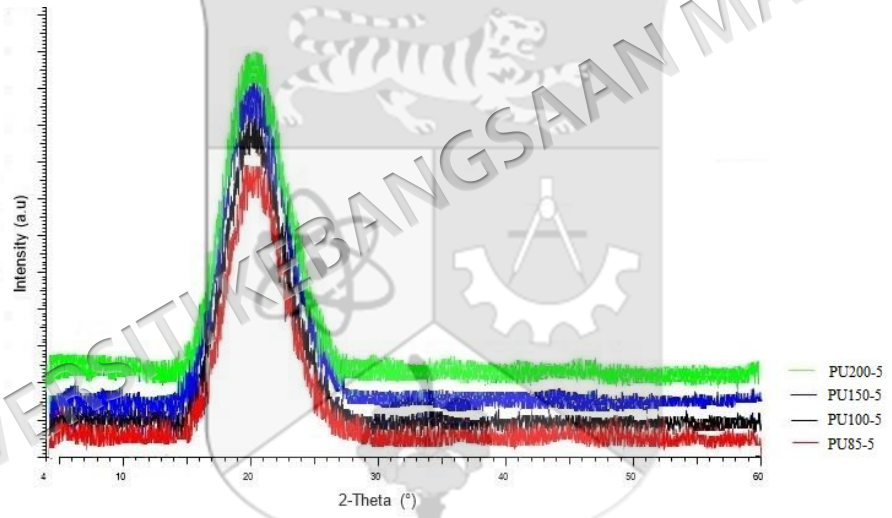

Figure 4.10 XRD diffractograms of PU-$LiClO_4$ films with different NCO/OH ratios

4.8.2 Effect of $LiClO_4$ loading

XRD diffractograms of PU-$LiClO_4$ and $LiClO_4$ are shown in Figure 4.11. The highly intense peaks of $LiClO_4$ were detected at 13.5°, 21.1°, 22.1° 23.3°, 30.9°, 31.7°, 33.1°, and 46.2° which are the same as peaks shown in Inorganic Crystal Structure Database (ICSD ID: 413238 165579) (Anon 2017). The important finding in this XRD analysis was the integration of $LiClO_4$ into the polyurethane decreased the crystallinity of the polyurethane by decreasing the broad peak in the region between 15° and 30° (Su'ait et al. 2014). This region was associated to the hard segment of PU (Hosseiny et al. 2017).

The height of the broad peak corresponded to the amount of hard segment (Ajit et al. 2010). This result is in consistency with the cross-linking analysis which shows a decrease in gel content from 69.18% to 50.36% proving the inhibition of polymerization could take place with the incorporation of more than 5 wt% of salt into the polyurethane (Ajit et al. 2010). Besides that, this is also attributed to the interaction between Li^+ ion and thus, it will affect the electrical conductivity of the PU-$LiClO_4$ films that will be discussed in Section 4.9. Moreover, small peaks at 21.1°, 23.2° and 30.9° were detected in PU200-25 and PU200-30 indicating the re-crystallization of $LiClO_4$ in these PU-$LiClO_4$ (Anon 2017). The re-crystallization of lithium salt occurred because of the ion association between the Li^+ cation and anion in PU at higher salt concentration (Su'ait et al. 2009). The salt affects the overall electrical conductivity through the formation of crystalline complexes, the intramolecular cross-linking of the polymer chains and the degree of salt dissociation-number of charge carriers (Gray 1997). \

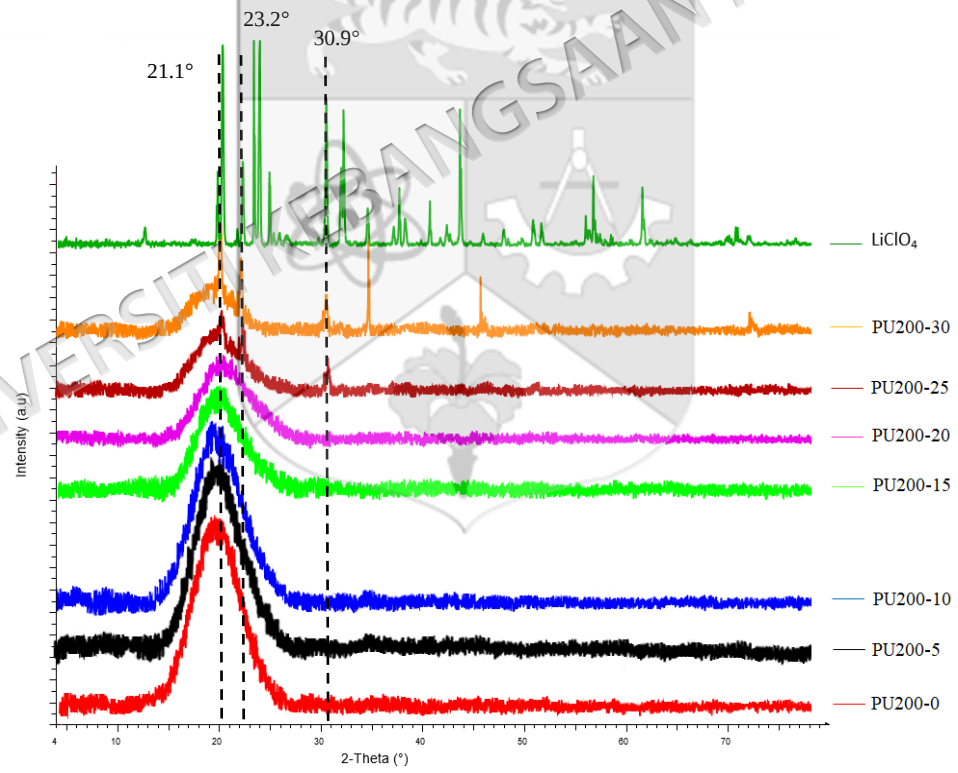

Figure 4.11 XRD diffractograms of PU-$LiClO_4$ films with different $LiClO_4$ content

4.9 Impedance analysis

From this point onwards, the discussion focuses on the pristine PU and PU-$LiClO_4$ films that are elastic, free standing and have homogeneous surface, namely PU200-0, PU200-5 and PU200-10.

4.9.1 Effect of NCO/OH ratios

Table 4.11 shows the electrical conductivity of polyurethane-$LiClO_4$ films. The values decreased from PU200-5 (2.00×10^{-7} $S.cm^{-1}$) to PU85-5 (1.10×10^{-9} $S.cm^{-1}$). PU1-5 which has the highest NCO/OH ratio induces coordination between urethane group and lithium ion leading to greater ion transport of lithium ions in the PU200-5. All samples of PU-$LiClO_4$ experienced lithium ion transport in polyurethane due to the increase in crystallinity of polyurethane-$LiClO_4$ as verified by DSC and XRD analysis (Saunier et al. 2002). Lithium ion could undergo intrachain or interchain ion transport as shown in Figure 4.12.

(a) (b)

Figure 4.12 (a) Intrachain lithium ion transport and (b) Interchain lithium ion transport

This impedance analysis proves that NCO content in PU can be varied to optimize the electrical conductivity of the PU-$LiClO_4$.

4.9.2 Effect of $LiClO_4$ loading

The effect of adding $LiClO_4$ in the PU on the electrical conductivity of PU200-0, PU200-5 and PU200-10 was determined and studied as shown in Appendix I1 to I6. However, due to the uneven surfaces caused by the incomplete polymerization in PU200-15, PU200-20, PU200-25 and PU200-30 as shown in Figure 4.1 (c) and 4.9 (d) to (g), their electrical conductivity could not be determined. In reference to the XRD analysis, even though there was reduction in crystallinity of PU-$LiClO_4$, the addition of

lithium salt is expected to give higher electrical conductivity (Wang et al. 2011). However, Table 4.5 shows that PU200-5 (2.00×10^{-7} $S.cm^{-1}$) has slightly higher electrical conductivity than PU200-10 (1.74×10^{-7} $S.cm^{-1}$) at room temperature because the Li^+ ion interacted with the N=C=O of MDI in PU200-10 as indicated in the FTIR analysis. There was less hard segment (urethane group) in PU200-10 (64.29%) compared to PU200-5 (69.18%) as verified through the gel content determination. Thus, the ion transport between Li^+ ion and urethane group is hardly to take place. Furthermore, small bubbles formed in PU200-10 as shown in Figure 4.9 (c) might restrict the lithium ion mobility. PU200-0 did not contain lithium salt therefore it showed the lowest conductivity. In addition, PU is an insulated material (Silva et al. 2012) and it does not conduct electricity.

Table 4.5 Electrical conductivity of PU-$LiClO_4$

Samples	Conductivity ($S.cm^{-1}$) at 298 K
PU200-0	1.86×10^{-10}
PU200-5	2.00×10^{-7}
PU200-10	1.74×10^{-7}
PU150-5	1.95×10^{-8}
PU100-5	2.65×10^{-9}
PU85-5	1.10×10^{-9}

4.10 Tensile Analysis

4.10.1 Effect of NCO/OH ratios

Tensile modulus, stress and strain of PU200-5, PU150-5, PU100-5 and PU85-5 are as shown in Appendix J1 and summarized in Table 4.6. Tensile modulus of PU-$LiClO_4$ films decreased with decreasing MDI content. MDI is the main component in the formation of hard segment in polyurethane. Hard segment determined the rigidity of PU. Hence, higher isocyanate content resulted in higher rigidity of PU (Petrovic et al. 2002). Thus, the polymer has higher resistance to deformation. Hence more stress could be transfer to the PU as shown in Table 4.6. Furthermore, lower MDI content would increase the flexibility of polyurethane. Hence, PU85-5 demonstrated greatest elongation with tensile strain at 281 % compared to PU100-5 at 217 %, PU150-5 at 215 % and PU200-5 at 170 %.

4.10.2 Effect of $LiClO_4$ Loading

Tensile modulus, stress and strain of PU200-0, PU200-5 and PU200-10 are as shown in Appendix J2 and Table 4.6. The tensile modulus of PUs increased with increasing $LiClO_4$ content. PU200-10 has the highest tensile modulus compared to other polyurethanes. $LiClO_4$ increased the stiffness of PU. This is associated to the coordination between PU and Li^+ ion that enhanced the interaction between PU and lithium salt. Addition of metallic salt enhanced the tensile modulus of PU (Saha et al. 2008). The tensile stress of PU-$LiClO_4$ increased too with increasing $LiClO_4$ loading. This result is tally with the pendulum and pencil hardness results. However, PU200-10 has a slightly lower tensile stress than PU200-10. This is attributed to the formation of shorter chains in PU200-10 as supported by the FTIR analysis compared to PU200-5.

Table 4.6 Tensile Modulus, stress and strain of PU200-0. PU200-5 and PU200-10, PU150-5, PU100-5 and PU85-5

Sample	Tensile Modulus (MPa)	Tensile Stress (MPa)	Tensile Strain (%)
PU200-0	1	2	277
PU200-5	2	5	170
PU200-10	10	5	106
PU150-5	2	2	215
PU100-5	2	2	217
PU85-5	1	2	281

4.11 Pendulum Hardness

Pendulum hardness refers to its resistance to deformation upon pressure by pendulum load. Table 4.7 shows the hardness of PU-$LiClO_4$ films increased with decreasing NCO/OH ratio. This is attributed to an increasing functionality of the polyol with increasing OH number, and it facilitates greater interaction between polyurethane chains by the formation of hydrogen bond (Lee & Kim 1995) and increases cohesive force between the polymeric chains (Suzana et al. 2016). Hence, PU85-5 had the greatest pendulum hardness among all the 5 wt% PU-$LiClO_4$.

Table 4.14 below reveals that PU200-10 had greater pendulum hardness than PU200-5 and PU200-0. The inclusion of $LiClO_4$ in the PU system increased the pendulum hardness of polyurethane. This is because of greater formation of coordinate bonds between polyurethane and lithium ion that increases the crosslinking between polyurethane chains. Hence, more stress could be transferred to the polyurethane.

However, PU200-15, PU200-20, PU200-25 and PU200-30 could not be tested by the pendulum hardness tester because they had uneven surfaces.

Table 4.7 Pendulum hardness of PU200-0. PU200-5 and PU200-10, PU150-5, PU100-5 and PU85-5

Sample	Pendulum hardness (%)
PU200-0	3.1
PU200-5	8.9
PU200-10	22.0
PU150-5	9.3
PU100-5	11.7
PU85-5	16.2

4.12 Pencil Hardness

Pencil hardness is the measure of the film resistance to the deformation caused by the applied pencil tip pressure. The results shown in Table 4.8 shows that PU85-5 has the highest pencil hardness compared to other PU-$LiClO_4$ with 5 wt% of lithium salt. These findings are consistent with the pendulum hardness results. Hence, PU85-5 with lower isocyanate content possessed greater flexibility. Benzene rings in MDI restricts the chain mobility, resulting in rigid and brittle material at higher NCO content. Thus, at lower MDI content, more elastic material is produced.

Pendulum hardness test could not be performed onto the PU200-15, PU200-20, PU200-25 and PU200-30 due to their uneven surfaces. Thus, only pencil hardness test was conducted. Table 4.8 reveals that hardness of PU200-10 had greater pencil hardness (H) than PU200-5 (6B) and PU200-0 (6B) which is tally with the pendulum hardness test result. It indicated the crystalline properties of $LiClO_4$ increases the rigidity of polyurethane. Besides, greater amount of $LiClO_4$ induces greater coordination between lithium ion and polyurethane chains. Hence, larger force could be absorbed by the polyurethane chain.

Table 4.8 Pencil hardness of PU200-0. PU200-5 and PU200-10, PU150-5, PU100-5 and PU85-5

Sample	Scale of hardness
PU200-0	6B
PU200-5	6B
PU200-10	H
PU150-5	6B
PU100-5	5B
PU85-5	4B

CHAPTER V

SYNTHESIS AND CHARACTERIZATION OF SELF-HEALING POLYURETHANE

This chapter is about the synthesis of self-healing polyurethane and optimization of the self-healing polyurethane with different 6,7-dihydoxycoumarin as an independent variable. The polymers are characterized by different analyse such as FTIR spectroscopy analysis; soxhlet analysis, DSC and TGA analysis; optical microscope; SEM-EDX; impedance analysis; tensile test; pendulum and pencil hardness tests. From this section onwards, four different self-healing polyurethanes with different NCO/DHCs ratios of 200/24 (PU200C24-5), 200/48 (PU200C48-5), 200/72 (PU200C72-5) and 200/96 (PU200C96-5) were synthesized, characterized and discussed. PU1-5 which did not have 6,7-dihydroxycoumarin was used as a control. All the films were flexible, flat, free-standing and have homogeneous surfaces except PU200C96-5 which was rigid. PEG and PKO-p contribute flexibility whereas 6,7-dihydroxycoumarin contributes rigidity to the polymer. To an extent, it is possible that coumarin becomes a hindrance for the PEG to function as chain extender and the existence of chain entanglement might be possible. That restricts the mobility of polymeric chains.

5.1 FTIR analysis

Figure 5.1 (a) and (b) show that the urethane group was detected in PU200-5, PU200C96-5, PU200C72-5, PU200C48-5 and PU200C24-5 with the emergence of N-H peak at 3350 cm^{-1}, carbonyl peak at 1707 cm^{-1}, C=C of aromatic ring peak at 1529 and 1508 cm^{-1} , carbamate (C-N) peak at 1600 cm^{-1} (overlapped with C=C of pyrone in coumarin) and C-O-C of urethane at 1060 cm^{-1}. The disappearance of NCO peak at

2250-2270 cm^{-1} in Figure 5.1 indicates the complete step-growth polymerization of self-healing polyurethanes has taken place. The detected carbonyl peak is hydrogen bonded carbonyl urethane group (Radice & Bradley; Wong & Badri 2012). According to previous studies (Clemitson 2008; Radice & Bradley 2007; Wong & Badri 2012), the existence of the peak at ~1740 cm^{-1} is referred to as non-hydrogen bonded urethane stretching where the peak around 1700 cm^{-1} is assigned to hydrogen bonded urethane stretching. This indicates the occurrence of intermolecular interaction during the curing process. The wagging vibration of =C-H peak of 6,7-dihydroxycoumarin in self-healing PU-$LiClO_4$ films were detected at ~830 cm^{-1}. Upon exposure to UV irradiation, the small increase in percentage transmittance of =C-H in PU200C72-5 is attributed to the formation of cyclobutane formed by dimerization of coumarins as shown in Figure 5.2 (Smith 2015; Ling et al. 2011). However, PU200C24-5, PU200C48-5 and PU200C96-5 did not exhibit any increase in the percentage of transmittance for =C-H peak as shown in Figure 5.1 (a), (b) and (c) and (e). This is because there is an insufficient amount of coumarin in PU200C24-5, PU200C48-5 and the high rigidity of PU200C96-5 protects them from undergoing dimerization process. Moreover, the intensities of carbonyl urethane and C=C of aromatic ring peaks in PU200-5, PU200C24-5 and PU200C48-5 decreased drastically upon exposure to UV irradiation compared to PU200C72-5. This indicates the degradation of urethane group as reported by Rashvand (2014) & Newman (2001). The photo-degradation mechanism of the aromatic diisocyanate based polyurethane was proposed by Osawa (1977) and as shown in Figure 5.3, 5.4 and 5.5.

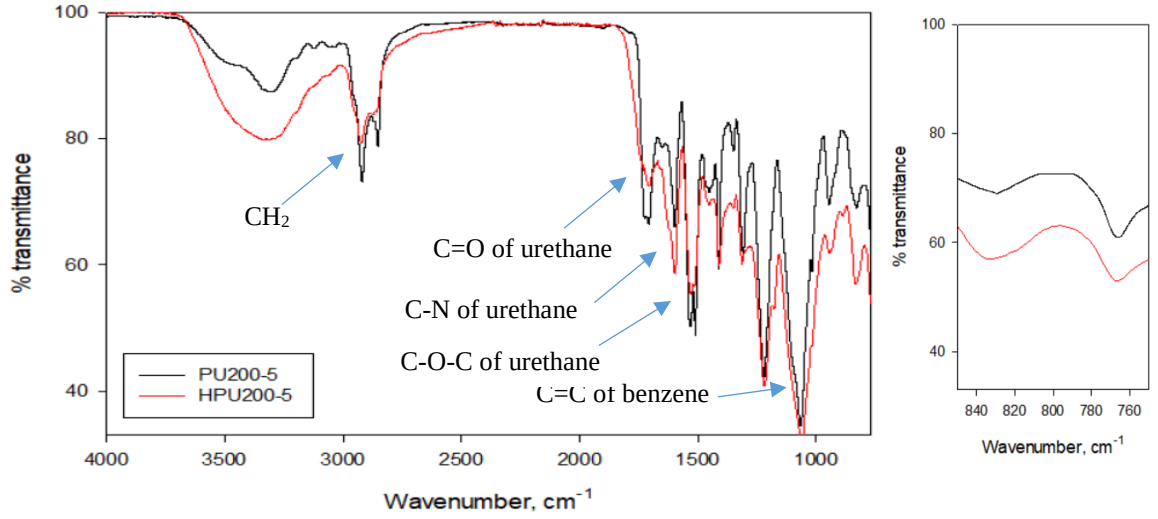

(a)

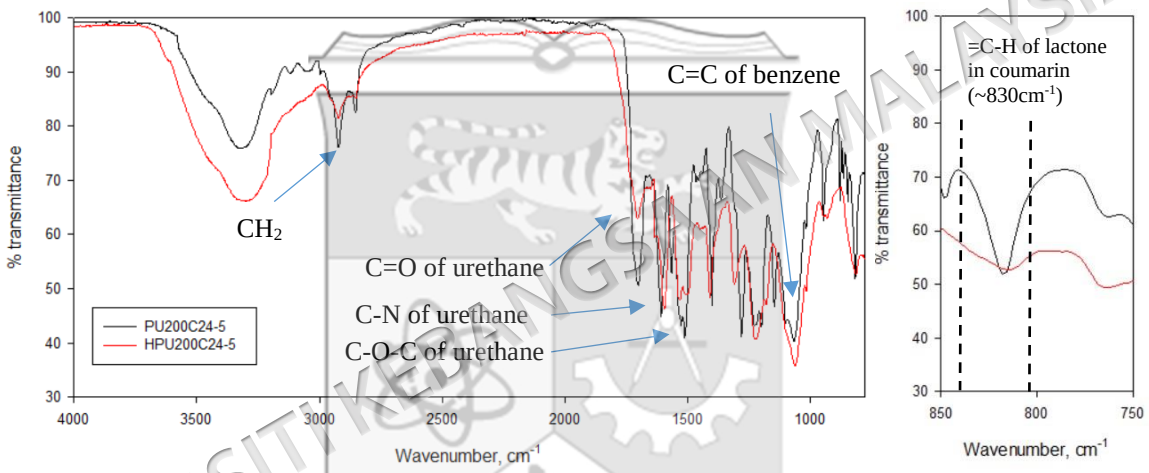

(b)

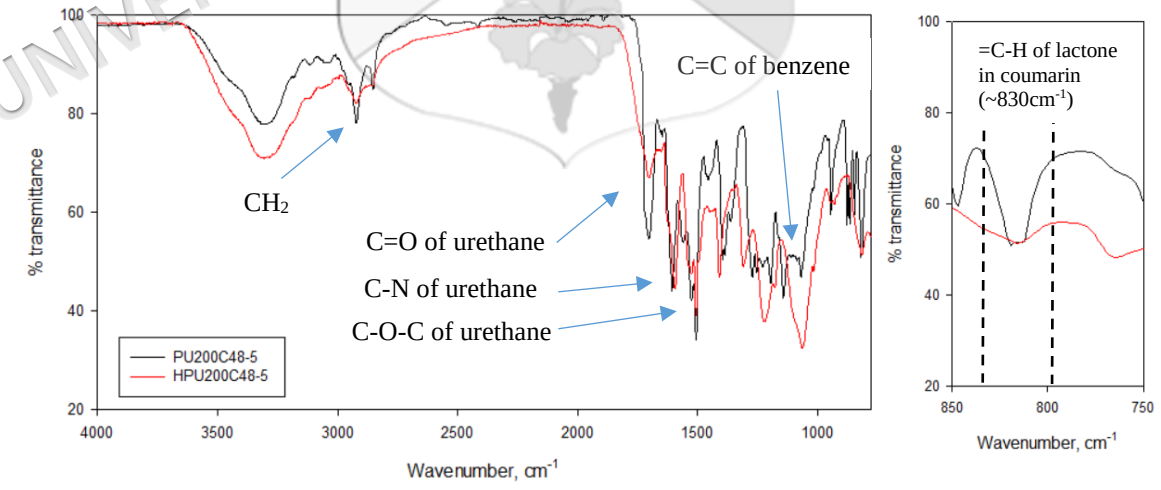

(c)

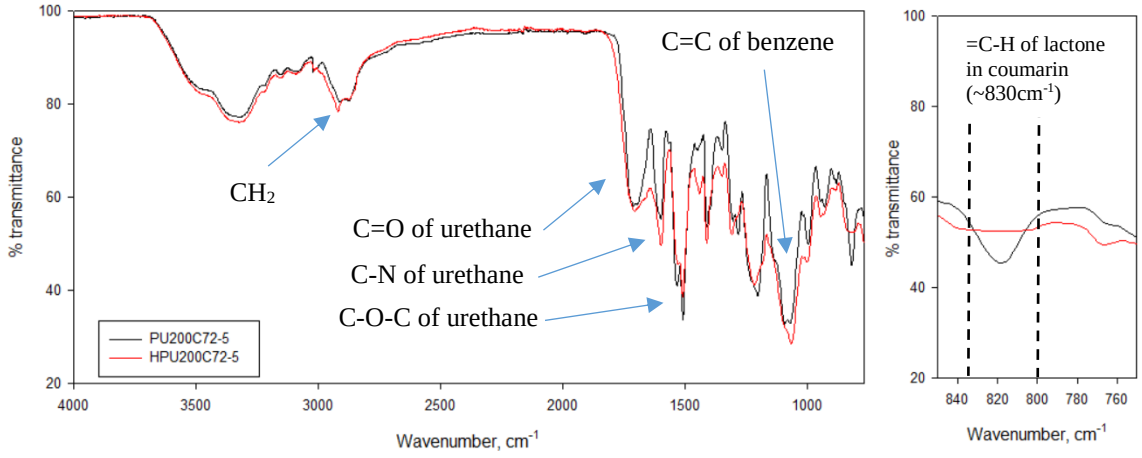

(d)

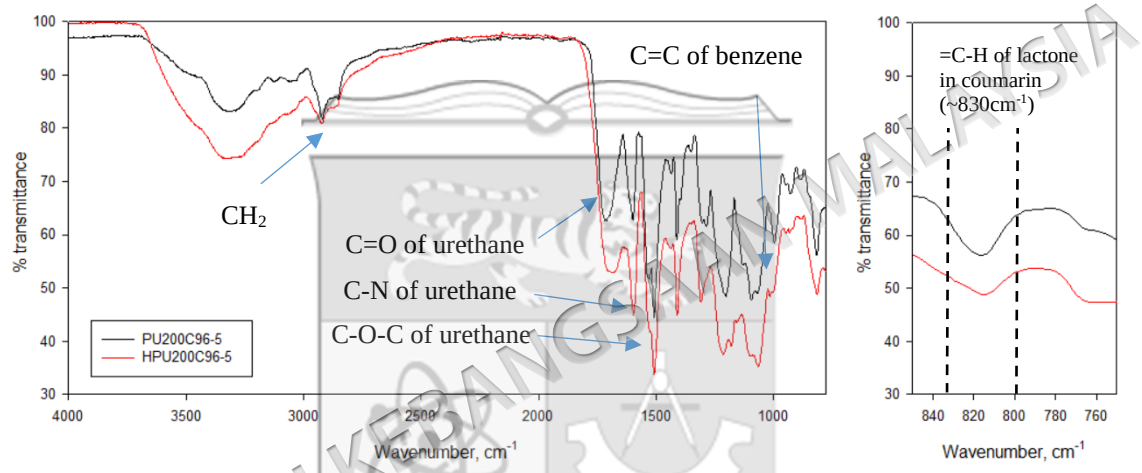

(e)

Figure 5.1 FTIR spectrum of non UV-irradiated and UV-irradiated (a) PU200-5,(b) PU200C24-5 (c) PU200C48-5, (d) PU200C72-5 and (e) PU200C96-5

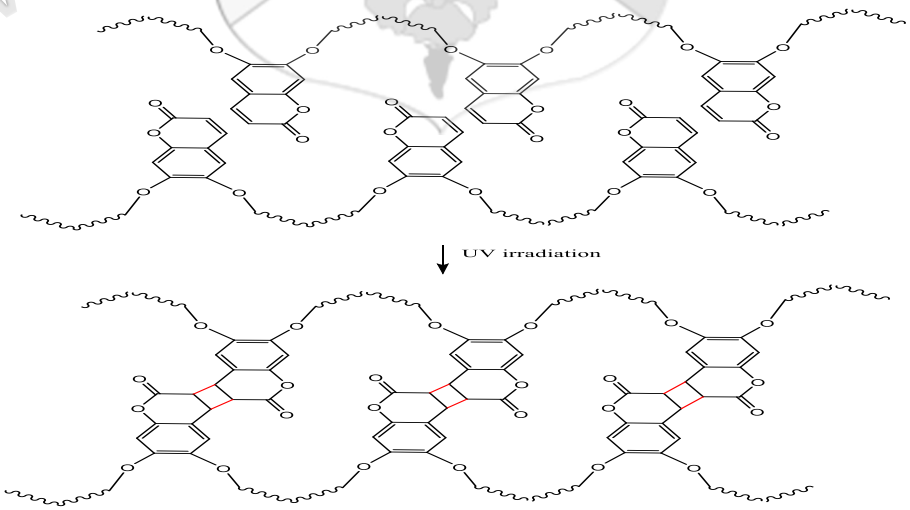

Figure 5.2 Dimerization mechanism between polyurethane chains

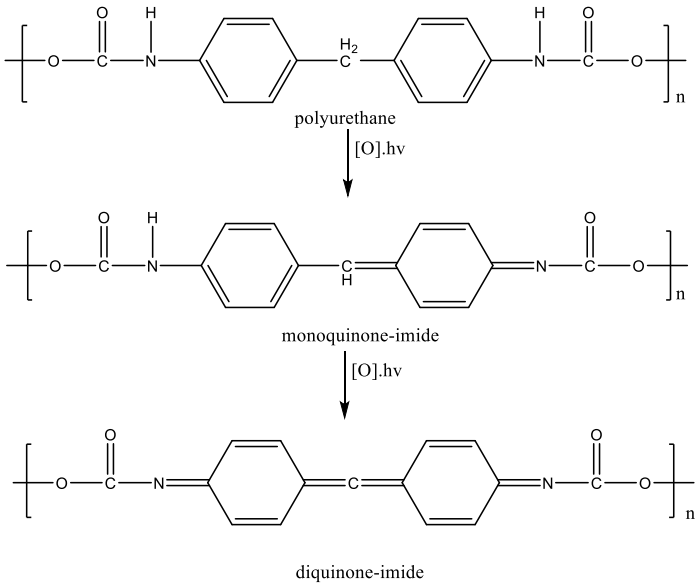

Figure 5.3 The oxidative photo-degradation mechanism of polyurethane

Besides that, another possible photo-degradation mechanism of polyurethane delivers CO and CO_2 as shown in Figure 6 and Figure 7.

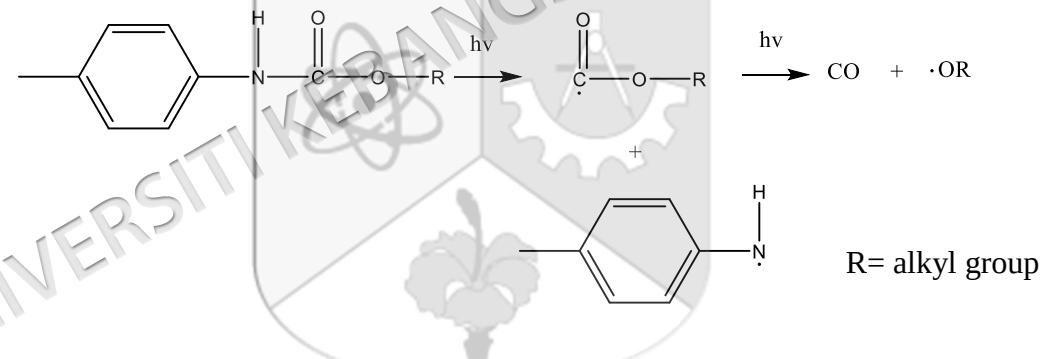

Figure 5.4 Photo-degradation mechanism of polyurethane forming CO, alkoxy and amino radicals

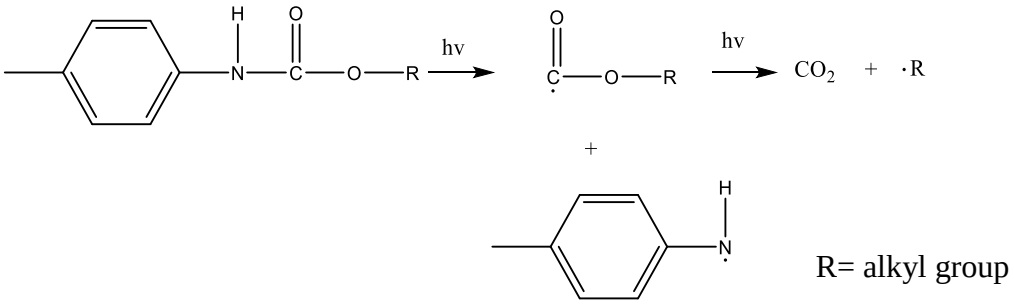

Figure 5.5 Photo-degradation mechanism of polyurethane forming CO_2, alkoxy and amino radicals

The alkoxy, amino and alkyl radicals formed as shown in Figure 5.4 and 5.5 could undergo further degradation reaction by forming diazo compounds (Newman et al. 2001; Rashvand et al. 2014). Besides that, the ordered complexed C=O of urethane was not detected in all self-healing polyurethanes. Coumarin disrupts the coordination between urethane group and Li^+ ion as the carbonyl group of ester in 6,7-dihydroxycoumarin competed with carbonyl group of urethane for the interaction.

Dimerization of coumarin could take place due to the photochemical [2+2] cycloaddition. Cycloaddition of 2 alkenes involves Highest Occupied Molecular Orbital (HOMO) and Lowest Unoccupied Molecular Orbital (LUMO) interaction. Before the dimerization of coumarin took place, the electron in π bonding orbital (π) is excited to π antibonding orbital (π*) with higher energy level through exposure to UV light. Thus, the lobes from HOMO and LUMO with same algebraic sign could overlap to form 2 sigma bonds which is called suprafacial bond formation as shown in Figure 5.6 (Jacobs 1997; Fleming 2015).

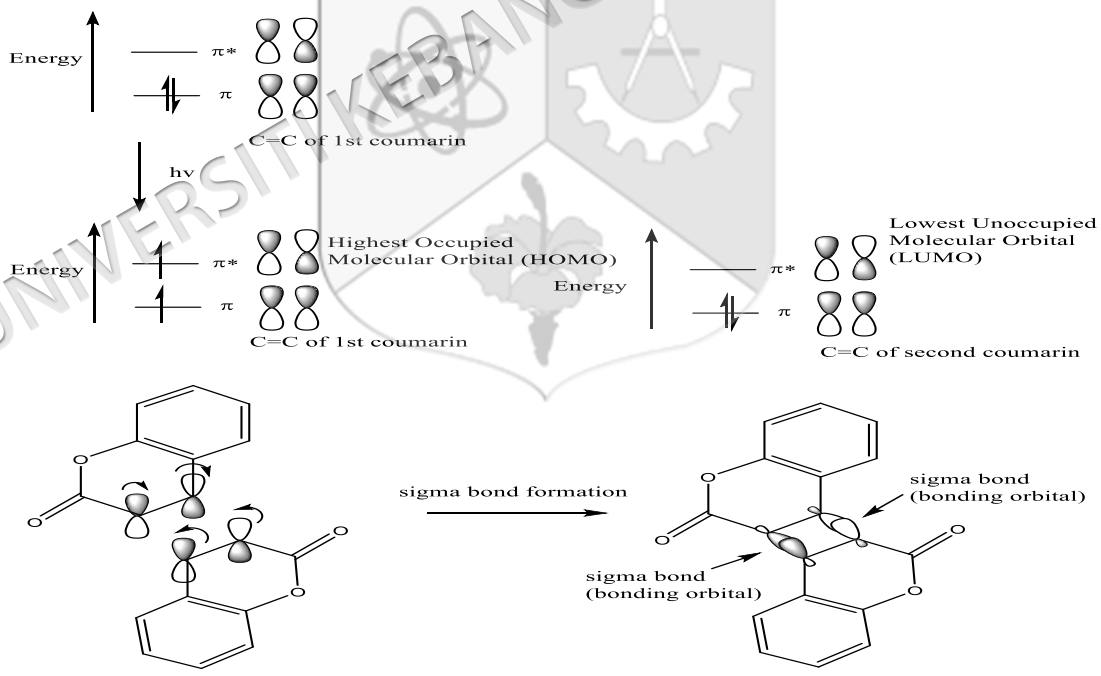

Figure 5.6 Mechanism of formation of bonding orbital between coumarin via photochemical [2+2] cycloaddition

However, [2+2] cycloaddition of coumarin could not happen by heating. This is because heating is not sufficient to excite electron π bonding orbital to π antibonding

orbital (π*). Hence, the HOMO and LUMO could not overlap to form 2 sigma bonds due to the formation of antibonding orbital that causes electron repulsion as shown in Figure 5.7 (Jacobs 1997; Fleming 2015).

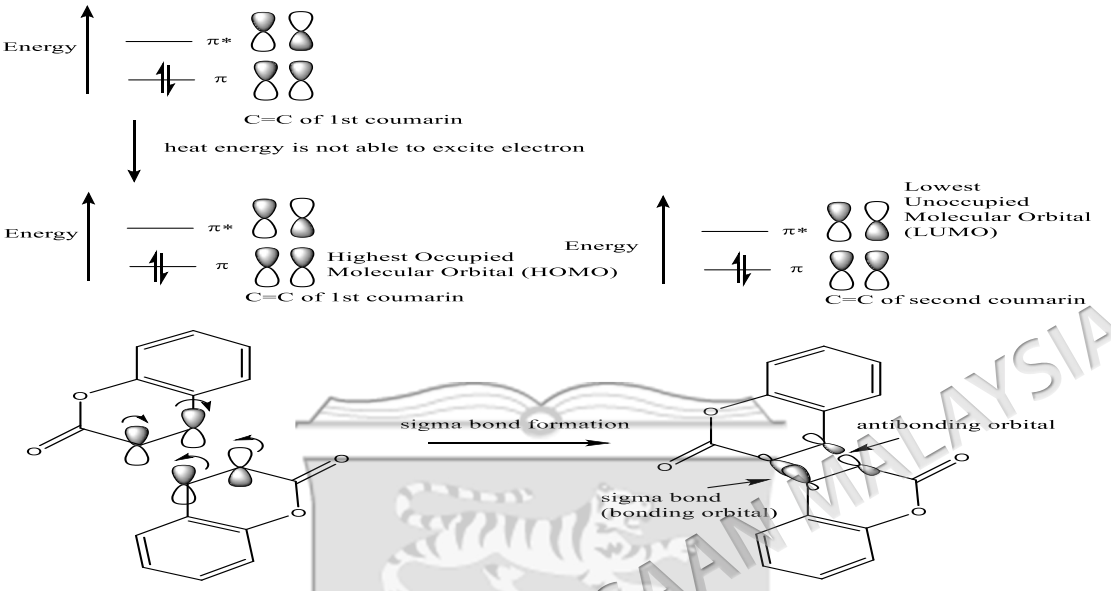

Figure 5.7 Mechanism of formation of bonding orbital and antibonding orbital between coumarin via thermal [2+2] cycloaddition

5.2 Cross-linking analysis

The soxhlet analysis shown in Table 5.1 revealed higher solid content of non UV irradiated self-healing polyurethanes compared to pristine PU due to rigidity of 6,7-dihydroxycoumarin in the polymer host. PU200-5, PU200C48-5 and PU200C24-5 showed a decrease in the gel content after exposure to UV irradiation as shown in Table 5.3. UV radiation releases energy in term of heat and initiated degradation. Hence, the degree of crosslinking in UV irradiated PU200-5, PU200C48-5 and PU200C24-5 became lower. However, PU200C72-5 and PU200C96-5 were able to maintain its resistance to UV degradation. This proves PU200C72-5 and PU200C96-5 which have higher amount of 6,7-dihydroxycoumarin could absorb more UV energy compared to PU200C48-5 and PU200C24-5. So, the crosslink in UV irradiated PU200C96-5 and PU200C72-5 could be retained.

Table 5.1 The gel content of non UV-irradiated and UV irradiated self-healing polyurethanes and control polyurethane

Samples	Gel content (%)	
	Non UV irradiated	UV irradiated
PU200-5	69.18	65.45
PU200C24-5	74.33	69.88
PU200C48-5	75.40	70.23
PU200C72-5	77.27	77.20
PU200C96-5	80.34	81.79

5.3 DSC analysis

The glass transition temperature for the self-healing polyurethanes are tabulated in Table 5.2 and shown in Appendix E3. The glass transition temperature of non UV irradiated PU200C96-5, PU200C72-5, PU200C48-5 and PU200C24-5 were above room temperature indicating the glassy state of self-healing PU-$LiClO_4$ films. T_g of polyurethane is affected by the mobility of the PKO-p polymeric chain and the urethane backbones in the macromolecular structure. The T_g of the self-healing polyurethanes were detected at 58.8 ºC for NCO/DHC ratio of 200/24, 59.7 ºC for 200/48, 61.0 ºC for 200/72 and 68.7 ºC for 200/96. Aliphatic polymers with single bonds have high degree of rotation. However, the presence of cyclic or aromatic structure in the polyurethane chain hindered this rotation (Pang et al. 2012). An increase in the DHC loading in the PU-$LiClO_4$ increased the T_g of the PU films. Hence, higher amount of 6,7-dihydroxycoumarin would restrict the segmental mobility of polyurethanes. The highest content of 6,7-dihydroxycoumarin in PU200C96-5 has 77.3 % gel (as discussed in the previous section) yielded the highest T_g with hard, stiff and brittle film characteristics. Acetone has been completely removed from the polyurethane system during curing process with absence of the endothermic peak at 56 °C for the boiling point of acetone. The absence of crystallization and melting temperatures (T_c and T_m) indicated that these self-healing polyurethanes are thermosetting materials. However, the UV-irradiated PU200-5, PU200C24-5 and PU200C48-5 experienced decrease in T_g as shown in Table 5.5 and Appendix E4. It is attributed to the insufficient amount of 6,7-dihydroxycoumarin in absorbing the UV irradiation that led to the photo-oxidation/degradation of PU chains as shown in Figure 5.2, 5.3 and 5.4 that resulted in lower T_g. However, PU200C72-5 and PU200C96-5 did not experience any decrease in

T_g due to their ability to absorb the UV irradiation that imposed onto the self-healing polyurethanes. Hence, the chains could remain intact. This result is tally with the soxhlet test and FTIR results. Furthermore, the UV-irradiated PU200C96-5 which has highest amount of dihydroxycoumarin experienced an increase in T_g from 68.7 °C to 76.6 °C. This is attributed to π to π stacking interaction between benzene rings of coumarins which are in planar shape (Rafael et al. 2017). This phenomenon restricted chain movement in UV irradiated PUC0-5 (Yamaguchi et al. 2009).

Table 5.2 Glass transition temperature of various non UV-irradiated and UV irradiated self-healing polyurethanes and control polyurethane

Sample	Glass transition temperature, Tg (°C)	
	Non UV irradiated	UV irradiated
PU200-5	49.1	35.8
PU200C24-5	58.8	36.1
PU200C48-5	59.7	39.3
PU200C72-5	61.0	61.2
PU200C96-5	68.7	76.6

5.4 Thermogravimetric analysis

Appendix F3-13 shows TGA thermograms and differential thermogravimetric (DTG) curves for non UV-irradiated and UV-irradiated self-healing polyurethanes containing different amount of 6,7-dihydroxycoumarin. The percentage of weight loss (wt.%) is summrarized in Table 5.6 and Table 5.7. The first thermal degradation (T_{d1}) stage of PU was observed at the region of 150 to 230 °C with thermal stability in the range between 150 °C -160 °C and achieved the maximum temperature at T_{max}, around 200 °C for all non UV-irradiated self-healing polyurethanes. Generally, the T_{max} declined from PU200-5 to PU200C96-5 because aliphatic polyurethane has greater thermal stability than aromatic polyurethane (Frish 1969; Lamba et al. 1998; Srinivasan 1998). The inclusion of 6,7-dihydroxycoumarin into polyurethane will reduce the thermal stability of urethane group in the polyurethane. It is obviously shown in the lowering of temperature for T_{d1}. T_{d1} corresponds to degradation of the hard segment that comprised of urethane linkages which resulted in three decomposition mechanisms for urethane bonds: (i) dissociation to isocyanate and alcohol, (ii) formation of primary amine, carbon dioxide and (iii) formation of secondary amine and carbon dioxide

(Chattopadhyay & Webster 2009; Chuayjuljit et al. 2007; Corcuera et al. 2011; Lu et al. 2002; Pan & Webster 2012; Rueda-Larraz et al. 2009).

The second step of T_{d2} for all self-healing polyurethanes was detected in the range of 230-430 °C. This region corresponds to the liberation of free isocyanate that led to the formation of thermally stable carbodiimide derivatives or compounds with isocyanurate rings as a result of a trimerization reaction (Apukhtina 1973). The third degradation (T_{d3}) stage started at the region of 430-520 °C which is contributed by the thermal decomposition of soft segments of PU (ester linkages), which is seldom being affected by the chemical composition and the three dimensional arrangement of polyurethane structure (Corcuera et al. 2011; Liu et al. 2002). The total weight loss decreased from 71.4 % to 61.6 % at higher amount of 6,7-dihydroxycoumarin. 6,7-dihydroxycoumarin has high degradation temperature as shown in the Figure 5.8 (k). 6,7-dihydroxycoumarin is a molecule containing functional groups such as ester, benzene and cyclic structure which increase the rigidity of self-healing polyurethane. Higher aromatic proposition in polyurethane resulted in higher thermal stability (Frisch 1969). Sharp DTG peak of 6,7-dihydroxycoumarin as shown in Figure 5.9 (k) was not detected in the DTG curves of all self-healing PUs indicating possible complete polymerization in the 6,7-dihydroxycoumarin containing PUs.

However, when PU200-5, PU200C24-5 and PU200C48-5 were exposed to UV irradiation, the total weight loss decreased by 4 to 10%. This is due to the susceptibility of PU200-5 PU200C24-5 and PU200C48-5 to UV irradiation attack and the damage induced free radical termination reaction (Boubakri et al. 2010; Rosu et al. 2005; Rashvand et al. 2014) that forming imide group in the polymer. The imide formed has excellent heat resistance that induced lower weight loss (Liao et al. 2007) in UV-irradiated PU200-5, PU200C24-5 and PU200C48-5 (HPU200-5, HPU200C24-5 and HPU200C48-5). UV irradiated PU200C48-5 gave highest residue percentage (39.4%) during thermal degradation. This might be attributed to the interaction of coumarin in PU with the amino radical formed during photodegradation forming dihydroquinolines which has high melting point via Skraup–Doebner–von Miller reaction (Nasim et al. 2014).

Table 5.3 Weight loss of various (a) non UV-irradiated self-healing PU-$LiClO_4$ films and pristine polyurethane and (b) UV-irradiated self-healing PU-$LiClO_4$ films and pristine polyurethane

(a)

Sample	T_{max}, °C	T_{d1}, 150-230°C	T_{d2}, 230-430°C	T_{d3}, 430-520°C	Total weight loss (%)	Residue after 520°C (%)
PU200-5	219.7	5.0	49.1	17.3	71.4	28.6
PU200C24-5	204.3	4.3	51.1	13.5	68.9	31.1
PU200C48-5	203.0	4.7	51.8	13.4	69.9	30.1
PU200C72-5	195.2	5.6	46.7	12.5	64.8	35.2
PU200C96-5	199	6.5	43.8	11.2	61.6	38.4

(b)

Sample	T_{max}, °C	T_{d1}, 150-230°C	T_{d2}, 230-430°C	T_{d3}, 430-520°C	Total weight loss (%)	Residue after 520°C (%)
HPU200-5	195.0	4.7	47.8	14.0	66.5	33.5
HPU200C24-5	199.2	5.4	44.4	15.7	65.5	34.5
HPU200C48-5	196.6	5.1	40.5	15.0	60.6	39.4
HPU200C72-5	196.6	5.1	47.3	11.7	64.2	35.9
HPU200C96-5	199.9	5.7	42.2	14.5	62.3	37.7

5.5 Optical Microscopy analysis

The microscopy images in Appendix H1 and Figure 5.8 reveal the average width of cut wound in samples was around 10-20 μm. After exposure to UV irradiation, the Appendix H1 show the cut wounds of UV-irradiated of PU200-5, PU200C24-5, PU200C48-5 respectively still remained intact. But the important discovery was the cut wound of UV-irradiated PU200C72-5 healed completely as shown in Figure 5.8. This result is tally with the soxhlet and FTIR analysis that indicated the ability of UV-irradiated PU200C72-5 in resisting photodegradation and efficient healing capability. Another discovery was the UV-irradiated PU200C96-5 failed to recover the cut wound even though it contains the highest amount of 6,7-dihydroxycoumarin as supported by FTIR and DSC analyse. It might be attributed to high rigidity of 6,7-dihydroxycoumarin that restricted the polymer chain mobility (Wu et al. 2008). Hence, the dimerization of PU200C96-5 was harder to take place between the polymeric chains compared to PU200C72-5.

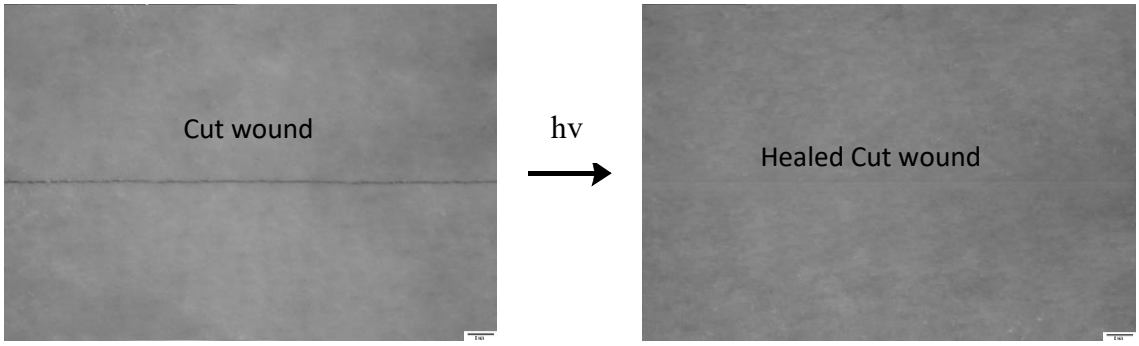

(a) (b)

Figure 5.8 Optical micrographs of (a) non UV-irradiated PU200C72-5, and (b) UV-irradiated PU200C72-5

5.6 SEM-EDX Morphology analysis

Figure 5.9 and Appendix H2 show the SEM micrographs and elemental composition of non UV irradiated and UV irradiated of pristine PU and self-healing PU200C24-5, PU200C48-5, PU200C72-5 and PU200C96-5 respectively. SEM-EDX analysis was carried out to investigate the healing ability of the self-healing PU films. The SEM-EDX images as shown in Figure. 5.9 proved the ability of PU200C72-5 to heal the cut wound by itself compared to other self-healing polyurethanes and PU200-5 through photo-cycloaddition reaction (Ling et al. 2012). Besides that, UV-irradiated PU200C96-5 exhibited slight healing as it contains the greatest amount of hydroxyl group coumarin enabled it to have more dangling chains. These dangling chains was able to diffuse between the polyurethane chains. But the dangling chains were not sufficient to heal the cut wound (Yamaguchi et al. 2009). The formation of cyclcobutane ring between coumarins is more favourable compared to unsaturated fatty acids in the PKO-based polyol such as oleic acid which is the main fatty acid in palm kernel oil, this is due to the the π- π* (pi to pi star) UV absorption wavelength of oleic acid is around 270 nm (equal to 443.06 $kJ.mol^{-1}$) (Coelho et al. 2011) which needs much higher energy to excite electron compared to coumarin that absorbs at 350 nm (equal to 341.79 $kJ.mol^{-1}$) to have π- π* transition. Hence, it is harder for the unsaturated fatty acid in polyol to undergo dimerization.

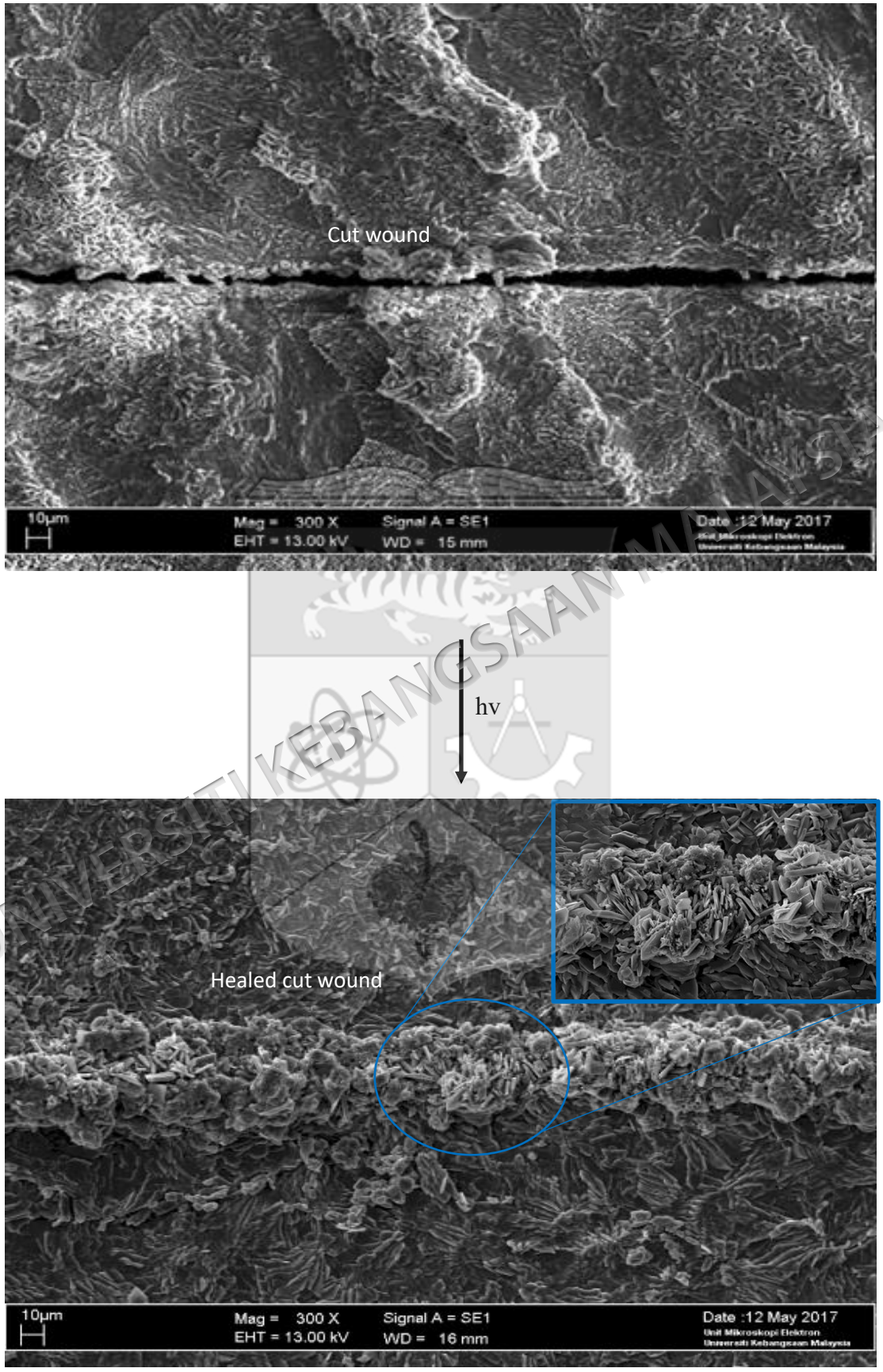

Figure 5.9 Scanning Electron Microscope images of UV irradiated PU200C72-5

5.7 Impedance analysis

The measured electrical conductivity of polyurethanes is shown in Appendix I1 and I7-I15 and summarized in Table 5.4. The conductivity of polymers is in the range of 10^{-7} to 10^{-8} S.cm^{-1} due to the incorporation of 5 wt% $LiClO_4$ in polyurethane. However, the UV irradiated PU200-5 demonstrated greatest decrease in Electrical conductivity compared to other UV irradiated self-healing PUs. This is attributed to the UV degradation of PU200-5 that induces degradation. The degradation of PU caused the lithium ion transport between polymeric chains in PU1-5 became harder. Besides that, UV irradiated PU200C72-5 experienced lowest decrease in Electrical conductivity due to the formation of cyclobutene rings between polymeric chains that increase the degree of crosslinking and restrict the lithium ions mobility in the polymer host (Vandiver et al. 2015). UV irradiated PU200C48-5 has great reduction in electrical conductivity during thermal degradation. This might be attributed to the interaction of dihydroxycoumarin in PU with the amino radical formed during photodegradation of PU200C48-5 forming dihydroquinolines (Nasim et al. 2014). This compound might hinder the lithium ion mobility.

Table 5.4 Electrical conductivity of non UV-irradiated and UV-irradiated PU200-5, PU200C24-5, PU200C48-5, PU200C72-5 and PU200C96-5

Samples (Non UV irradiated)	Electrical Conductivity, S.cm^{-1}	Samples (UV irradiated)	Electrical Conductivity, S.cm^{-1}	Reduction in electrical conductivity (%)
PU200-5	2.00×10^{-7}	HPU200-5	1.59×10^{-10}	99.92
PU200C24-5	1.74×10^{-8}	HPU200C24-5	4.30×10^{-9}	75.86
PU200C48-5	8.78×10^{-8}	HPU200C48-5	5.62×10^{-9}	93.60
PU200C72-5	2.08×10^{-7}	HPU200C72-5	9.77×10^{-8}	53.03
PU200C96-5	4.18×10^{-8}	HPU200C96-5	1.94×10^{-8}	53.59

5.8 Tensile analysis

Appendix J3 and Table 5.5 indicated that the tensile modulus of non UV-irradiated self-healing PUs increased at higher amount of 6,7-dihydroxycoumarin due to greater rigidity of hard segment which was contributed by 6,7-dihydroxycoumarin that cause greater resistance to deformation. Hence, PU200C96-5 showed the highest tensile modulus. However, after these PUs were irradiated by UV light, the tensile modulus of

PU200-5, PU200C24-5 and PU200C48-5 increased but their tensile stress and strain decreased as revealed in Table 5.6. The photodegradation of PU200-5, PU200C24-5 and PU200C48-5 rupture the chains and the free volume in these polymers decreases. Hence, this increases the sheer force PU200-5, PU200C24-5 and PU200C48-5. Besides, photodegradation of PU200-5, PU200C24-5 and PU200C48-5 could produce diazo compound which is rigid (Sergei 2011) as explained in the FTIR analysis. Thus, the toughness of polymer increases and the viscoelasticity of polymer decreases. Hence, the UV irradiated PU200-5, PU200C24-5 and PU200C48-5experienced decrease in stress and strain (Boubakri et al. 2010) as stated in Appendix J4 and J5. This finding is tally with the FTIR analysis which proved the inefficient amount of coumarin in PU200C24-5 and PU200C48-5restricted the photodegradation of polyurethane. However, PU200C72-5 showed insignificant change in tensile modulus. This is attributed to the stability of the polymeric chains in PU200C72-5 to UV irradiation. Besides that, UV irradiated PU200C96-5 also demonstrated higher tensile modulus upon exposure to UV irradiation. This might be attributed π to π stacking interaction between benzene rings of coumarins (Sergei 2011; Kandasamy et al. 1998) as PU200C96-5 contains the greatest amount of 6,7-dihydroxycoumarin (Yamaguchi et al. 2009). This restricts the mobility of self-healing polyurethane chains and enhances the mechanical strength.

Table 5.5 Tensile modulus, stress and strain of non UV-irradiated self-healing PU-$LiClO_4$ and control polyurethane

Samples	Tensile Modulus (MPa)	Tensile Stress (MPa)	Tensile Strain (%)
PU200-5	2	5	170
PU200C24-5	212	11	40
PU200C48-5	322	10	10
PU200C72-5	458	14	7
PU200C96-5	533	23	5

Table 5.6 Tensile modulus, stress and strain of UV irradiated self-healing PU-$LiClO_4$ and control polyurethane

Samples	Tensile Modulus (MPa)	Tensile Stress (MPa)	Tensile Strain (%)
HPU200-5	10	5	114
HPU200C24-5	266	3	5
HPU200C48-5	381	7	7
HPU200C72-5	465	22	11
HPU200C96-5	592	17	2

5.9 Pendulum Hardness

The pendulum hardness increased with higher amount of 6,7-dihydroxycoumarin as shown in Table 5.7. The mobility of self-healing polyurethane decreased at higher amount of 6,7-dihydroxycoumarin. More 6,7-dihydroxycoumarin could resist greater external force applied to it as the benzene ring in the coumarin enhances the rigidity of polymer. This result is consistent with the tensile analysis. After the exposure of UV irradiation, UV irradiated PU200-5, PU200C24-5, PU200C48-5 and PU200C96-5 showed greater increase of hardness compared to PU200C72-5 as shown in Table 5.14. It is because of the photo degradation in UV irradiated PU200-5, PU200C24-5 and PU200C48-5 which induced molecular and chemical changes such as chain scissions (Malassenet et al. 2015). The chain scissions caused higher molecular cohesion in the polyurethane with smaller free volume in the polymer and thus greater hardness and brittleness (Sonmez et al. 2011). This result is tally with pencil hardness and tensile results.

Table 5.7 Pendulum hardness of non UV-irradiated and UV irradiated self-healing PU-$LiClO_4$ and control polyurethane

	Pendulum hardness, %	
Samples	Non UV irradiated	UV irradiated
PU200-5	8.96	14.32
PU200C24-5	27.15	32.12
PU200C48-5	30.34	34.12
PU200C72-5	38.12	38.44
PU200C96-5	44.67	47.61

5.10 Pencil Hardness

PUC0-5 showed the highest pencil hardness in Table 5.8 upon the exposure of UV irradiation, all UV-irradiated PU200-5, PU200C24-5, PU200C48-5 and PU200C96-5 samples have higher pencil hardness whereas UV-irradiated PU200C72-5 maintained its hardness value. This result is consistent with pendulum hardness and tensile analysis. The UV-irradiated PU200-5, PU200C24-5, PU200C48-5 samples undergone photo-degradation that induced smaller free volume in the polymer that caused higher rigidity and brittleness.

Table 5.8 Pencil hardness of non UV-irradiated self-healing polyurethanes and pristine polyurethane

Samples	Scale of Hardness	
	Non UV irradiated	UV irradiated
PU200-5	6B	4B
PU200C24-5	3B	2B
PU200C48-5	3B	2B
PU200C72-5	2B	2B
PU200C96-5	B	F

CHAPTER VI

CONCLUSION

6.1 SUMMARY

A self-healing PU-$LiClO_4$ was successfully developed by prepolymerization technique derived from palm kernel oil based polyol (PKO-p), a promising low-cost sustainable material for the synthesis of polyurethane (PU)

In the first stage, PU-$LiClO_4$ was successfully synthesized via pre-Spolymerization technique by varying the NCO/OH ratio and adding $LiClO_4$ in acetone under nitrogen atmosphere and reacted at room temperature. The effect of different NCO/OH ratio on the formation of urethane linkages (NHCO backbone), degree of cross linking, thermal properties, morphological and electrochemical studies of PU films has been successfully conducted. The formation of urethane linkages (NHCO backbone) after the polymerization was confirmed by the disappearance of v(N=C=O) peaks at ~2241 cm^{-1} and the appearances of (N–H) peaks at ~3300 cm^{-1}, carbonyl v(C=O) at ~1710 cm^{-1}, carbamate (C–N) at ~1600 cm^{-1}, ether (C-O-C) at ~1065 cm^{-1}, v(C=C) benzene ring at ~1535 cm^{-1} and ~510 cm^{-1} in the PU chain. Besides, ordered complexed C=O was detected at ~1650 cm^{-1} in PU due to the coordination between Li^+ ion and carbonyl urethane group. The soxhlet test proved highest NCO/OH ratio. Lowest amount of $LiClO_4$ gave higher gel content due to the hard segment formed by the reaction between isocyanate and the hydroxyl groups and the inhibition of the formation of hard segment in polyurethane which led to shorter polymer chain and lower solid content. Besides, DSC and TGA analyse showed that greater glass transition temperature and thermal degradation temperature were observed

at higher NCO/OH ratio. Moreover, SEM micrographs revealed the cracking in PU-$LiClO_4$ with more than 5wt% of $LiClO_4$ due to the high crystallinity of $LiClO_4$ and shorter polyurethane chain. The appearance of bubbles in SEM micrographs was because of the reaction between free NCO groups of urethane prepolymer and water. PU200-5 gave the highest electrical conductivity compared to PU1-10 due to the incomplete polymerization took place in PU200-10 forming shorter polyurethane chain lead to restriction of lithium ion transport along the polyurethane chain. Mechanical analysis also proved PU with highest NCO/OH ratio had greatest tensile modulus but lowest pendulum and pencil hardness. Hence PU200-5 with NCO/OH (200/100) was chosen as the polymeric host for the synthesis of self-healing PU-$LiClO_4$.

In the second stage, self-healing PU-$LiClO_4$ (HPU) was prepared by mixing PKO-p, PEG, 6,7-dihydroxycoumarin and MDI in acetone flask under nitrogen gas atmosphere to form HPU. The UV irradiated SHPU was prepared by exposure to UV light. FTIR analysis showed the photodegradation of SEwith the reduction of C=O and C=C peaks at ~1710 cm^{-1} and ~1530 cm^{-1} corresponded to the breaking of urethane bond. The FTIR analysis result is supported by the decrease of gel content analysis. It proved the low amount of 6,7-dihydroxycomarin (less than NCO/DHC of 200/72) was insufficient in preventing the photodegradation of HPU. However, PU200C72-5 with NCO/DHC ratio of 200/72 was not just able to withstand UV photodegradation, but also could undero photo-dimerization which is crucial is healing of polymeric film. DSC and TGA analysis also proved HPU with less than NCO/DHC of 200/72 had lower glass transition and degradation temperatures after exposure to UV light due to the degradation of urethane bond that induced shorter chain. Micrograph analysis proved the high efficiency of HPU with NCO/DHC ratio of 200/72 in repairing the cut wound compared to other HPUs . Lastly, HPU with higher 6,7-dihydroxycoumarin experienced lower decrease in electrical conductivity due to its capability in absorbing more photons that induced HPU chains remained intact. This facilitated the lithium ion transport in HPUs. Higher 6,7-dihydroxycoumarin could maintain its mechanical properties even after exposure to UV light as proven by tensile, pendulum and pencil hardness analysis. These properties exhibited promising potentials for this HPU with NCO/DHC ratio of 200/72 in different applications.

6.2 FUTURE STUDIES

In order to increase the healing efficiency of HPU, other coumarins should be explored and modified in order to increase the healing speed of HPU. Besides that, electrical conductivity of HPU could be increased by increasing the polar groups in HPU so the ion transport in polymeric chains is enhanced.

1. An attempt should be made by using a functional compound such as dihydroxyketone that acts a chain extender in synthesizing the polymer to increase the conductivity of self-healing PU-$LiClO_4$.
2. Another alternative to synthesize chain extended dihydroxycoumarin is using more stable reagents such as 1-bromopropanol or 1-bromobutanol. These stable reagents can possibly offer more sites for reaction. Besides that, 5,7-dihydroxy-4-methylcoumarin could be used as a healing agent in the self-healing polyurethane due to the methyl group bonded to the lactone in the coumarin that could enhance the dimerization between coumarins. This will increase the healing efficiency of the self-healing polyurethane.
3. Polyacrylamide or polyacrylic acid which are polar polymers that act as grafting polymer or copolymer to create the self-healing polyurethane. This is to ensure not only the self-healing is achieved, but also to enhance the mechanical properties of the self-healing polymer.

REFERENCES

Abate, A. R. & Weitz, D. A. 2009. High-order multiple emulsions formed in poly(dimethylsiloxane) microfluidics. *Small* 5(18): 2030-2032.

Adebahr, J., Byrne, N., Forsyth, M., MacFarlane, D. R. & Jacobsson, P. 2003. Enhancement of ion dynamics in PMMA-based gels with addition of TiO_2 nano-particles. *Electrochimica Acta* 48(14): 2099-2103.

Adzima, B. J., Aguirre, H. A., Kloxin, C. J., Scott, T. F. & Bowman, C. N. 2008. Rheological and chemical analysis of reverse gelation in a covalently cross-linked Diels− Alder polymer network. *Macromolecules* 41(23): 9112-9117.

Agrawal, R. C. & Pandey, G. P. 2008. Solid polymer electrolytes: materials designing and all-solid-state battery applications: an overview. *Physics D: Applied Physics* 41: 18.

Aguirresarobe, R. H. & Irusta, L. 2014. UV-light responsive waterborne polyurethane based on coumarin : synthesis and kinetics of reversible chain extension. *Journal of Polymer Research* 21: 505-514.

Ahmad, S., Ahmad, S. & Agnihotry, S. A. 2005. Nanocomposite electrolytes with fumed silica in poly (methyl methacrylate): thermal, rheological and conductivity studies. *Journal of Power Sources* 140(1): 151-156.

Ahmad, A., Rahman, M. Y. A. & Su'ait, M. S. 2012. Morphological, Infrared and Ionic Conductivity Studies of PEO–MG49–$LiClO_4$ Based Solid Polymer Electrolyte. *Journal of Applied Polymer Science* 124: 4222-4229.

Ajit, R. K., Balaji, R. & Raman, S. S. 2010. Structural Investigation of Polyurethane Based Gel Polymer Electrolytes Using Small Angle X-ray Scattering. *Journal of the Physical Society of Japan* 79: 154-159.

Alam, M. & Alandis, N.M. 2014. Corn Oil Based Poly(Ether Amide Urethane) Coating Material—Synthesis, Characterization and Coating Properties. *Industrial Crops and Products* 57: 17-28.

Alloin, F., Aprea, A.D., El-Kissi, N., Dufresne, A. & Bossard, F. 2010. Nanocomposite polymer electrolyte based on whisker or microfibrils polyoxyethylene nanocomposites. *Electrochimica Acta* 55: 5186-5194.

Andreeva, D. V., Fix, D., Mohwald, H. & Shchukin, D. G. 2008. Buffering polyelectrolyte multilayers for active corrosion protection. *Journal of Materials Chemistry.* 18(15): 1738-40.

Ang, K.P., Lee, C.S., Cheng, S.F. & Chuah, C.H. 2014. Synthesis of Palm Oil - Based Polyester Polyol for Polyurethane Adhesive Production. *Journal of Applied Polymer Science* 131(6).

Anon. 2017. Lithium perchlorate. https://materialsproject.org/materials/mp-30301/

Apukhtina, N. P. 1973. Methods for Increasing the Thermal Stability of Polyurethanes. In. Gingold, K. (trans.). Schiller, A.M. (Ed. 1). *Soviet Urethane Technology: Soviet Progress in Polyurethanes Series*. Connecticut, USA: Technomic publication.

Aramaki, K. 2008. Preparation of chromate-free, self-healing polymer films containing sodium silicate on zinc pretreated in a cerium(III) nitrate solution for preventing zinc corrosion at scratches in 0.5 M NaCl. *Corrosion Science* 44(6): 1375-1389.

Asahara, H., Iwamoto, T., Kida, T., & Akashi, M. 2013. Unique catalytic effect of a cyclodextrin host on photodimerization of coumarin in nonpolar solvents. *Tetrahedron Letters 54*(7), 688-691.

Ataollahi, N., Ahmad, A., Hamzah, H., Rahman, M. Y. A. & Mohamed, N. S. 2013. Ionic conduction of blend poly (vinylidene fluoride-hexafluoro propylene) and poly (methyl methacrylate) grafted natural rubber based solid polymer electrolyte. *International Journal of Electrochemical Science* 8: 7875-7884.

Ataollahi, N., Ahmad, A., Lee, T. K., Abdullah, A. R. & Rahman, M. Y. A. 2014. Prepration and characterization of PVDF-MG49-$NH_4CF_3SO_3$ based solid polymer electrolyte. *E-polymers* 14(2): 115-120.

Auria, M. D. & Racioppi, R. 2004. The photodimerisation of coumarin. *Journal of Photochemistry and Photobiology A: Chemistry* 163: 557-559.

Aziz,S.B. & Abidin, Z.H.Z. 2013. Electrical conduction mechanism in solid polymer electrolytes: new concepts to Arrhenius equation. *Journal of Soft Matter*.

Badri, K.H. 2011. *Process for the Production of Vegetable Oil-based Polyurethane Polyols*. MY 145094-A

Badri, K.H. 2012. Chapter 20: Biobased Polyurethane from Palm Kernel Oil-Based Polyol. In. Zafar, F. & Sharmin, E. (Ed. 1). *Polyurethane*, pp 447-470. InTech DOI: 10.5772/47966.

Badri, K.H., Ahmad, S.H. & Zakaria, S. 2000. Development of Zero ODP Rigid Polyurethane Foam from RBD Palm Kernel Oil. *Journal of Material Science Letters* 19(15): 1355-1456.

Badri, K.H., Ahmad, S.H. & Zakaria, S. 2001. The Production of a High-Functionality RBD Palm Kernel-Based Polyester Polyol. *Journal of Applied Polymer Science* 82: 827-832.

Badri, K.H., Othman, Z. & Mohd Razali, I. 2005. Mechanical Properties of Polyurethane Composites from Oil Palm Resources. *Iranian Polymer Journal* 14 (5): 441-448.

Badri, K.H., Shahaldin, F.H. & Othman, Z. 2004. Indigenous Coating Material from Palm Oil-Based Polyamide. *Journal of Materials Science* 39 (13): 4331-4333.

Bailey, B. M., Leterrier, Y., Garcia, S. J. & Zwaag, S. Van Der. 2015. Electrically conductive self-healing polymer composite coatings. *Progress in Organic Coatings* 85: 189-198.

Baskaran, R., Selvasekarapandian, S., Kuwata, N., Kawamura, J. & Hattori, T. 2006. Conductivity and thermal studies of blend polymer electrolytes based on PVAc–PMMA. *Solid State Ionics* 177: 2679-2682.

Baskaran, R., Selvasekarapandian, S., Kuwata, N., Kawamura, J. & Hattori, T. 2007. Structure, thermal and transport properties of PVAc–LiClO 4 solid polymer electrolytes. *Journal of Physics and Chemistry of Solids* 68(3): 407-412.

Beiermann, B. A., Keller, M. W., & Sottos, N. R. 2009. Self-healing flexible laminates for resealing of puncture damage. *Smart Materials and Structures* 18(8): 1-7.

Berta, M., Lindsay, C., Pans, G., & Camino, G. 2006. Effect of chemical structure on combustion and thermal behaviour of polyurethane elastomer layered silicate nanocomposites. *Polymer Degradation and Stability* 91: 1179-1191.

Bielawski, C. W. & Grubbs, R. H. 2007. Living ring-opening metathesis polymerization. *Progress in Polymer Science* 32(1): 1-29.

Biggs, P., Jones, L., Wellborn, B. & Lewis, G. 2009. A self-healing PMMA bone cement: Influence of crystal size of Grubbs' catalyst. *IFMBE Proceedings* 14: 147-150.

Biswajit, Ghosh & Marek, W. U. 2009. Self-repairing oxetane-substituted chitosan polyurethane networks. *Science* 323: 1458-1460.

Blaiszik, B. J., Caruso, M. M., Mcilroy, D. A., Moore, J. S., White, S. R. & Sottos, N. R. 2009. Microcapsules filled with reactive solutions for self-healing materials. *Polymer 50*(4): 990-997.

Blaiszik, B. J., Kramer, S. L. B., Olugebefola, S. C., Moore, J. S., Sottos, N. R. & White, S. R. 2010. Self-Healing Polymers and Composites. *Annual Review of Materials Research* 40: 179-211.

Bleay, S. M., Loader, C. B., Hawyes, V. J., Humberstone, L. & Curtis, P. T. 2001. A smart repair system for polymer matrix composites. *Composites Part A*, 32(12): 1767-76.

Boubakri, A., Guermazi, N., Elleuch, K. & Ayedi, H. F. 2010. Study of UV-aging of thermoplastic polyurethane material. *Materials Science & Engineering A*, 527(7–8): 1649-S1654.

Bouridah, A., Dalard, F., Deroo, D., Cheradame, H., & Le Nest, J. F. 1985. Poly (dimethylsiloxane)-poly(ethylene oxide) based polyurethane networks used as electrolytes in lithium electrochemical solid state batteries. *Solid State Ionics* 15(3): 233-240.

Brown, E. N., Sottos, N. R. & White, S. R. 2002. Fracture testing of a self-healing polymer composite. *Experimental Mechanics* 42(4): 372-379.

Brown, E. N. 2003. Fracture and fatigue of a self-healing polymer composite material. *PhD thesis*, University of Illinois Urbana-Champaign, USA.

Brown, E. N., Kesslers, M. R., Sotttos, N. R. & White, S. R. 2003. In situ poly(urea-formadehyde) microencapsulation of dicyclopentadiene. *Journal of Microencapsulation* 20(6): 719-730.

Brown, E. N., White, S. R. & Sottos, N. R. 2005[a]. Retardation and repair of fatigue cracks in a microcapsule toughened epoxy composite–Part I: Manual infiltration. *Composites Science and Technology* 65(15): 2466-2473.

Brown, E. N., White, S. R. & Sottos, N. R. 2005[b]. Retardation and repair of fatigue cracks in a microcapsule toughened epoxy composite—Part II: In situ self-healing. *Composites Science and Technology* 65(15): 2474-2480.

Bruce, P. 1995. *Solid State Electrochemistry*. Cambridge, UK: Cambridge University Press.

Cangemi, J. M., Neto, S. C., Chierice, G. O. & dos Santos, A. M. 2006. Study of the Biodegradation of a Polymer Derived from Castor Oil by Scanning Electron Microscopy, Thermogravimetry and Infrared Spectroscopy. *Polímeros* 16(2): 129-135.

Chan, Y., Min, Z. R. & Ming, Q.Z. 2014. Self-healing polyurethane elastomer with thermally reversible alkoxyamines as crosslinkages. *Polymer* 55: 1782-1791.

Chattopadhyay, D. K. & Raju, K. V. S. N. 2007. Structural Engineering of Polyurethane Coatings For High Performance Applications. *Progress in Polymer Science* 32: 352-418.

Chattopadhyay, D.K. & Webster, D. C. 2009. Thermal Stability and Flame Retardancy of Polyurethanes. *Progress in Polymer Sciences* 34: 1068-1133.

Chen, X., Dam, M. A., Ono, K., Mal, A., Shen, H., Nutt, S. R., Sheran, K. & Wudl, F. 2002. A thermally re-mendable cross-linked polymeric material. *Science* 295: 1698-1702.

Chen, Y. & Chou, C. F. 1995. Reversible photodimerization of coumarin derivatives dispersed in poly (vinyl acetate). *Journal of Polymer Science Part A: Polymer Chemistry* 33: 2705-2714.

Chen, Y. & Jean, C. S. 1997. Polyethers containing coumarin dimer components in the main chain. I. Synthesis by photopolymerization of 7,7′ - (polymethylenedioxy) dicoumarins. *Journal of Applied Polymer Science* 64(9): 1749-1758.

Chen, Y. & Jean, C. S. 1997. Polyethers containing coumarin dimer components in the main chain. II. Reversible photocleavage and photopolymerization. *Journal of Applied Polymer Science* 64(9): 1759-1768.

Chen, Y. & Wu, J. D. 1994. Preparation and photoreaction of copolymers derived from N(1-phenylethyl) acrylamide and 7-acryloyloxy-4-methyl coumarin. *Journal of Polymer Science Part A: Polymer Chemistry 32*(10): 1867-1875.

Chian, K.S. & Gan, L.H. 1998. Development of a Rigid Polyurethane Foam from Palm Oil. *Journal of Applied Polymer Science* 68(3): 509-515.

Chipara, M. D., Chipara, M., Shansky, E. & Zaleski, J. M. 2009. Self - healing of high elasticity block copolymers. *Polymers for Advanced Technologies* 20(4): 427-431.

Cho, S. H., Andersson, H. M., White, S. R., Sottos, N. R. & Braun, P. V. 2006. Polydimethylsiloxane-Based Self-Healing Materials. *Advanced Materials* 18: 997-1000.

Cho, S. Y., Kim, J. G. & Chung, C. M. 2008. A fluorescent crack sensor based on cyclobutane-containing crosslinked polymers of tricinnamates. *Sensors and Actuators B: Chemical* 134(2): 822-825.

Chuang, F. S., Tsen, W. C. & Shu, Y. C. 2004. The effect of different siloxane chain-extenders on the thermal degradation and stability of segmented polyurethanes. *Polymer Degradation and Stability* 84: 69-77.

Chuayjuljit, S., Sangpakdee, T. & Saravari, O. 2007. Processing and Properties of Palm Oil-Based Rigid Polyurethane Foam. *Journal of Metals, Materials and Minerals* 17(1): 17-23.

Chujo, Y., Sada, K. & Saegusa, T. 1990. Polyoxazoline having a coumarin moiety as a pendant group. Synthesis and photogelation. *Macromolecules* 23(10): 2693-2697.

Chung, C. M., Roh, Y. S., Cho, S. Y., & Kim, J. G. 2004. Crack healing in polymeric materials via photochemical [2+ 2] cycloaddition. *Chemistry of Materials 16*(21): 3982-3984.

Clark, A.J. & Hoong, S.S. 2014. Copolymers of Tetrahydrofuran and Epoxidized Vegetable Oils: Application to Elastomeric Polyurethanes. *Polymer Chemistry* 5: 3238-3244.

Clemitson, I. 2008. *Castable Polyurethane Elastomers*. New York, USA: Taylor & Francis Group.

Coelho, C. S., Gama, J. A. N., Oliveira, J. L. A. T., Silva, B. S. F., Souza, V. R. C., Endringerm D. C. & Lenz, D. 2012. Use of extracts of sunflower-seed oil (Helianthus annus L.) for the treatment of cutaneous injuries in equine metatarsus: a case report. *Revista Brasileira de Plantas Medicinais* 14: 125-129.

Coll, M. C., Babb, D. & Ryan, A. J. 2008. Characterisation of polyurethane networks based on vegetable derived polyol. *Polymer* 49: 3279-3287.

Colvin, B.G. 1995. Low Cost Polyols From Natural Oils. *U'Tech Asia* 95(36): 1-10.

Corcuera, M. A., Rueda, L., Saralegui, A., Martin, M .D., Fernandez-d'Arlas, B., Mondragon, I. & Eceiza, A. 2011. Effect of Diisocyanate Structure on the Properties and Microstructure of Polyurethanes Based on Polyols Derived from Renewable Resources. *Journal of Applied Polymer Science* 122: 3677-3685.

Cordier, P., Tournilhac, F., Soulié-Ziakovic, C. & Leibler, L. 2008. Self-healing and thermoreversible rubber from supramolecular assembly. *Nature* 451(7181): 977-980.

Cosco, S., Ambrogi, V., Musto, P. & Carfagna, C. 2007. Properties of poly (urea‐formaldheyde) microcapsules containing an epoxy resin. *Journal of Applied Polymer Science* 105(3): 1400-1411.

Cuve, L. & Pascault, J. P. 1991. Synthesis and properties of polyurethanes based on polyolefine: 1. Rigid polyurethanes and amorphous segmented polyurethanes prepared in polar solvents under homogeneous conditions. *Polymer* 32(2): 343-352.

Conceição, P.V.S., Faria, L.O., Santos, A.P. & Furtado, C.A. 2003. Study of Bare and Functionalized Zicronia Nanoparticles filled Polymer Electrolytes Based on Polyurethane. *Material Research Society Symposium Proceeding* 756: EE3.14.1-EE3.14.6.

Caruso, M. M., Delafuente, D. A., Ho, V., Sottos, N. R., Moore, J. S. & White, S. R. 2007. Solvent-promoted self-healing epoxy materials. *Macromolecules* 40(25): 8830-8832.

Caruso, M. M., Blaiszik, B. J., White, S. R., Sottos, N. R. & Moore, J. S. 2008. Full recovery of fracture toughness using a nontoxic solvent‐based self‐healing system. *Advanced Functional Materials* 18(13): 1898-1904.

Daud, F.N., Ahmad, A. & Badri, K.H. 2013. Preparation and Characterization of Plasticized Palm-Based Polyurethane Solid Polymer Electrolyte. *AIP Conference Proceedings* 1571(1): 775-781.

Daud, F.N., Ahmad, A. & Badri, K.H. 2014. An Investigation on the Properties of Palm-Based Polyurethane Solid Polymer Electrolyte. *International Journal of Polymer Science* 326716: 1-5.

Deka, M. & Kumar, A. 2011. Electrical and electrochemical studies of poly(vinylidene fluoride)eclay nanocomposite gel polymer electrolytes for Li-ion batteries, *Journal of Power Sources* 196: 1358-1364.

Dias, E. L., Nguyen, S. T. & Grubbs, R. H. 1997. Well-defined ruthenium olefin metathesis catalysts: mechanism and activity. *Journal of the American Chemical Society* 119(17): 3887-3897.

Edman, L., Doeff, M.M., Ferry, A., Kerr, J. & De Jonghe, L.C. 2000. Transport properties of the solid polymer electrolyte system P(EO)n LiTFSI. *Journal of Physical Chemistry* B 104: 3476-3480.

Ermolovich, O. A. 2005. Structure and properties of biodegradable film materials based on compatibilized polyethylene/starch compositions. *Polimernyj Zhurnal* 27 (3): 174-180.

European Palm Oil Alliance. 2016. Palm Oil Production. https://www.palmoilandfood.eu/en/palm-oil-production/

Fenton, D.E., Parker, J.M. & Wright, P.V. 1973. Complexes of Alkali Metal Ions with Poly (ethylene oxide). *Polymer* 14(11): 589.

Fleming, I. 2015. *Pericyclic reactions*. Oxford: Oxford University Press.

Fomin, V. A. & Guzeev, V.V. 2001. Biologically degradable polymers. *Plasticheskie Massy* 2: 2-46.

Fridrihsone-Girone, A. & Stirna, U. 2014. Characterization of Polyurethane Networks Based on Rapeseed Oil Derived Polyol. *European Polymer Journal* 49(6): 1204-1214

Frisch, K. C. 1969. *Polyurethane Technology*. New York: John Wiley & Sons Inc.

Fujiwara, M., Shiokawa, K., Kawasaki, N. & Tanaka, Y. 2003. Photodimerization of Coumarin ‐ Derived Pentacyclooctasiloxane to Fabricate a Three ‐ Dimensional Organic – Inorganic Hybrid Material. *Advanced Functional Materials* 13(5): 371-376.

Fukushima, T., Matsuda, Y., Hashimoto H. & Arakawa, R. 2001. Studies on Solvation of Lithium Ions in Organic Electrolyte Solutions by Electrospray Ionization-Mass Spectroscopy. *Electrochemical and Solid-State Letters* 4: 127-128.

Garrison, T.F., Zhang, Z., Kim, H.J., Mitra, D., Xia, Y., Pfister, D.P., Brehm-Stecher, B.F., Larock, R.C. & Kessler, M.R. 2014. Thermo‐Mechanical and Antibacterial Properties of Soybean Oil‐Based Cationic Polyurethane Coatings: Effects of Amine Ratio and Degree of Crosslinking. *Macromolecular Materials and Engineering* 299(9): 1042-1051

Ghouili, A., Dusek, M., Petricek, V., Ayed, T. B. & Hassen, R. Ben. 2014. Synthesis, crystal structure and spectral characteristics of highly fluorescent chalcone-based coumarin in solution and in polymer matrix. *Journal of Physics and Chemistry of Solids 75*(2): 18-193.

Gotsmann, B., Duerig, U., Frommer, J. & Hawker, C. J. 2006. Exploiting chemical switching in a Diels–Alder polymer for nanoscale probe lithography and data storage. *Advanced functional materials* 16(11): 1499-1505.

Graf, C., Schärtl, W. & Hugenberg, N. 2000. Photoinduced Cluster Formation of Coumarin‐Labeled Organosilicon Micronetworks. *Advanced Materials* 12(18): 1353-1356.

Gray, F.M. 1991. *Solid Polymer Electrolytes*. New York, USA: Wiley-VCH.

Gray, F.M. 1997. *Polymer electrolytes*. United Kingdom: The Royal Society of Chemistry.

Grubbs, R. H. 2006. Olefin‐metathesis catalysts for the preparation of molecules and materials (Nobel lecture). *Angewandte Chemie International Edition* 45(23): 3760-3765.

Gurusiddappa, J., Madhuri, W., Padma, S.R. & Priya, K.D. 2016. Studies on the morphology and conductivity of PEO/$LiClO_4$. *Materials Today: Proceedings* 3: 1451-1459.

Haddad, S., Zanina, N., Othmane, A. & Mora, L. 2011. Polyurethane films modified by antithrombin–heparin complex to enhance endothelialization: An original impedimetric analysis. *Electrochimica Acta* 56: 7303-7011.

Hansen, C. J., Wu, W., Toohey, K. S., Sottos, N. R., White, S. R. & Lewis, J. A.. 2009. Self-healing materials with interpenetrating microvascular networks. *Journal of Advanced Materials* 21(41): 41434-4147.

Ha, S. W., Camalier, C. E., Beck Jr, G. R. & Lee, J. K. 2009. New method to prepare very stable and biocompatible fluorescent silica nanoparticles. *Chemical Communications* (20): 2881-2883.

Hossieny, N., Shaayegan, V., Ameli, A., Saniei, M. and Park, C.B. 2017. Characterization of hard-segment crystalline phase of thermoplastic polyurethane

in the presence of butane and glycerol monosterate and its impact on mechanical property and microcellular morphology. *Polymer* 112: 208-218

Husić, S., Javni, I. & Petrović, Z.S. 2005. Thermal and Mechanical Properties of Glass Reinforced Soy-Based Polyurethane Composites. *Composites Science and Technology* 65(1): 19-25.

Ibrahim, S., Yasin, S.M.M., Ahmad, R. & Johan, M.R. (2012). Conductivity, thermal and morphology studies of PEO based salted polymer electrolytes. *Solid State Science*, 14:1111-1116.

Ionescu, M. & Petrović, Z.S. 2010. High Functionality Polyether Polyols Based on Polyglycerol. *Journal of Cellular Plastics* 46(3): 223-237

Jacobs, A. 1997. *Understanding Organic Reaction Mechanisms*. Cambridge: Cambridge University Press.

Jian-he, H., Li, S., Xin-wen, Z., Kahirou, D. & Ke-li, Z. 2010. Non-isothermal Decomposition Mechanism and Kinetics of $LiClO_4$ in Nitrogen. *Chemistry Research of Chinese Universities* 26: 300-303.

Jones, A. S., Rule, J. D., Moore, J. S., Sottos, N. R. & White, S. R. 2007. Life extension of self-healing polymers with rapidly growing fatigue cracks. *Journal of the Royal Society Interface* 4(13): 395-403.

Judit, C., Han, G. & Bert, L. 2011. Self-Healing Materials Based on Disulfide Links. *Macromolecules* 44: 2536-2541.

Jung, D., Hegeman, A., Sottos, N. R., Geubelle, P. H. & White, S. R. 1997. Self-healing composites using embedded microspheres. *American Society of Mechanical Engineers, Materials Division (Publication)* 80: 265-275.

Kalista, S., Ward, T. C & Oyetunji, Z. 2007. Self-healing of poly(ethylene-comethacrylic acid) copolymers following projectile puncture. *Mechanics of Advanced Materials and Structures* 14(5): 391-97.

Kandasamy, C., Hoong, K.F., Kamaraja, S., Vayalakkavoor, T.R. & Ibrahim, A.R. 1998. An N-substituted 6,7-benzocoumarin-8,9-aziridine derivative. *Acta Crystallographica Section C:* 1299-1301.

Kang, Y., Seo, Y. H. & Lee, C. 2000. Synthesis and Conductivity of PEGME Branched Poly(ethylene-alt-maleimide) Based Solid Polymer Electrolyte. *Bulletin-Korean Chemical Society* 21: 241.

Kaur, S., Rana, D., Matsuura, T., Sundarrajan, S. & Ramakrishna, S. 2012. Preparation and characterization of surface modified electrospun membranes for higher filtration flux. *Membrane Science* 390-391: 235-242.

Keller, B. M. W., White, S. R., & Sottos, N. R. 2007. A Self-Healing Poly (Dimethyl Siloxane) Elastomer. *Advanced Functional Materials* 17: 2399-2404.

Keller, M. W., White, S. R., & Sottos, N. R. 2008. Torsion fatigue response of self-healing poly (dimethylsiloxane) elastomers. *Polymer* 49(13): 3136-3145.

Kessler, M. R., & White, S. R. 2002. Cure kinetics of the ring-opening metathesis polymerization of dicyclopentadiene. *Journal of Polymer Science Part A: Polymer Chemistry* 40(14): 2373-2383.

Khoon Poh, A., Choy Sin, L., Sit Foon, C. & Cheng Hock, C. 2014. Polyurethane Wood Adhesive from Palm Oil-Based Polyester Polyol. *Journal of Adhesion Science and Technology* 28(11): 1020-1033.

Kim, B. K., Seo, J. W. & Jeong, H. M. 2003. Morphology and properties of waterborne polyurethane/clay nanocomposites. *European Polymer Journal* 39: 85-91.

Kim, B. S. & Kim, B. K. 2005. Enhancement of hydrolytic stability and adhesion of waterborne polyurethanes. *Journal of Applied Polymer Science* 97: 1961-1969.

Kim, H. C., Hartner, S. & Hampp, N. 2008. Single- and two-photon absorption induced photocleavage of dimeric coumarin linkers: Therapeutic versus passive photocleavage in ophthalmologic applications. *Journal of Photochemistry and Photobiology* 197: 239-244.

Kirk, J. G., Naik, S., Moosbrugger, J. C., Morrison, D. J., Volkov, D. & Sokolov, I. 2009. Self-healing epoxy composites based on the use of nanoporous silica capsules. *International journal of fracture* 159(1): 101-102.

Koerner, H., Liu, W., Alexander, M., Mirau, P., Dowty, H. & Vaia, R. A. 2005. Deformation–morphology correlations in electrically conductive carbon nanotube-thermoplastic polyurethane nanocomposites. *Polymer* 46: 4405-20.

Koichi, T. 2012. Supramolecular Photodimerization of coumarins. *Molecules* 17: 1408-1418.

Kuo, C. W., Li, W. B., Chen, P. R., Liao, J. W., Tseng, C. G. & Wu, T. Y. 2013. Effect of Plasticizer and Lithium Salt Concentration in PMMA-based Composite Polymer Electrolytes. *Electrochemical Science* 8: 5007-5021.

Lamba, N. M. K., Woodhouse, K. A. & Cooper, S. L. 1998. *Polyurethanes in Biomedical Applications*. Boca Raton: CRC Press.

Larin, G. E., Bernklau, N., Kessler, M. R. & DiCesare, J. C. 2006. Rheokinetics of ring‐opening metathesis polymerization of norbornene‐based monomers intended for self‐healing applications. *Polymer Engineering & Science* 46(12): 1804-1811.

La Scala, J.J., Sands, J.M., Orlicki, J.A., Robinette, E.J. & Palmese, G.R. 2004. Fatty Acid-Based Monomers as Styrene Replacements for Liquid Molding Resins. *Polymer* 45(22): 7729-7737.

Lee, J. S. & Kim, B. K. 1995. Poly(urethane) cationomers from poly(propylene) glycol and isophorone diisocyanate: emulsion characteristics and tensile properties of cast films. *Progress in Organic Coatings* (*25*): 311-318.

Lee, J. K., Liu, X., Yoon, S. H., & Kessler, M. R. 2007. Thermal analysis of ring‐opening metathesis polymerized healing agents. *Journal of Polymer Science Part B: Polymer Physics* 45(14): 1771-1780.

Lewis, G., Wellborn, B., Jones, I. I., & Biggs, P. 2009. A room-temperature autonomically-healing PMMA bone cement: influence of composition on fatigue crack propagation rate. *Journal of Applied Biomaterials & Biomechanics* 7(2): 90-96.

Liao, S. K., Jang, S. C. & Lin, M. F. 2008. Phase Behaviour and Thermal Stability of Imide-Containing Siloxane- Urethane Copolymers. *Journal of Polymers and Polymer Composites* 16(2): 153-164.

Liew, C. W., Ong, Y.S., Lim, J.Y., Lim, C.S., Teoh, K.H. & Ramesh, S. 2013. Effect of ionic liquid on semi–crystalline poly(vinylidene fluoride–co–hexafluoropropylene) solid copolymer electrolytes. *International Journal of Electrochemical Science* 8: 7779-7794.

Lin, C. K., Kuo, J. F., Chen C. Y. & Fang, J. J 2012. Investigation of bifurcated hydrogen bonds within the thermotropic liquid crystalline polyurethanes. *Polymer* 53: 254-258.

Ling, J., Rong, M. Z. & Zhang, M. Q. 2011. Coumarin imparts repeated photochemical remendability to polyurethane. *Journal of Materials Chemistry* 21: 18373.

Ling, J., Rong, M. Z. & Zhang, M. Q. 2012. Photo-stimulated self-healing polyurethane containing dihydroxyl coumarin derivatives. *Polymer* 53: 2691-2698.

Liu, Y. L., & Hsieh, C. Y. 2006. Crosslinked epoxy materials exhibiting thermal remendablility and removability from multifunctional maleimide and furan compounds. *Journal of Polymer Science Part A: Polymer Chemistry* 44(2): 905-913.

Liu, X., Sheng, X., Lee, J. K. & Kessler, M. R. 2007. Isothermal cure characterization of dicyclopentadiene. *Journal of Thermal Analysis and Calorimetry* 89(2): 453-457.

Liu, H. A., Gnade, B. E. & Balkus, K. J. 2008. A Delivery System for Self‐Healing Inorganic Films. *Advanced Functional Materials* 18(22): 3620-3629.

Liu, B., Wang, R., Mi, W., Li, X. & Yu, H. 2012. Novel Branched Coumarin Dyes for Dye-Sensitized Solar Cells: Significant Improvement in Photovoltaic Performance by Simple Structure Modification. *Journal of Materials Chemistry* 22: 15379-15387.

Liu, B. T., Wang, D. H., Syu, J. R. & Lin, S. H. 2014. Enhanced electrical conductivity of polyurethane-polyaniline composites containing core-shell particles through conductive-shell effect. *Taiwan Institute of Chemical Engineers* 45: 2047-2051.

Liu, L., Wu, X. & Li, T. 2014. Novel polymer electrolytes based on cationic polyurethane with different alkyl chain length. 2014. *Journal of Power Sources* 249: 397-404.

Liu, L., Wu, X. & Li, T. 2014. Novel polymer electrolytes based on cationic polyurethane with different alkyl chain length. *Journal of Power Sources* 249: 397-404.

Liu, X., Sheng, X., Lee, J. K., & Kessler, M. R. 2009. Synthesis and Characterization of Melamine- Urea-Formaldehyde Microcapsules Containing ENB-Based Self-Healing Agents. *Macromolecular Materials and Engineering* 294: 389-395.

Loutfy, R. O. & Mayo, P. D. 1972. Primary Bond Formation in the Addition of Cyclopentenone to Chloroethylenes. *Canadian Journal of Chemistry* 50: 3465.

Lu, M. G., Lee, J. Y., Shim, M. J. & Kim, S. W. 2002. Thermal Degradation of Film Cast from Aqueous Polyurethane Dispersion. *Journal of Applied Polymer Science* 85(12): 2552-2558.

Lumcharoen, D. & Saravari, O. 2014. Preparation and Characterization of Flexible Polyurethane Foams from Palm Oil-Based Polyol. *Advanced Materials Research* 911: 352-356.

Ma, X. Huang, X., Gao, J., Zhang, S., Deng, Z. & Suo, J. 2014. Compliant gel polymer electrolyte based on poly(methyl acrylate-co-acrylonitrile)/poly(vinyl alcohol) for flexible lithium-ion batteries. *Electrochimica Acta* 115: 216-222.

Malassenet, L., George, B., Merlin, A. & Podgorski, L. 2015. Persoz hardness: a useful property to study performance of exterior wood coatings. *International Wood Products Journa*l 6:174-180.

Mal, N. K., Fujiwara, M. & Tanaka, Y. 2003. Photocontrolled reversible release of guest molecules from coumarin-modified mesoporous silica. *Nature* 421(6921): 350-353.

Mark, B., Liming, T., Justin, R. K., Andrew, J. D., Frederick, L. B., Gina, L. F., Stuart, J. R. & Christoph, W. 2011. Optically healable supramolecular polymers. *Nature* 472: 334-337.

Mascaraque, N., Fierro, J. L. G. Duran, A. & Munoz, F. 2013. An interpretation for the increase of ionic conductivity by nitrogen incorporation in LiPON oxynitride glasses. *Solid State Ionics* 233: 73-79.

Michael, B. 1996. Bond polarity and electronegativity. http://www.mikeblaber.org/oldwine/chm1045/notes/Bonding/Polarity/Bond05.html

Mishra, K., Narayan, R., Raju, K. V. S. N. & Aminabhavi, T. M. 2012. Hyperbranched polyurethane (HBPU)-urea and HBPU-imide coatings: Effect of chain extender and NCO/OH ratio on their properties. *Progress in Organic Coatings* 74: 134-141.

Mobarak, N. N., Ahmad, A., Abdullah, M. P., Ramli N. & Rahman, M. Y. A. 2013. Conductivity enhancement via chemical modification of chitosan based green polymer electrolyte. *Electrochimica Acta*. 92: 161-167.

Mondal, S. & Martin, D. 2012. Hydrolytic Degradation of Segmented Polyurethane Copolymers for Biomedical Applications. *Polymer Degradation and Stability* 97(8): 1553-1561.

Montarnal, D., Tournilhac, F., Hidalgo, M., Couturier, J. L. & Leibler, L. 2009. Versatile one-pot synthesis of supramolecular plastics and self-healing rubbers. *Journal of the American Chemical Society* 131(23): 7966-7967.

Mookhoek, S. D., Blaiszik, B. J., Fischer, H. R., Sottos, N. R., White, S. R. & Zwaag, S.V.D. 2008. Peripherally decorated binary microcapsules containing two liquids. *Journal of Materials Chemistry* 18: 5390-5394.

Murphy, E. B., Bolanos, E., Schaffner-Hamann, C.,Wudl, F., Nutt, S. R. & Auad, M. L. 2008. Synthesis and characterization of a single-component thermally remendable polymer network: Staudinger and Stille revisited. *Macromolecules* 41(14): 5203-5209.

Mutsuhisa, F., Ken, K. & Shohei, N. 2007. Microphase-separated structure and mechanical properties of norbornane diisocyanate-based polyurethanes. *Polymer* 48: 997-1004.

Nasim, M.K., Suman, P., Shaik, K. & Lokman, H.C. 2014. Multicomponent reactions for facile access to coumarin-fused dihydroquinolines and quinolines: synthesis and photophysical studies. New Journal of Chemistry 38: 4722-4729

Nelson, G. L., & Chaiw-Liang, K. U. O. 1975. An improved procedure for the preparation of exo-dicyclopentadiene. *Synthesis* 105(02): 105-106.

Newman, C. R. & Forciniti, D. 2001. Modeling the Ultraviolet Photodegradation of Rigid Polyurethane Foams. *Industrial & Engineering Chemistry Research* 40: 3346-3352.

Ng, W.K., Lim, P.K. & Boey, P.L. 2003. Dietary Lipid and Palm Oil Source Affects Growth, Fatty Acid Composition and Muscle A-Tocopherol Concentration of African Catfish, *Clarias gariepinus*. *Aquaculture* 215: 229-243.

Ngai, T. & Wu, C. 2003. Effect of Cross-Linking on Dynamics of Semidilute Copolymer Solutions: Poly (methyl methacrylate-co-7-acryloyloxy-4-methylcoumarin) in Chloroform. *Macromolecules* 36(3): 848-854.

Nguyen, S. T., Johnson, L. K., Grubbs, R. H. & Ziller, J. W. 1992. Ring-opening metathesis polymerization (ROMP) of norbornene by a group VIII carbene complex in protic media. *Journal of the American Chemical Society* 114(10): 3974-3975.

Nguyen, S. T., Grubbs, R. H. & Ziller, J. W. 1993. Syntheses and activities of new single-component, ruthenium-based olefin metathesis catalysts. *Journal of the American Chemical Society* 115(21): 9858-9859.

Nicotera, I., Coppola, L., Oliviero, C., Castriota, M., & Cazzanelli, E. 2006. Investigation of ionic conduction and mechanical properties of PMMA–PVdF blend-based polymer electrolytes. *Solid State Ionics* 177(5): 581-588.

Nik Norulaini, N.A., Md Zaidul, I.S., Anuar, O. & Mohd Omar, A.K. 2004. Supercritical Enhancement for Separation of Lauric Acid and Oleic Acid in Palm Kernel Oil (PKO). *Separation and Purification Technology* 39: 133-138.

Noor, S.A.M., Ahmad, A., Talib, I.A. & Rahman, M.Y.A. 2010. Morphology, Chemical Interaction, and Conductivity of a PEO-ENR50 Based on Solid Polymer Electrolyte. *Ionics* 16(2): 161-170.

Ooi, T.L., Salmiah, A., Hazimah, A.H. & Chong, Y.J. 2006. An Overview of R&D in Palm Oil-Based Polyols and Polyurethanes in MPOB. *Palm Oil Developments 44*, 1-7.

Osawa, Z., Cheu, E. L. & Nagashima, K. 1977. Study of the degradation of polyurethanes. III. Mechanism of the photodegradation of polyurethane. *Polymer Chemistry* 15(2): 445-450.

Palmese, G.R., A.M. Peterson, A.M. & R.E. Jensen. 2008. Remendable polymeric materials using reversible covalent bonds‘, In Proceedings of 26th Army Science Conference, Orlando, Florida, USA.

Pan, X. & Webster, D. C. 2012. New Biobased High Functionality Polyols and Their Use in Polyurethane Coatings. *ChemSusChem* 5: 419-429.

Pang, H., Xu, L., Yan, D. & Li, Z. 2014. Progress in Polymer Science Conductive polymer composites with segregated structures. *Progress in Polymer Science 39*(11): 1908-1933.

Pang, J. W. C. & Bond, I. P. 2005. 'Bleeding composites': damage detection and self-repair using a biomimetic approach. *Composites A* 36(2): 183-88.

Pang, Y., Luo, L., Chen, Y., Zhang, P., Wang, X., Peng, C. & Liu, X. 2012. Influence of steric hindrance between Hydrogen atoms of linkage Groups and Adjacent Phenyls on Properties of Polyimide. *Chemical Research in Chinese Universities* 28(5): 926-930.

Park, J. S., Kim, H. S. & Hahn, H. T. 2009. Healing behavior of a matrix crack on a carbon fiber/mendomer composite. *Composites Science and Technology* 69(7-8): 1082-1088.

Park, J. S., Takahashi, K., Guo, Z., Wang, Y., Bolanos, E., Hamann-Schaffner, C., Murphy, E., Wudl, F. & Hahn, H.T. 2008. Towards development of a self-healing composite using a mendable polymer and resistive heating. *Journal of Composite Materials* 42(26): 2869-81.

Petcharoen, K. & Sirivat, A. 2013. Electrostrictive properties of thermoplastic polyurethane elastomer: Effects of urethane type and soft–hard segment composition. *Current Applied Physics* 13: 1119-1127.

Petrović, Z. S., Zhang, W., Zlatanić, A., Lava, C. C. & Ilavskyý, M. 2002. Effect of OH/NCO molar ratio on properties of soy-based polyurethane networks. *Journal of Polymers and the Environment* 10(1): 5-12.

Petrović, Z.S. 2008. Polyurethanes from Vegetable Oils. *Polymer Reviews* 48(1): 109-155.

Pfister, D.P., Xia, Y. & Larock, R.C. 2011. Recent Advances in Vegetable Oil ‐ Based Polyurethanes. *ChemSusChem* 4(6): 703-717.

Philippe, C., Francois, T., Corinne, S. Z. & Ludwik, L. 2008. Self-healing and thermoreversible rubber from supramolecular assembly. *Nature* 451: 977-980.

Plaisted T. A, Nemat-Nasser S. 2007. Quantitative evaluation of fracture, healing and rehealing of a reversibly cross-linked polymer. *Acta Materialia.* 55(17): 5684-96.

Pradhan, D.K., Choudhary, R.N.P., & Samantaray, B.K. 2009. Studies of dielectric and electrical properties of plasticized polymer nanocomposite electrolytes. *Materials Chemistry and Physics* 115: 557-561.

Quartarone, E., Mustarelli, P. & Magistris, A. 1998. PEO-based composite polymer electrolytes. *Solid State Ionics* 110(1): 1-14.

Radice, S. & Bradley, M. 2007. Time-Based FT-IR Analysis of Curing of Polyurethanes. *Thermoscientific Application Note* 51255. https://www.thermo.com. [October 2011].

Radojčić, D., Ionescu, M. & Petrović, Z.S. 2013. Novel Potentially Biodegradable Polyurethanes from Bio-Based Polyols. *Contemporary Materials* 1(4): 9-21.

Rafael, A.R., Mauricio, M.D., Javier, O.H., Margarita, R.A., Norberto, F. & Maria, P.C.C. 2017. 3-Substituted-7-(diethylamino)coumarins as molecular scaffolds for the bottom-up self-assembly of solids with extensive π-stacking. *Journal of Molecular Structure* 1130: 914-921

Rahmathullah, M. A. M. & Palmese, G. R. 2009. Crack-healing behavior of epoxy-amine thermosets. *Journal of Applied Polymer Science* 113(4): 2191-2201.

Rajendran, S., Mahendran, O. & Kannan, R. 2002. Characterization of [(1-x)PMMA-xPVdF] polymer blend electrolyte with Li^+ ion. *Fuel* 81: 1077-1081.

Rajendran, S., Sivakumar, M., & Subadevi, R. 2004. Investigations on the effect of various plasticizers in PVA–PMMA solid polymer blend electrolytes. *Materials Letters* 58(5): 641-649.

Rashvand, M., & Ranjbar, Z. 2014. Degradation and stabilization of an aromatic polyurethane coating during an artificial aging test via FTIR spectroscopy. Materials and Corrosion 65: 1.

Ren, T., Ren, J. & Tang, X. 2005. Microporous Polyurethane/Acrylate Gel Polymer Electrolyte Obtained by Emulsion Polymerization. *Polymer International* 54(1): 185-190.

Ren, D. & Frazier, C. E. 2013. Structure–property behaviour of moisture-cure polyurethane wood adhesives: Influence of hard segment content. *Adhesion and Adhesives* 45: 118-124.

Respoet, G., Nguyen, M.T., McGarraghy, M. & Hegarty, A.F. 1998. The Alcoholysis Reaction of Isocyanates Giving Urethanes: Evidence for a Multimolecular Mechanism. *The Journal of Organic Chemistry* 63: 6878-6885.

Rint, P. S., Felix, H. B., Luc, B., Brigitte, J. B.F., Hirschberg, J.H.K.K., Ronald, F. M. L., Jimmy, K. L. L. & Meijer, E. W. 1997. Reversible Polymers Formed from Self-Complementary Monomers Using Quadruple Hydrogen Bonding. *Science* 278: 1601-1604.

Rivas, B.L., Pereira, E.D. & Moreno-Villoslada, I. 2003. Water-soluble polymer-metal ion interactions. *Progress of Polymer Science* 28: 173-208.

Rong, M. Z., Zhang, M. Q. & Zhang, W. 2007. A novel self-healing epoxy system with microencapsulated epoxy and imidazole curing agent. *Advanced Composites Letters* 16(5): 167-172.

Rosu, L., Cascaval, C. N., Ciobanu, C., Rosu, D., Ion, E. D., Morosanu, C. & Enachescu, M. 2005. Effect of UV radiation on the semi-interpenetrating polymer networks

based on polyurethane and epoxy maleate of bisphenol A. *Journal of Photochemistry and Photobiology A: Chemistry* 169, 177-185.

Rozman, H. D., Yeo, Y. S., Tay, G. S. & Abubakar, A. 2003. The mechanical and physical properties of polyurethane composites based on rice husk and polyethylene glycol. *Polymer Testing* 22: 617-623.

Rueda-Larraz, L., d'Arlas B. F., Tercjak, A., Ribes, A., Mondragon, I. & Eceiza, A. 2009. Synthesis and Microstructure–Mechanical Property Relationships of Segmented Polyurethanes Based on a PCL–PTHF–PCL Block Copolymer as Soft Segment. *European Polymer Journal* 45: 2096-2109.

Rule, J. D., Brown, E.N., Sottos, N. R., White, S. R. & Moore, J. S. 2005. Wax-protected catalyst microspheres for efficient self-healing materials. *Journal of Advanced Materials* 17(2): 205-208.

Saha, M. C., Kabir, M. E., & Jeelani, S. 2008. Enhancement in thermal and mechanical properties of polyurethane foam infused with nanoparticles. *Materials Science and Engineering: A* 479(1): 213-222.

Salih, A.M., Ahmad, M.B., Ibrahim, N.A., Dahlan, K.Z.H.M., Tajau, R., Mahmood, M.H. & Yunus, W.M.Z.W. 2014. Thermal and Mechanical Properties of Palm Oil-Based Polyurethane Acrylate/Clay Nanocomposites Prepared by In-Situ Intercalative Method and Electron Beam Radiation. *Advancing Nuclear Research and Energy Development: Proceedings of the International Nuclear Science, Technology & Engineering Conference 2013* 1584(1): 117-124.

Salleh, M.Z., Badri, K.H., Mahmood, M.H. & Ahmad, S.H. 2010. Synthesis of UV-Curable Hyperbranched Urethane Acrylate from Palm Oil Oleic Acid. *Journal of Nuclear and Related Technologies* 7: 39-48.

Salmiah, I., Azizan, A. & Nor, S.M. 2015. Characterization of Castor Oil-Based Polyurethane Electrolytes. Polymers 7:747-759

Sami, S., Yildirim, E., Yurtsever, M., Yurtsever, E., Yilgor, E., Yilgor, I. & Wilkes, G.L. 2014. Understanding the influence of hydrogen bonding and diisocyanate symmetry on the morphology and properties of segmented polyurethanes and polyureas: Computational and experimental study. *Polymer* 55: 4563-4567.

Sanford, M. S., Love, J. A., & Grubbs, R. H. 2001. Mechanism and activity of ruthenium olefin metathesis catalysts. *Journal of the American Chemical Society* 123(27): 6543-6554.

Sang, S., Zhang, J., Wu, Q. & Liao, Y. 2007. Influences of Bentonite on conductivity of composite solid alkaline polymer electrolyte PVA-Bentonite-KOH-H_2O. *Electrochimica Acta* 52: 7315-732.

Sato, E., Nagai, S. & Matsumoto, A. 2013. Reversible thickness control of polymer thin films containing photoreactive coumarin derivative units. *Progress in Organic Coatings* 76: 1747-1751.

Saunier, J., Chaix, N., Alloin, F., Belieres, J.P. & Sanchez, J.Y. 2002. Electrochemical study of polymethacrylonitrile electrolytes: Conductivity study of polymer/salt complexes and plasticized polymer electrolytes. Part I. *Electrochimica Acta* 47: 1321-1326.

Sauvant-Moynot, V., Gonzalez, S. & Kittel, J. 2008. Self-healing coatings: An alternative route for anticorrosion protection. *Progress in Organic Coatings* 63(3): 307-315.

Sebenik, U. & Krajnc, M. 2007. Influence of the soft segment length and content on the synthesis and properties of isocyanate-terminated urethane prepolymers. *International Journal of Adhesion & Adhesives* 27: 527-535.

Segal, E., Haba, Y., Narkis, M. & Siegmann, A. 2001. On the structure and electrical conductivity of polyaniline/polystyrene blends prepared by an aqueous-dispersion blending method. *Journal of Polymer Science Part B: Polymer Physics* 39: 611-21.

Seoane, R., Bilbao, P., Gondra, K., Gonzalez-jimenez, A., Valentin, J. L. & Marcos-fernandez, A. 2016. Synthesis and characterization of a photo-crosslinkable polyurethane based on a coumarin-containing polycaprolactone diol. *European Polymer Journal 76*: 245-255.

Septevani, A. a., Evans, D. a. C., Chaleat, C., Martin, D. J. & Annamalai, P. K. 2015. A systematic study substituting polyether polyol with palm kernel oil based polyester polyol in rigid polyurethane foam. *Industrial Crops and Products* 66: 16-26.

Sergei, M.K. 2011. Valence Isomerization between diazo compounds and diazirines. *European Journal of Organic Chemistry* 6153-6175.

Shchukin, D. G., Zheludkevich, M., Yasakau, K., Lamaka, S., Ferreira, M. G. & Möhwald, H. 2006. Layer ‐ by ‐ Layer assembled nanocontainers for self ‐ healing corrosion protection. *Advanced Materials* 18(13): 1672-1678.

Sheba, D. B. & Fred, W. 2008. Mendable polymers. *Journal of Materials Chemistry* 18: 41-62.

Silva, M. J., Kanda, D. H. F. & Nagashima, H. N. 2012. Mechanism of charge transport in castor oil-based polyurethane/carbon black composite (PU/CB). *Non Crystalline Solids* 358: 270-275.

Simon, D., Borreguero, A. M., Lucas A. D. & Rodriguez, J. F. 2015. Glycolysis of viscoelastic flexible polyurethane foam wastes. *Polymer Degradation and Stability* 116: 23-35.

Smith, B. C. 2015. How to Properly Compare Spectra, and Determining Alkane Chain Length from Infrared Spectra. *Spectroscopy* 40-46.

Sonmez, A., Budakei, M., Demirci, Z. & Akkus, M. Effects of thermal aging on the film hardness of some wood varnishes. *Bioresources* 6(4): 4594-4605.

Srinivasan, K. S. V. 1998. *Macromolecules New Frontiers*. New Delhi: Allied Publishers Limited.

Su'ait, M.S., Ahmad, A., Hamzah, H. & Rahman, M.Y.A. 2009. Preparation and Characterization of PMMA-MG49-$LiClO_4$ Solid Polymeric Electrolyte. *Journal of Physics D: Applied Physics* 42: 55410.

Su'ait, M .S., A. Ahmand, A., Hamzah, H. & Rahman, M. Y. A. 2011. Effect of lithium salt concentrations on blended 49% poly(methyl methacrylate) grafted natural rubber and poly(methyl methacrylate) based solid polymer electrolyte. *Electrochimica Acta* 57: 123-131.

Su'ait, M. S., Ahmad, A., Badri, K. H., Mohamed, N. S., Rahman, M. Y. A., Azanza Ricardo, C. L. & Scardi, P. 2014. The potential of polyurethane bio-based solid polymer electrolyte for photochemical cell application. *International Journal of Hydrogen Energy* 39: 3005-3017.

Sun, X. X. & Song, M. 2009. Highly conductive carbon nanotube/polymer nanocomposites achievable. *Macromolecular Theory Simulations* 18: 155-61.

Suzana, m.c., Ivan, S.R., Milena, M.C., Dragan, T.S. & Jaroslava,, B.S. 2016. Preparation and characterization of waterborne polyurethane/silica hybrid dispersions from castor oil polyols obtained by glycolysis poly(ethylene terephthalate) waste. *International Journal of Adhesion and Adhesives* 70: 329-341

Tan, I.K.P., Kumar, K.S., Theanmalar, M., Gan, S.N. & Gordon III, B. 1997. Saponified Palm Kernel Oil and Its Major Free Fatty Acids as Carbon Substrates for the Production of Polyhydroxyalkanoates in *Pseudomonas putida* PGA1. *Applied Microbiology and Biotechnology* 47(3): 207-211.

Tanaka, R., Hirose, S. & Hatakeyama, H. 2008. Preparation and Characterization of Polyurethane Foams Using a Palm Oil-Based Polyol. *Bioresource Technology* 99(9): 3810-3816.

Tian, L.Y., Zhu, W.H. & Tang, X. 2003. Polymer Gel Electrolytes Based on Thermoplastic Polyurethane. *Journal of Applied Polymer Science* 90(9): 2310-2315.

Tian, Q., Yuan, Y. C., Rong, M. Z. & Zhang, M. Q. 2009. A thermally remendable epoxy resin. *Journal of Materials Chemistry* 19(9): 1289-1296.

Toohey, K. S., Sottos, N. R., Lewis, J. A., Moore, J. S. & White, S. R. 2007. Self-healing materials with microvascular networks. *Nature Materials* 6(8): 581-85.

Träger, J., Heinzer, J., Kim, H. C. & Hampp, N. 2008. Polymers for in vivo tuning of refractive properties in intraocular lenses. *Macromolecular Bioscience* 8(2): 177-183.

Träger, J., Kim, H. C., & Hampp, N. 2006. Polymers for refractive index change in intraocular lenses: A novel approach for photoinduced tuning of focal length. Proc. SPIE 6138, Ophthalmic Technologies XVI, 61381D (March 07, 2006); http://dx.doi.org/10.1117/12.646214.

Träger, J., Kim, H. C. & Hampp, N. 2007. Ophthalmology: Two-photon treatment. *Nature Photonics* 1(9): 509-511.

Trnka, T. M., & Grubbs, R. H. 2001. The development of L2X2Ru CHR olefin metathesis catalysts: an organometallic success story. *Accounts of Chemical Research* 34(1): 18-29.

Uc, J. M. C., Espinosa, J. I. M., Rodriguez, J. V. C., Ortega, A. A., Torres, H. V., Fernandez, A. M. & Roman, J. S. 2009. TGA/FTIR studies of segmented aliphatic polyurethanes and their nanocomposites prepared with commercial montmorillonites. *Polymer degradation and stability* 94: 1666-1677.

Ulihin, A. S., Uvarov, N.F., Mateyshina, Y. G., Brezhneva, L. I. & Matvienko, A. A. 2006. Composite solid electrolytes $LiClO_4$-Al_2O_3. *Solid State Ionics* 177: 2787-2790.

Vandiver, M. A., Caire, B. R., Ertem, S. P., Tsai, T., Coughlin, E. B., Herring, A. M. & Liberatore, M. W. 2015. Mechanical Performance of Polyiosoprene Copolymer Anion Exchange Membranes by Varying Crosslinking Methods *162*(4): 206-212.

Varley, R. J. & van der Zwaag, S. 2008. Development of a quasi-static test method to investigate the origin of self-healing in ionomers under ballistic conditions. *Polymer Testing* 27(1): 11-19.

Varley, R. J., & van der Zwaag, S. 2008. Towards an understanding of thermally activated self-healing of an ionomer system during ballistic penetration. *Acta Materialia* 56(19): 5737-5750.

Velayutham, T.S., Majid, W.H., Ahmad, A.B., Kang, G.Y. & Gan, S.N. 2009. Synthesis and Characterization of Polyurethane Coatings Derived from Polyols Synthesized with Glycerol, Phthalic Anhydride and Oleic Acid. *Progress in Organic Coatings* 66(4): 367-371.

Wang, S. & Min, K. 2011. Solid Polymer Electrolytes of Blends of Polyurethane and Polyether Modified Polysiloxane and Their Ionic Conductivity. *Polymer* 51: 2621-2628.

Wang, W., Xu, L., Li, X., Yang, Y. & An, E. 2014. Self-healing properties of protective coatings containing diisocyanate microcapsules on carbon steel surfaces. *Corrosion Science* 80: 528-535.

Watanabe, M., Nagano, S., Sanui, K. & Ogata, N. 1986. Ion conduction mechanism in network polymers from poly (ethylene oxide) and poly (propylene oxide) containing lithium perchlorate. *Solid State Ionics* 18: 338-342.

Weston, J.E., & Steele, B.C.H. 1982. Effects of inert fillers on the mechanical and electrochemical properties of lithium salt-poly(ethylene oxide) polymer electrolytes. *Solid State Ionics* 7: 75-79.

White, S. R., Sottos, N. R., Geubelle, P. H. & Moore, J. S. 2001. Autonomic healing of polymer composites. *Nature* 409(6822): 794.

White, S. R., Caruso, M. M. & Moore, J. S. 2008. Autonomic healing of polymers. *Mrs Bulletin* 33(8): 766-769.

Williams, H. R., Trask, R. S., Weaver, P. M. & Bond, I. P. 2008. Minimum mass vascular networks in multifunctional materials. *Journal of the Royal Society Interface* 5(18): 55-65.

Wilson, G. O., Moore, J. S., White, S. R., Sottos, N. R. & Andersson, H. M. 2008. Autonomic healing of epoxy vinyl esters via ring opening metathesis polymerization. *Advanced Functional Materials* 18(1): 44-52.

Wolff, T. & Görner, H. 2010. Photocleavage of dimers of coumarin and 6-alkylcoumarins. *Journal of Photochemistry and Photobiology A: Chemistry* 2010: 219-223.

Wong, C.S. & Badri, K.H. 2010 Thermal and Fire Resistant Properties of Palm Kernel Oil and Soybean Oil-Based Polyurethanes. *Sains Malaysiana* 39(5): 775-784.

Wong, C. S. & Badri, K. H. 2012. Chemical Analyses of Palm Kernel Oil-Based Polyurethane Prepolymer. *Materials Sciences and Applications* 3: 78-86.

Wright, P. V. 1975. Electrical conductivity in ionic complexes of poly (ethylene oxide). *Polymer International* 7(5): 319-327.

Wu, D. Y., Meure, S. & Solomon, D. 2008. Self-healing polymeric materials: A review of recent developments. *Progress in Polymer Science 33*(5): 479-522.

Xiao, D. S., Yuan, Y. C., Rong, M. Z. & Zhang, M. Q. 2009. Hollow polymeric microcapsules : Preparation, characterization and application in holding boron trifluoride diethyl etherate. *Polymer 50*(2), 560-568.

Xiong, S., Yang, F., Ding, G., Mya, K. Y., Ma, J. & Lu, X. 2012. Covalent bonding of polyaniline on fullerene: Enhanced electrical, ionic conductivities and electrochromic performances. *Electrochimica Acta* 67: 194-200.

Xu, J. J. & Ye, H. 2005. Polymer gel electrolytes based on oligomeric polyether/cross-linked PMMA blends prepared via in situ polymerization. *Electrochemistry communications* 7(8): 829-835.

Xu, K. 2004. Nonaqueous liquid electrolytes for lithium-based rechargeable batteries. *Chemical reviews* 104(10): 4303-4418.

Xu, T., Yuan, W., Wang, S.J., Li, Z.F., Sun, B.Q. & Wang, M.X. 2008. Synthesis of Polyurethane Modified Bismaleimide (UBMI) and Polyurethane-Imide Elastomer. *Chinese Journal of Polymer Science* 26(1): 117-119.

Yamaguchi, M., Ono, S. & Okamoto, K. 2009. Interdiffusion of dangling chains in weak gel and its application to self-repairing material. *Journal of Materials Science and Engineering: B* 162(3):189-194.

Yeganeh, H. & Hojati-Talemi, P. 2007. Preparation and Properties of Novel Biodegradable Polyurethane Networks Based on Castor Oil and Poly (Ethylene Glycol). *Polymer Degradation and Stability* 92(3): 480-489.

Yeom, C. K., Oh, S. B., Rhim, J. W. & Lee, J. M. 2000. Microencapsulation of water-soluble herbicide by interfacial reaction. I. Characterization of microencapsulation. *Journal of Applied Polymer Science* 78(9):1645-55.

Yin, T., Rong, M. Z., Zhang, M. Q. & Yang, G. C. 2007. Self-healing epoxy composites–preparation and effect of the healant consisting of microencapsulated epoxy and latent curing agent. *Composites Science and Technology* 67(2): 201-212.

Yuan, F., Chen, H. Z., Yang, H. Y., Li, H. Y. & Wang, M. 2005. PAN–PEO solid polymer electrolytes with high ionic conductivity. *Materials chemistry and physics* 89(2): 390-394.

Yuan, Y. C., Rong, M. Z., Zhang, M. Q., Chen, J., Yang, G. C., & Li, X. M. 2008. Self-Healing Polymeric Materials Using Epoxy/ Mercaptan as the Healant. *Macromolecules* 41: 5197-5202.

Yuan, Y. C., Rong, M. Z. & Zhang, M. Q. 2008. Preparation and characterization of microencapsulated polythiol. *Polymer* 49: 2531-2541.

Zafar, F. & Eram, S. 2012. *Polyurethane*, USA: InTech Open.

Zhang, M. Q. 2012. Sunlight stimulated repeated self healing. *Express Polymer Letters* 6(2): 95.

Zhao, L., Loy, D. A. & Shea, K. J. 2006. Photodeformable spherical hybrid nanoparticles. *Journal of the American Chemical Society* 128(44): 14250-14251.

APPENDIX A

^{1}H NMR spectrum of the synthesized chain extended dihydroycoumarin

A1 ^{1}H NMR spectrum of the product obtained from Experiment 1

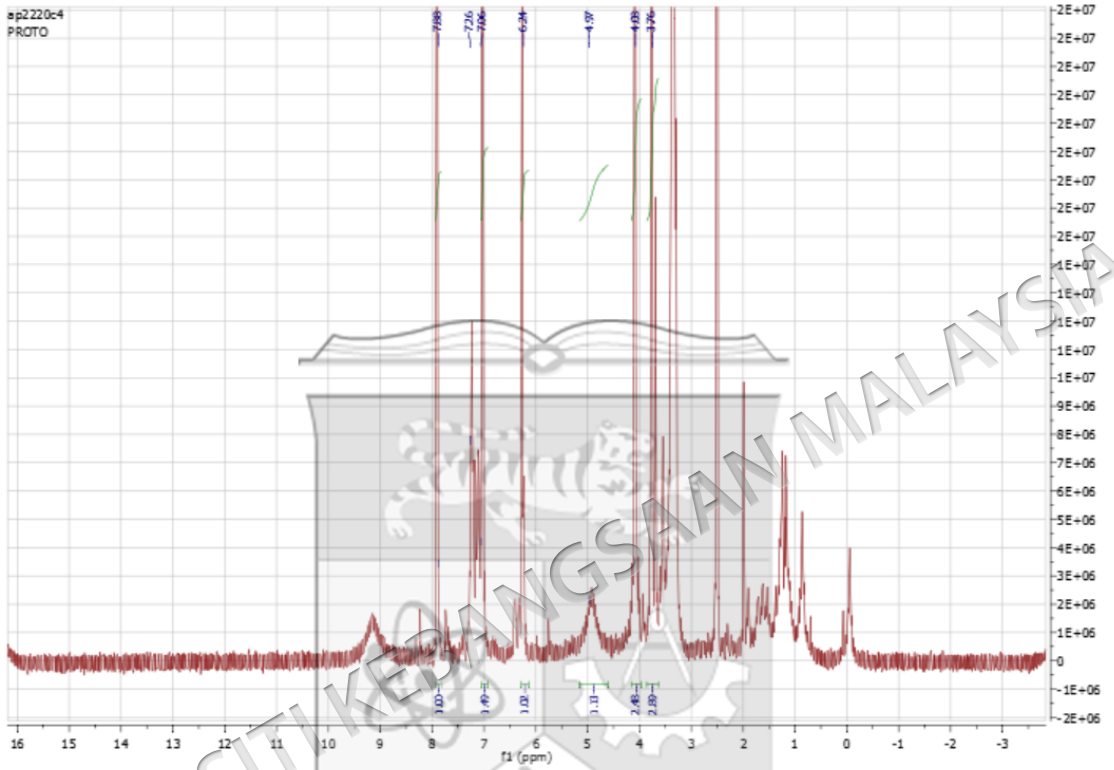

A2 ^{1}H NMR spectrum of the product obtained from Experiment 2

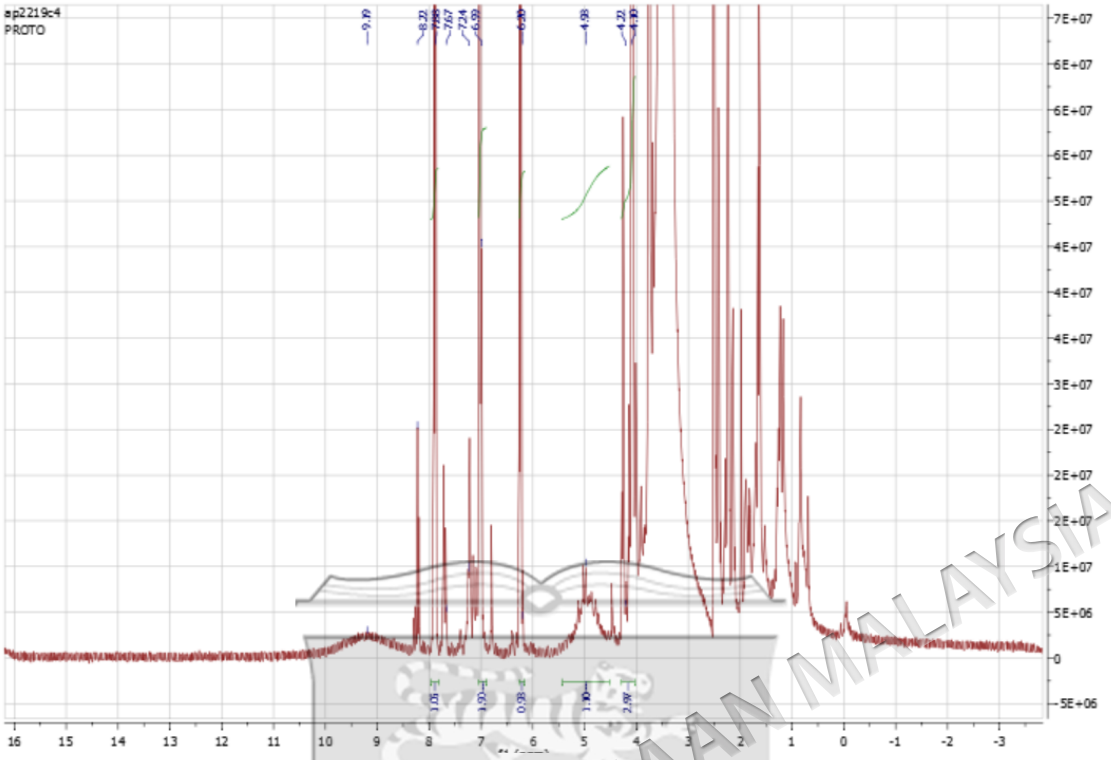

A3 ^{1}H NMR spectrum of the product obtained from Experiment 3

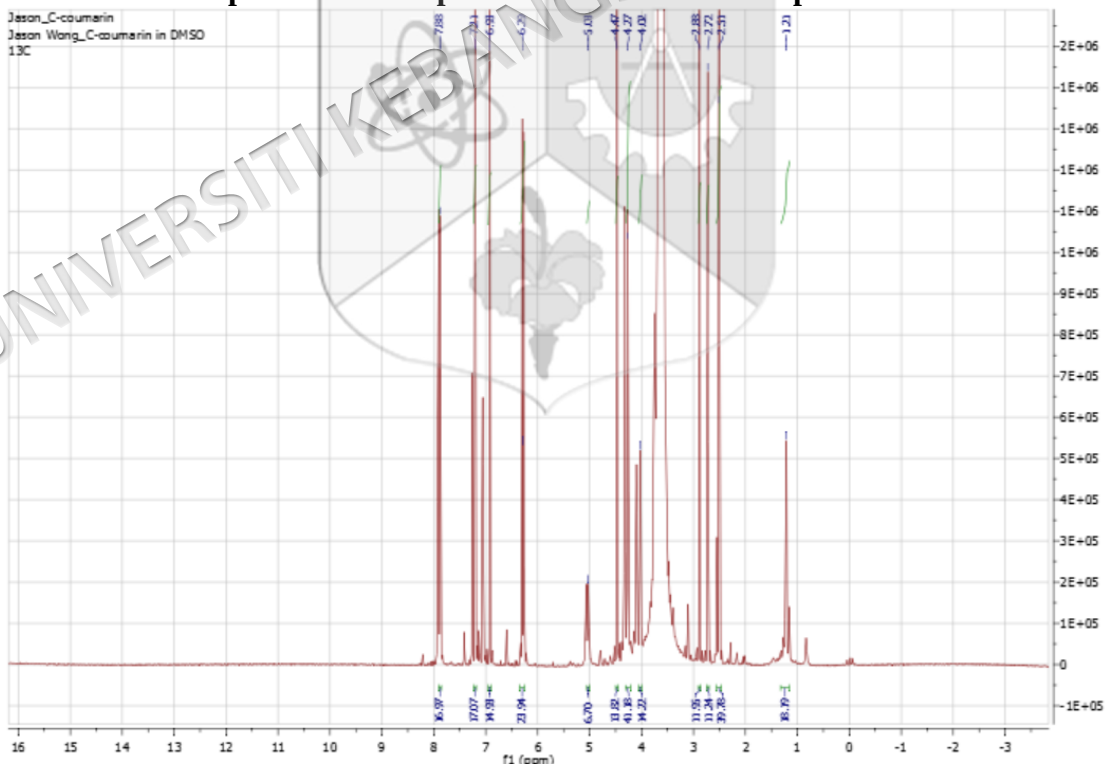

A4 ^{1}H NMR spectrum of the product obtained from Experiment 4

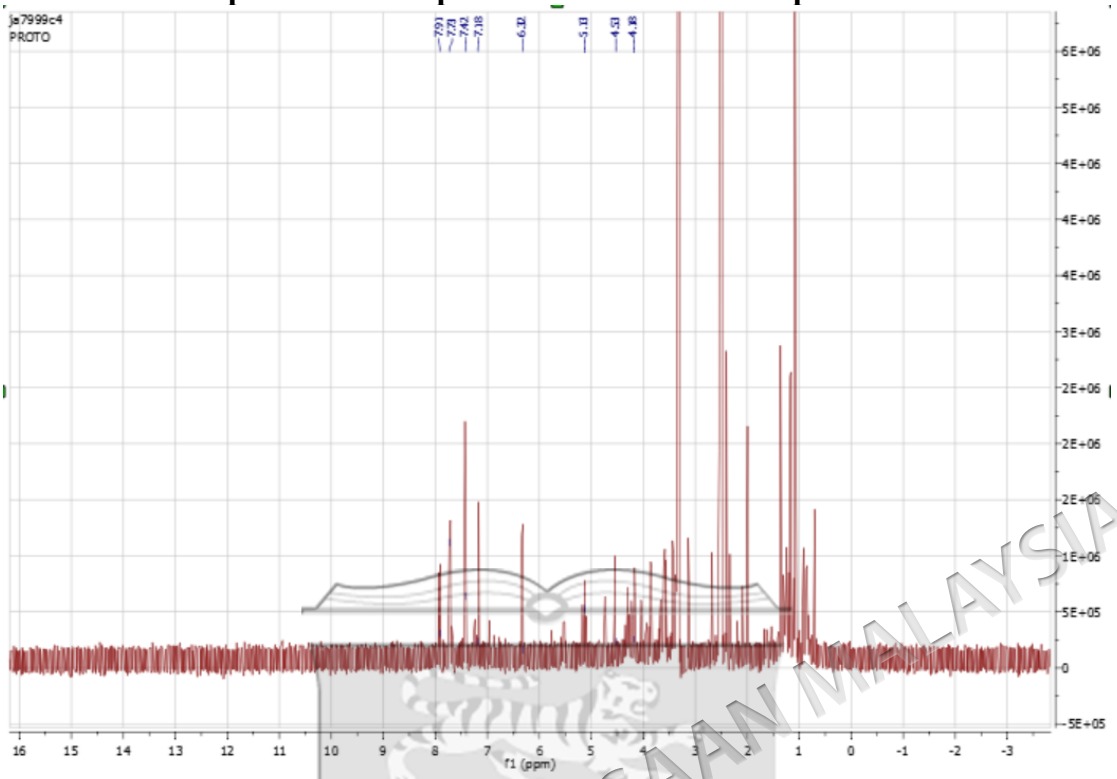

A5 ^{1}H NMR spectrum of the product obtained from Experiment 5

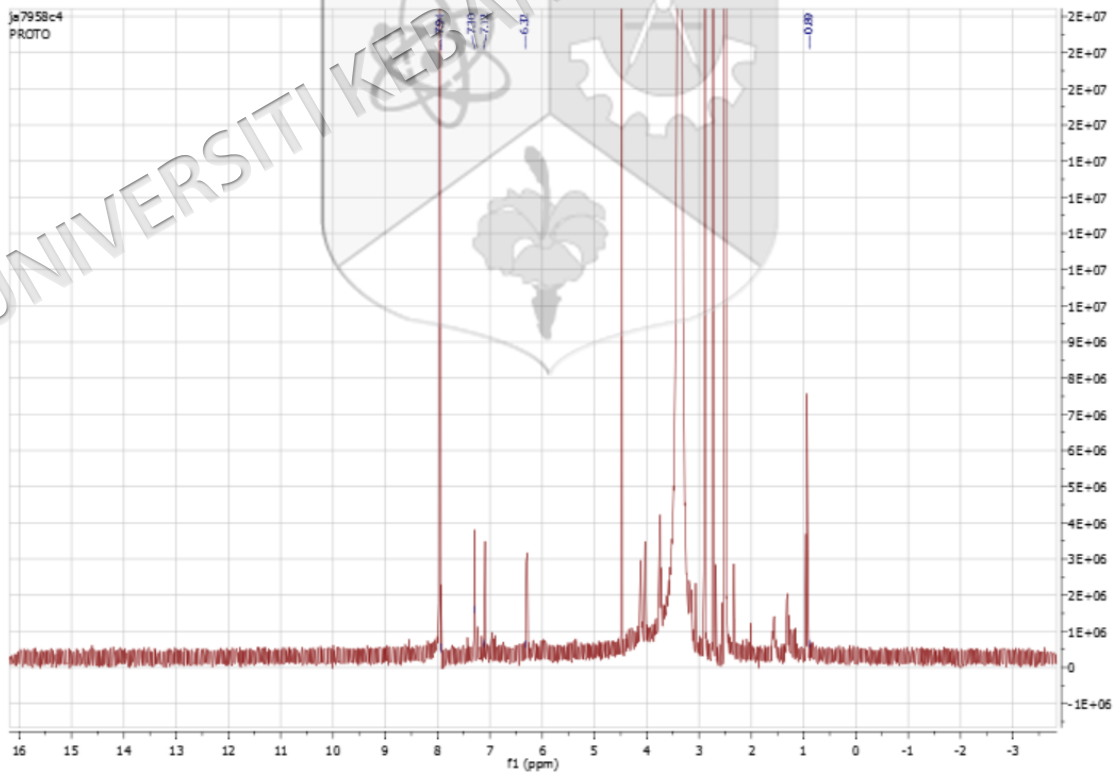

A6 ^{1}H NMR spectrum of the product obtained from Experiment 6

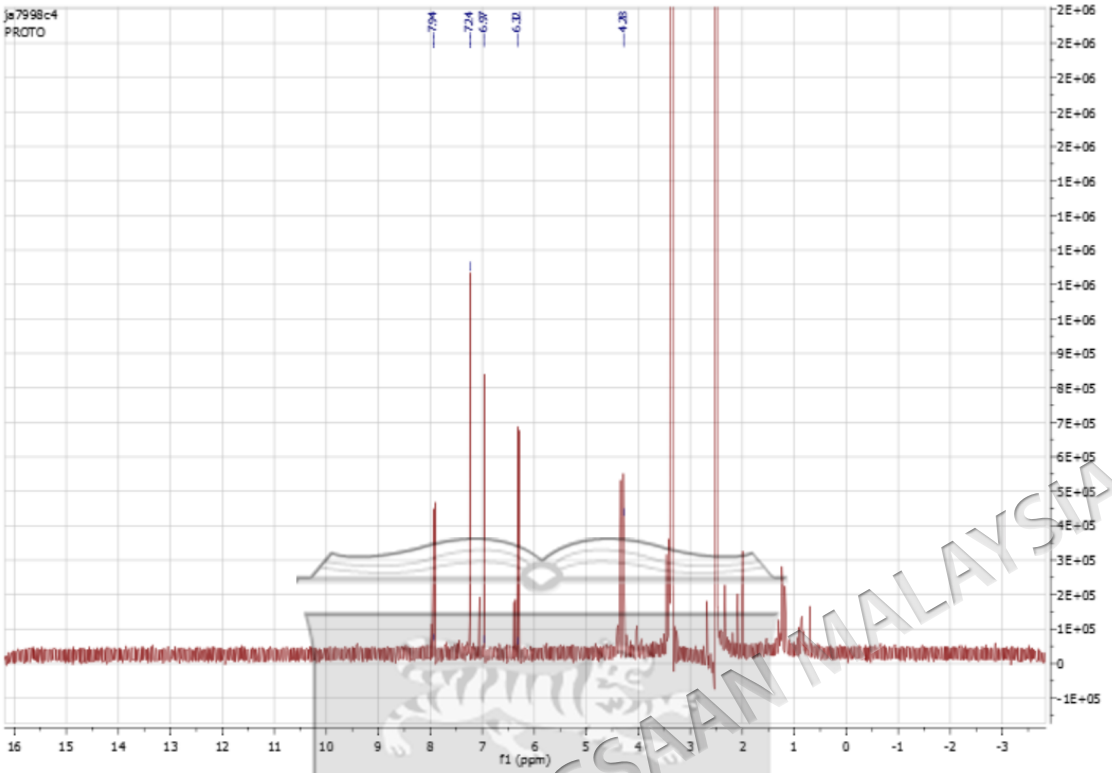

A7 ^{1}H NMR spectrum of the product obtained from Experiment 7

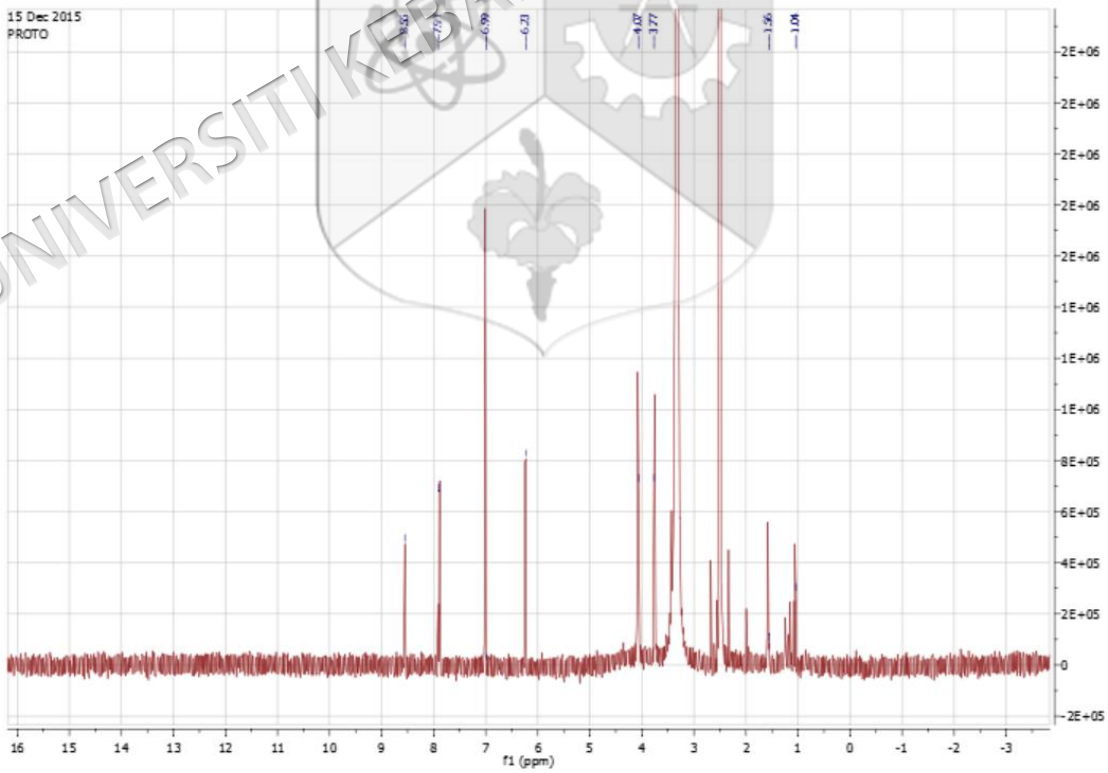

APPENDIX B

Chemical shifts, spitting patterns and integration ratio of chain extended dihydroxycoumarin and various extracted poroducts from experiments 1 to 7

Chain extended dihydroxycoumarin		
Chemical shift	Integration	Splitting patterns
7.94	1	Doublet
6.98	2	Singlet
6.22	1	Doublet
4.9	2	Singlet
4.33	4	Triplet
3.69	4	Triplet

Experiment 1 sample		
Chemical shift	Integration	Splitting patterns
7.93	1	Singlet
6.93	1	Quartet
6.29	1	Triplet
5.03	1	Singlet
4.27	4	Triplet
3.70	overlap with solvent peak	-

Experiment 2 sample		
Chemical shift	Integration	Splitting patterns
7.88	1	Doublet
6.99	2	Singlet
6.24	1	Singlet
4.93	1	Doublet
4.22	3	Doublet
3.70	overlap with solvent peak	-

Experiment 3 sample		
Chemical shift	Integration	Splitting patterns
7.90	3	Doublet
7.00	5	Singlet
6.23	3	Doublet
5.00	1	Doublet
4.23	2	Doublet
3.73	overlap with solvent peak	-

Experiment 4 sample		
Chemical shift	Integration	Splitting patterns
7.90	3	Doublet
7.00	4	Singlet
6.40	4	Singlet
5.31	1	Triplet
4.23	2	Triplet
3.73	overlap with solvent peak	-

Experiment 5 sample		
Chemical shift	Integration	Splitting patterns
8.00	7	Singlet
7.09	1	Doublet
6.43	1	Singlet
4.41	1	Doublet
3.71	Overlap with solvent peak	-

Experiment 6 sample		
Chemical shift	Integration	Splitting patterns
7.95	1	Singlet
7.00	5	Singlet
6.32	2	Doublet
4.10	3	Singlet
3.72	3	Singlet

Experiment 7 sample		
Chemical shift	Integration	Splitting patterns
7.90	1	Doublet
7.00	3	Singlet
6.33	1	Singlet
4.11	2	Singlet
3.83	2	Singlet

APPENDIX C

Stress-Strain Curve Of Various PU-$LiClO_4$ and Self-Healing PU-$LiClO_4$

C1 Stress-Strain curve of PU200-5

TNB

ASTM D 638

Test: Rate 1	10.00000 mm/min

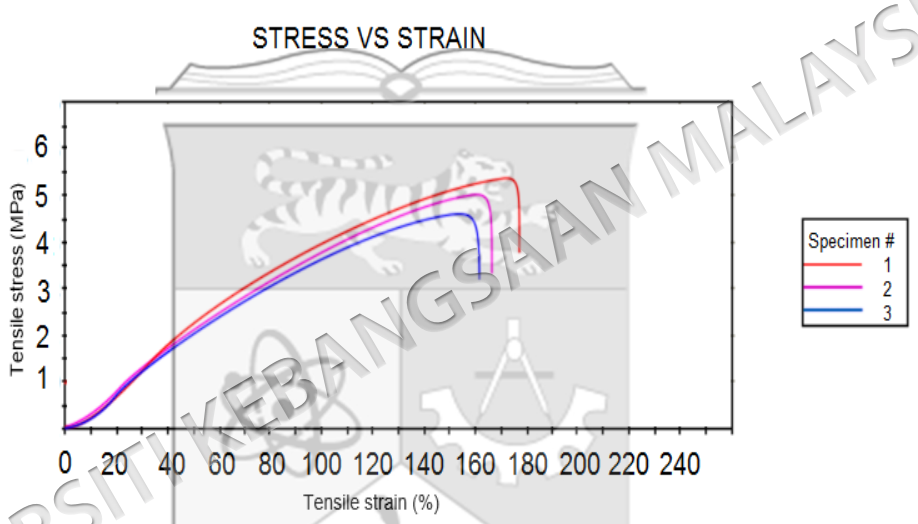

	Tensile stress at Maximum Load (MPa)	*Modulus (Automatic Young's) (MPa)*	*Tensile strain at Break (Standard) (%)*	*Tensile stress at Break (Standard) (MPa)*
1	5.404	2.523	178.739	5.404
2	4.994	2.619	167.431	4.994
3	4.530	2.317	163.882	4.530
Maximum	5.404	2.619	178.739	5.404
Minimum	4.530	2/317	163.882	4.530
Mean	4.976	2.486	170.017	4.976

C2 Stress-Strain curve of PU150-5

TNB

ASTM D 638

Test: Rate 1	10.00000 mm/min

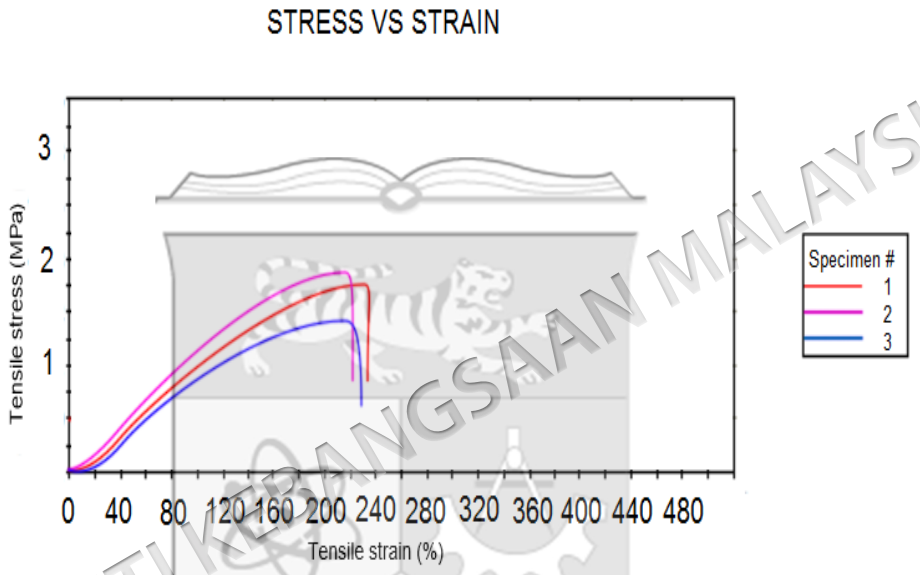

	Tensile stress at Maximum Load (MPa)	*Modulus (Automatic Young's) (MPa)*	*Tensile strain at Break (Standard) (%)*	*Tensile stress at Break (Standard) (MPa)*
1	2.104	1.884	219.645	2.104
2	2.286	1.983	205.340	2.286
3	2.485	1.946	222.034	2.485
Maximum	2.485	1.983	222.034	2.485
Minimum	2.104	1.946	205.340	2.104
Mean	2.292	1.938	215.673	2.292

C3 Stress-Strain curve of PU150-5

TNB

ASTM D 638

Test: Rate 1	10.00000 mm/min

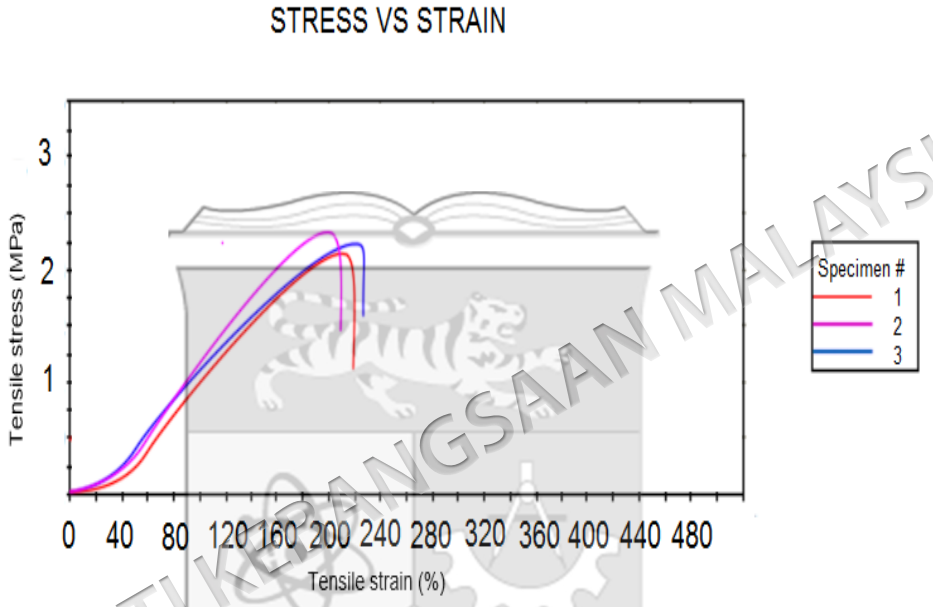

	Tensile stress at Maximum Load (MPa)	*Modulus (Automatic Young's) (MPa)*	*Tensile strain at Break (Standard) (%)*	*Tensile stress at Break (Standard) (MPa)*
1	2.127	1.857	218.670	2.127
2	2.316	1.994	208.453	2.316
3	2.245	1.768	224.143	2.245
Maximum	2.316	1.994	224.143	2.316
Minimum	2.127	1.768	208.453	2.127
Mean	2.229	1.873	217.089	2.229

C4 Stress-Strain curve of PU85-5

TNB

ASTM D 638

Test: Rate 1	10.00000 mm/min

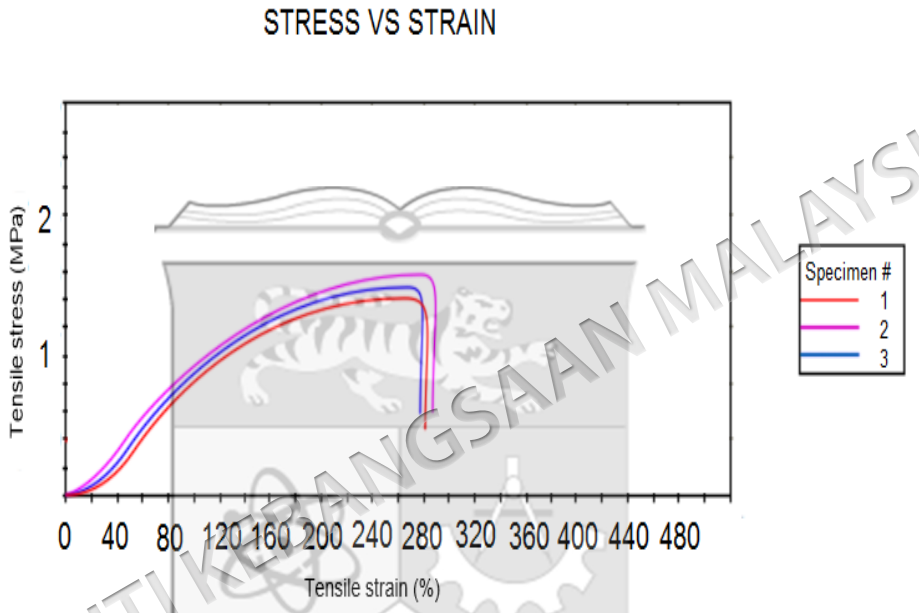

	Tensile stress at Maximum Load (MPa)	*Modulus (Automatic Young's) (MPa)*	*Tensile strain at Break (Standard) (%)*	*Tensile stress at Break (Standard) (MPa)*
1	1.532	1.067	281.461	1.532
2	1.604	1.152	287.539	1.604
3	1.478	1.045	275.338	1.478
Maximum	1.604	1.152	287.539	1.604
Minimum	1.478	1.045	275.338	1.478
Mean	1.538	1.088	281.446	1.538

C5 Stress-Strain curve of PU200-0

TNB

ASTM D 638

Test: Rate 1	10.00000 mm/min

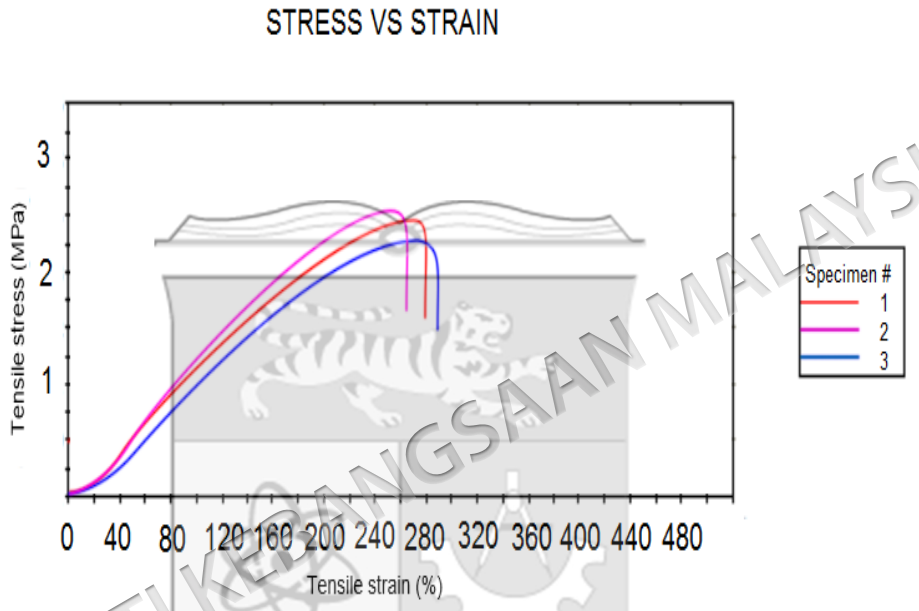

	Tensile stress at Maximum Load (MPa)	*Modulus (Automatic Young's) (MPa)*	*Tensile strain at Break (Standard) (%)*	*Tensile stress at Break (Standard) (MPa)*
1	2.496	1.461	278.423	2.496
2	2.517	1.598	262.946	2.517
3	2.258	1.053	291.944	2.258
Maximum	2.517	1.598	291.944	2.517
Minimum	2.258	1.053	262.946	2.258
Mean	2.424	1.371	277.771	2.424

C6 Stress-Strain curve of PU200-10

TNB

ASTM D 638

Test: Rate 1	10.00000 mm/min

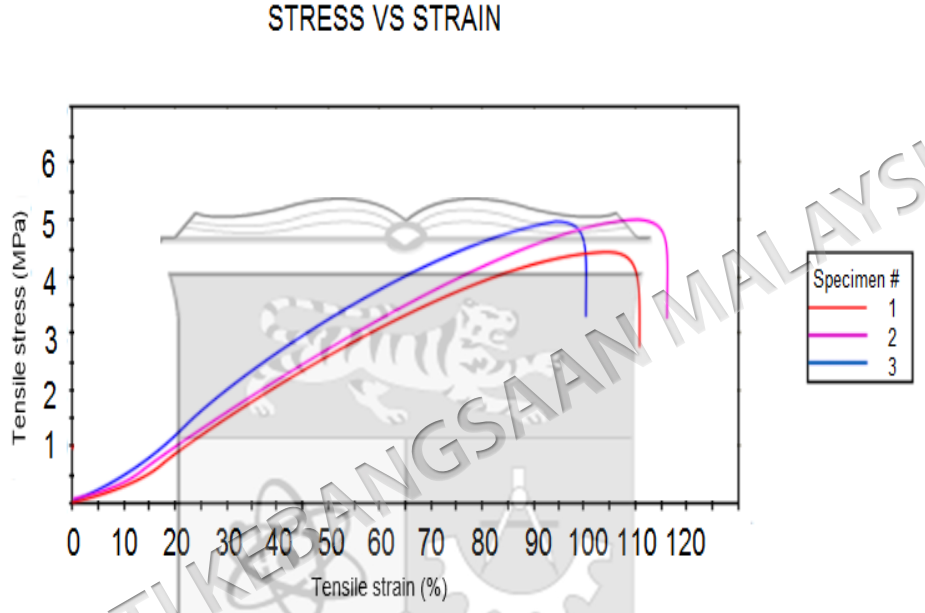

	Tensile stress at Maximum Load (MPa)	*Modulus (Automatic Young's) (MPa)*	*Tensile strain at Break (Standard) (%)*	*Tensile stress at Break (Standard) (MPa)*
1	4.486	10.424	108.175	4.486
2	5.132	9.281	113.433	5.132
3	5.045	11.237	96.573	5.045
Maximum	5.132	11.237	113.433	5.132
Minimum	4.486	9.281	96.573	4.486
Mean	4.888	10.314	106.060	4.888

C7 Stress-Strain curve of PU200C96-5

TNB

ASTM D 638

Test: Rate 1	10.00000 mm/min

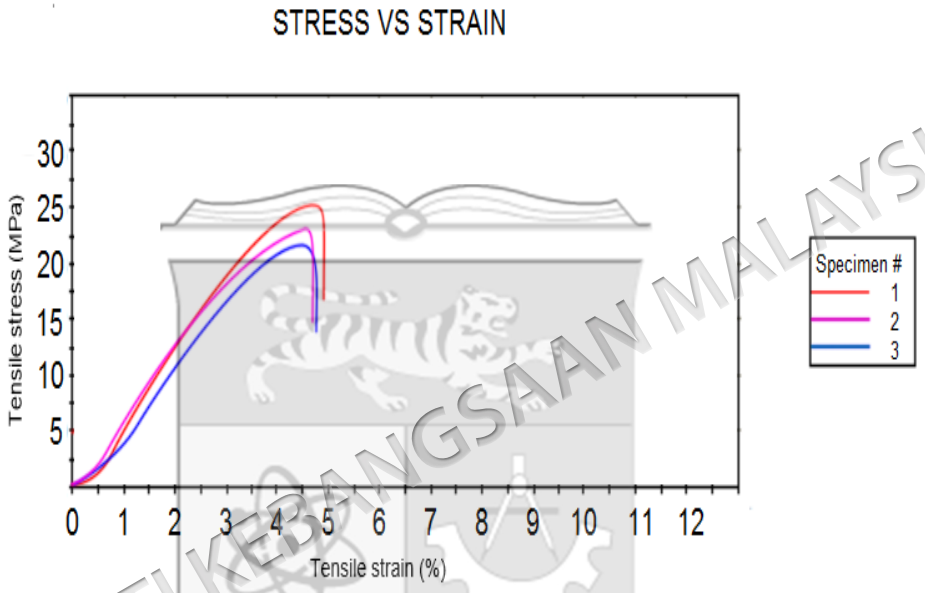

	Tensile stress at Maximum Load (MPa)	*Modulus (Automatic Young's) (MPa)*	*Tensile strain at Break (Standard) (%)*	*Tensile stress at Break (Standard) (MPa)*
1	25.087	534.143	4.956	19.987
2	22.613	541.066	4.712	18.184
3	20.374	523.634	4.812	16.034
Maximum	25.087	541.066	4.956	19.987
Minimum	20.374	523.634	4.712	16.034
Mean	22.691	532.948	4.827	18.068

C8 Stress-Strain curve of PU200C72-5

TNB

ASTM D 638

Test: Rate 1	10.00000 mm/min

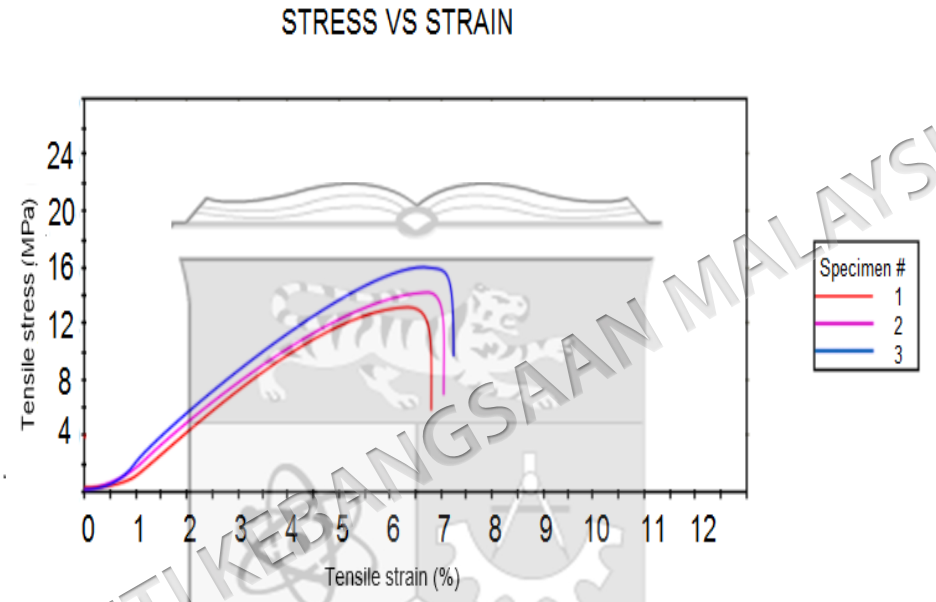

	Tensile stress at Maximum Load (MPa)	*Modulus (Automatic Young's) (MPa)*	*Tensile strain at Break (Standard) (%)*	*Tensile stress at Break (Standard) (MPa)*
1	12.034	445.863	6.812	12.034
2	14.321	453.213	7.041	14.321
3	16.213	475.421	7.351	16.213
Maximum	16.213	475.421	7.351	16.213
Minimum	12.034	445.863	6.812	12.034
Mean	14.189	458.165	7.068	14.189

C9 Stress-Strain curve of PU200C48-5

TNB

ASTM D 638

Test: Rate 1	10.00000 mm/min

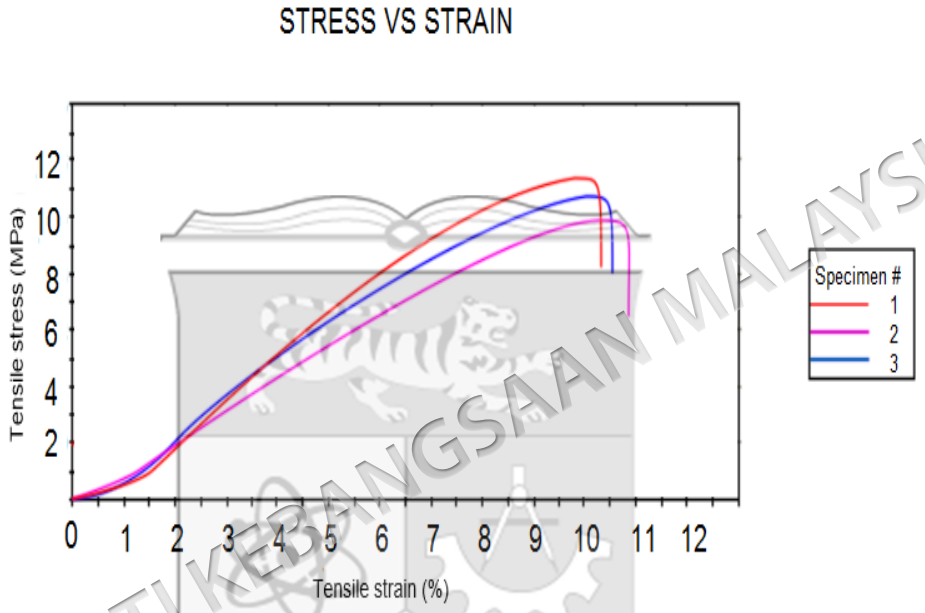

	Tensile stress at Maximum Load (MPa)	*Modulus (Automatic Young's) (MPa)*	*Tensile strain at Break (Standard) (%)*	*Tensile stress at Break (Standard) (MPa)*
1	11.275	335.123	10.733	11.275
2	9.312	298.857	10.696	9.312
3	10.886	331.266	10.489	10.886
Maximum	11.275	335.123	10.733	11.275
Minimum	9.312	298.857	10.489	9.312
Mean	10.491	321.749	10.639	10.491

C10 Stress-Strain curve of PU200C24-5

TNB

ASTM D 638

Test: Rate 1	10.00000 mm/min

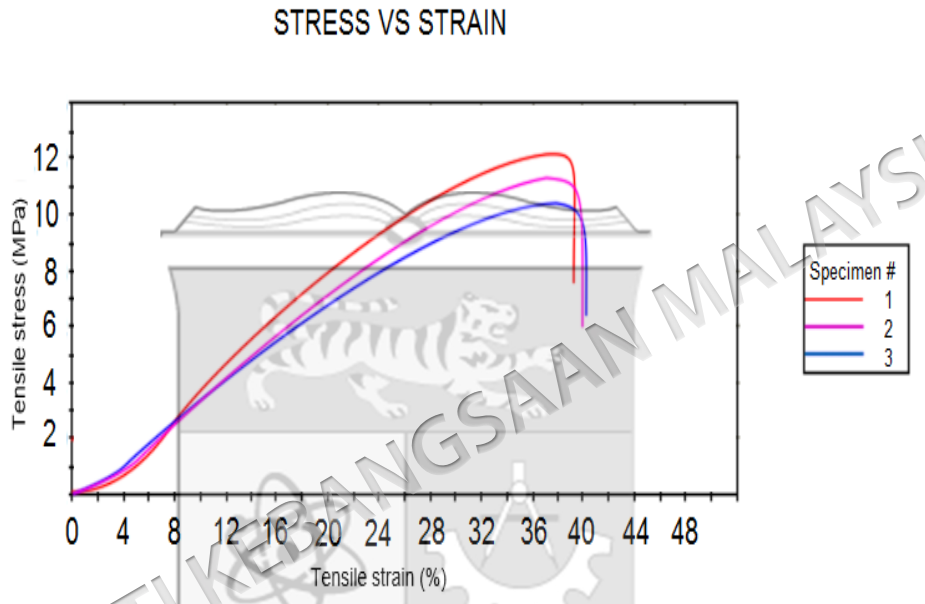

	Tensile stress at Maximum Load (MPa)	*Modulus (Automatic Young's) (MPa)*	*Tensile strain at Break (Standard) (%)*	*Tensile stress at Break (Standard) (MPa)*
1	12.112	223.135	38.856	12.112
2	11.245	210.885	39.944	11.245
3	10.264	203.128	40.794	10.264
Maximum	12.112	223.135	40.794	12.112
Minimum	10.264	203.128	38.856	10.264
Mean	11.207	212.383	39.865	11.207

C11 Stress-Strain curve of HPU200C96-5

TNB

ASTM D 638

Test: Rate 1	10.00000 mm/min

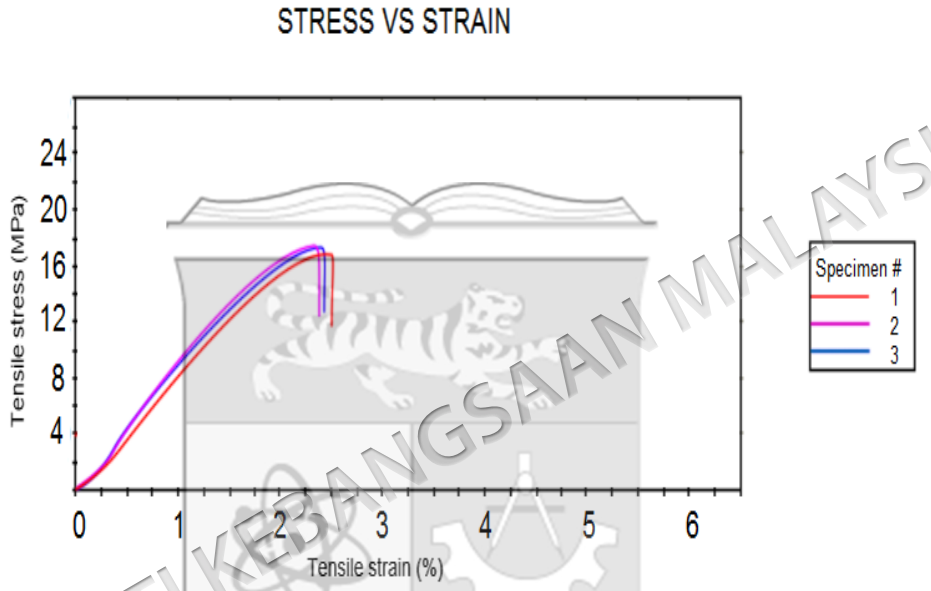

	Tensile stress at Maximum Load (MPa)	*Modulus (Automatic Young's) (MPa)*	*Tensile strain at Break (Standard) (%)*	*Tensile stress at Break (Standard) (MPa)*
1	16.351	581.843	2.523	16.351
2	17.030	601.235	2.162	17.030
3	16.957	593.127	2.471	16.957
Maximum	17.030	601.235	2.523	17.030
Minimum	16.351	581.843	2.162	16.351
Mean	16.779	592.098	2.385	16.779

C12 Stress-Strain curve of HPU200C72-5

TNB

ASTM D 638

Test: Rate 1	10.00000 mm/min

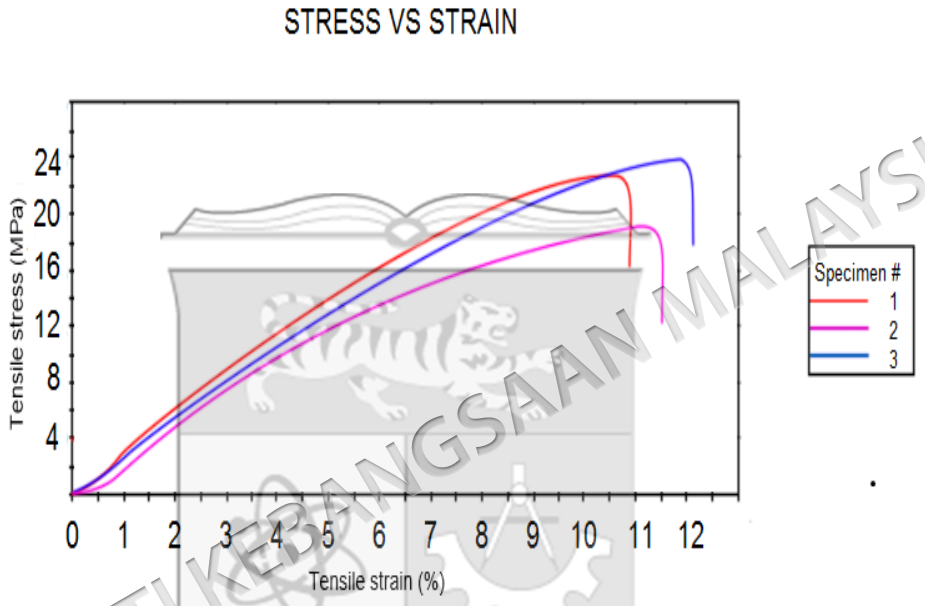

	Tensile stress at Maximum Load (MPa)	*Modulus (Automatic Young's) (MPa)*	*Tensile strain at Break (Standard) (%)*	*Tensile stress at Break (Standard) (MPa)*
1	22.321	465.161	10.654	22.321
2	19.846	454.322	11.501	19.846
3	24.102	475.123	12.143	24.102
Maximum	24.102	475.123	12.143	24.102
Minimum	19.846	454.322	10.654	19.846
Mean	22.090	464.869	11.433	22.090

C13 Stress-Strain curve of HPU200C48-5

TNB

ASTM D 638

Test: Rate 1	10.00000 mm/min

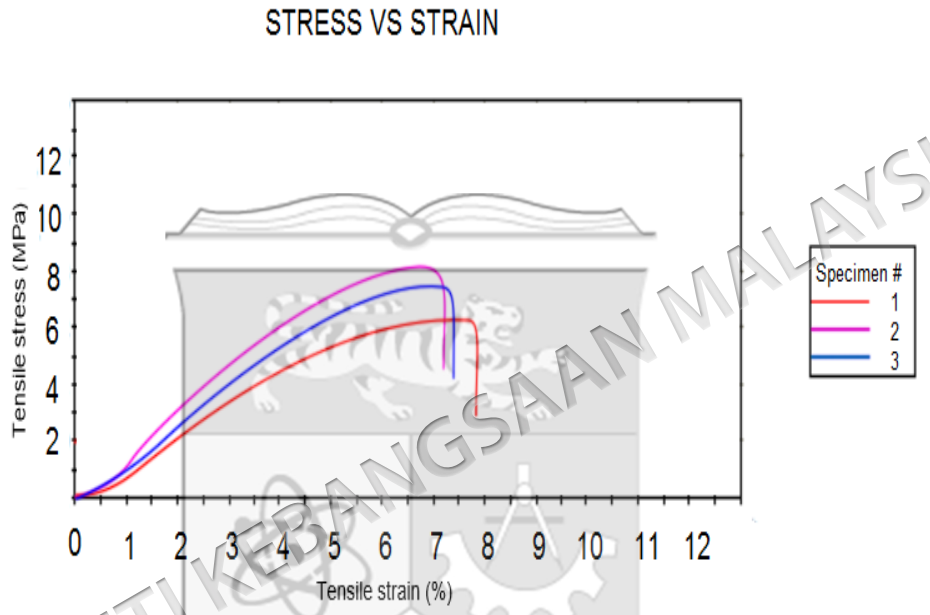

	Tensile stress at Maximum Load (MPa)	*Modulus (Automatic Young's) (MPa)*	*Tensile strain at Break (Standard) (%)*	*Tensile stress at Break (Standard) (MPa)*
1	6.236	354.853	7.854	6.236
2	8.096	401.965	7.163	8.096
3	7.379	386.199	7.412	7.379
Maximum	8.096	401.965	7.163	8.096
Minimum	6.236	354.853	7.854	6.236
Mean	7.235	381.006	7.476	7.235

C14 Stress-Strain curve of HPU200C24-5

TNB

ASTM D 638

Test: Rate 1	10.00000 mm/min

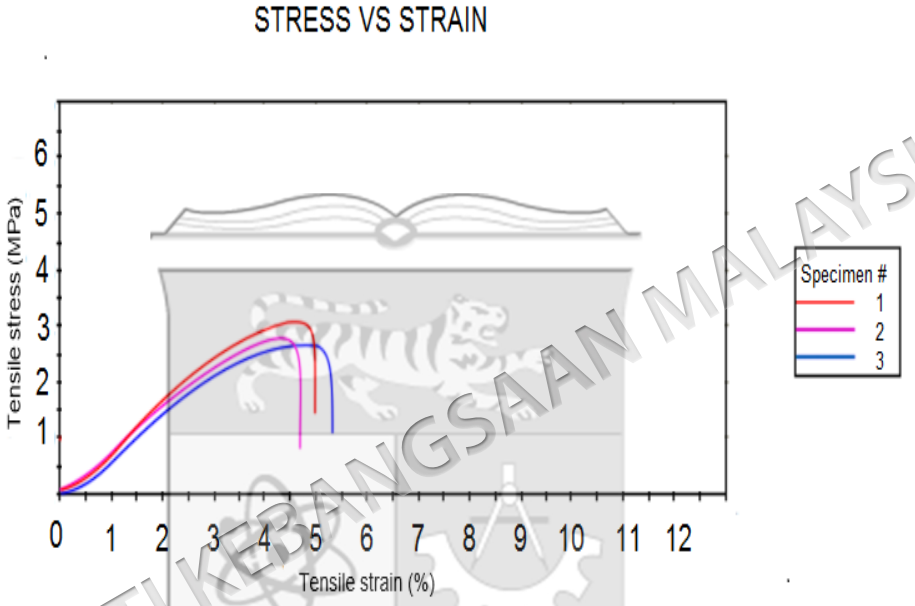

	Tensile stress at Maximum Load (MPa)	*Modulus (Automatic Young's) (MPa)*	*Tensile strain at Break (Standard) (%)*	*Tensile stress at Break (Standard) (MPa)*
1	2.957	283.845	4.996	2.957
2	2.613	262.387	4.686	2.613
3	2.487	252.645	5.387	2.487
Maximum	2.957	283.845	5.387	2.957
Minimum	2.487	252.645	4.686	2.487
Mean	2.686	266.292	5.023	2.686

C15 Stress-Strain curve of HPU200-5

TNB

ASTM D 638

Test: Rate 1	10.00000 mm/min

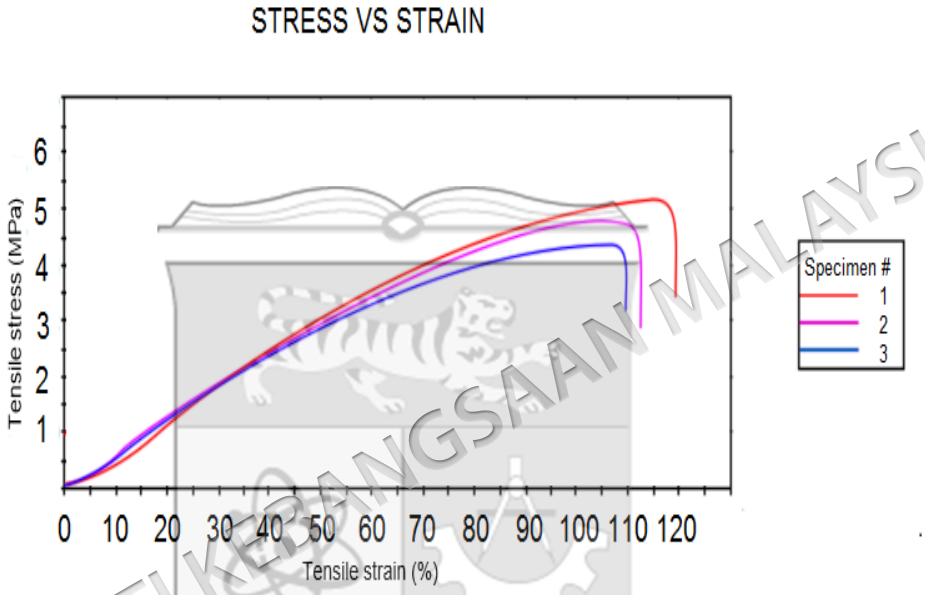

	Tensile stress at Maximum Load (MPa)	*Modulus (Automatic Young's) (MPa)*	*Tensile strain at Break (Standard) (%)*	*Tensile stress at Break (Standard) (MPa)*
1	5.032	9.746	119.262	5.032
2	4.869	9.329	112.795	4.869
3	4.353	9.425	109.320	4.353
Maximum	5.032	9.746	119.262	5.032
Minimum	4.353	9.329	109.320	4.353
Mean	4.751	9.500	113.792	4.751

APPENDIX D

Wavenumbers of Various PU-$LiClO_4$ and Self-Healing PU-$LiClO_4$

D1 FTIR spectroscopy analysis data of the pristine polyurethane and the PU-$LiClO_4$ at various NCO/OH ratio

Functional group	Wavenumber, cm^{-1}				
	PU200-0	PU200-5	PU150-5	PU100-5	PU85-5
C=O (urethane)	1725, 1711	1708	1708	1708	1708
C-N (urethane)	1598	1599	1598	1598	1599
N-H (urethane)	3296	3352	3327	3341	3336
C=C (benzene ring)	1533, 1510	1535, 1509	1534, 1509	1533, 1510	1534, 1510
C-O-C (urethane)	1067	1067	1067	1067	1067
N=C=O (isocyanate)	-	-	-	-	-
Ordered complexed C=O(urethane)	-	1649	-	-	-

D2 FTIR spectroscopy analysis data of the prestine polyurethane and the PU-$LiClO_4$ at various $LiClO_4$ content

Functional group	Wavenumber, cm^{-1}						
	PU200-0	PU200-5	PU200-10	PU200-15	PU200-20	PU200-25	PU200-30
C=O (urethane)	1725, 1711	1708	1707	1707	1708	1708	1707
C-N (urethane)	1598	1597	1597	1597	1597	1598	1598
N-H (urethane)	3296	3352	3359	3356	3363	3359	3359
C=C (benzene ring)	1533, 1510	1535, 1509	1534, 1510	1533, 1509	1533, 1509	1535, 1510	1535, 1509
C-O-C (urethane)	1067	1067	1067	1067	1069	1070	1068
N=C=O (isocyanate)	-	-	2282	2282	2277	2274	2275
Ordered complexed C=O (urethane)	-	1649	1649	1632	1637	1639	1636

D3 The wavenumber of different functional Groups in PU200-5, PU200C24-5, PU200C48-5, PU200C72-5 and PU200C96-5

Functional group	Wavenumber [cm^{-1}]					
	PU200-5	PU200C24-5	PU200C 48-5	PU200C 72-5	PU200C96-5	Condition
C=O	1708	1700	1702	1710	1710	Non irradiated
(urethane)	1708	1702	1702	1702	1700	UV irradiated
C-N	1599	1608	1602	1599	1596	Non irradiated
(urethane)	1597	1594	1595	1597	1594	UV irradiated
N-H	3352	3311	3303	3325	3316	Non irradiated
(urethane)	3316	3301	3297	3326	3319	UV irradiated
C=C	1535,	1527,	1527,	1533,	1529,	Non irradiated
(benzene ring)	1509	1511	1506	1508	1508	
	1531,	1531,	1525,	1527,	1521,	UV irradiated
	1513	1510	1506	1508	1508	
C-O-C	1067	1066	1068	1068	1068	Non irradiated
(urethane)	1063	1063	1063	1064	1064	UV irradiated
C=C	-	823	823	825	825	Non irradiated
(coumarin	-	823	823	825	825	UV irradiated
N=C=O	-	-	-	-	-	Non irradiated
(isocyanate)	-	-	-	-	-	UV irradiated
Ordered	1649	-	-	-	-	Non irradiated
complexed	-	-	-	-	-	UV irradiated
C=O						
(urethane)						

APPENDIX E

DSC thermograms of various PU-$LiClO_4$ and self-healing PU-$LiClO_4$

E1 DSC thermogram of PU-$LiClO_4$ with different NCO/OH ratios

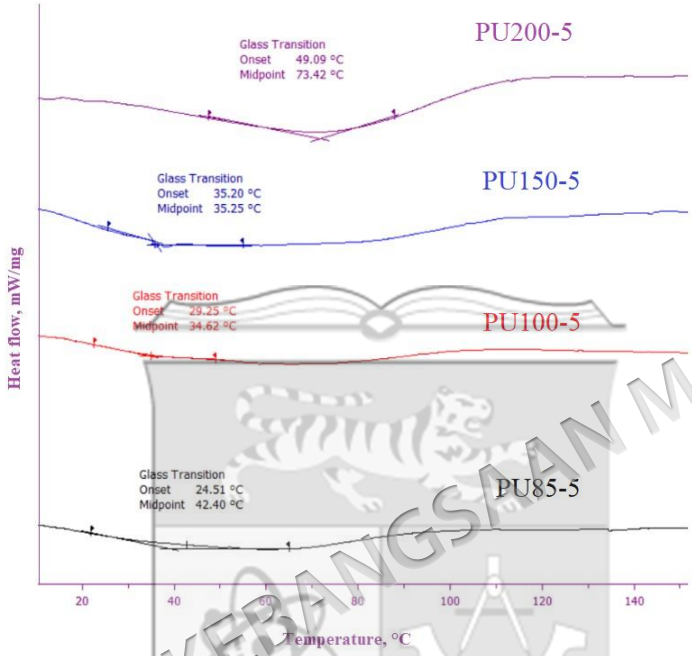

E2 DSC thermogram of PU-$LiClO_4$ with different $LiClO_4$ loading

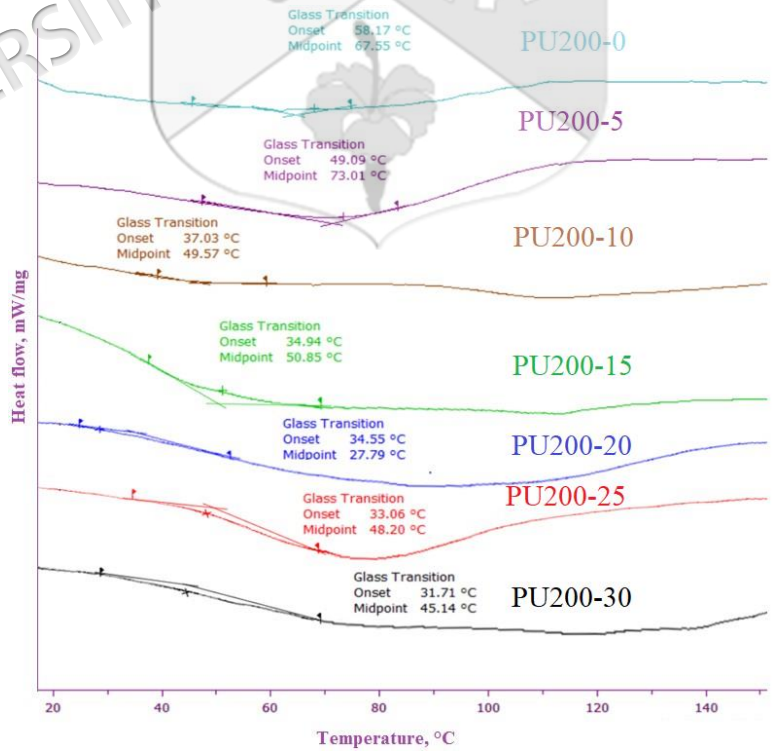

E3 DSC thermograms of non UV-irradiated self-healing polyurethanes and prestine polyurethane (PU200C96-5, PU200C72-5, PU200C48-5, PU200C24-5 and PU200-5)

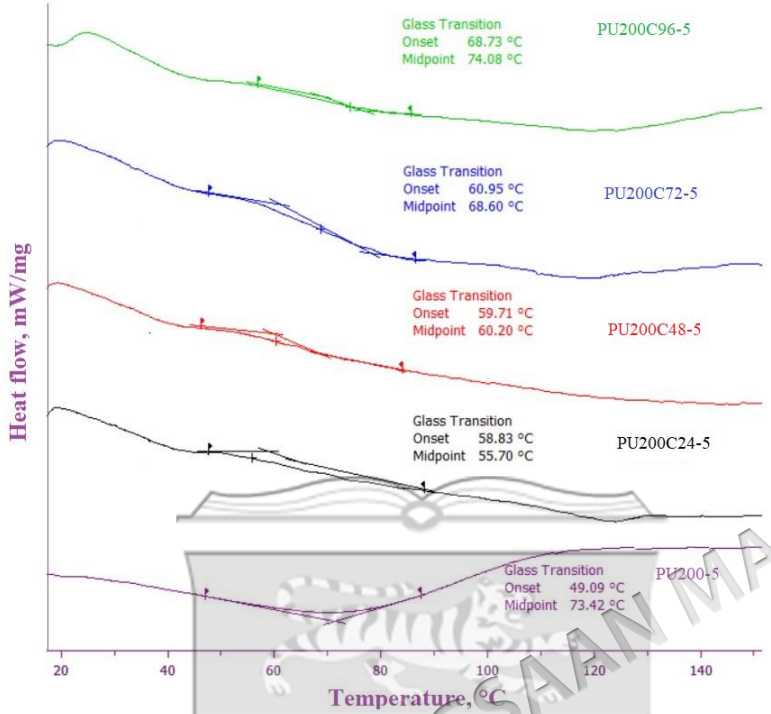

E4 DSC thermograms of UV-irradiated self-healing polyurethanes and prestine polyurethane (HPU200C96-5, HPU200C72-5, HPU200C48-5, HPU200C24-5 and HPU200-5)

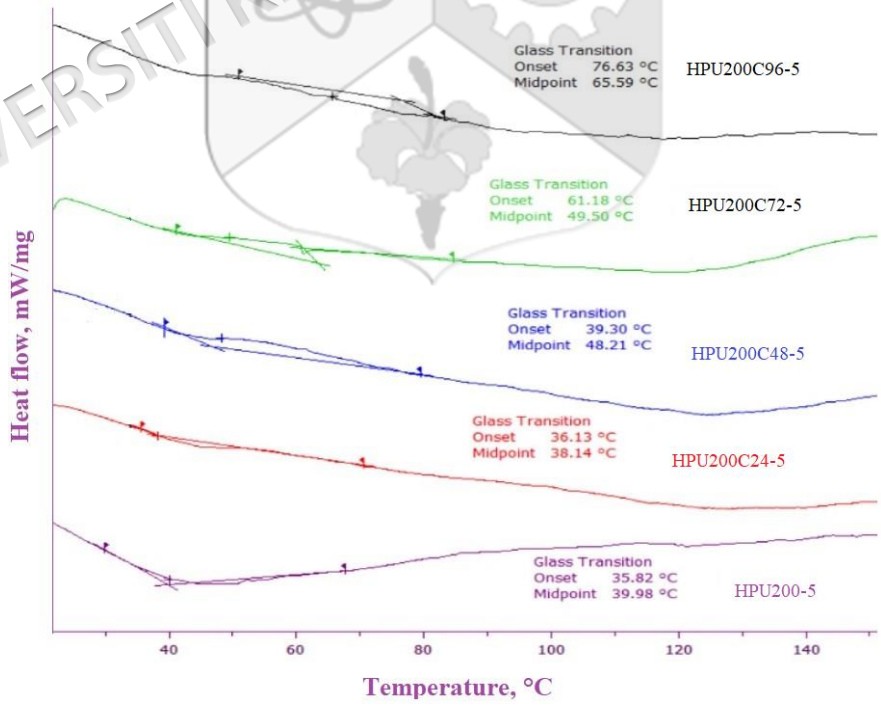

APPENDIX F

TGA thermograms and DTG curves for various PU-$LiClO_4$ and self-healing PU-$LiClO_4$

F1 **TGA thermograms and DTG curves for PU-$LiClO_4$ films with varying NCO/OH contents**

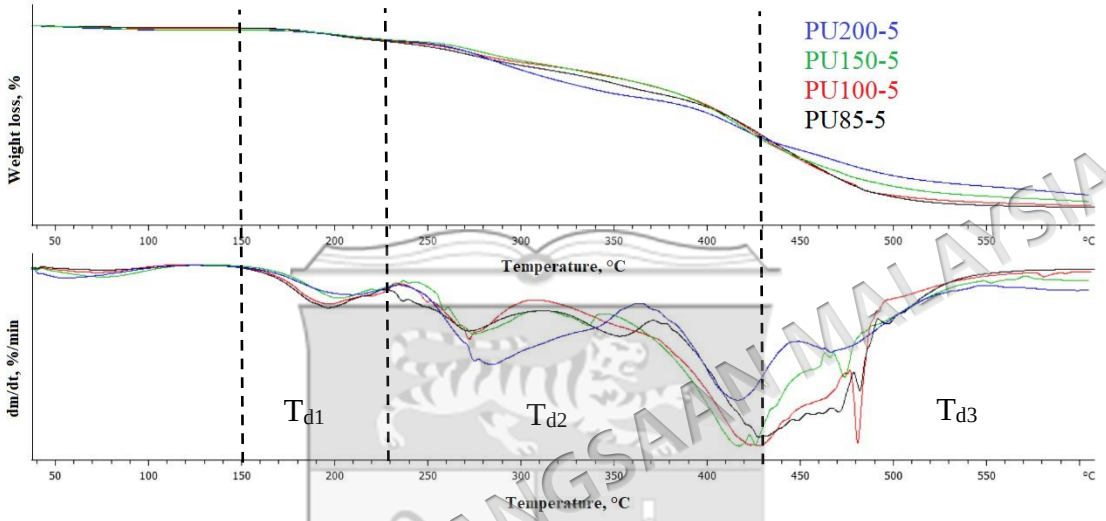

F2 **TGA thermograms and DTG curves for pristine PU and PU-$LiClO_4$ films at varying $LiClO_4$ content with 200/100 of NCO/OH ratio**

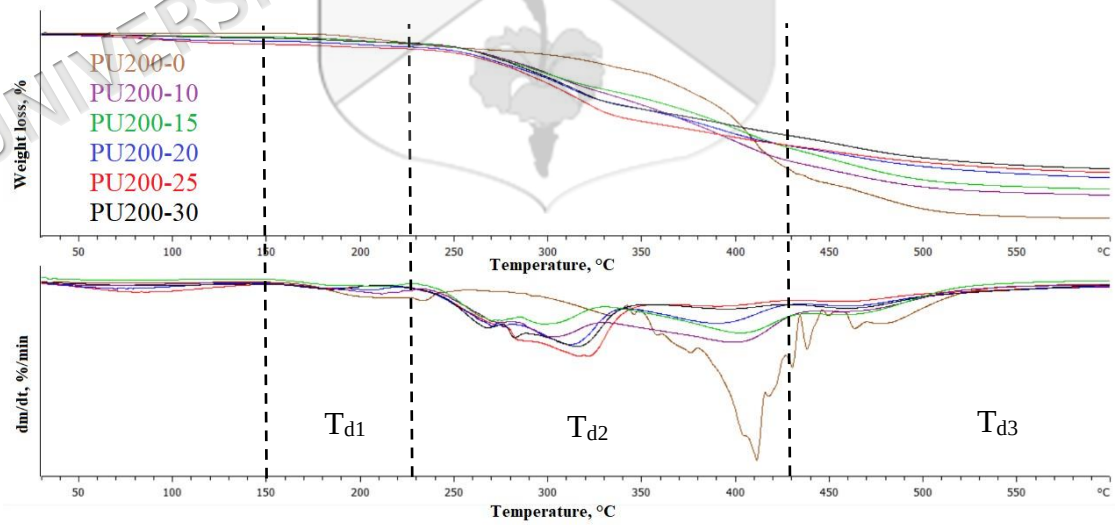

F3 Thermograms and DTG curves of non UV-irradiated PU200-5

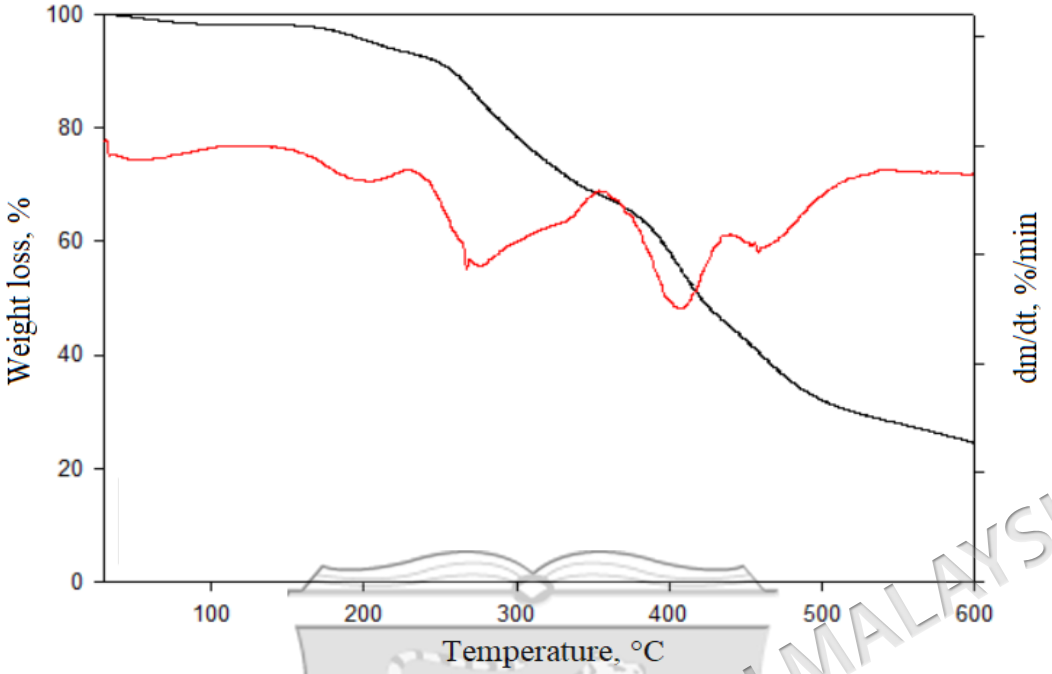

F4 Thermograms and DTG curves of UV-irradiated PU200-5

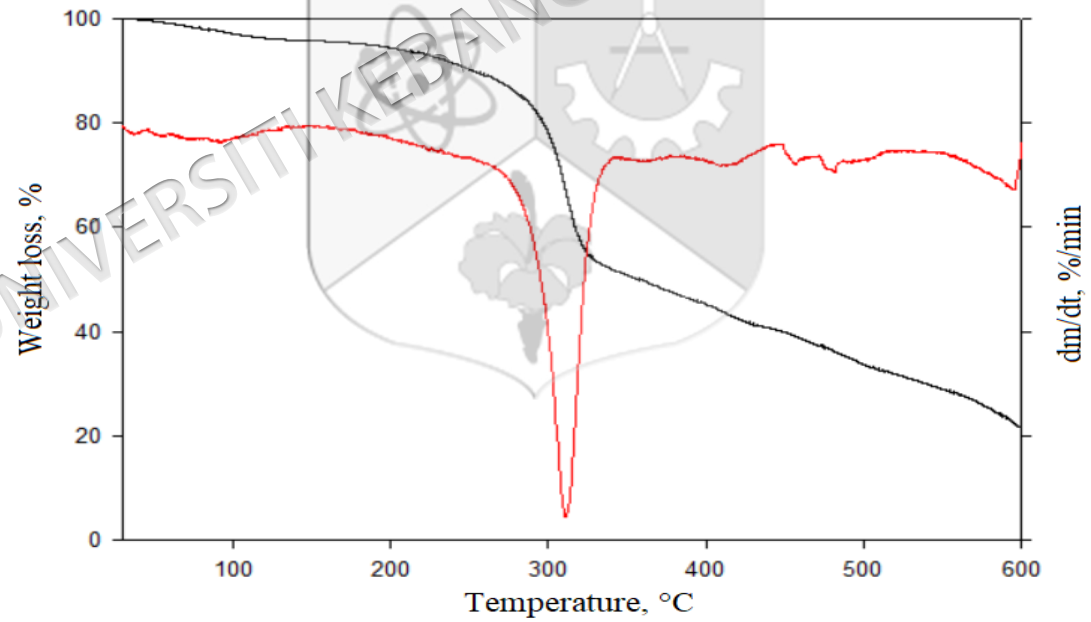

F5 Thermograms and DTG curves of non UV-irradiated PU200C24-5

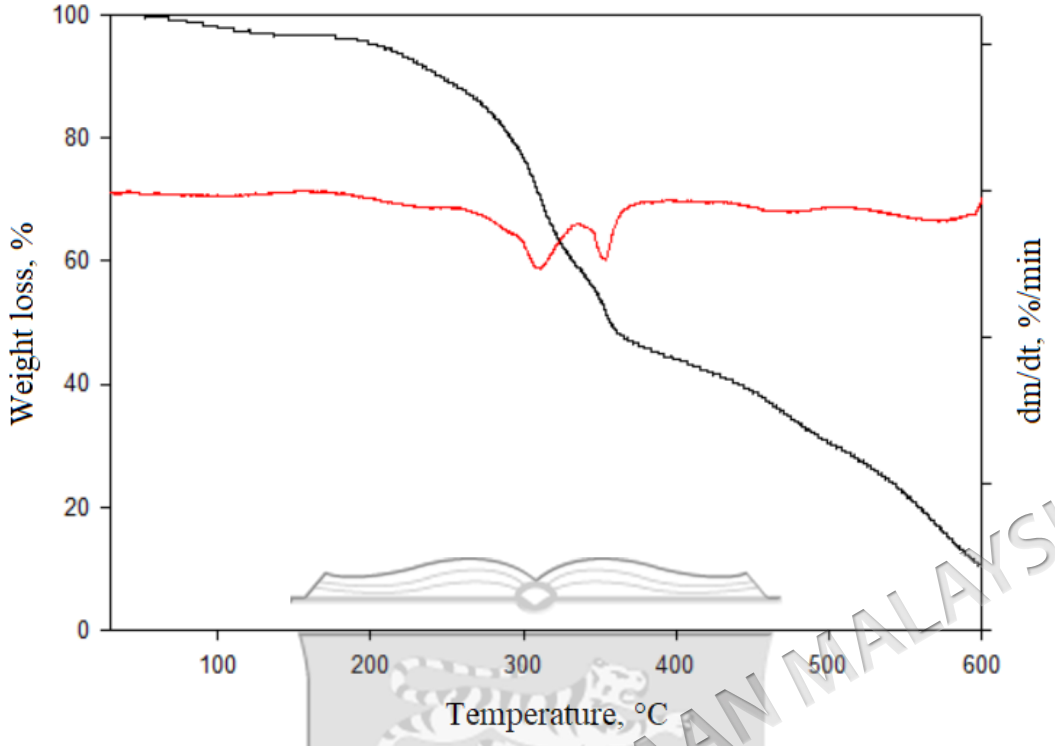

F6 Thermograms and DTG curves of UV-irradiated PU200C24-5

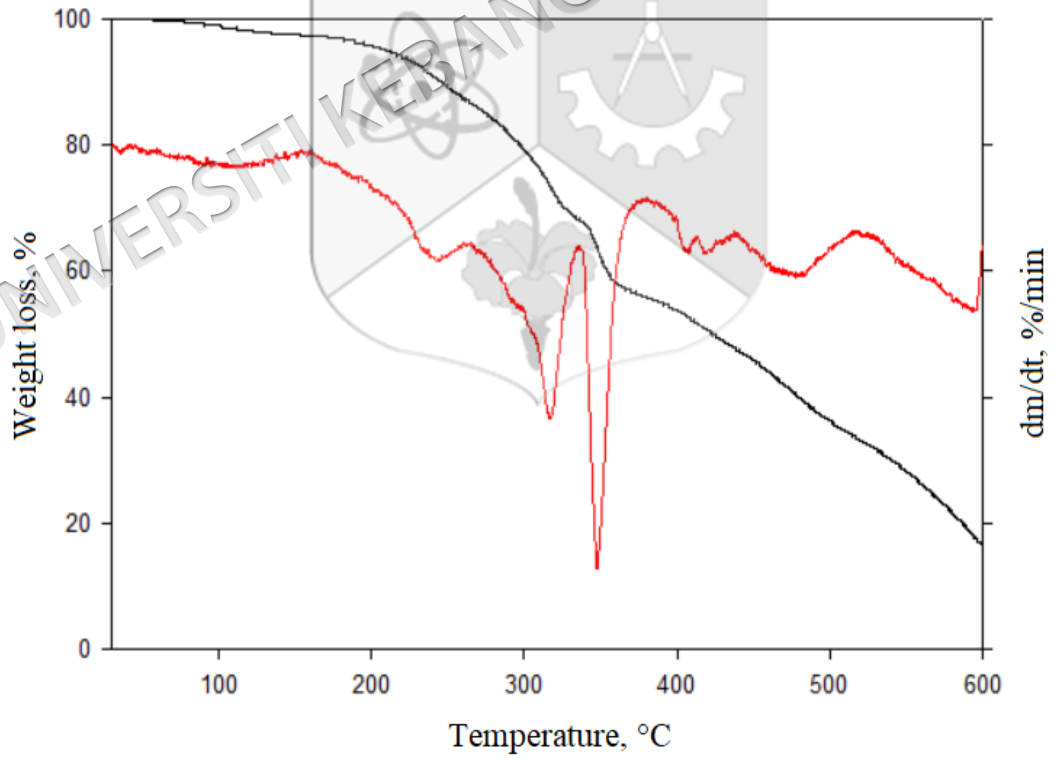

F7 Thermograms and DTG curves of non UV-irradiated PU200C48-5

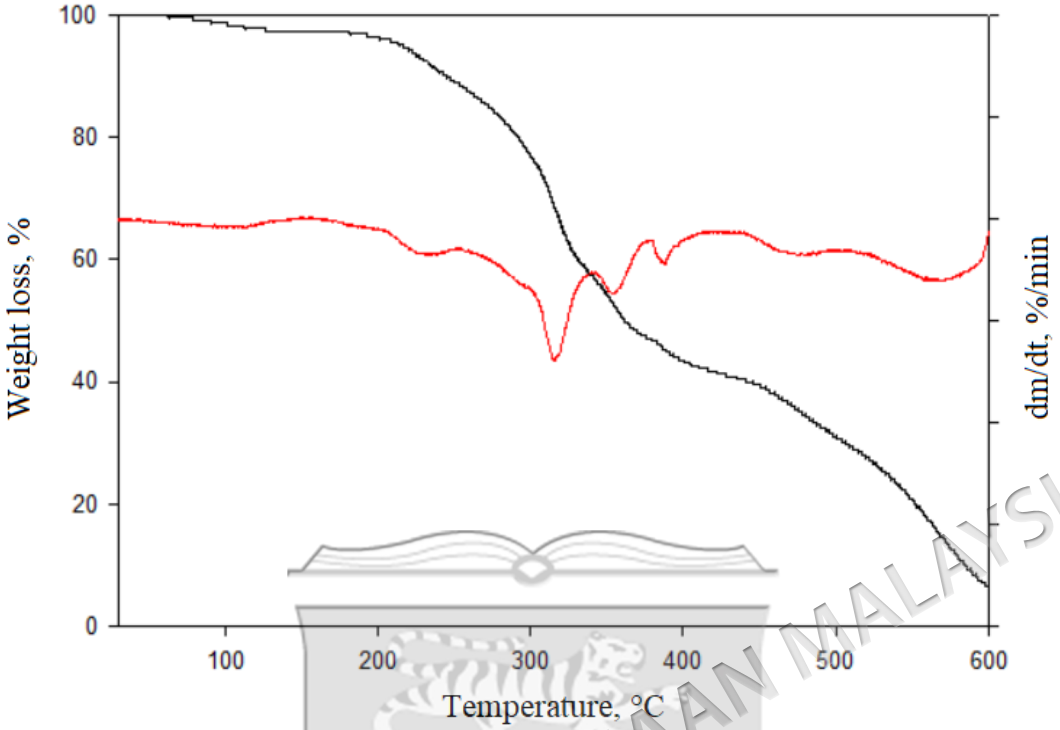

F8 Thermograms and DTG curves of UV-irradiated PU200C48-5

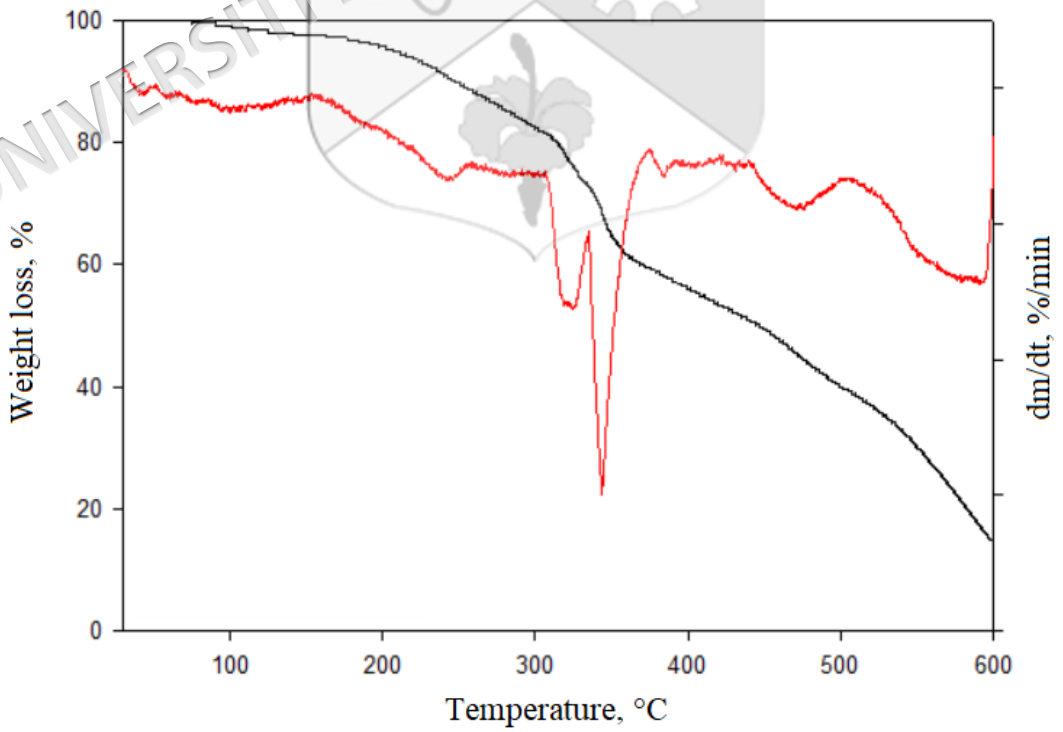

F9 Thermograms and DTG curves of non UV-irradiated PU200C72-5

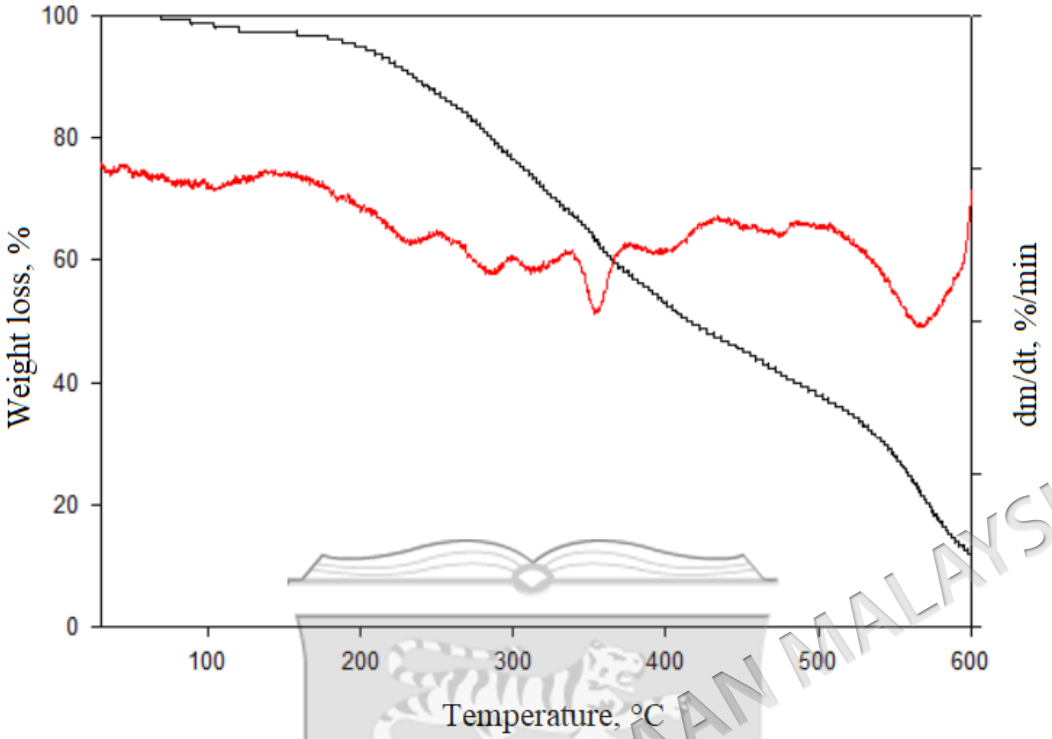

F10 Thermograms and DTG curves of UV-irradiated PU200C72-5

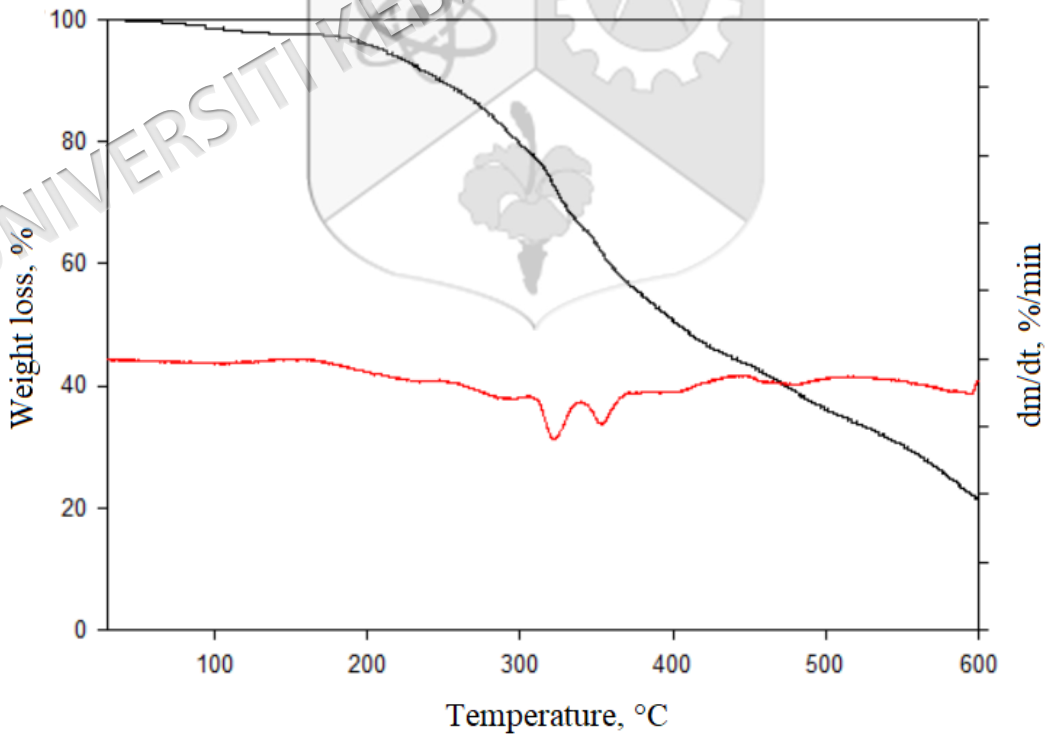

F11 Thermograms and DTG curves of non UV-irradiated PU200C96-5

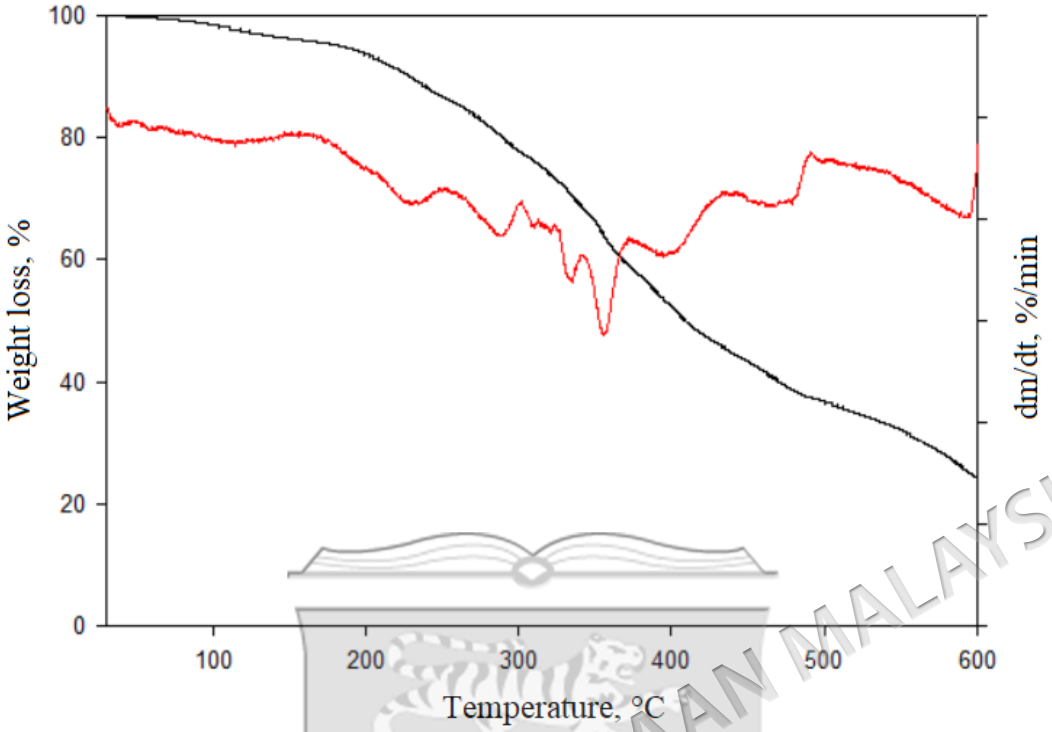

F12 Thermograms and DTG curves of UV-irradiated PU200C96-5

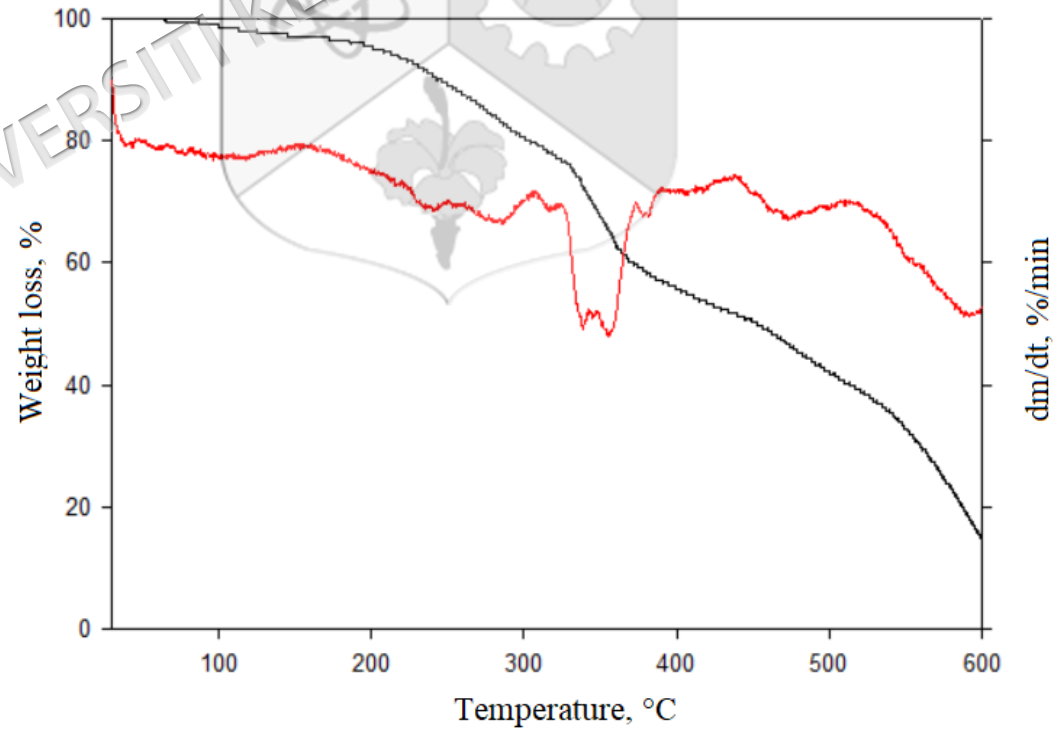

F13 Thermograms and DTG curves of 6,7-dihydroxycoumarin

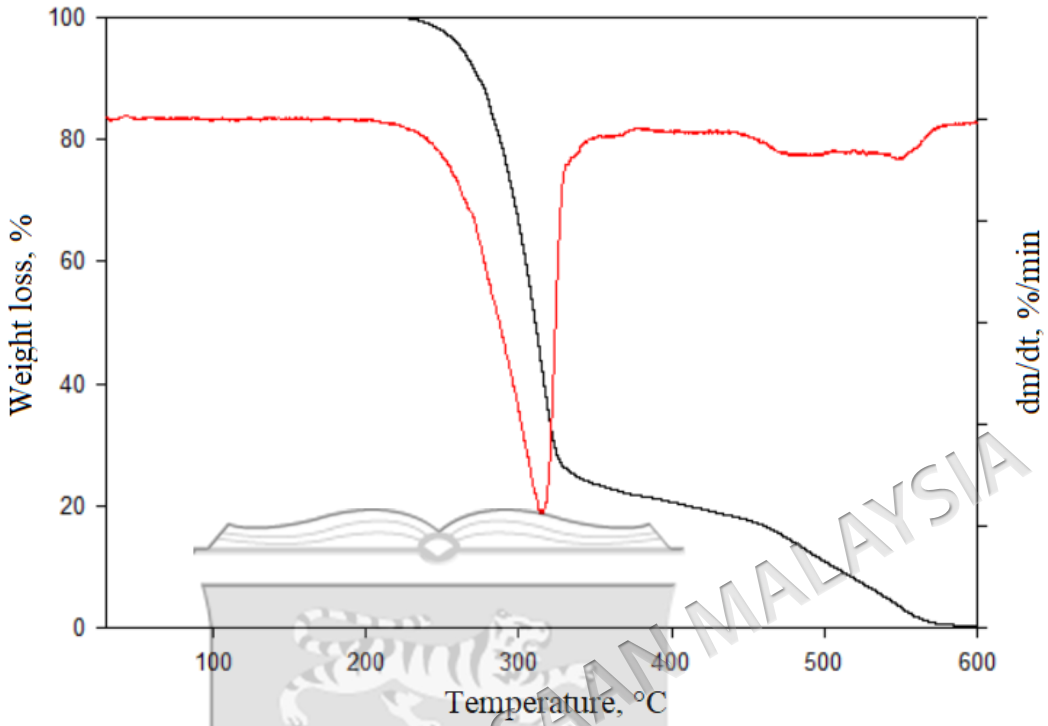

APPENDIX G

Elemental composition of various PU-$LiClO_4$ and self-healing PU-$LiClO_4$

G1 Elemental composition of PU films with varying NCO/OH ratios

Sample	Element	Average mass %	Average atomic %
PU200-5	C	78.64	87.88
	N	0.19	0.21
	O	11.91	10.47
	Cl	3.62	1.44
PU150-5	C	78.76	81.98
	N	0.22	0.25
	O	15.02	15.05
	Cl	6.00	2.71
PU100-5	C	74.62	75.62
	N	0.17	0.19
	O	20.51	21.92
	Cl	4.7	2.27
PU85-5	C	76.42	88.02
	N	0.11	0.12
	O	20.67	10.43
	Cl	3.23	1.42

G2 Elemental composition of PU films with varying $LiClO_4$ content

Samples	Element	Average mass %	Average atomic %
PU200-0	C	86.21	89.05
(0 wt% $LiClO_4$)	N	0.45	0.51
	O	13.34	10.44
	Cl	0.00	0.00
PU200-5	C	78.64	87.88
(5 wt% $LiClO_4$)	N	0.19	0.21
	O	11.91	10.47
	Cl	3.62	1.44
PU200-10	C	64.91	73.82
(10 wt% $LiClO_4$)	N	0.94	0.91
	O	25.84	22.06
	Cl	8.31	3.20
PU200-15	C	54.05	63.35
(15 wt% $LiClO_4$)	N	3.41	3.43
	O	33.81	29.75
	Cl	8.73	3.47
PU200-20	C	51.34	62.48
(20 wt% $LiClO_4$)	N	5.27	5.38
	O	30.67	22.45
	Cl	12.72	9.69
PU200-25	C	53.17	64.19
(25 wt% $LiClO_4$)	N	2.99	3.10
	O	29.2	26.94
	Cl	14.12	5.78
PU200-30	C	50.41	62.48
(30 wt% $LiClO_4$)	N	2.91	3.10
	O	29.03	27.01
	Cl	17.64	7.41

G3 Elemental composition in non UV-irradiated PU200-5, PU200C24-5, PU200C48-5, PU200C72-5 and PU200C96-5

Samples	Element	Average mass %	Average atomic %
PU200-5	C	78.64	87.88
	N	0.19	0.15
	O	17.55	10.47
	Cl	3.62	1.51
PU200C24-5	C	60.87	67.53
	N	0.04	0.06
	O	33.75	27.28
	Cl	5.34	5.13
PU200C48-5	C	62.58	69.00
	N	0.07	0.09
	O	34.32	27.90
	Cl	3.03	3.01
PU200C72-5	C	62.03	68.57
	N	0.05	0.07
	O	34.68	28.27
	Cl	3.24	3.09
PU200C96-5	C	68.43	73.70
	N	0.06	0.08
	O	26.48	20.84
	Cl	5.03	5.38

G4 Elemental composition in UV-irradiated UV-irradiated PU200-5, PU200C24-5, PU200C48-5, PU200C72-5 and PU200C96-5

Samples	Element	Average mass %	Average atomic %
HPU200-5	C	75.17	82.13
	N	0.25	0.17
	O	21.57	16.49
	Cl	3.01	1.21
HPU200C24-5	C	61.21	69.16
	N	0.07	0.09
	O	34.09	26.51
	Cl	4.63	4.24
HPU200C48-5	C	63.09	69.47
	N	0.07	0.09
	O	32.79	26.42
	Cl	4.05	4.02
HPU200C72-5	C	62.13	68.66
	N	0.06	0.07
	O	34.61	28.2
	Cl	3.2	3.07
HPU200C96-5	C	65.17	71.55
	N	0.05	0.07
	O	30.15	24.15
	Cl	4.62	4.23

D9 Tensile modulus, stress and strain of PU200-5. PU150-5, PU100-5 and PU85-5

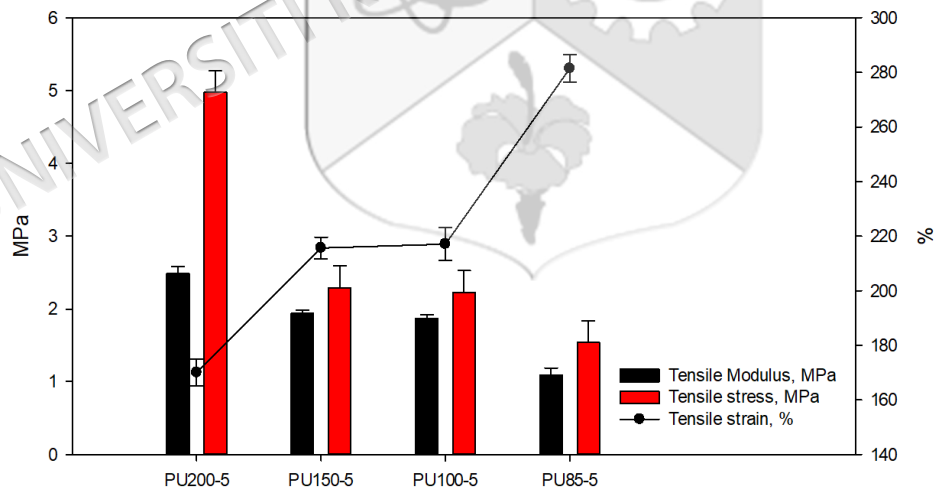

D10 Tensile modulus, stress and strain of PU200-0, PU200-5 and PU200-10

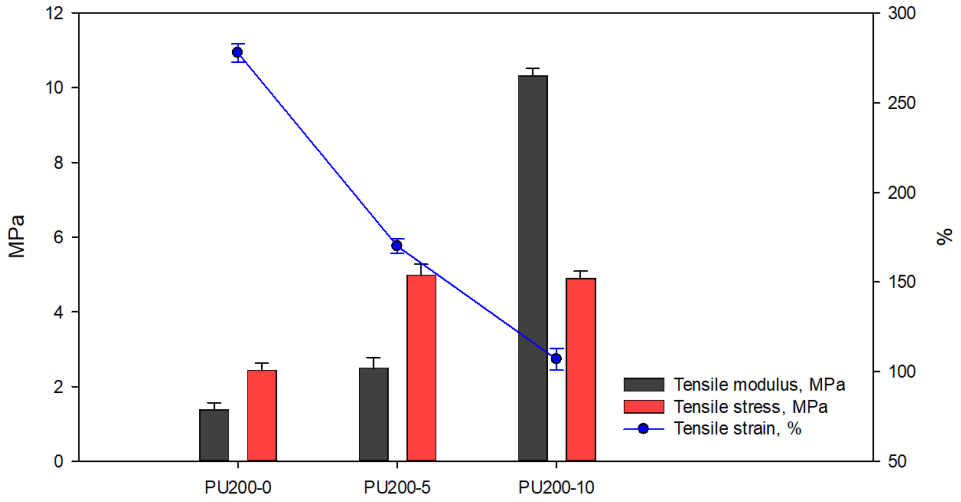

APPENDIX H

Optical and Scanning electron micrographs of various PU-$LiClO_4$ and self-healing PU-$LiClO_4$

H1 Optical micrographs of non UV-irradiated (a) PU200-5, (c) PU200C24-5, (e) PU200C48-5, (g) PU200C96-5 and UV-irradiated (b) HPU200-5, (d) HPU200C24-5, (f) HPU200C48-5 and (h) HPU200C96-5

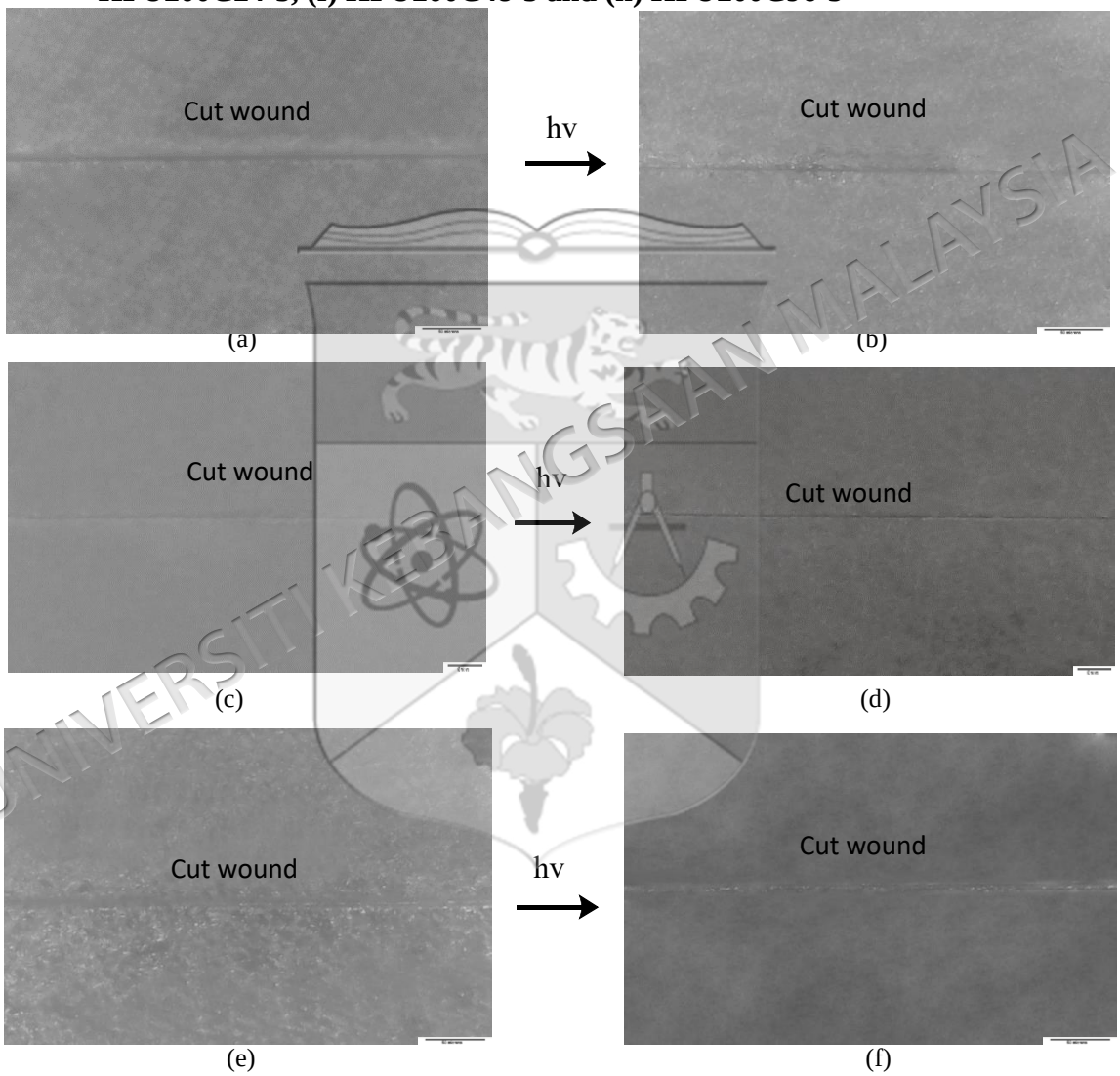

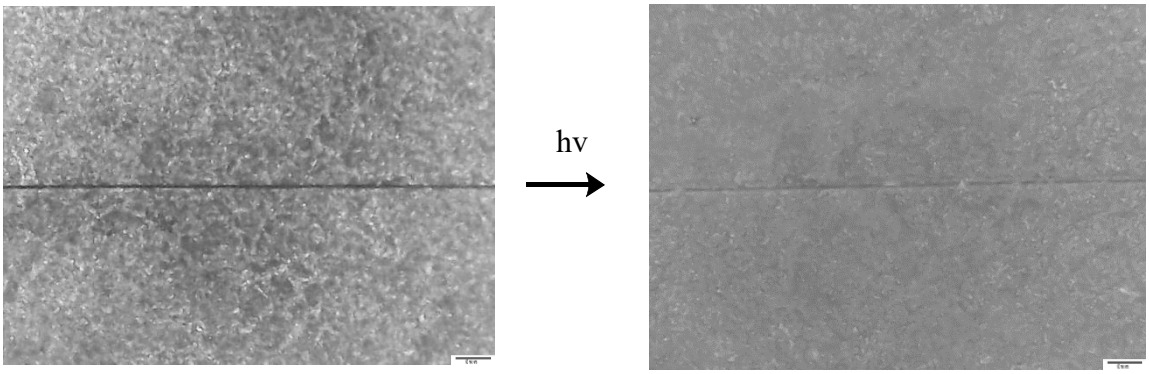

(g) (h)

H2 Scanning Electron Microscope micrographs of UV irradiated (a) PU200-5, (b) PU200C24-5, (c) PU200C48-5 and (d) PU200C96-5

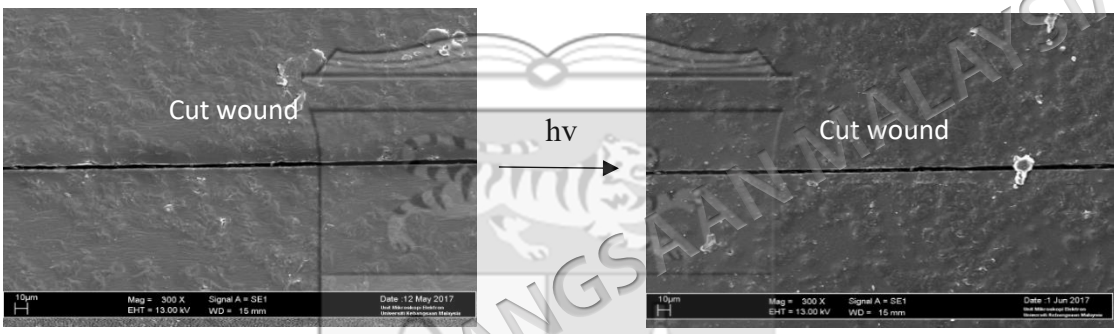

(a)

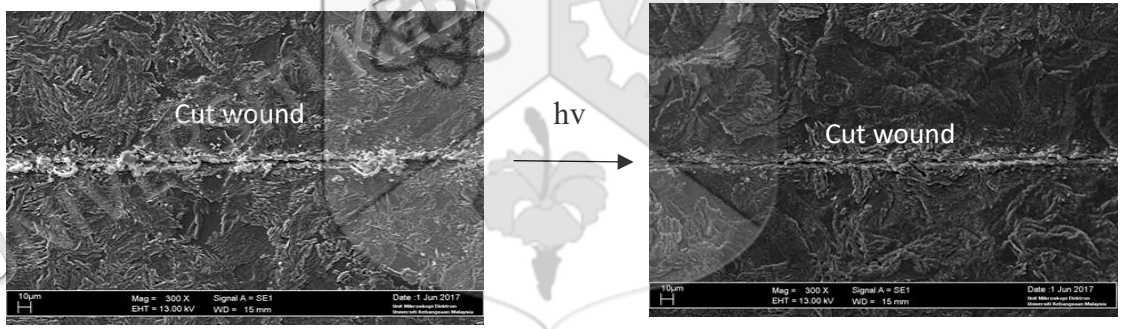

(b)

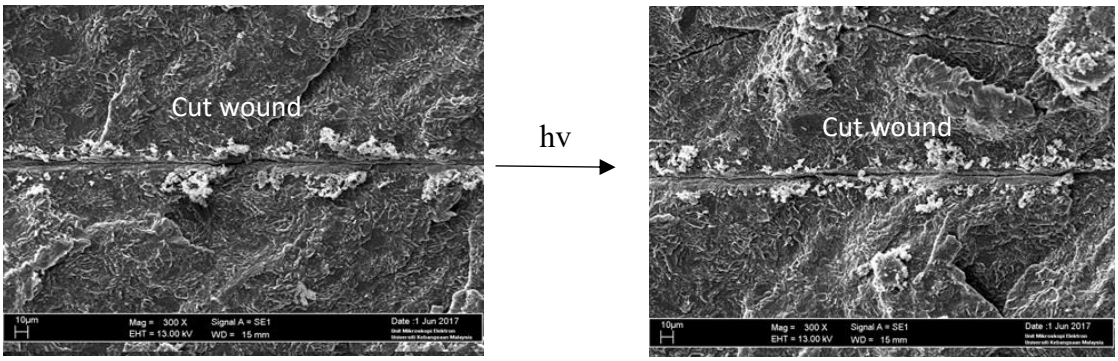

(c)

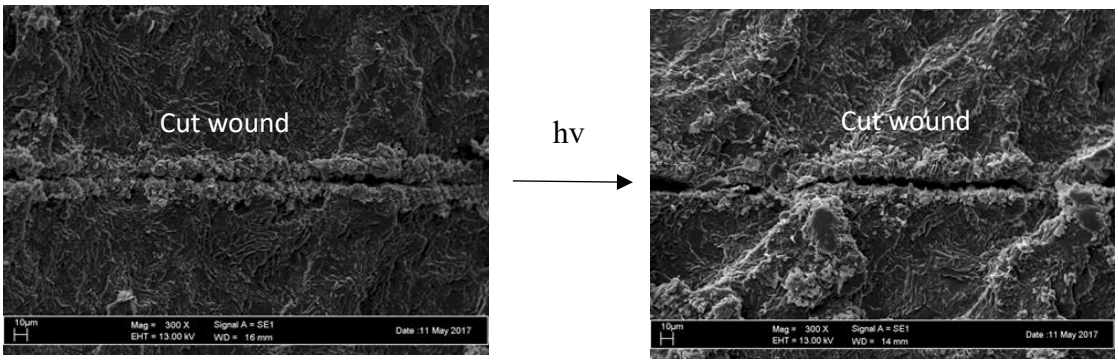

(d)

APPENDIX I

Bulk Resistance Of Various PU-$LiClO_4$ And Self-Healing PU-$LiClO_4$

I1 Bulk Resistance Of PU200-0

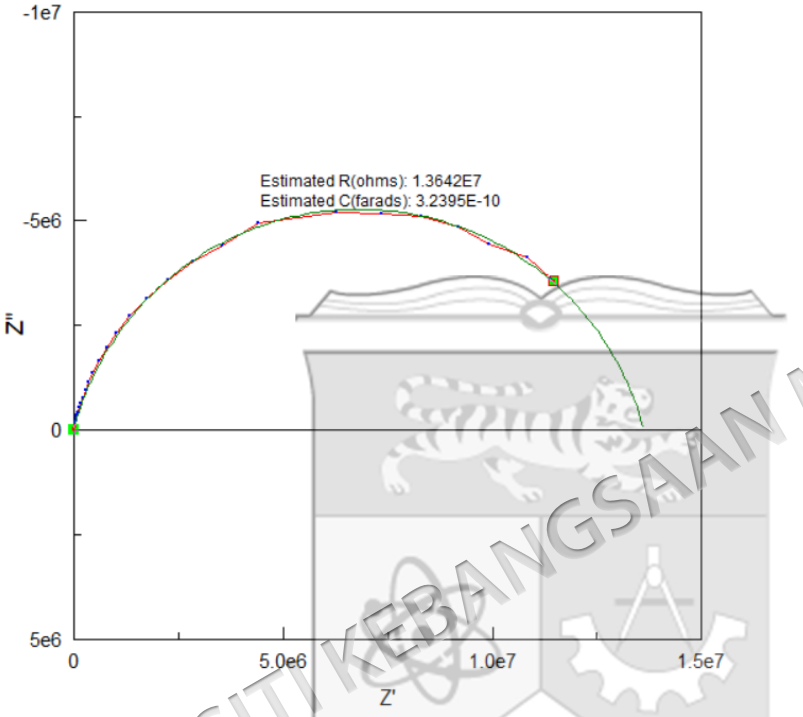

I2 Bulk Resistance Of PU200-5

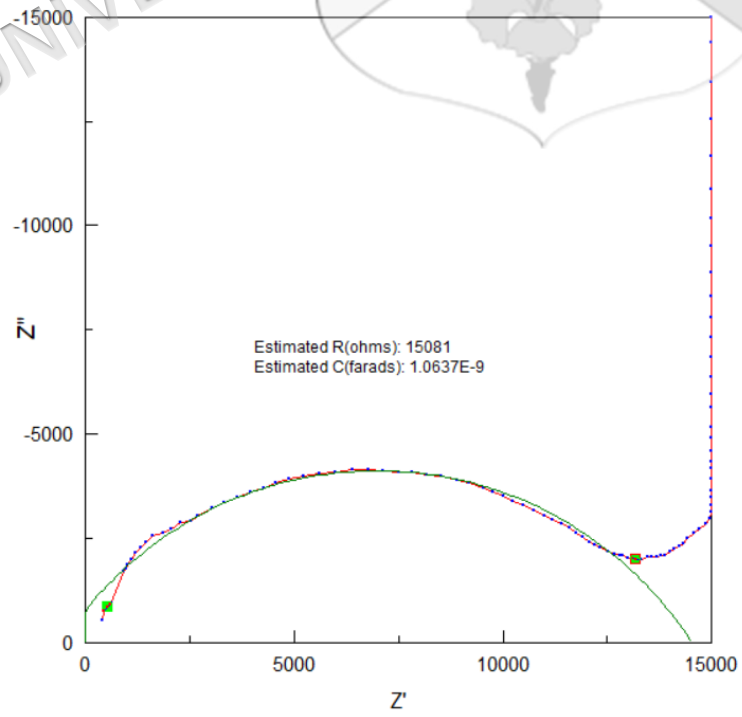

I3 Bulk Resistance Of PU200-10

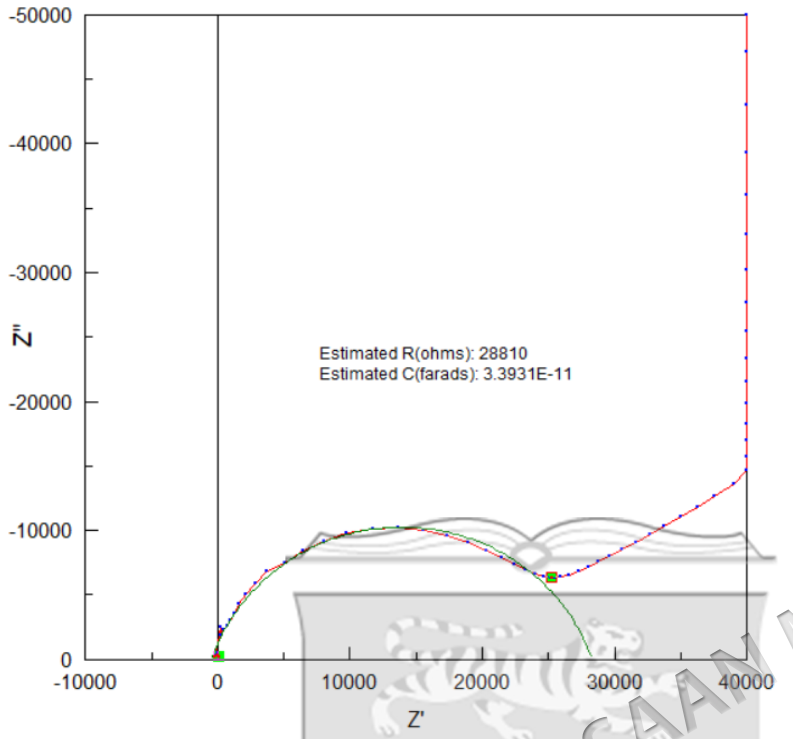

I4 Bulk Resistance Of PU150-5

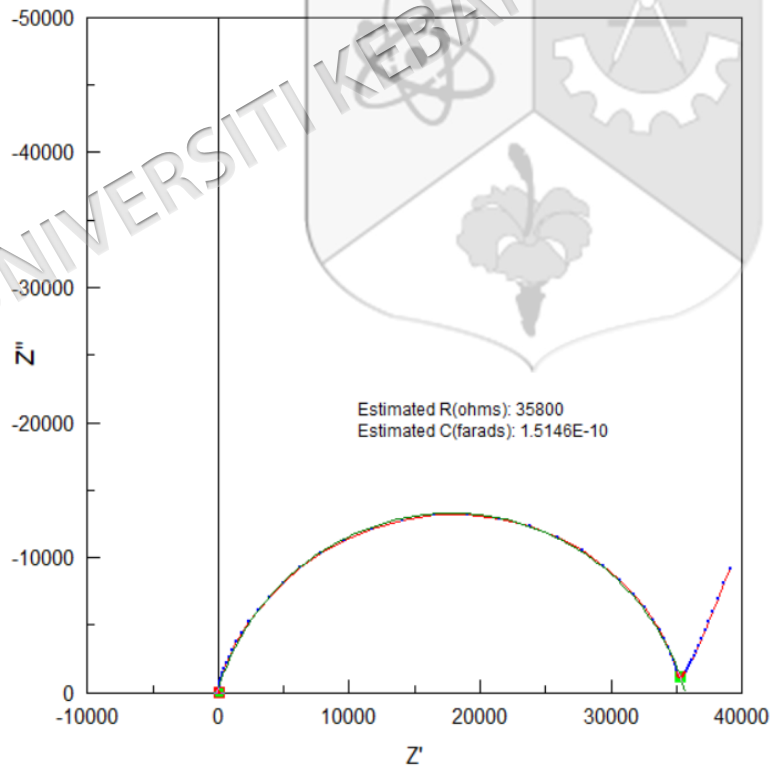

I5 Bulk Resistance Of PU100-5

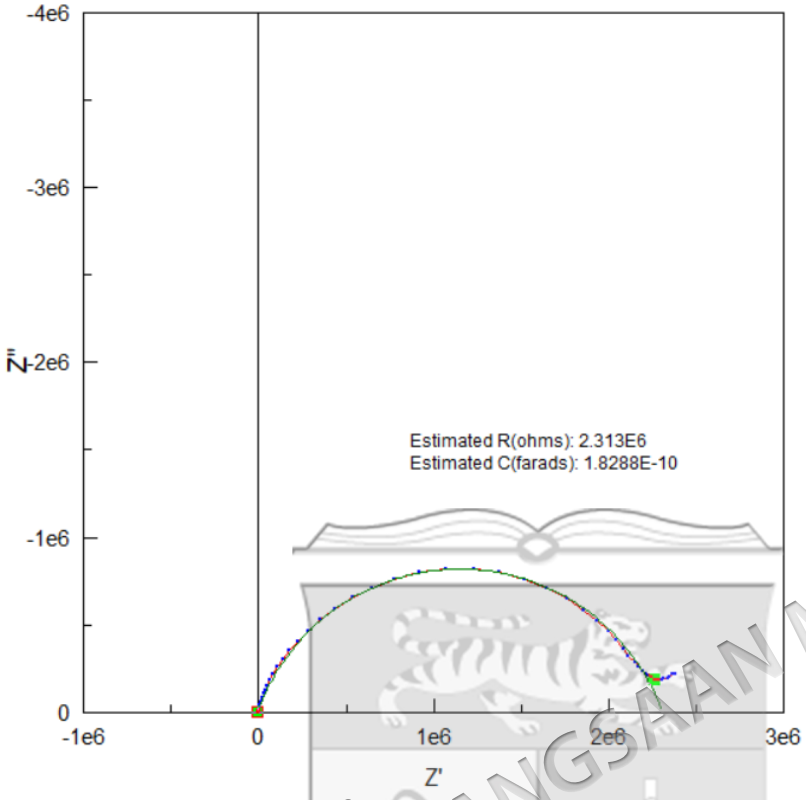

I6 Bulk Resistance Of PU85-5

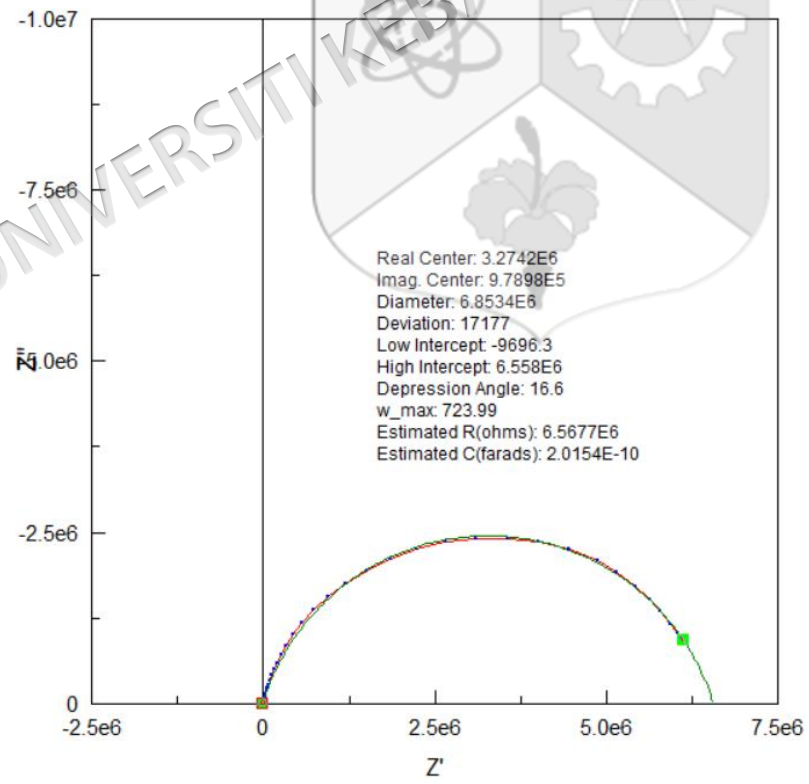

I7 Bulk Resistance Of HPU200-5

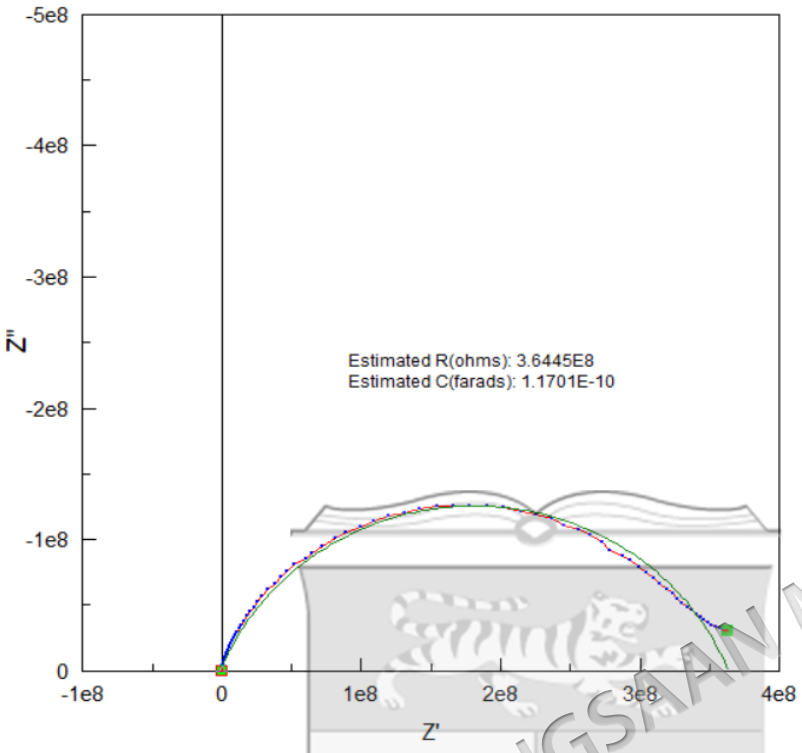

I8 Bulk Resistance Of PU200C24-5

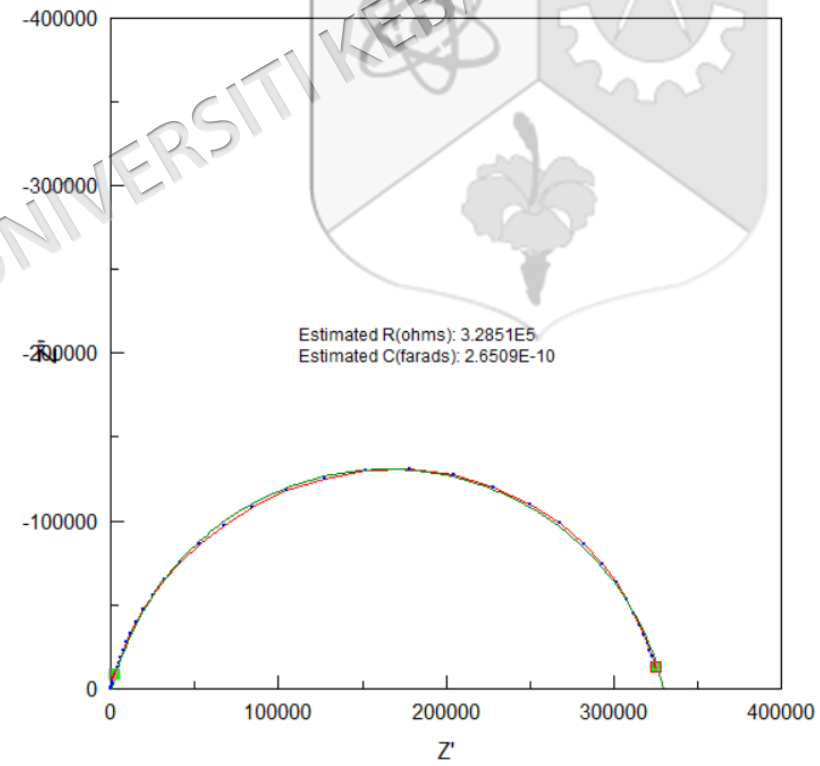

I9 Bulk Resistance Of HPU200C24-5

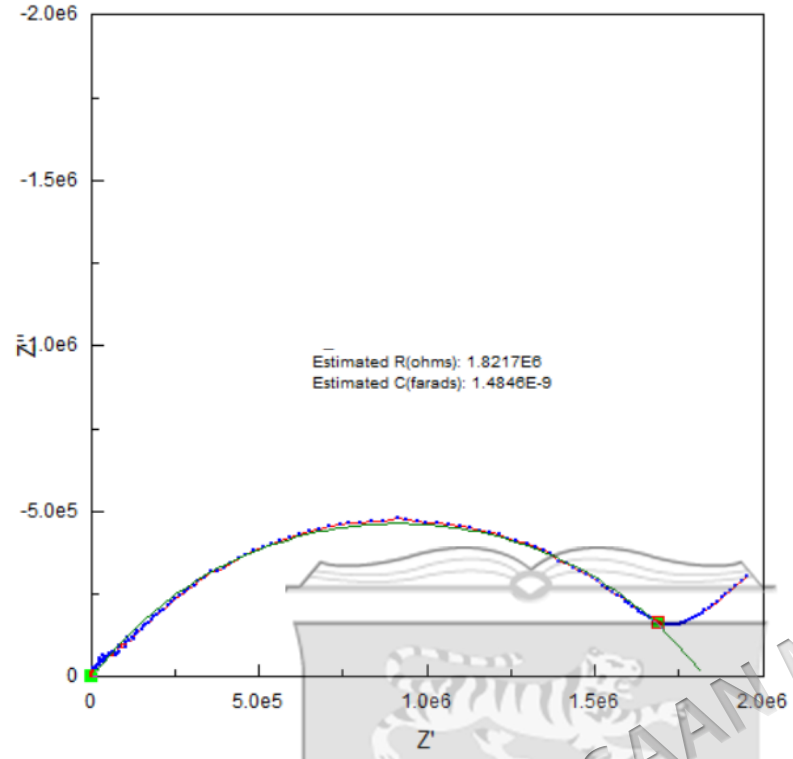

I10 Bulk Resistance Of PU200C48-5

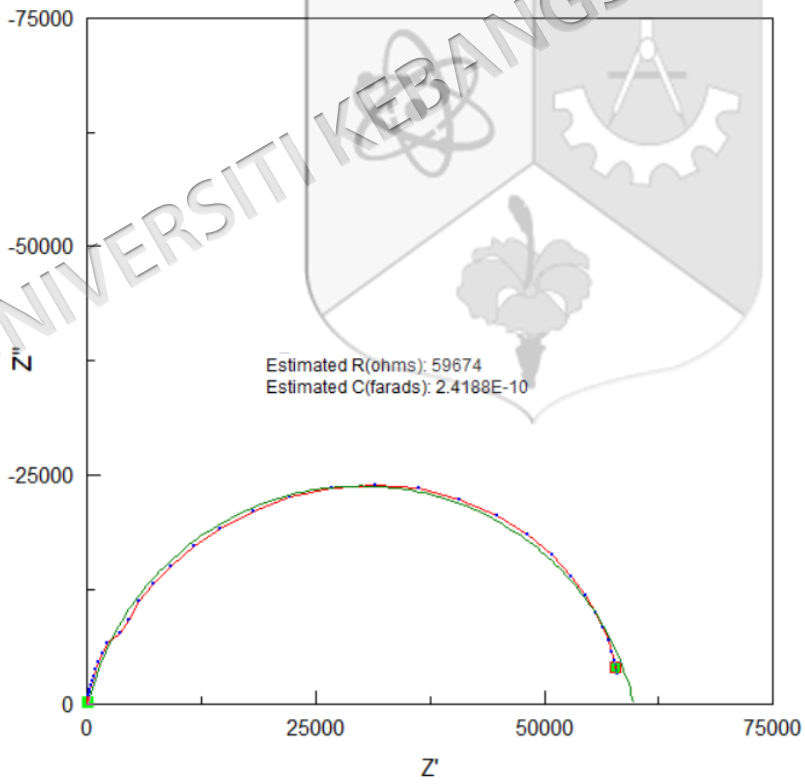

I11 Bulk Resistance Of HPU200C48-5

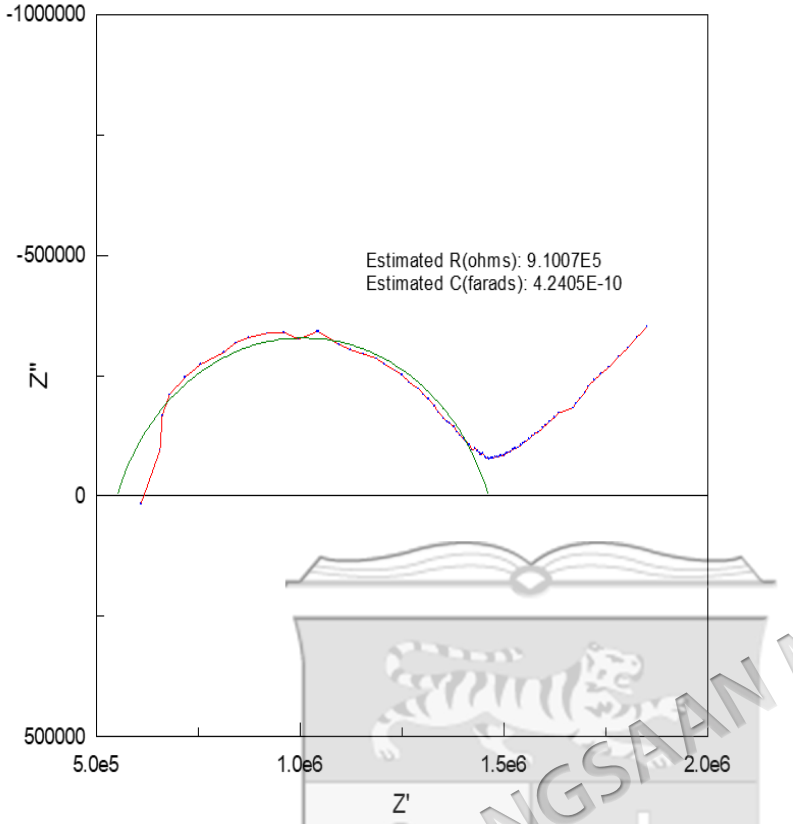

I12 Bulk Resistance Of PU200C72-5

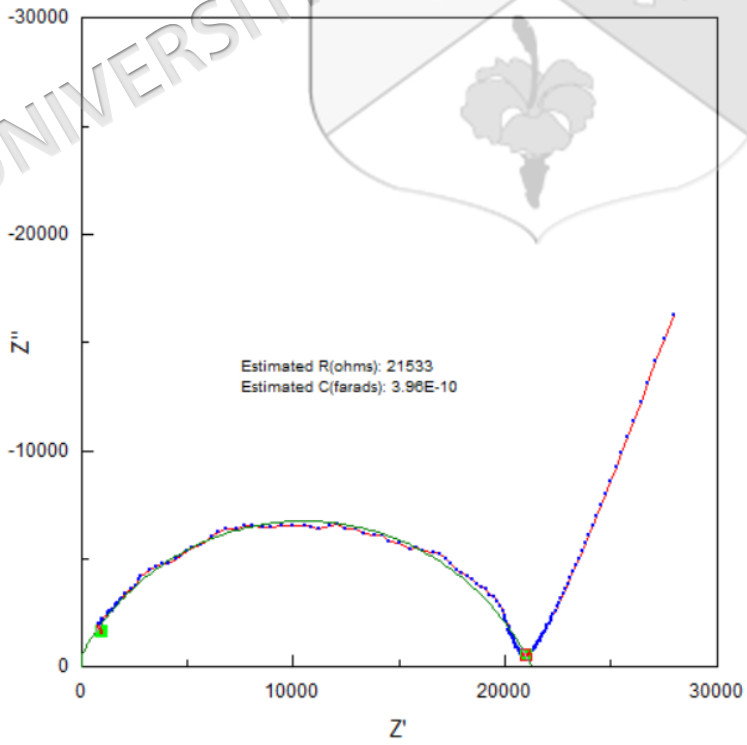

I13 Bulk Resistance Of HPU200C72-5

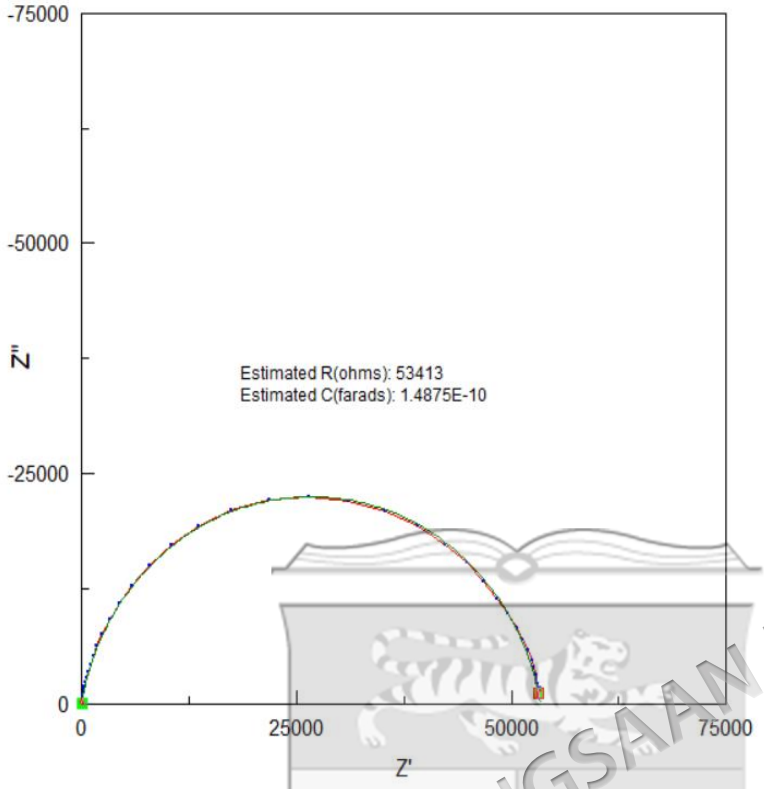

I14 Bulk Resistance Of PU200C96-5

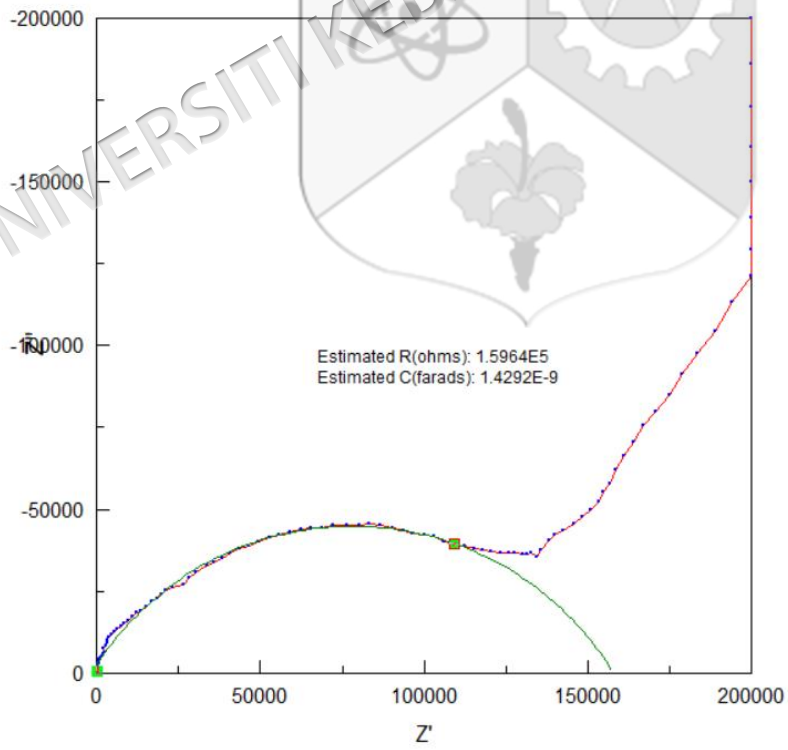

I15 Bulk Resistance Of HPU200C96-5

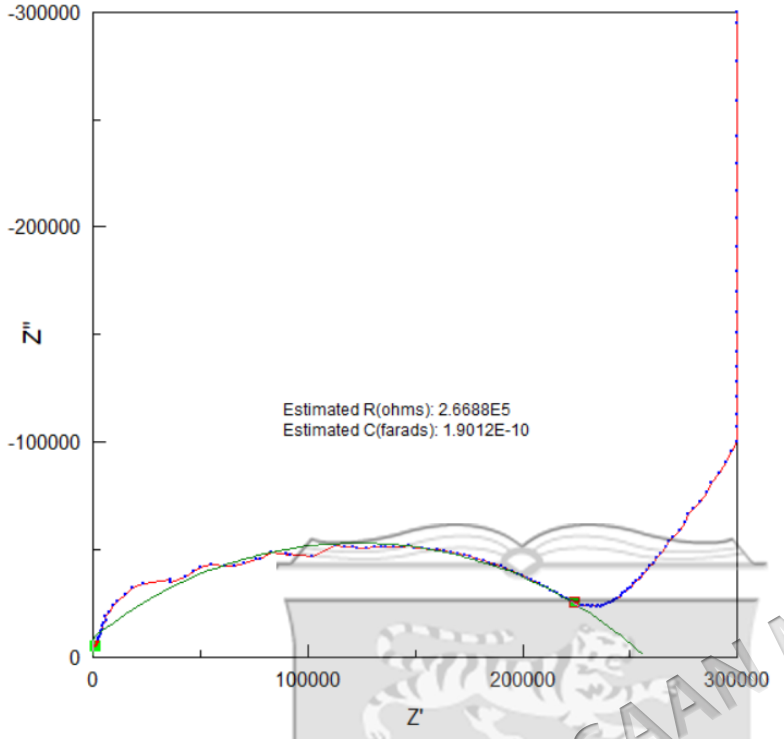

APPENDIX J

Tensile modulus, stress and strain of various PU-$LiClO_4$ and self-healing PU-$LiClO_4$

J1 Tensile modulus, stress and strain of PU200-5. PU150-5, PU100-5 and PU85-5

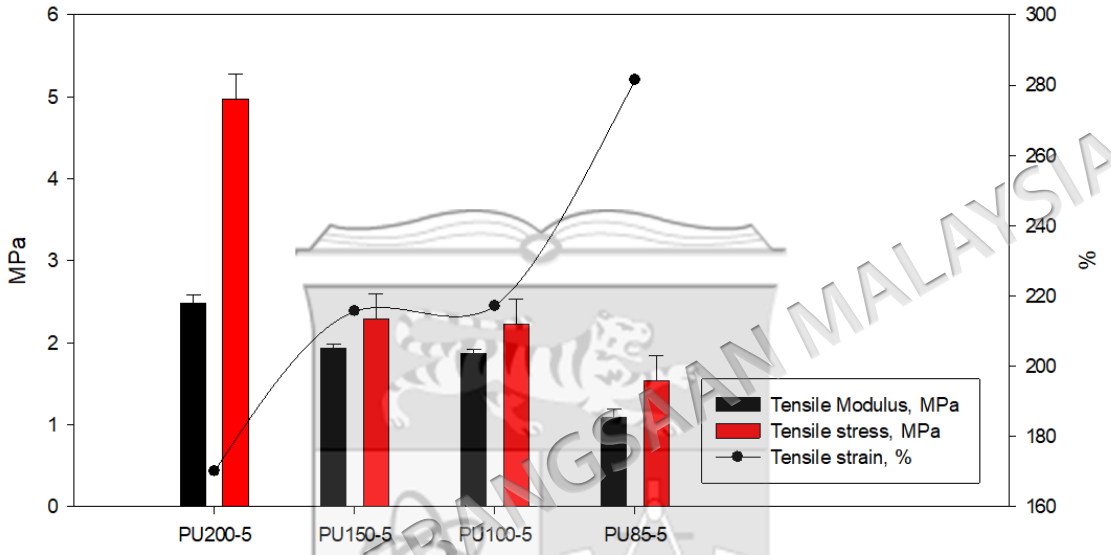

J2 Tensile modulus, stress and strain of PU200-0, PU200-5 and PU200-10

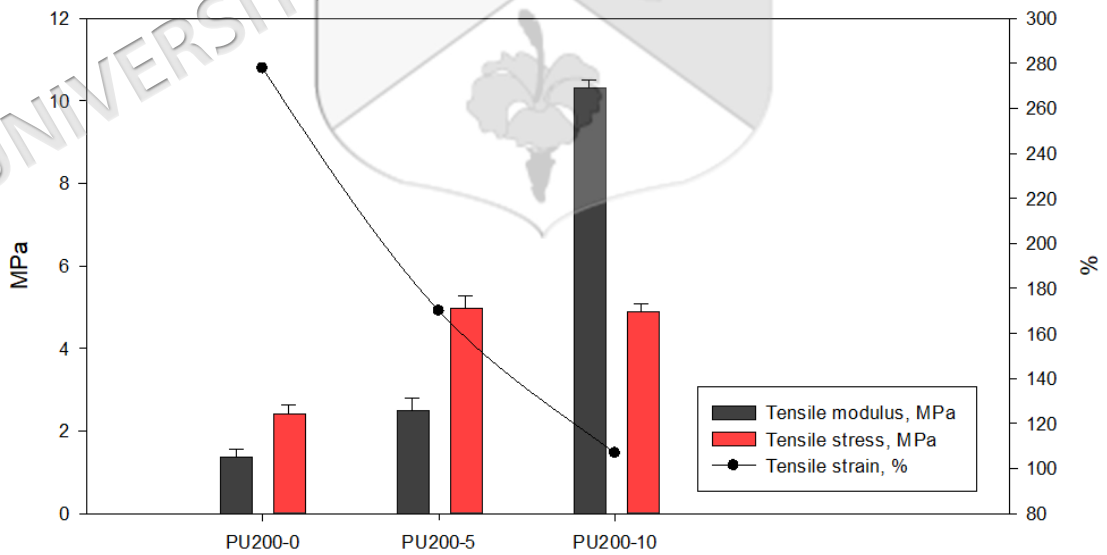

J3 Tensile modulus of non UV-irradiated and UV-irradiated PU200-5, PU200C24-5, PU200C48-5, PU200C72-5 and PU200C96-5

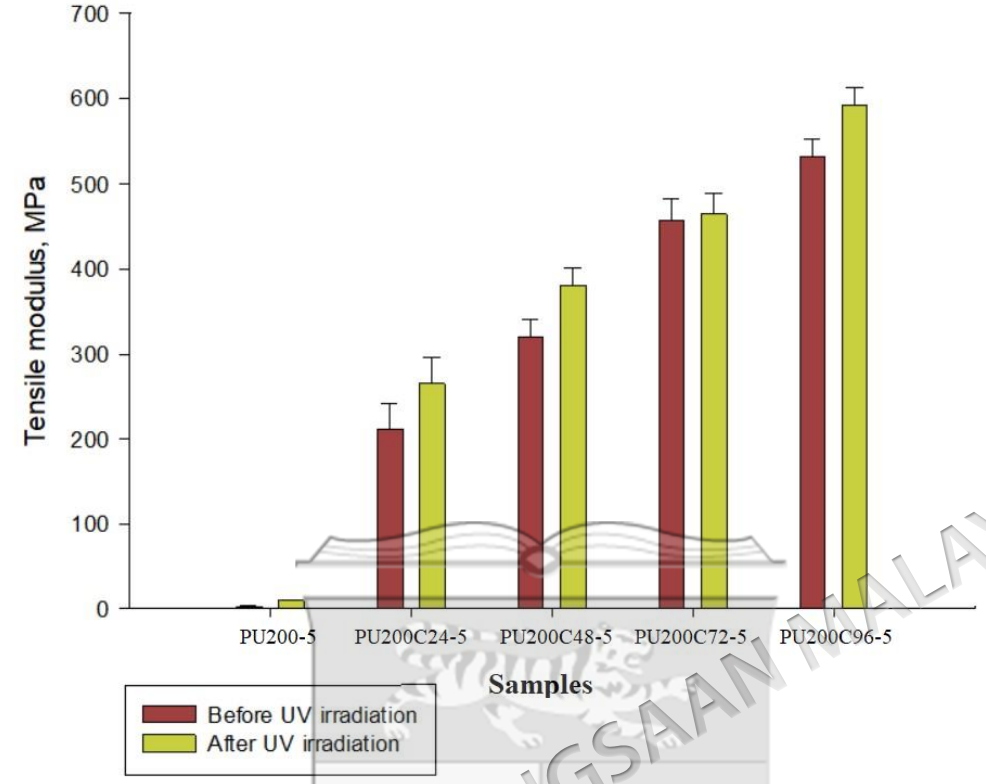

J4 Tensile stress of non UV-irradiated and UV-irradiated PU200-5, PU200C24-5, PU200C48-5, PU200C72-5 and PU200C96-5

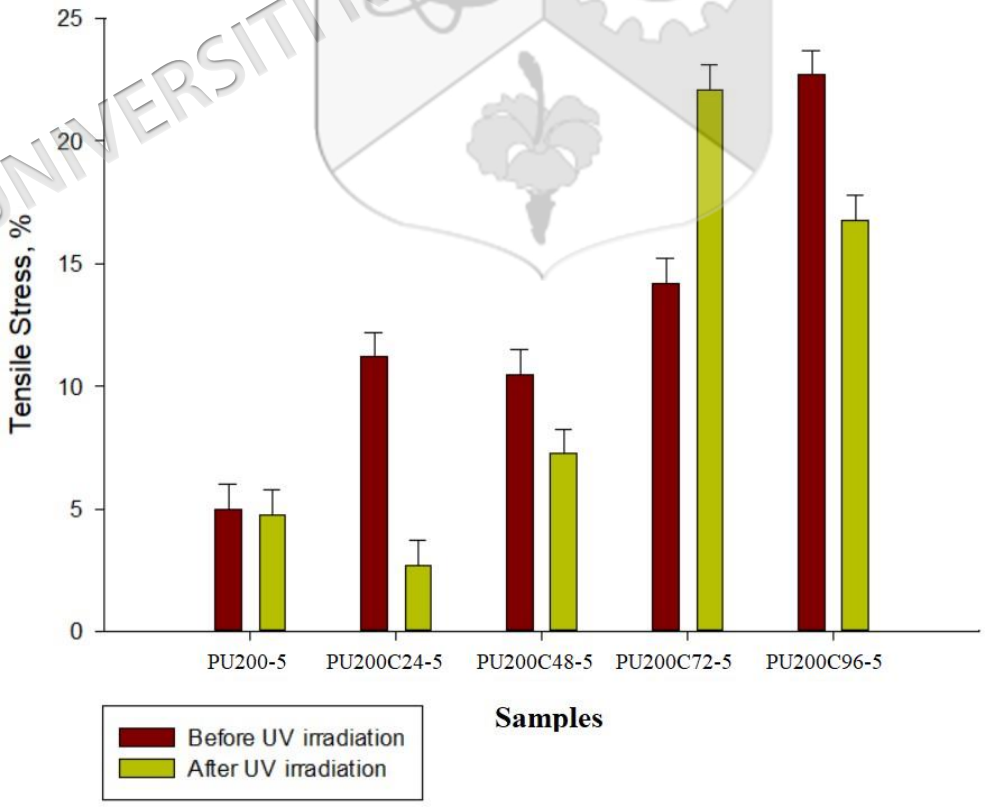

J5 Tensile strain of non UV-irradiated and UV-irradiated PU200-5, PU200C24-5, PU200C48-5, PU200C72-5 and PU200C96-5

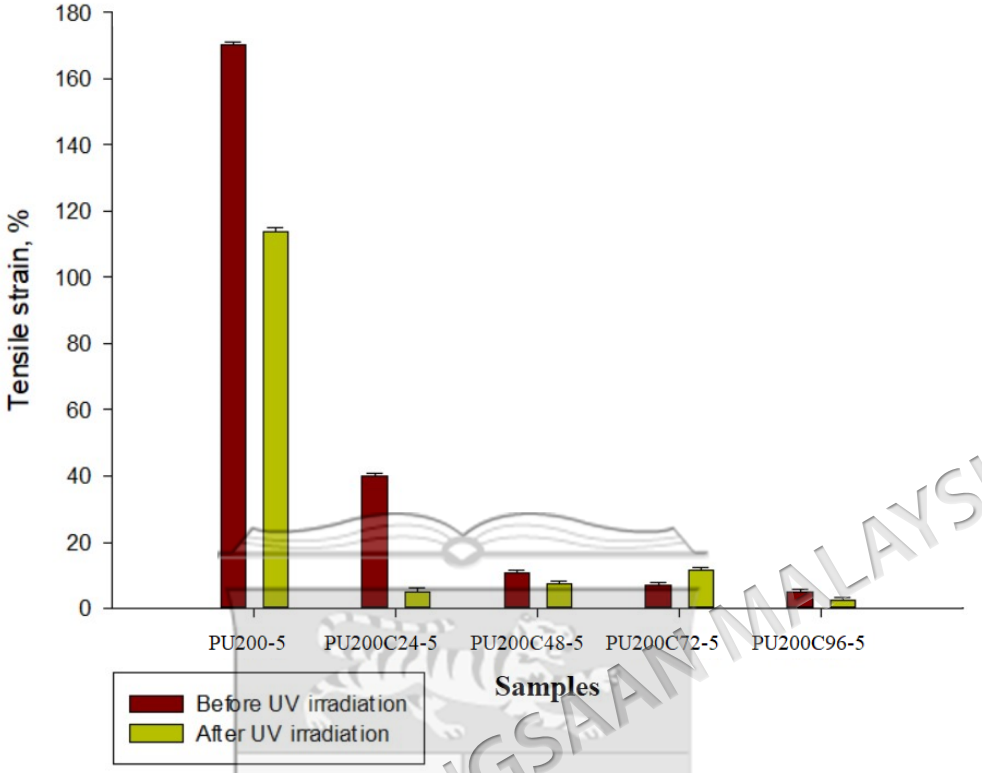

APPENDIX K

LIST OF PUBLICATIONS AND PATENTS

1) JOURNALS (*h* index = 4 Scopus/ISI 2018)

Wong,L.S. & **Wong, C.S.** 2015. A New Method of Heavy Metals and Aluminium Detection using Biopolymer-Based Optical Biosensor, *Sensor journal, IEEE* 15 (1): 471-475. ISI/SCOPUS (Thomson Reuters)

Wong, C.S., Badri, K.H., Ataollahi, N.., Law, K.P., Su'ait, M.S. & Hassan, N.I. 2014. Synthesis of New Bio-based Solid Polymer Electrolyte Polyurethane-$LiClO_4$ via Prepolymerization Method: Effect of NCO/OH Ratio on Their Chemical, Thermal Properties and Ionic Conductivity, International Journal of Chemical Nuclear, *Materials and Metallurgical Engineering* 1(11): 216.

Wong, C.S. & Badri, K.H. 2013. Thermal, Mechanical and Chemical Analyses Of Rapid and Self-Cured Prepolymerized Polyurethane Coatings, Applied Mechanics and Materials, 313-314:227-231. ISI/SCOPUS (Thomson Reuters)

Wong, C.S. & Badri, K.H. 2012. Chemical Analyses of Palm Kernel Oil-Based Polyurethane Prepolymer, Materials Sciences and Applications. 3(2): pp 78-86 ISI/SCOPUS (Thomson Reuters)

Wong, C.S. & Badri, K.H. 2010. Thermal and Fire Resistant Properties of Palm Kernel Oil and Soybean Oil-Based Polyurethanes, 39 (5): 775-784. ISI/SCOPUS (Thomson Reuters)

Badri, K.H., **Wong, C.S.**, Shahrom, M.S, Liow, C.H., Baderuliksan, N.Y & Norzali, N.A. 2010. FTIR Spectroscopy Analysis of the Prepolymerization of Palm-Based Polyurethane, Solid State Science and Technology 18 (2): 1-8.

2) CHAPTER IN BOOK

Badri, K.H. & **Wong, C.S.** 2014. Chapter 1: Castable palm-based polyurethane prepolymer. Pandalai, S. G. Ed. Recent Research Developments in Polymer Science, 12: 1-16 ISBN: 978-81-7895-611-4 Kerala, India:Transworld Research Network (INTERNATIONAL)

3) PATENTS

Badri, K.H., Wong,K.C. & **Wong C.S.** UV-RadMach reactor. Filing Date: 25/3/2014, Filing number UKM IKB/108/2/1850.

APPENDIX L

AWARDS AND ACHIEVEMENTS

Research Innovation Award Production of Palm-Based Polyurethane Polyol Majlis Anugerah Inovasi UKM/Puri Pujangga/UKM. 13 April 2012

Erasmus Mundus (Techno II), University of Girona, Spain (€15000), September 2015 to June 2016